August 1982
Final Report

DOT HS-806 280

US Department of Transportation
National Highway Traffic Safety Administration

VALIDATION OF THE CRASH VICTIM SIMULATOR
Volume II: Engineering Manual --Part II
Validation Effort

John T. Fleck
Frank E. Butler
Norman J. DeLeys

Calspan Corporation
Advanced Technology Center
4455 Genesee Street
Buffalo, N.Y.   14225

Contract No. DOT-HS-6-01300
Contract Amount $492,175

TECHNICAL REPORT STANDARD TITLE PAGE

1. Report No.
DOT-HS-806 280

2. Government Accession No.

3. Recipient's Catalog No.

4. Title and Subtitle
Validation of the Crash Victim Simulator
Volume 2, Engineering Manual - Part II:
Validation Effort

5. Report Date
August, 1982

6. Performing Organization Code
W69

7. Author(s)
John T. Fleck, Frank E. Butler, Norman J. DeLeys

8. Performing Organization Report No.
ZS-5881-V-2

9. Performing Organization Name and Address
Calspan Corporation
Advanced Technology Center
4455 Genesee Street
Buffalo, NY 14225

10. Work Unit No.

11. Contract or Grant No.
DOT-HS-6-01300

12. Sponsoring Agency Name and Address
U. S. Department of Transportation
National Highway Traffic Safety Administration
400 Seventh Street, S.W.
Washington, DC 20590

13. Type of Report and Period Covered
Final Report
January 1976 - August 1982

14. Sponsoring Agency Code

15. Supplementary Notes

16. Abstract

A combined analytical and experimental research project was carried out to develop and examine the validity of an improved version of the computer program used to simulate the three-dimensional dynamic gross motion responses of motor vehicle crash victims. Among the improvements incorporated in the new (CVS-IV) version of the program are a more efficient integration technique, a routine to automatically position a seated occupant in equilibrium, and modifications of the input and output control routines that make it easier to use the program. Measurements of a Part 572 50th percentile male anthropomorphic dummy were made to define an input data set for a simulation model of the dummy. Dynamic pendulum impact tests of dummy sub-assemblies were performed and modeled with the computer program. Detailed comparisons of predicted system responses with those measured in special impact sled tests of the dummy restrained by a three-point restraint belt and by a pre-inflated air bag are also presented.

Results of the project are documented in four manuals as follows:

Volume 1 - Engineering Manual - Part I: Analytical Formulation
Volume 2 - Engineering Manual - Part II: Validation Effort
Volume 3 - User's Manual
Volume 4 - Programmer's Manual

17. Key Words
Computer Simulation
Three-Dimensional Dynamics
Mathematical Models
Crash Victim Simulation
Rigid Body Dynamics

18. Distribution Statement
Document is available to the U. S. public through the National Technical Information Service, Springfield, Virginia 22161

19. Security Classif. (of this report)
Unclassified

20. Security Classif. (of this page)
Unclassified

21. No. of Pages
246

22. Price

Form DOT F 1700.7 (8-69)

METRIC CONVERSION FACTORS

Approximate Conversions to Metric Measures

Symbol	When You Know	Multiply by	To Find	Symbol
		LENGTH		
in	inches	*2.5	centimeters	cm
ft	feet	30	centimeters	cm
yd	yards	0.9	meters	m
mi	miles	1.6	kilometers	km
		AREA		
in^2	square inches	6.5	square centimeters	cm^2
ft^2	square feet	0.09	square meters	m^2
yd^2	square yards	0.8	square meters	m^2
mi^2	square miles	2.6	square kilometers	km^2
	acres	0.4	hectares	ha
		MASS (weight)		
oz	ounces	28	grams	g
lb	pounds	0.45	kilograms	kg
	short tons (2000 lb)	0.9	tonnes	t
		VOLUME		
tsp	teaspoons	5	milliliters	ml
Tbsp	tablespoons	15	milliliters	ml
fl oz	fluid ounces	30	milliliters	ml
c	cups	0.24	liters	l
pt	pints	0.47	liters	l
qt	quarts	0.95	liters	l
gal	gallons	3.8	liters	l
ft^3	cubic feet	0.03	cubic meters	m^3
yd^3	cubic yards	0.76	cubic meters	m^3
		TEMPERATURE (exact)		
°F	Fahrenheit temperature	5/9 (after subtracting 32)	Celsius temperature	°C

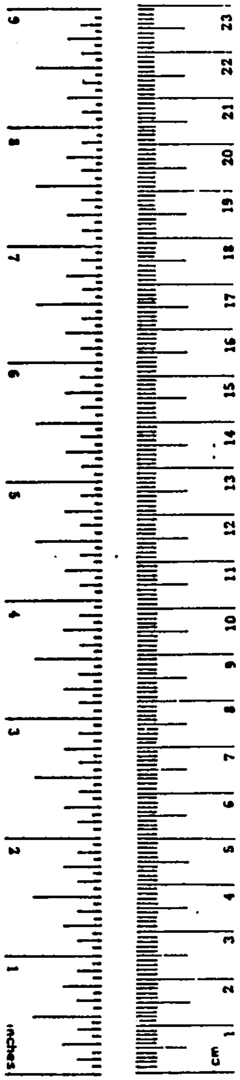

Approximate Conversions from Metric Measures

Symbol	When You Know	Multiply by	To Find	Symbol
		LENGTH		
mm	millimeters	0.04	inches	in
cm	centimeters	0.4	inches	in
m	meters	3.3	feet	ft
m	meters	1.1	yards	yd
km	kilometers	0.6	miles	mi
		AREA		
cm^2	square centimeters	0.16	square inches	in^2
m^2	square meters	1.2	square yards	yd^2
km^2	square kilometers	0.4	square miles	mi^2
ha	hectares (10,000 m^2)	2.5	acres	
		MASS (weight)		
g	grams	0.035	ounces	oz
kg	kilograms	2.2	pounds	lb
t	tonnes (1000 kg)	1.1	short tons	
		VOLUME		
ml	milliliters	0.03	fluid ounces	fl oz
l	liters	2.1	pints	pt
l	liters	1.06	quarts	qt
l	liters	0.26	gallons	gal
m^3	cubic meters	35	cubic feet	ft^3
m^3	cubic meters	1.3	cubic yards	yd^3
		TEMPERATURE (exact)		
°C	Celsius temperature	9/5 (then add 32)	Fahrenheit temperature	°F

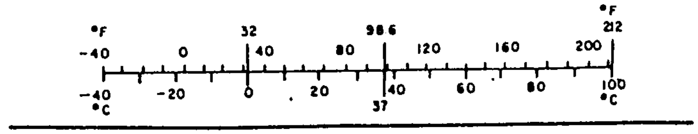

---

*1 in = 2.54 (exactly). For other exact conversions and more detailed tables, see NBS Misc. Publ. 286, Units of Weights and Measures, Price $2.25, SD Catalog No. C13.10:286.

FOREWORD

This document is one of four manuals that constitute the final report of the research project conducted under Contract No. DOT-HS-6-01300 for the National Highway Traffic Safety Administration. Dr. John T. Fleck and Mr. Frank E. Butler of J & J Technologies, Inc. served as Principal Investigator and Project Engineer, respectively, during their earlier tenure as members of the Calspan Transportation Research Department. Subsequently, Mr. Norman J. DeLeys coordinated the efforts of Calspan and J & J Technologies, Inc., who was retained as a subcontractor to maintain the continuity necessary to preparation of the report.

The Contract Technical Monitor for this project was Dr. Lee Ovenshire of the National Highway Traffic Safety Administration.

This report has been reviewed and approved by:

Anthony L. Russo

Anthony L. Russo, Head
Transportation Research Department

TABLE OF CONTENTS

Table of Contents (Cont'd)

LIST OF FIGURES

List of Figures (Cont'd)

List of Figures (Cont'd)

List of Figures (Cont'd)

LIST OF TABLES

1.0 INTRODUCTION

In 1970 Calspan Corporation (formerly Cornell Aeronautical Laboratory, Inc.) began development of a mathematical model for simulating the three-dimensional dynamic responses of a motor vehicle crash victim. Under the joint sponsorship of the Motor Vehicle Manufacturers Association (MVMA) and the National Highway Traffic Safety Administration (NHTSA), the original development and validation of the program was accomplished in two phases (Ref. 1 and 2). Except for a special version of the Phase II crash victim simulation (CVS) program created for the MVMA (Ref. 3), the next major developmental effort was accomplished for the NHTSA and resulted in what was designated as the CVS-III computer program (Ref. 4).

Recognizing the CVS-III as a potentially valuable tool for aiding studies of crew member dyanmics during ejection from high-speed aircraft, the Air Force Aerospace Medical Research Laboratory (AFAMRL) sponsored the development of a special version of the program that formed the basis of the AFAMRL "Articulated Total Body" model or ATB (Ref. 5). Later, the ATB model was updated and some new features were added under another contract with the AFAMRL (Ref. 6).

This report documents work performed in the research project entitled "Validation of the Crash Victim Simulator" under Contract No. DOT-HS-6-01300 with the NHTSA which states the general objective as "the development of the CVS to a level that it can be used for a variety of rulemaking activities". A significant goal was "to conduct studies that specifically, quantitatively and validly pertain to the Part 572 dummy in several realistic crash safety compliance test situations". The project consisted of two principal areas of effort: (1) further development, improvement and refinement of the computer program, culminating in a version designated as the CVS-IV, and (2) the performance of detailed measurements and tests to define inputs for modeling the 50th percentile male dummy conforming to government specifications (Ref. 7) and executing computer simulations of experiments performed with the dummy to examine the validity of the model results.

The CVS-IV version of the computer program incorporates many modifications and features developed in this project as well as in conjunction with other closely related research studies (e.g., Ref. 5, 6 and 8). Among the improvements implemented in the CVS-IV are the following:

- a new, more efficient integration technique.
- a routine to automatically position a seated occupant in equilibrium.
- an advanced harness belt formulation that treats interaction of belts connected at a common junction point, belt slippage on deformable segments, and allows use of rate-dependent functions for calculation of belt forces.
- simulation of aerodynamic forces acting on body segments that may be partially shielded.
- improved routines for calculating joint torques.
- use of the main program integrator for computing vehicle and air bag motions.
- the ability to specify the motion of as many as six segments.
- a provision to account for segment principal axes that are not coincident with geometric axes, thereby allowing use of any convenient geometric axis system as the reference for segment input data.
- generality in specifying axes about which segments are rotated, and the sequence of rotations, to achieve a desired initial orientation.
- elimination of the need for multiple output units.
- routines for computing injury criteria values (HIC, HSI, and CSI) and for plotting any output variable(s) against any other variable or time.

During the course of the present study, several interim versions of the computer program were distributed to numerous users throughout the world. However, it should be noted that the modifications of each version were incorporated in such a way that, in most instances, input data decks remained upward compatible and useable with successive versions of the program.

The final report of this project is composed of four volumes:

Volume 1 - Engineering Manual - Part I: Analytical Formulation
Volume 2 - Engineering Manual - Part II: Validation Effort
Volume 3 - User's Manual
Volume 4 - Programmer's Manual

Volume 1 describes the analytical formulations, assumptions and the detailed development of the mathematical equations and relations used in the program.* Volume 2 documents the measurement of the dummy geometric, inertial and joint characteristics and experiments performed to validate computer models of the physical systems tested. The experiments simulated include static tests of an ellipsoidal air bag to check the validity of the idealized bag shape and force algorithms, dynamic pendulum impact tests of dummy component sub-assemblies, and impact sled tests in which the dummy was restrained by an air bag and a three-point belt restraint system (Ref. 9). The third volume provides instruction on how to use the program. Besides giving a detailed description of all data furnished on each input card, it explains the special input and output features and provides examples of program applications along with the Job Control Language needed to execute a simulation run. Volume 4 is intended primarily for use by programmers interested in the detailed structure of the program. Included in Volume 4 are descriptions of each subroutine, cross reference charts showing the subroutines called by other subroutines, labeled common blocks used by each subroutine and usage of each variable in the labeled common blocks in every subprogram, and a complete listing of the computer Fortran source deck.

---

*See also References 5 and 6 which document the analytical formulation of some algorithms and features not described in detail herein.

2.0 DUMMY COMPONENT MEASUREMENTS

Extensive measurements were made on a new Part 572 50th percentile male crash test dummy manufactured by Alderson Research Laboratories. The dummy (Serial No. 749) was disassembled into discrete elements which represent the major articulated segments for measurement of the segment inertial properties and joint characteristics. These data together with dimensional information provided by the official NHTSA dummy design drawings, were used to develop inputs for the CVS model of the dummy. The following sections describe in detail the measurements performed on the dummy.

2.1 Segment Weights and Center of Gravity Locations

The dummy segments for which the weight and C.G. position were measured are as follows: head, neck, upper torso (including the neck bracket assembly, B/04,* and the lumbar adapter, D/03), lower torso (including the lumbar spine, D/01, abdominal insert, E/04, and left and right femur assemblies, E/05 and E/06), right upper leg, right lower leg, right foot, right upper arm and the right lower arm (including the hand assembly, H/07). The dummy left limb segments were not measured since, being designed as mirror images of right limbs, any differences of inertial properties were deemed likely to be small and within the error of measurements.

A coordinate axis system was defined in each segment so the C.G. could be conveniently measured and related to geometric features of the component hardware such as, for example, a line connecting joint pivot centers. The weight and C.G. location were determined by supporting the segment on three load cells and with one of the three orthogonal reference planes horizontal. With the locations and reactions of the load cells known, the weight of the segment and

---

* Refer to NHTSA Drawing No. SA 150M002 and dummy parts list for components identified by symbols B/04, D/03, etc.

the position of the C.G. (after measuring and correcting for the tare weight of support fixtures) in the horizontal plane was calculated from application of force and moment equilibrium equations. The third coordinate of the C.G. was determined by repeating this procedure with the segment rotated 90° about one of the horizontal axes. The photographs of Figure 2-1 show typical set-ups of the apparatus as used to measure the weight and C.G. location of the lower arm and hand segment.

The measured segment weight and C.G. position data are summarized in Table 2-1. The geometric coordinate axis reference system defined for each segment is illustrated and described in Figure 2-2.

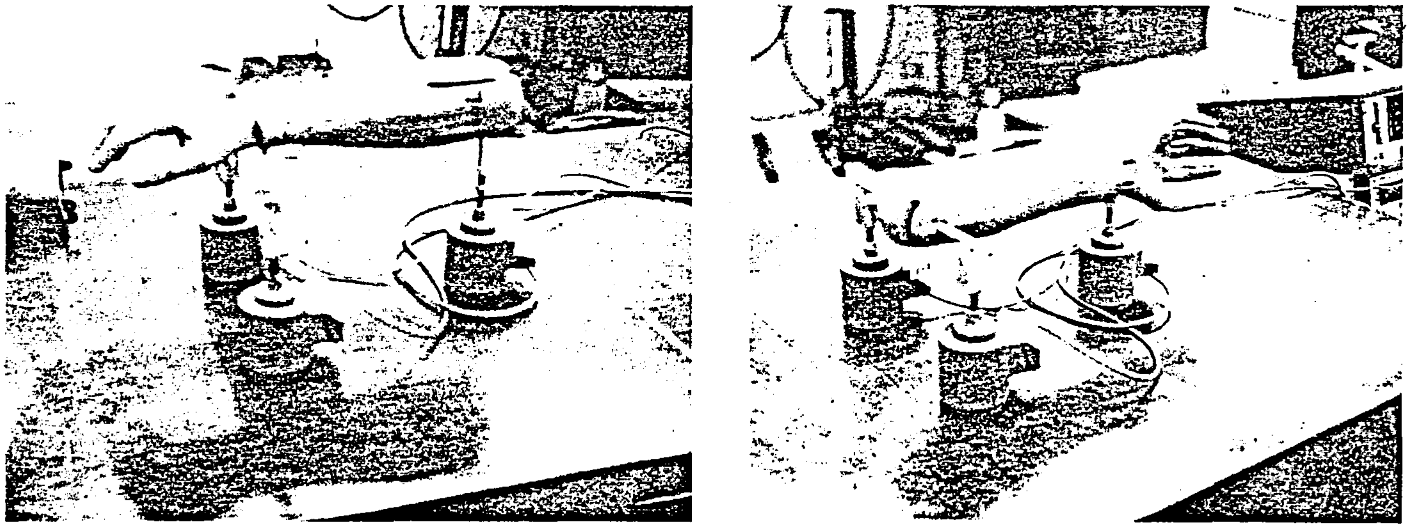

(a) Measurement of C.G. Location in XZ Plane (b) Measurement of C.G. Location in YZ Plane

Figure 2-1 SETUP FOR MEASUREMENT OF WEIGHT AND C.G. LOCATION OF LOWER ARM AND HAND SEGMENT

TABLE 2-1

SEGMENT WEIGHT AND CENTER OF GRAVITY LOCATION

Segment	Weight∿lb	Center of Gravity Coordinates(1)∿in.		
		X	Y	Z
Head	9.67	0.37	-0.043	-1.14
Neck	1.82	0.0	0.0	-2.43
Upper Torso(2)	37.87	1.131	N.M.	-6.309
Lower Torso(3)	38.04	1.794	0.061	-2.268
Right Upper Leg	18.00	0.043	0.10	-6.74
Right Lower Leg	7.00	0.097	N.M.	7.365
Right Foot	2.76	2.03	-0.13	N.M.
Right Upper Arm	4.76	-0.047	0.03	4.69
Right Lower Arm & Hand	4.61	-0.11	0.25	6.34

Notes: (1) Local geometric reference system - see Figure 2-2.

(2) Includes neck bracket assembly B/04 and lumbar adaptor bracket D/03.

(3) Includes lumbar spine D/01 (3.01 lb.), abdominal insert E/04 (3.17 lb.), and femur and retainer assembly E/06 (3.1 lb.).

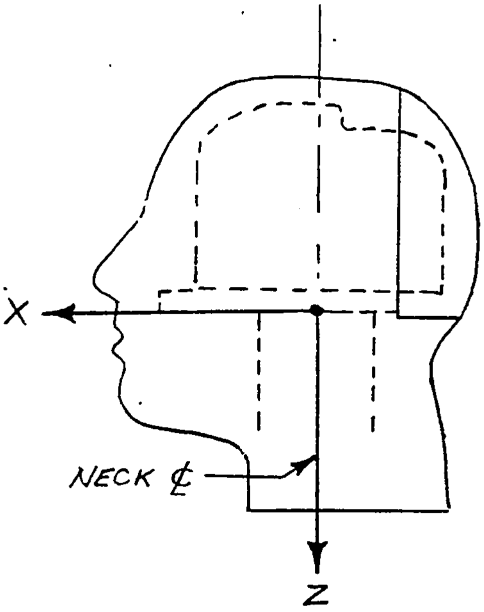

Origin: Intersection of Neck Centerline with head/neck attachment surface

+X Axis is forward, perpendicular to neck centerline in mid sagittal plane

+Y Axis is toward right

+Z Axis is downward along neck centerline

(a) HEAD

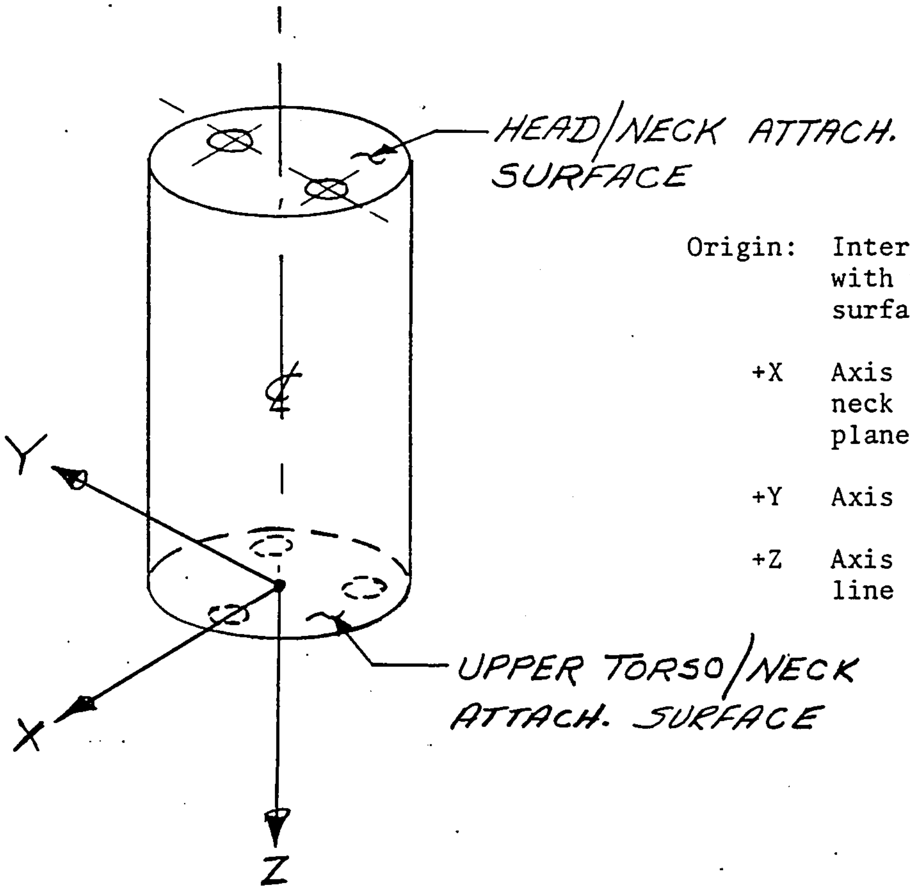

Origin: Intersection of Neck Centerline with upper torso/neck attachment surface

+X Axis is forward, perpendicular to neck centerline in mid sagittal plane

+Y Axis is toward right

+Z Axis is downward along neck centerline

(b) NECK

Figure 2-2 REFERENCE AXES FOR SEGMENT MEASUREMENTS

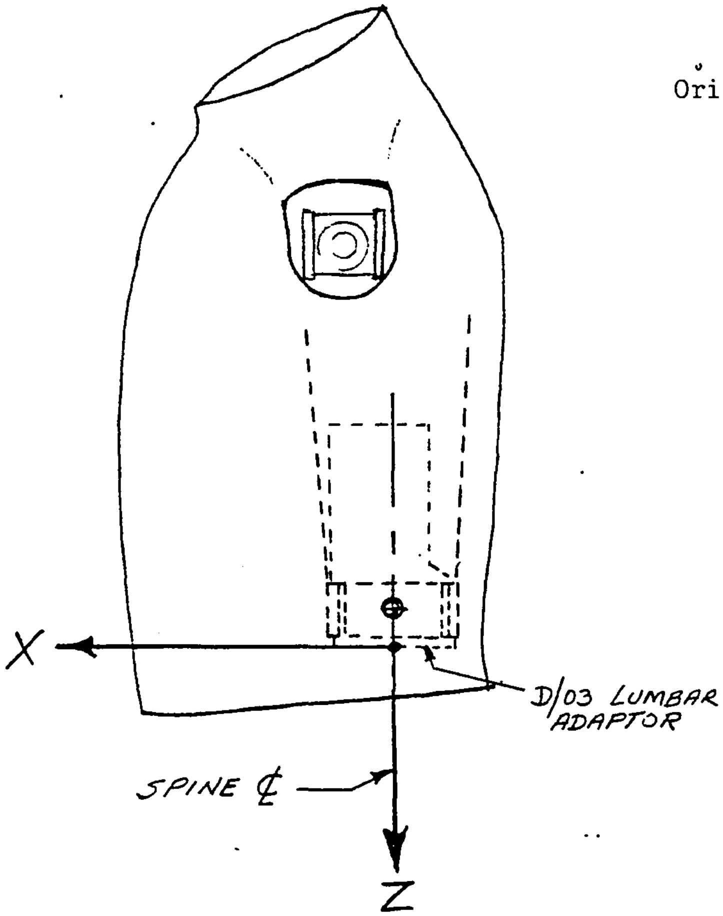

Origin:	Intersection of spine centerline with attachment surface of lumbar adaptor
+X	Axis is forward, perpendicular to lumbar spine centerline in mid-sagittal plane
+Y	Axis is toward the right
+Z	Axis is downward along lumbar spine centerline

(c) UPPER TORSO

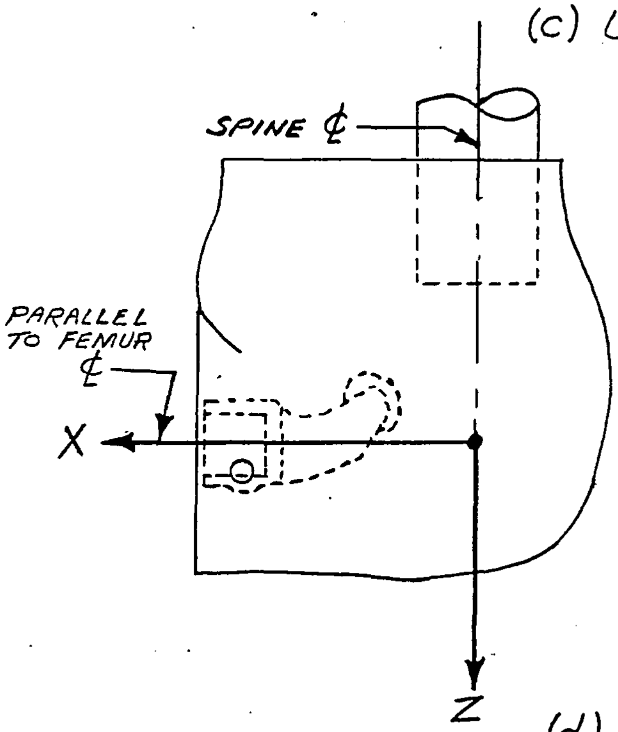

Origin:	Intersection of extension of lumbar spine centerline with perpendicular plane through centerline of femur shafts
+X	Is forward, perpendicular to lumbar spine centerline in mid-sagittal plane
+Y	Is toward the right
+Z	Is downward along lumbar spine centerline

(d) LOWER TORSO

Figure 2-2 REFERENCE AXES FOR SEGMENT MEASUREMENTS (Cont'd.)

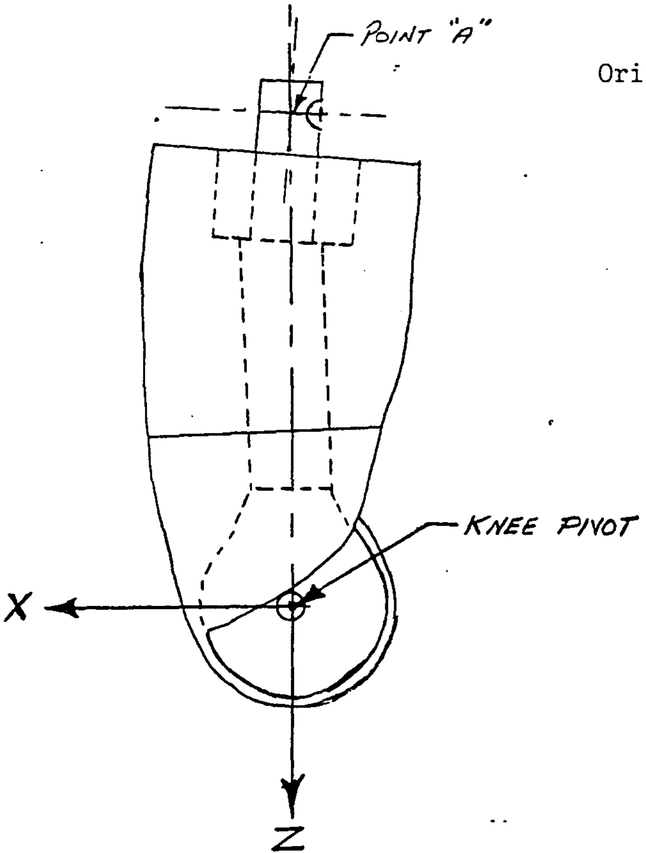

Origin: Center of knee joint

+X	Axis is toward the top of the leg, perpendicular to Y and Z axes
+Y	Axis is toward the right along centerline of knee pivot bolt
+Z	Axis is along a line from Point "A" on the centerline of the upper leg bone (at the station of the femur attachment bolt) to the center of the knee pivot

(e) UPPER LEG

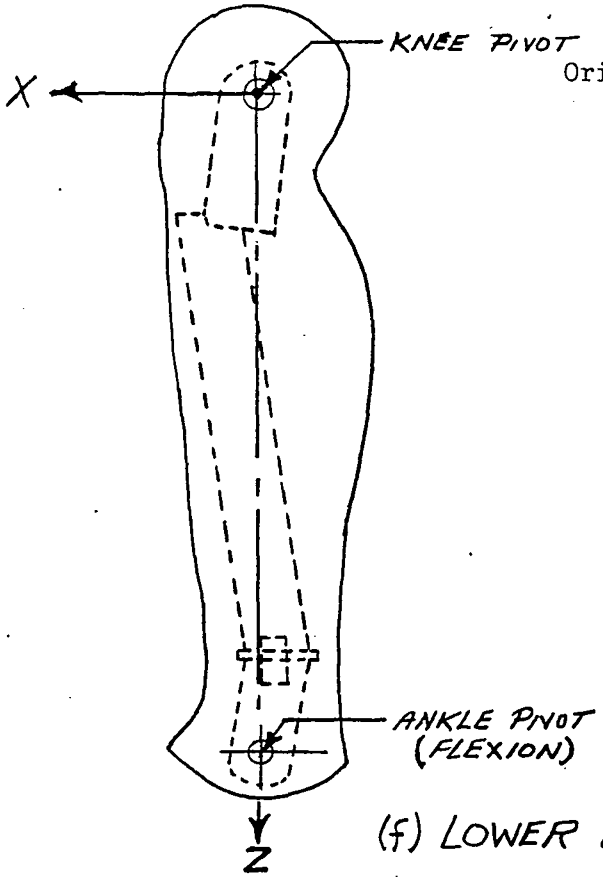

Origin: Center of the knee pivot

+X	Axis is toward the front of the leg, perpendicular to Y and Z axes
+Y	Axis is toward the right along centerline of knee pivot bolt
+Z	Axis is along a line from the center of the knee pivot to the center of the ankle pivot for flexion motion of the foot. Knee and ankle pivot axes are parallel

(f) LOWER LEG

Figure 2-2 REFERENCE AXES FOR SEGMENT MEASUREMENTS (Cont'd.)

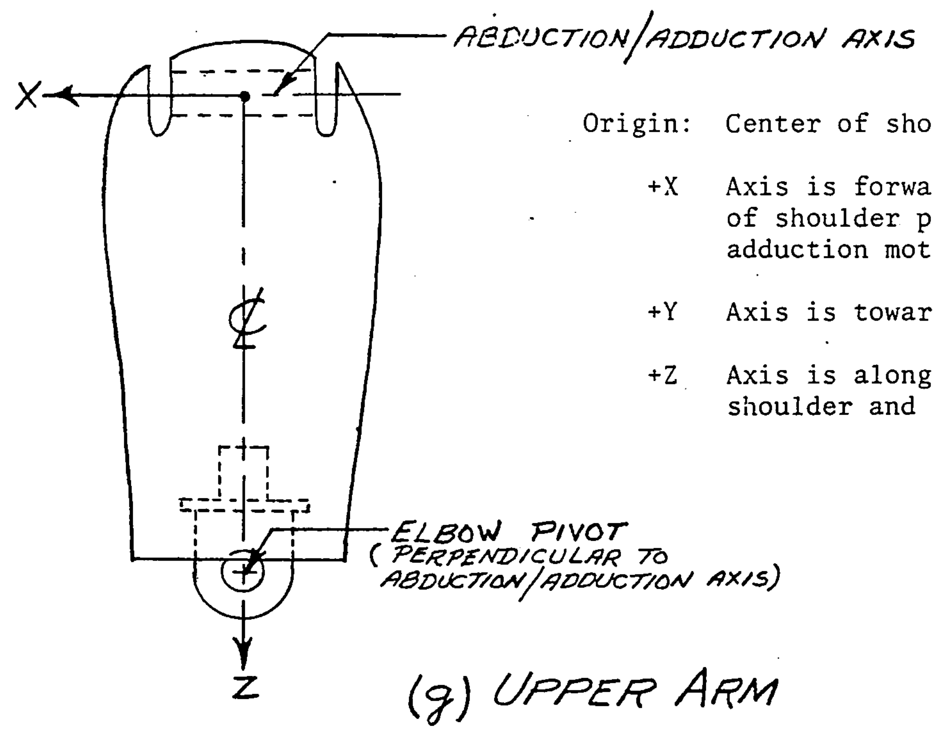

Origin: Center of shoulder pivot

+X Axis is forward along centerline of shoulder pivot for abduction/adduction motion

+Y Axis is toward the right

+Z Axis is along the line between shoulder and elbow pivot centers

(g) UPPER ARM

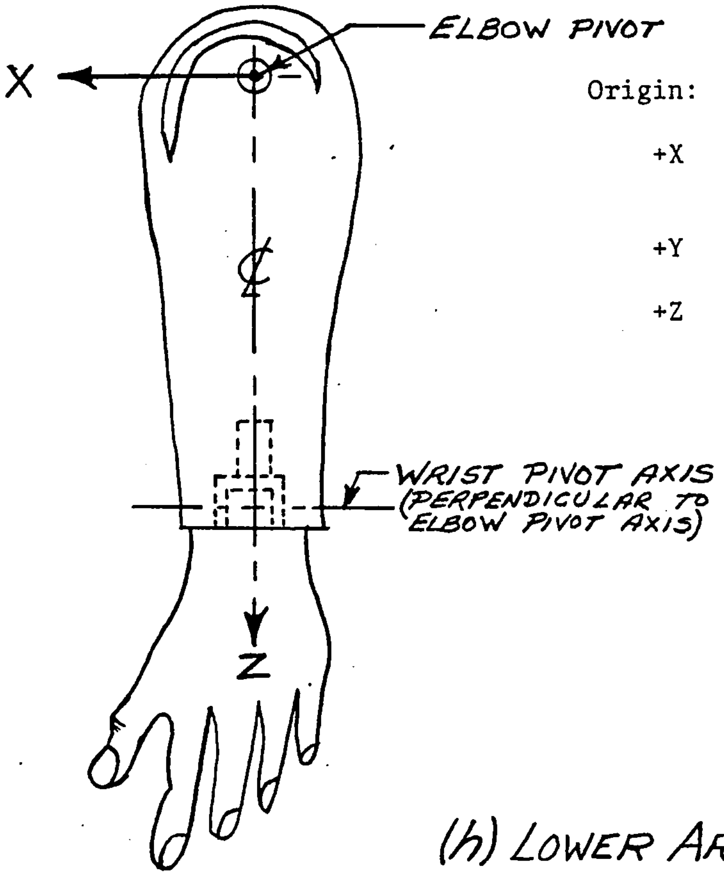

Origin: Center of elbow pivot

+X Axis is forward, parallel to wrist pivot axis

+Y Axis is toward the right

+Z Axis is along the line between elbow and wrist pivot centers

(h) LOWER ARM & HAND

Figure 2-2 REFERENCE AXES FOR SEGMENT MEASUREMENTS (Cont'd.)

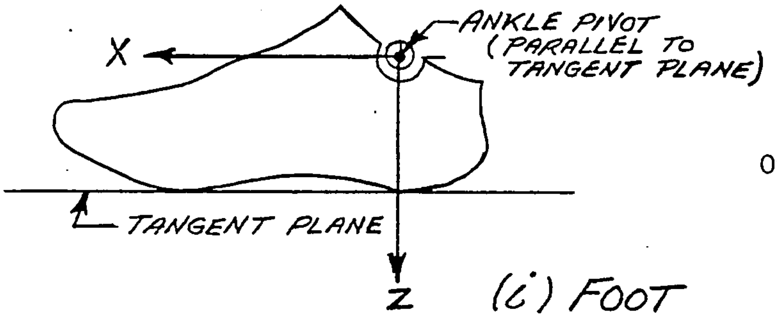

Origin:	Center of ankle pivot
+X	Axis is forward from heel to toe
+Y	Axis is toward the right along ankle pivot centerline
+Z	Axis is toward the sole of the foot, perpendicular to tangent plane

Figure 2-2 REFERENCE AXES FOR SEGMENT MEASUREMENTS (Cont'd.)

2.2 Segment Moments of Inertia

Segment principal moments of inertia and the directions of the principal axes were determined from measurements using a torsional pendulum. The pendulum consisted of a long slender steel rod to which a fixture for holding the segment in place was attached. The fixture was adjustable which allowed the segment orientation to be readily changed while maintaining the center of gravity on the pendulum torsional axis. From measurements of the periods of oscillation of the pendulum both with and without the segment mounted in the fixture, the moment of inertia of the segment about a given axis was computed from the following expression:

$$I = \frac{K}{4\pi^2}(T_C + T_F)(T_C - T_F)$$

where: K = pendulum rod torsional spring rate, in.-lb./rad.

T_C = oscillation period of the pendulum for the segment and fixture combined; sec.

T_F = oscillation period of the pendulum with the fixture alone.

Repeated measurements of the moment of inertia about six axes of each segment were made to define the inertia tensor components of each segment. The first three moment measurements were made by sequentially orienting each of the three orthogonal geometric reference axes of the segment coincident with the pendulum twist axis to obtain I_x, I_y and I_z. Three additional similar measurements with the segment rotated 45 degrees in the respective planes formed by these axes allowed the products of inertia I_{xy}, I_{xz} and I_{yz} to be calculated using the direction cosine parameters for the appropriate test configurations. The photographs of Figure 2-3 show typical test set-ups for measurement of the moment of inertia of the head about the geometric Y axis and also with the head rotated 45 degrees in the YZ plane.

The relationship between the measured and principal moments of inertia can be expressed as:

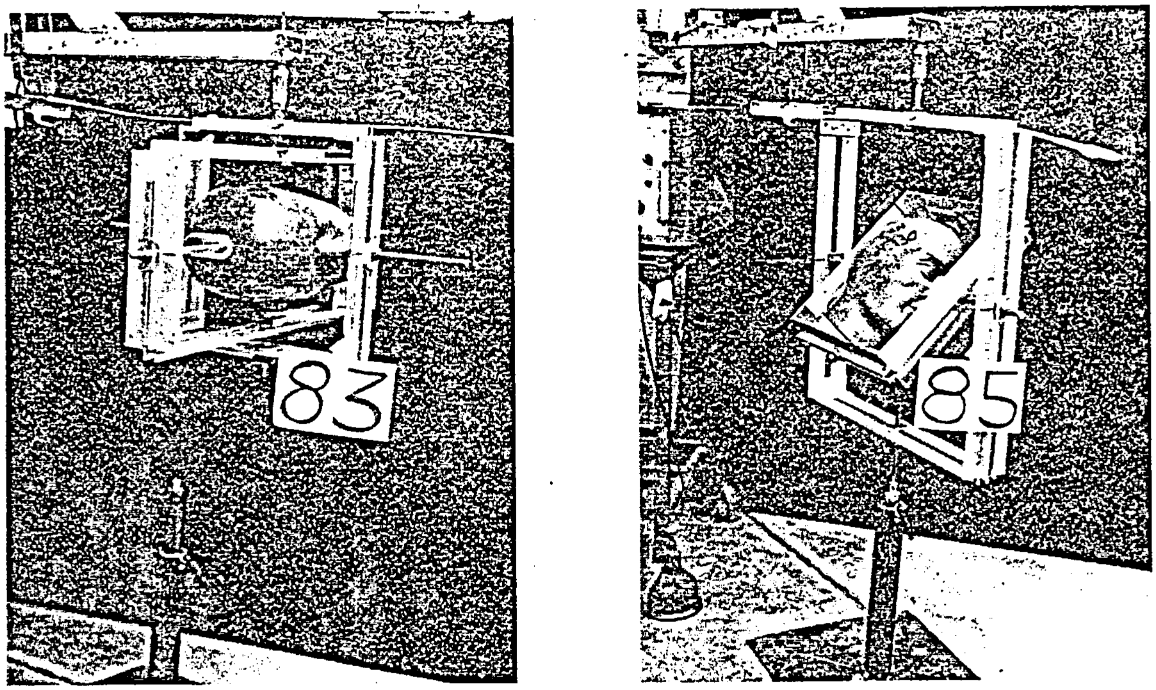

Figure 2-3 SEGMENT MOMENT OF INERTIA MEASUREMENT APPARATUS

$$\begin{vmatrix} I_p - I_x & I_{xy} & I_{xz} \\ I_{xy} & I_p - I_y & I_{yz} \\ I_{xz} & I_{yz} & I_p - I_z \end{vmatrix} = 0$$

An expansion of this determinant yields a cubic equation in I_p having three real roots corresponding to principal moments of inertia I_{p_1}, I_{p_2} and I_{p_3}.

$$I_p^3 + AI_p^2 + BI_p + C = 0$$

The coefficients A, B, and C are combinations of the moments I_x, I_y, I_z and products I_{xy}, I_{xz}, I_{yz} all of which are known from measured data.

Once having determined the roots I_{p_1}, I_{p_2}, and I_{p_3}, the results can be substituted in the following equations to obtain the angles between the principal axes and the selected body axes of the segment.

$$(I_x - I_{p_1})\ell_1 - I_{xy} m_1 - I_{xz} \eta_1 = 0$$

$$-I_{xy} \ell_2 + (I_y - I_{p_2})m_2 - I_{yz} \eta_2 = 0$$

$$-I_{xz} \ell_3 - I_{zy} m_3 + (I_z - I_{p_3})\eta_3 = 0$$

It should be noted that ℓ_1, m_1, and η_1 are the relative direction cosines indicating the angular offset between the principal axis of I_{p_1} and the axis to which measured moments and products of inertia are referenced. The same restriction holds for ℓ_2, m_2, and η_2 and ℓ_3, m_3, and η_3 which are the direction cosines corresponding to prinicpal moments I_{p_2} and I_{p_3}, respectively.

Since the above equations in determinant form yield a matrix equal to zero, no unique solution exists for ℓ, m, and η variables. Through a manipulation of these equations it is possible to determine the direction ratio of the axis of the principal moment of inertia. These equations for ℓ, m, and η in general are:

$$C_1 = \frac{\ell}{m} = \frac{I_{xy} I_{yz} + (I_y - I_p)I_{xz}}{(I_x - I_p)I_{yz} + I_{xz} I_{xy}}$$

$$C_2 = \frac{\ell}{\eta} = \frac{I_{xy} I_{yz} + (I_y - I_p)I_{xz}}{(I_x - I_p)(I_y - I_p) - I_{zy}^2}$$

$$C_3 = \frac{m}{\eta} = \frac{C_2}{C_1}$$

Using the identity

$$\ell^2 + m^2 + \eta^2 = 1$$

it is possible to solve the ratio equations above for specific direction cosines. The following equations are applicable for determining ℓ, m and η in general.

$$\ell = \sqrt{\frac{(C_1C_2)^2}{C_1^2 + C_2^2 + (C_1C_2)^2}} \qquad m = \sqrt{\frac{C_3^2}{C_3^2 + (C_1C_3)^2 + 1}} \qquad \eta = \sqrt{\frac{1}{C_2^2 + C_3^2 + 1}}$$

The segment principal moments of inertia calculated from the measured periods of the torsional pendulum are listed in Table 2-2. Note that the values for the left side segments have been assumed to be the same as the counterparts on the right side which were measured. It may also be noted that a negative principal moment of inertia was computed for the foot. Since a negative moment of inertia is physically impossible, this result must be due to erroneous experimental data. Also shown in the table are the rotation angles (yaw, pitch, and roll) of the principal axes with respect to the geometric reference axes.

TABLE 2-2

SEGMENT PRINCIPAL MOMENTS OF INERTIA

```
      SEGMENT                 I(X)           I(Y)           I(Z)

    LOWER TORSO           1.98735737     1.38368328     1.48021498
    UPPER TORSO           2.08147970     1.59185041     1.33422484
        HEAD               .21937682      .25739099      .16291044
  RIGHT UPPER LEG          .77407808      .77146310      .11529577
  RIGHT LOWER LEG          .59503229      .59081682      .03183907
     RIGHT FOOT          -.00523000      .06878830      .04613990
   LEFT UPPER LEG          .77407808      .77146310      .11529577
   LEFT LOWER LEG          .59503229      .59081682      .03183907
      LEFT FOOT          -.00523000      .06878830      .04613990
  RIGHT UPPER ARM          .13774171      .14268908      .01249418
  RIGHT LOWER ARM          .27270385      .25851130      .01237108
   LEFT UPPER ARM          .13774171      .14268908      .01249418
   LEFT LOWER ARM          .27270385      .25851130      .01237108
```

```
        ROTATION ANGLES - INERTIA WITH RESPECT TO GEOMETRIC

      SEGMENT                 YAW            PITCH           ROLL

    LOWER TORSO          -3.11130645    23.82151095    -1.08449813
    UPPER TORSO          -2.99566172     -.83587151     4.74471064
        HEAD              7.22443852    42.33767798     -.60777648
  RIGHT UPPER LEG       -42.18654999     -.16057733     2.32866653
  RIGHT LOWER LEG        11.88017565    -3.94095220      .57696403
     RIGHT FOOT         -29.02030477    24.84928585    21.66698254
   LEFT UPPER LEG        42.18654999     -.16057733    -2.32866653
   LEFT LOWER LEG       -11.88017565    -3.94095220     -.57696403
      LEFT FOOT          29.02030477    24.84928585   -21.66698254
  RIGHT UPPER ARM         5.45524163     1.27289002   -11.44956287
  RIGHT LOWER ARM        27.09974937      .89678174     1.25844211
   LEFT UPPER ARM        -5.45524163     1.27289002    11.44956287
   LEFT LOWER ARM       -27.09974937      .89678174    -1.25844211
```

2.3 Joint Characteristics

Except for the flexible rubber neck and lumbar spine of the Part 572 dummy, adjoining segments are all connected by one or more pin type joints. The quasi-static resistance to rotation about the pin joint axis was measured by securing one segment of a connected pair in a suitable fixture and recording the angular orientation and the applied torque as the other segment was moved manually throughout the joint range of motion. A load cell was used to measure the force applied at a known distance from the joint axis and the rotation was measured with a rotary potentiometer mounted coaxially with the axis. For most of the tests, the joint rotational axis was oriented vertically to avoid gravitational effects on the torque measurements.

2.3.1 Shoulder Assembly

Each shoulder assembly includes four pin joints that provide for flexion-extension and abduction-adduction motions of the upper arm and elevation-depression and anterior-posterior motions of the shoulder girdle relative to the upper torso.

(a) Upper Arm Flexion-Extension

The static torque characteristics of the joint permitting flexion-extension motion of the upper and arm were measured with the arm positioned at constant abduction angles of 1.7, 15, 30, 45 and 60 degrees. The reference orientation of the arm for these tests is depicted in Figure 2-4.

Data records obtained in the tests with the upper arm abducted 15 degrees and at 60 degrees are given in Figures 2-5 and 2-6, respectively. This joint has hard (metal to metal) stops at 178 degrees of flexion and 72 degrees of extension. The increase of torque evident in the plot for 15 degrees abduction at flexion angles greater than about 60 degrees resulted from interference of the upper arm flesh with the acromion process of the scapula. The

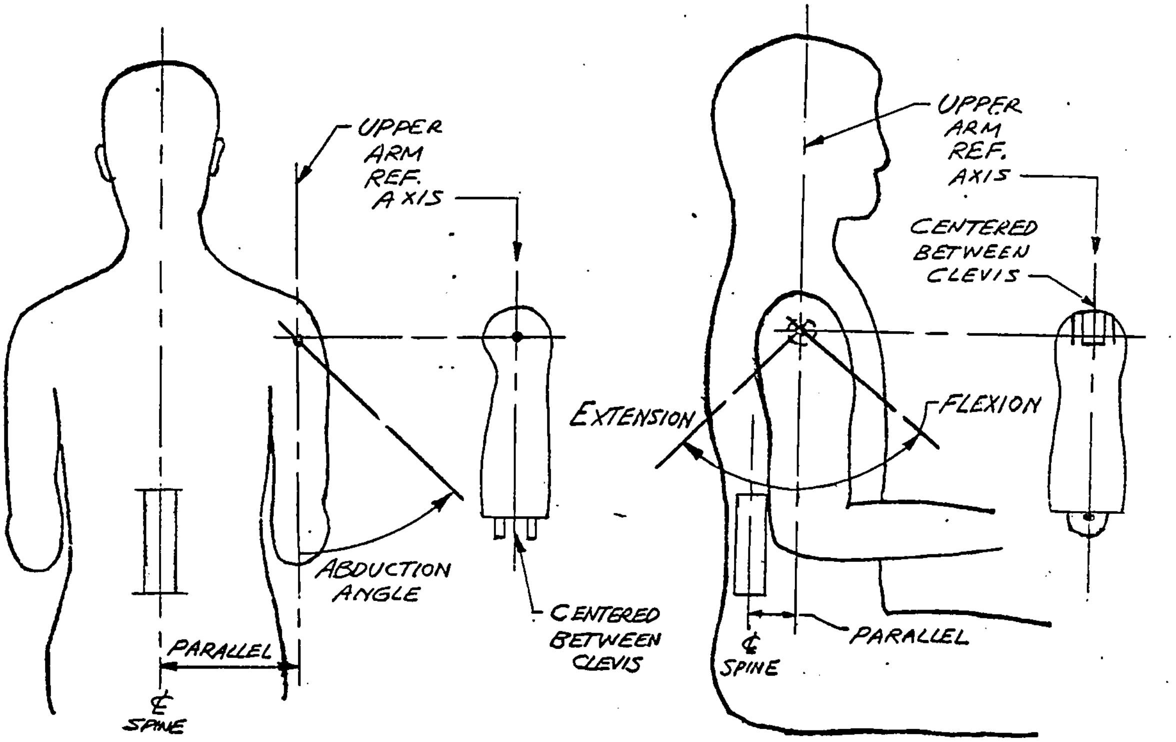

Figure 2-4 UPPER ARM REFERENCE ORIENTATION FOR MEASUREMENT OF FLEXION-EXTENSION TORQUES

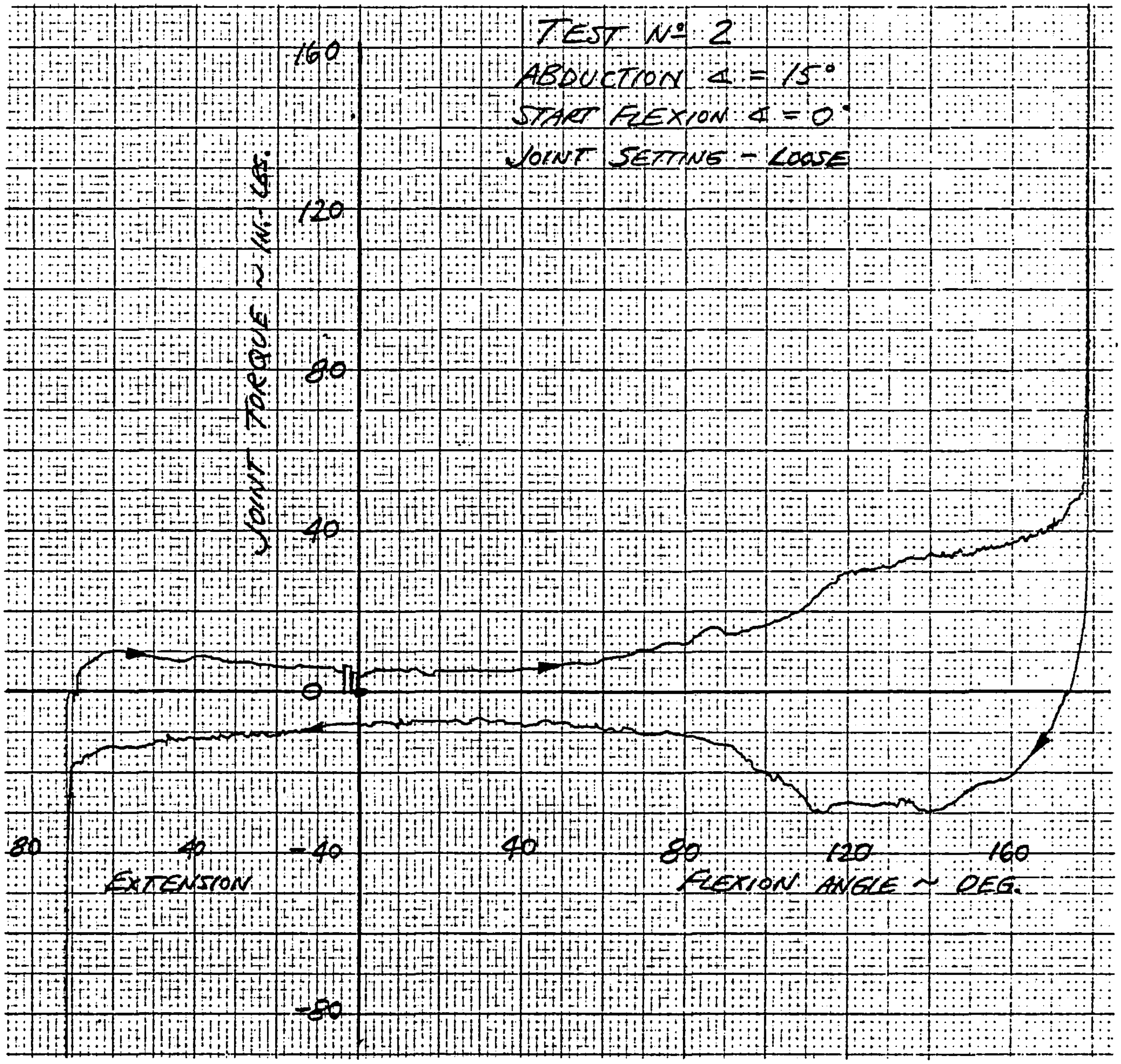

Figure 2-5 SHOULDER JOINT TORQUE FOR FLEXION-EXTENSION OF THE UPPER ARM WITH ARM ABDUCTED 15 DEGREES

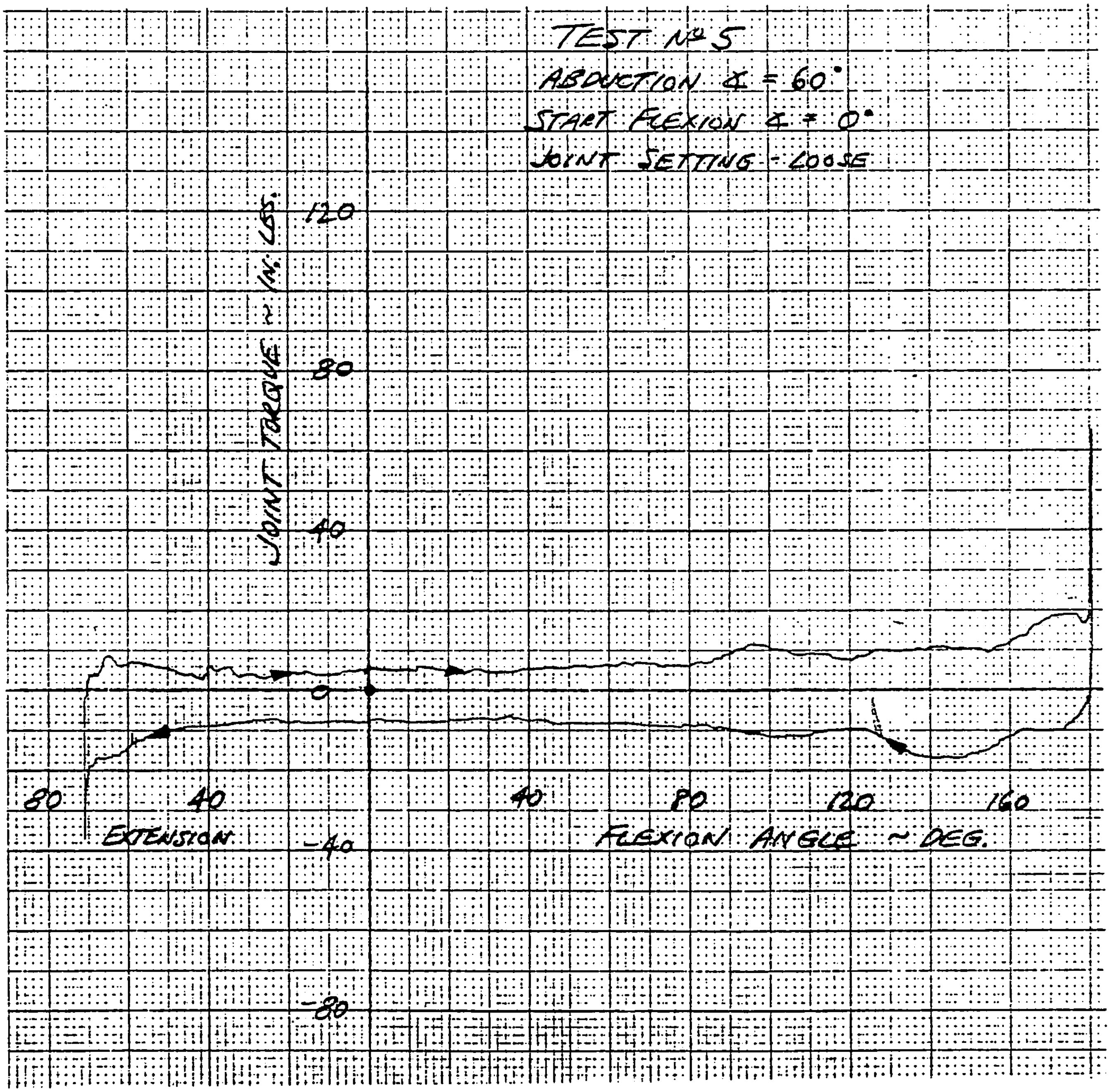

Figure 2-6 SHOULDER JOINT TORQUE FOR FLEXION-EXTENION OF THE UPPER ARM WITH ARM ABDUCTED 60 DEGREES

interference varies with the arm abduction angle and, as may be seen in Figure 2-6, did not have a large effect on the torque in the test with the arm abducted 60 degrees. Interference of the arm with the side of the upper torso occurs for abduction angles less than about 7 degrees, and thus increases the torque requirements for arm positions between 40 degrees of flexion or extension from the reference position.

Several additional similar tests were made with the joint tightened to support the weight of the extended arm (including the lower arm and hand segment). The indicated coulumb friction torque was increased from the less than 10 in.-lb. value measured with the loose joint setting to about 110 in.-lb. but torques of more than twice that amount were required to effect "breakaway" of the joint.

(b) Upper Arm Abduction-Adduction

Torques required to rotate the upper arm throughout the range of abduction-adduction motion for various constant flexion or extension angles were measured in a second series of tests. The reference orientation and definition of angular motion is shown in Figure 2-7 where it may be seen that the zero angle position is with the arm raised laterally so the long bone (Z) axis is perpendicular to the sagittal plane. With the arm in the position shown, bringing the arm downward toward the body is defined as positive angular motion (in the zero flexion plane). Similarly, with the arm flexed 90 degrees (i.e., 90° flexion plane), a positive rotation about the abduction-adduction joint axis results when the arm is rotated forward.

Measurements of the joint torque were obtained at 30 degree increments of the complete range of flexion-extension angles. An example record of the joint torque during abduction-adduction motion for the case of 60 degree flexion angle is presented in Figure 2-8. The coulomb friction of the loose joint indicated in this test is about 20 in.-lb. The increase of joint resistance at about +90 degrees results from contact of the arm with the torso whereas a hard

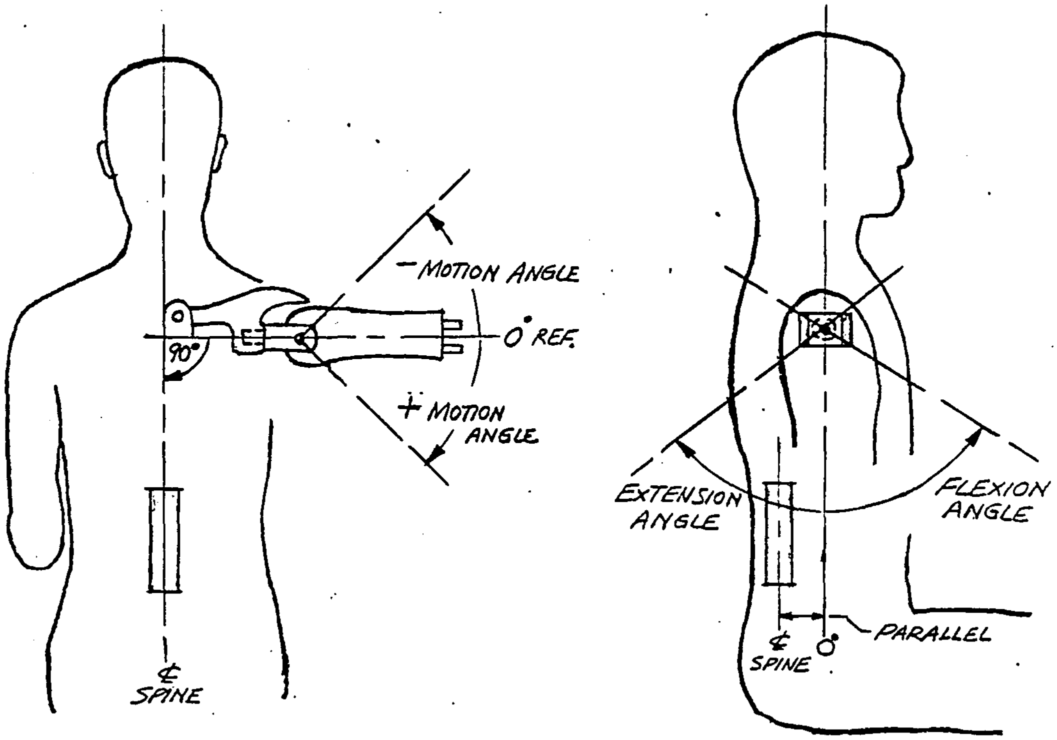

Figure 2-7 UPPER ARM REFERENCE ORIENTATION FOR MEASUREMENT OF ABDUCTION-ADDUCTION TORQUES

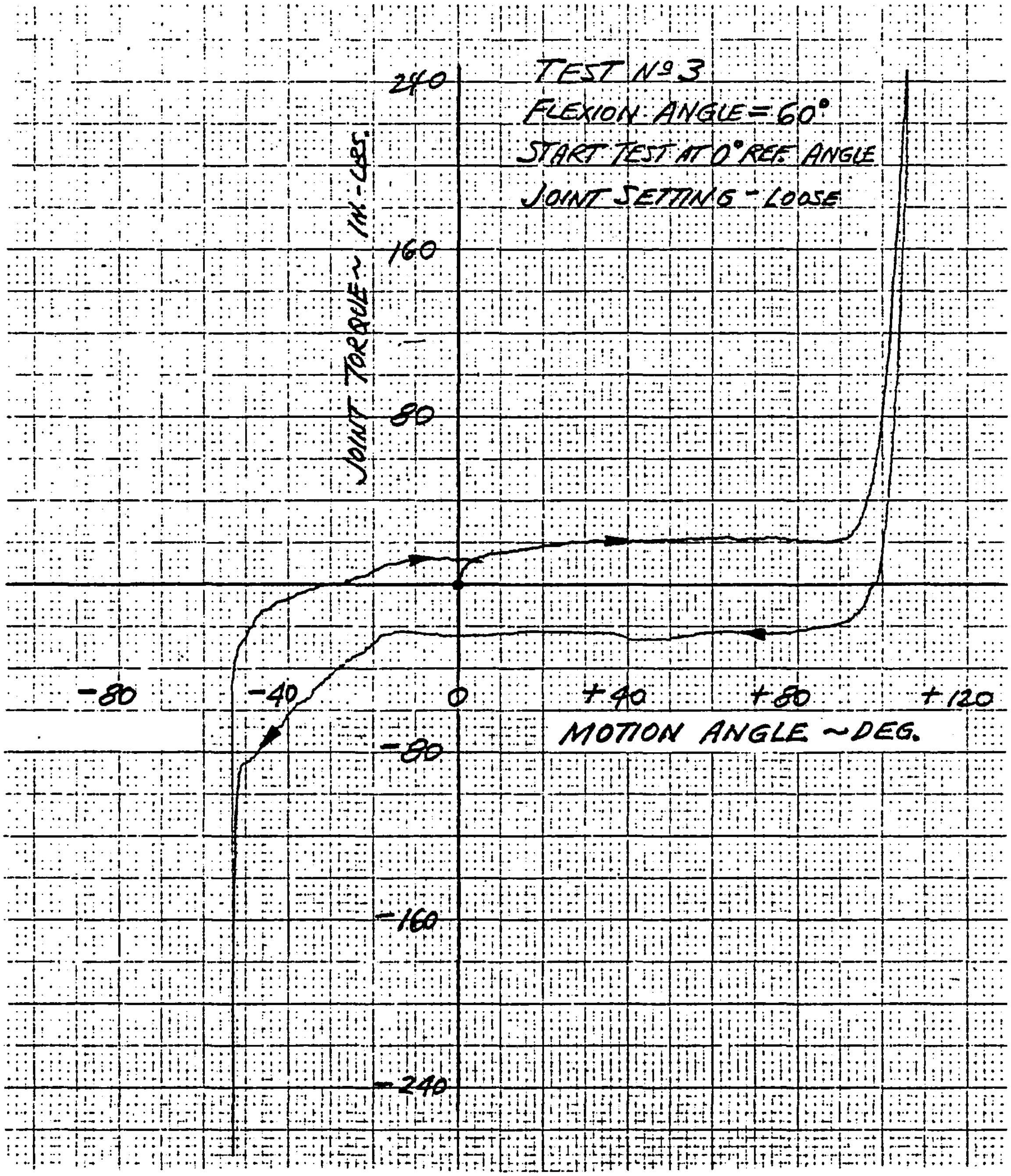

Figure 2-8 SHOULDER JOINT CHARACTERISTICS FOR ABDUCTION-ADDUCTION MOTION OF UPPER ARMS

metal-to-metal stop is engaged at an angle of approximately -53 degrees for motion in the opposite direction. Increased resistive torque due to interference of the flesh of the upper arm either with the skin of the upper torso or with the acromion process of the scapula is evidenced by the results of tests performed with the arm positioned at larger flexion angles.

(c) Shoulder Girdle

Angular motions of the shoulder girdle are depicted in Figure 2-9. Rotation about the pin joint for elevation-depression motion of the shoulder is resisted by forces developed in compressing rubber discs in the shoulder cylinder assembly. Anterior-posterior rotation of the shoulder girdle is resisted by a cap screw in contact with hard rubber stops.

Measured torque characteristics for the elvation-depression and anterior-posterior rotations of the shoulder girdle are presented in Figures 2-10 and 2-11, respectively. In each case, the coulomb friction adjustment of the joint was loose.

2.3.2 Elbow

Motion of the lower arm with respect to the upper arm is provided by two pin joints at the elbow. One of these joints allows flexion-extension motion and the other permits lateral-medial rotation about the long bone axis of the upper arm. Flexion-extension torques were measured for the zero medial angle position (i.e., x-z planes of upper and lower arms parallel) and are shown in Figure 2-12. The torque versus angle characteristic is highly assymetric due to interference of the upper and lower arm flesh that occurs for part of the motion range.

Joint torques for lateral-medial rotations of the arm were measured for several fixed flexion angles since the torque is affected by the aforementioned interference of the arm flesh. Lateral-medial rotation data were obtained for

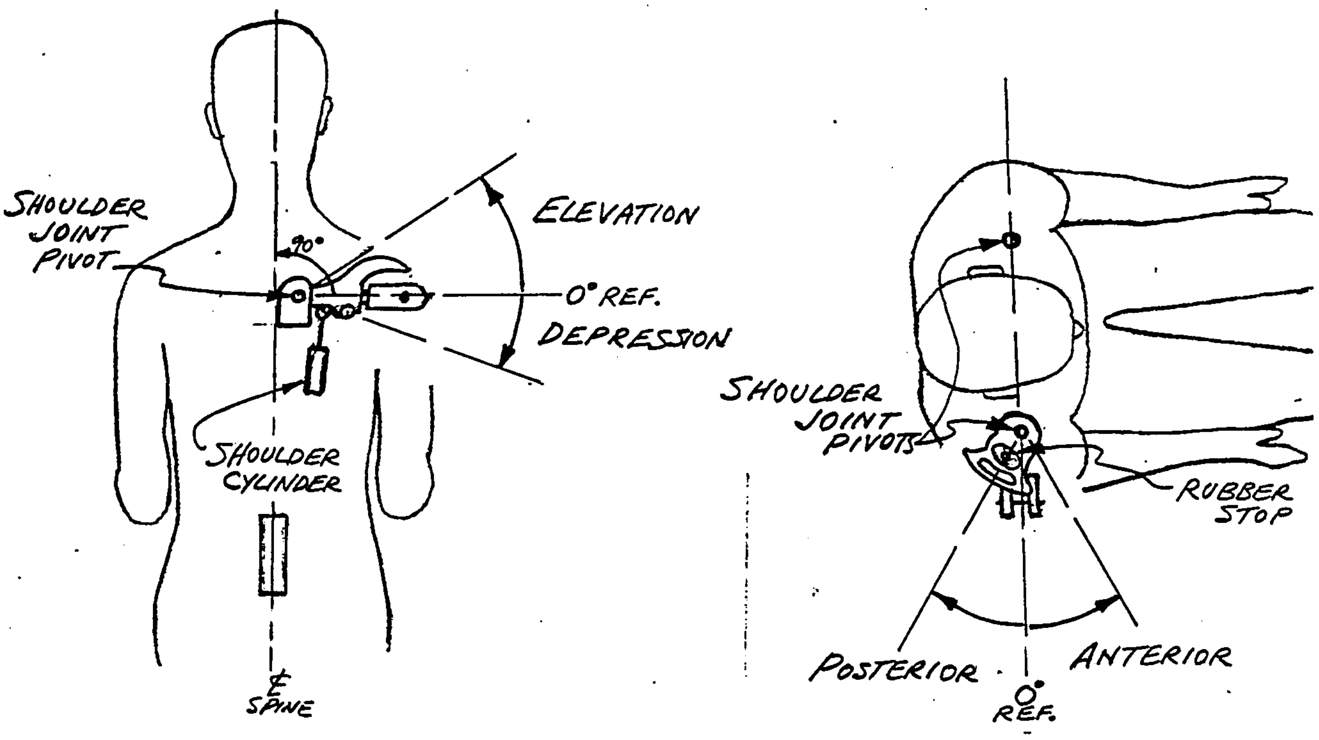

Figure 2-9 DEFINITION OF SHOULDER GIRDLE ANGULAR MOTIONS

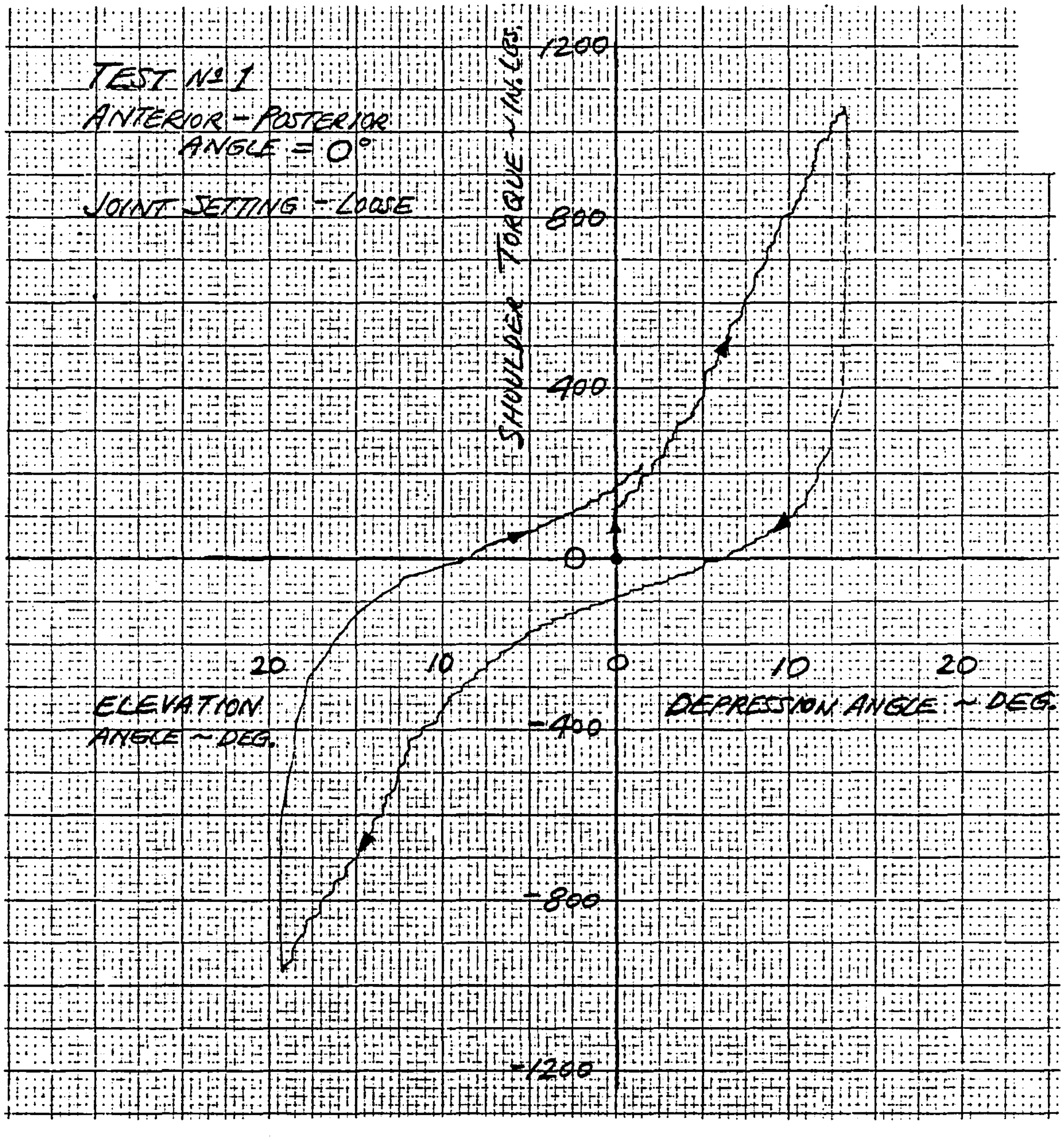

Figure 2-10 JOINT TORQUE CHARACTERISTICS FOR ELEVATION/
DEPRESSION MOTION OF THE SHOULDER

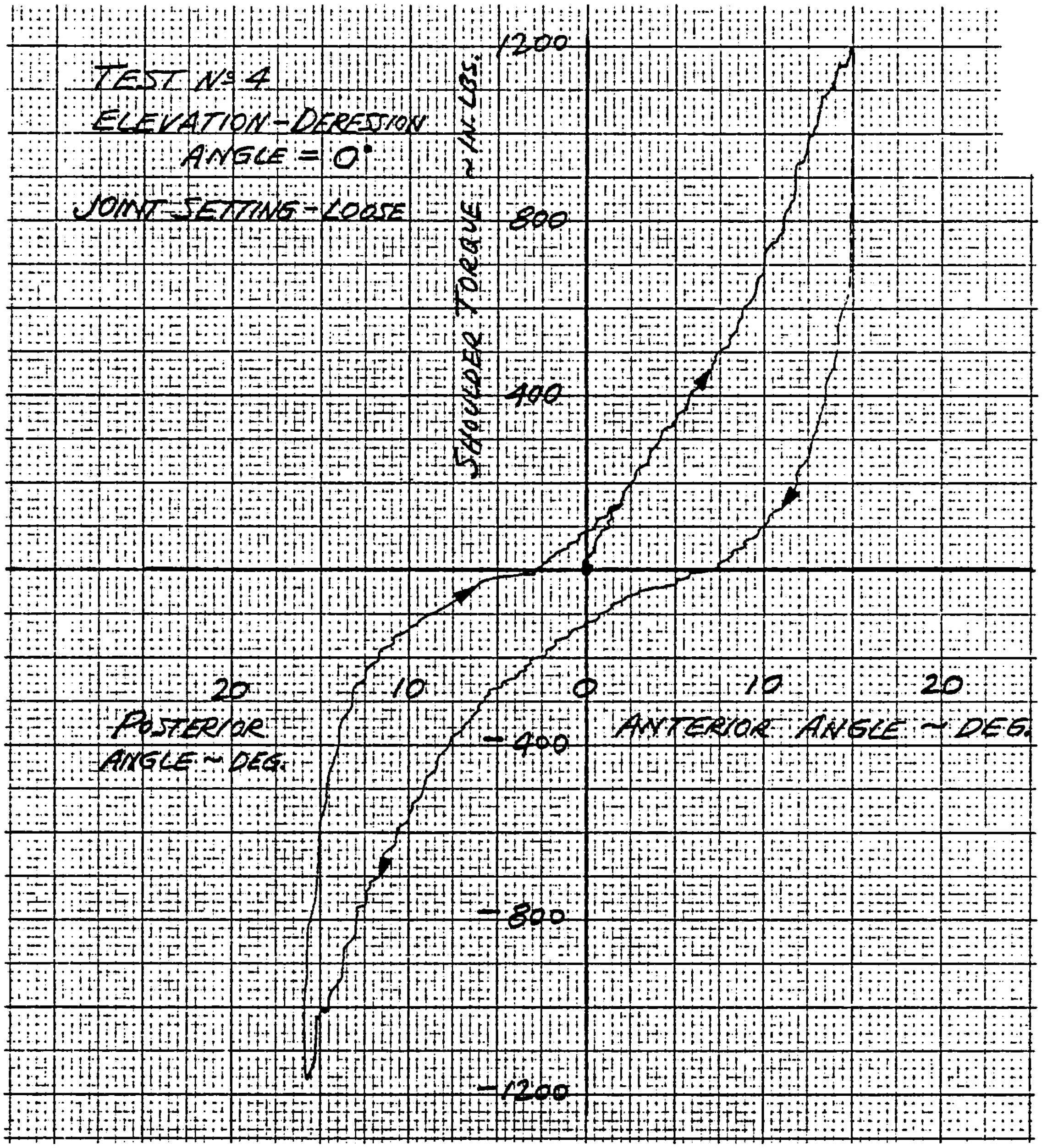

Figure 2-11 JOINT TORQUE CHARACTERISTICS FOR ANTERIOR/
POSTERIOR MOTION OF THE SHOULDER

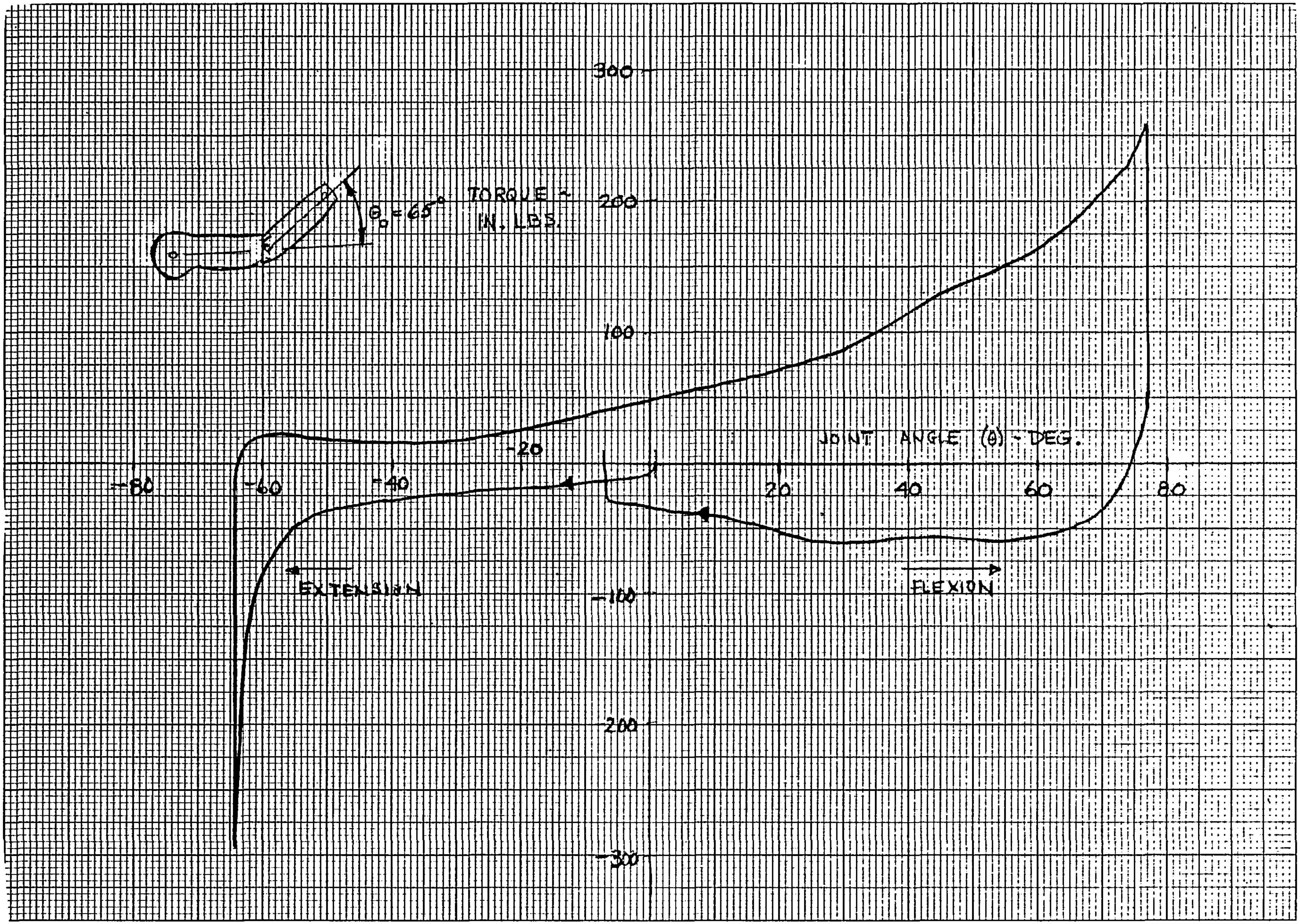

Figure 2-12 ELBOW JOINT FLEXION-EXTENSION TORQUE

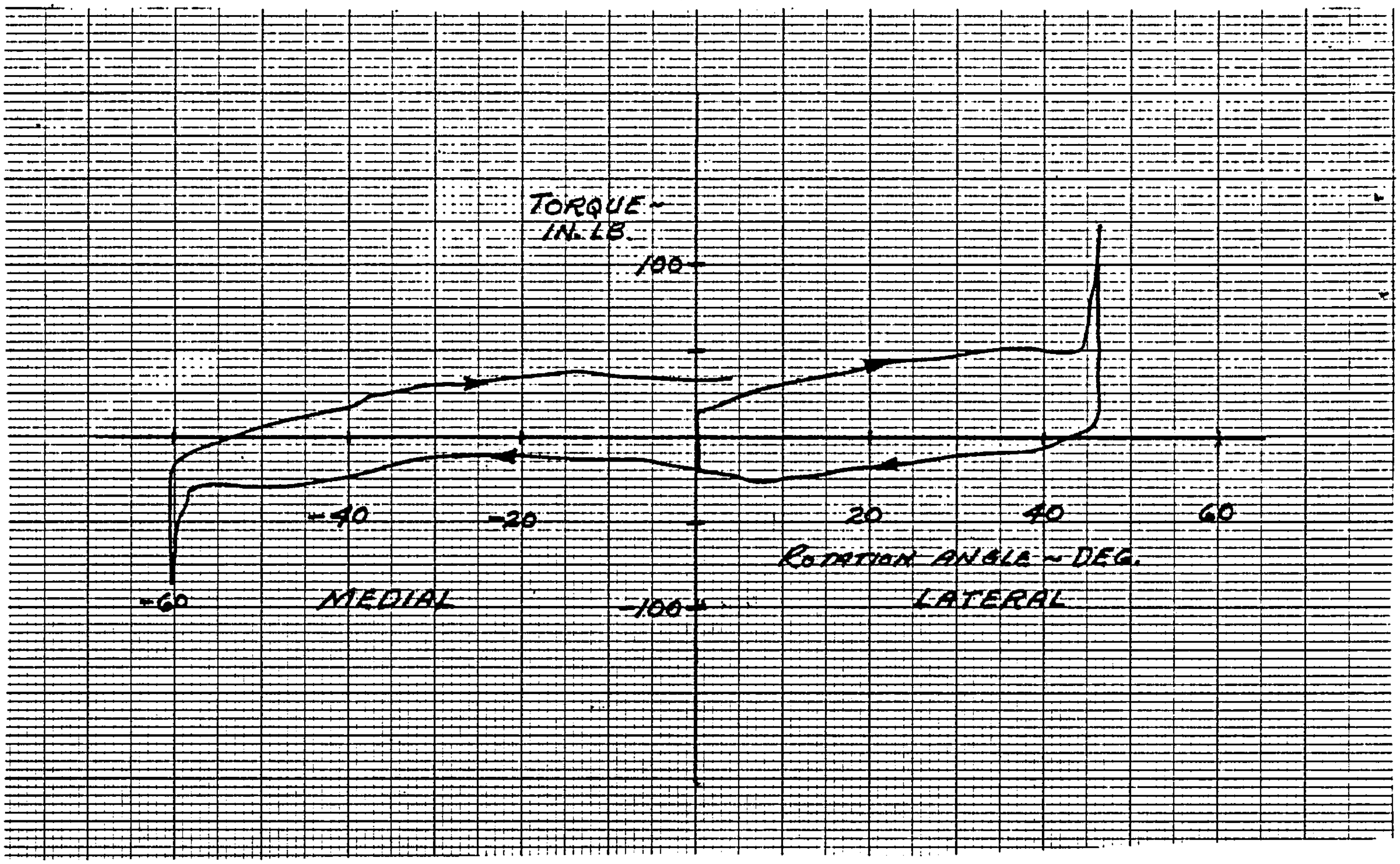

Figure 2-13 ELBOW JOINT LATERAL-MEDIAL ROTATION TORQUE

included angles of 56, 90, 110, 135 and 180 (full extension) degrees between the upper and lower arms. The torque measured for the case of 110 degree included angle is given in Figure 2-13. For this test, the lower arm was also initially positioned near the center of the motion range at a medial angle of 42.5 degrees.

2.3.3 Hip

Motions of the upper leg permitted by the hip joint were first investigated using only the skeletal structure (pelvic and femur and retainer assembly) without the flesh surrounding the lower torso to aid in deciding how the joint torques would be measured. The hip joint is a ball and socket, but motion is partly constrained by a pin which protrudes from the pelvis socket and rides in a circumferential slot machined in the ball of the femur. The construction and geometry of the joint is such that, except when the upper leg is at zero abduction/adduction angle, the leg cannot move in flexion/extension wihout simultaneous twist. Throughout most of the abduction motion range (approximately 65 degrees) the flexion and extension motion limits are about 50 degrees and 100 degrees, respectively, and requires the leg to twist over 60 degrees at maximum abduction. At the limit of adduction (approximately 18 degrees), the flexion limit is only about 30 degrees while twisting 8 degrees, and the maximum extension angle is approximately 75 degrees accompanied by 20 degrees of twist.

Torque measurements of the left hip joint were made with the right leg removed to avoid interference when the left leg was abducted. For these tests, the dummy lower torso was rigidly supported in a fixture above a flat table and and torque required to move the leg in abduction/adduction for several fixed angles of flexion and extension was measured. In this way, twist motions of the leg were avoided. Measurements were obtained for constant flexion angles of 0, 15, 30 and 40 degrees and for leg extension angles of 15, 30 40 and 50 degrees. Resistance of the joint to flexion/extension motion was measured in an additional test with the leg at an abduction angle of zero degrees.

The test apparatus is illustrated in the photographs of Figure 2-14 where it may be seen that the lower torso was tilted relative to the table top to obtain the desired leg flexion angle and allow the leg to be moved in a horizontal plane to avoid gravitational effects. Torques were monitored by applying a horizontal force at the end of the leg extension with a hand-held load cell. Vertical support of the leg was provided by means of another load cell mounted on a small dolly that rolled on the flat table surface. This load cell was used to indicate variations of the joint torque in the flexion/extension plane as the limb was moved in abduction-adduction motion. Joint angular measurements were obtained with a rotary potentiometer whose shaft was aligned with the joint axis of rotation.

The records of the hip joint torque for abduction/adduction motion with the leg maintained at 0 and 30 degrees of flexion are shown in Figure 2-15.

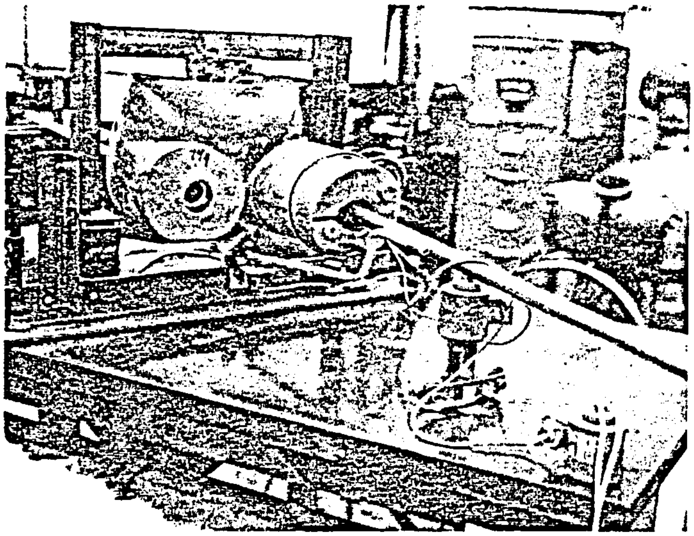

(a) Zero Leg Flexion

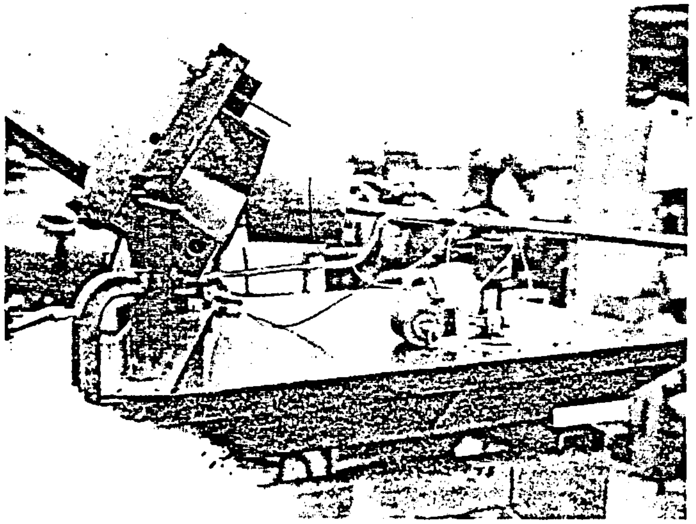

(b) 30° Leg Flexion

Figure 2-14 APPARATUS FOR MEASUREMENT OF HIP JOINT TORQUE CHARACTERISTICS

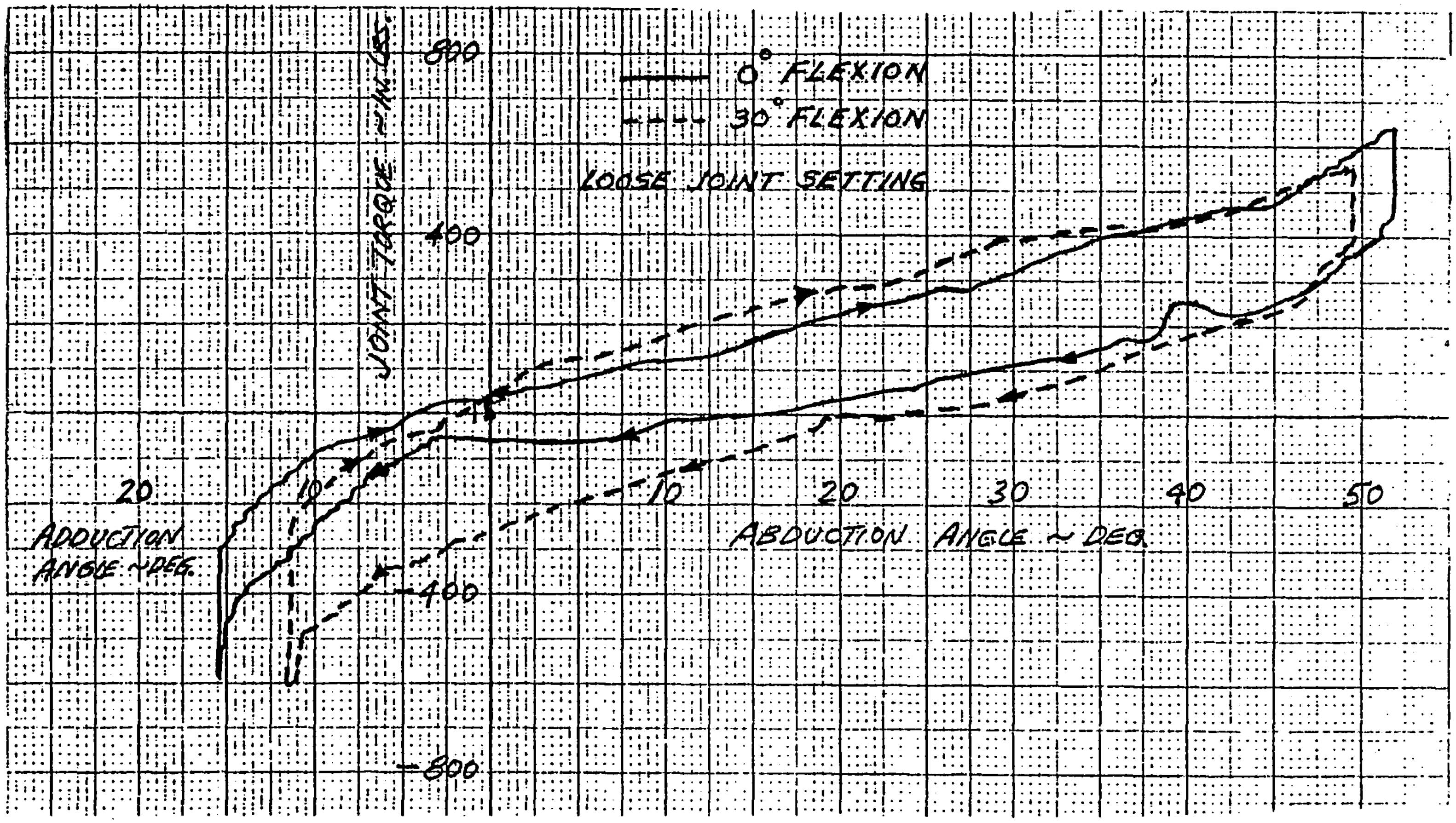

Figure 2-15 HIP JOINT TORQUE FOR UPPER LEG ABDUCTION/ADDUCTION MOTION

The data from all of the tests with the upper leg flexed or extended from the reference position indicates negative torques were required to prevent abduction. It is possible this results from compression of the lower torso flesh against the laterally sloping front surface of the pelvis structure which produces torques tending to abduct the leg. The measurements also show little variation of the initial flexion/extension moment as the leg was moved throughout the range of abduction/adduction motion.

The torque characteristics of the hip joint for flexion/extension motion of the upper leg at zero abduction angle are given in Figure 2-16. The plot indicates the resistances for flexion and extension are nearly the same for angles up to 40 degrees. At larger rotations, the flexion torque increases rapidly until the metal-to-metal stop is engaged at a flexion angle of about 49 degrees.

2.3.4 Thigh Joint

A pin type joint in the dummy thigh permits lateral and medial rotations of the lower leg as depicted in Figure 2-17. Resistive torques for this joint were obtained by placing the lower torso in a supine position with the upper leg aligned vertically and using a horizontal lever attached to the thigh to slowly rotate the joint between the joint stops. The resulting torque characteristics with the joint adjusted loose to minimize the coulomb friction are shown in Figure 2-18. As is evident from the plot, the joint provides a motion range of 60 degrees before engaging hard stops for both lateral and medial rotations from the reference orientation. The slightly increasing torque with increasing lateral rotation angles (and vice versa) is primarily due to interference between the skin surfaces of the thigh and the lower torso at the leg parting plane.

2.3.5 Knee

The measured resistive torque of the pin joint of the dummy knee that allows flexion and extension motion of the lower leg is presented in Figure 2-19.

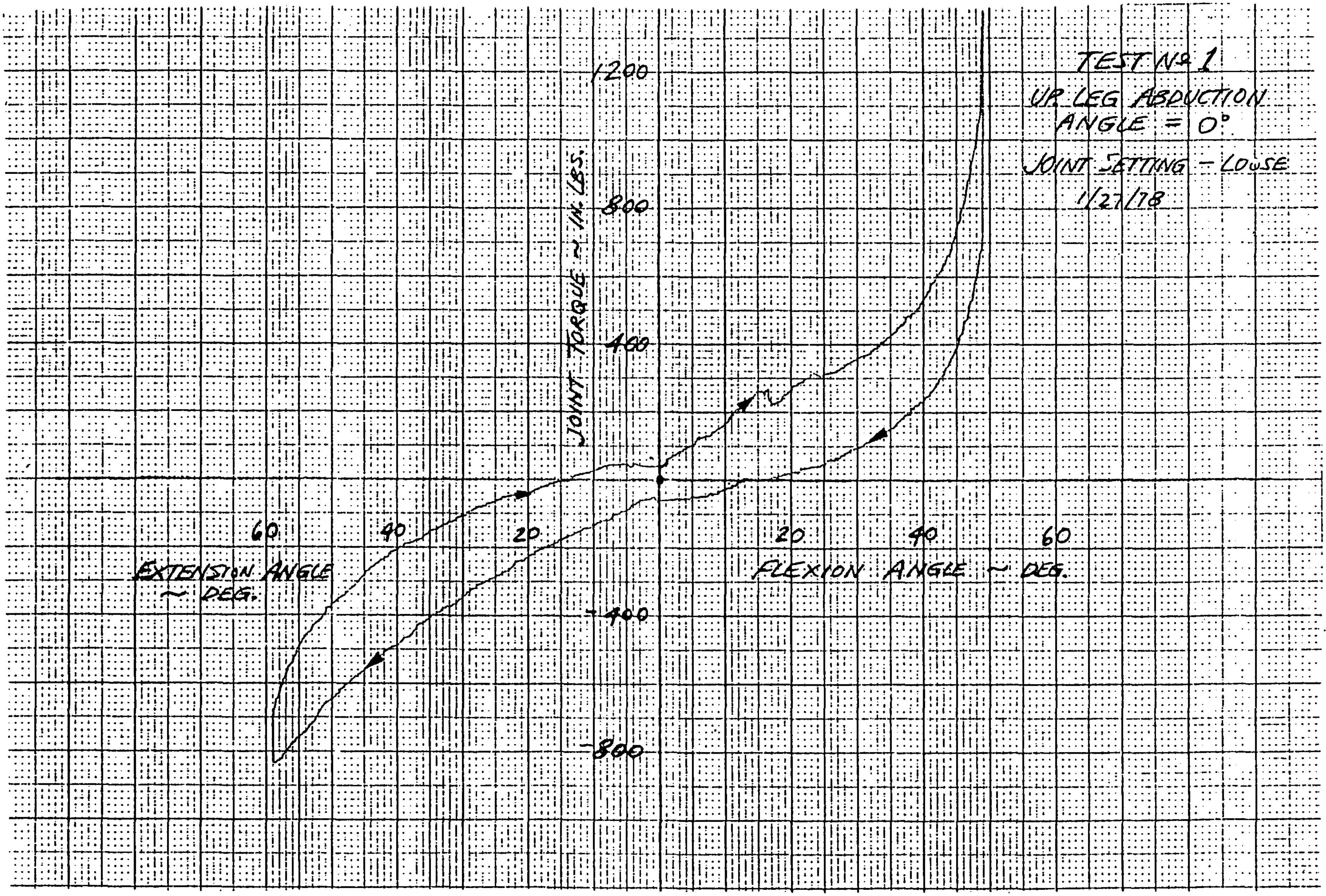

Figure 2-16 HIP JOINT TORQUE FOR UPPER LEG FLEXION/EXTENSION MOTION

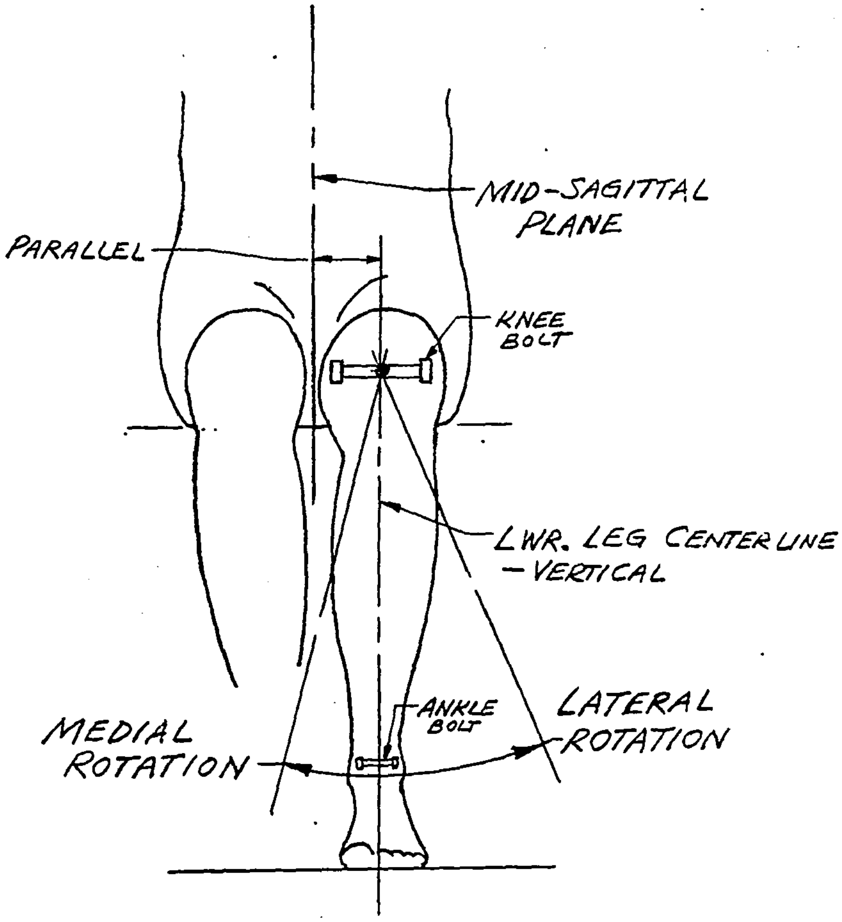

Figure 2-17 LOWER LEG REFERENCE ORIENTATION FOR MEDIAL AND LATERAL ROTATION OF THE THIGH JOINT

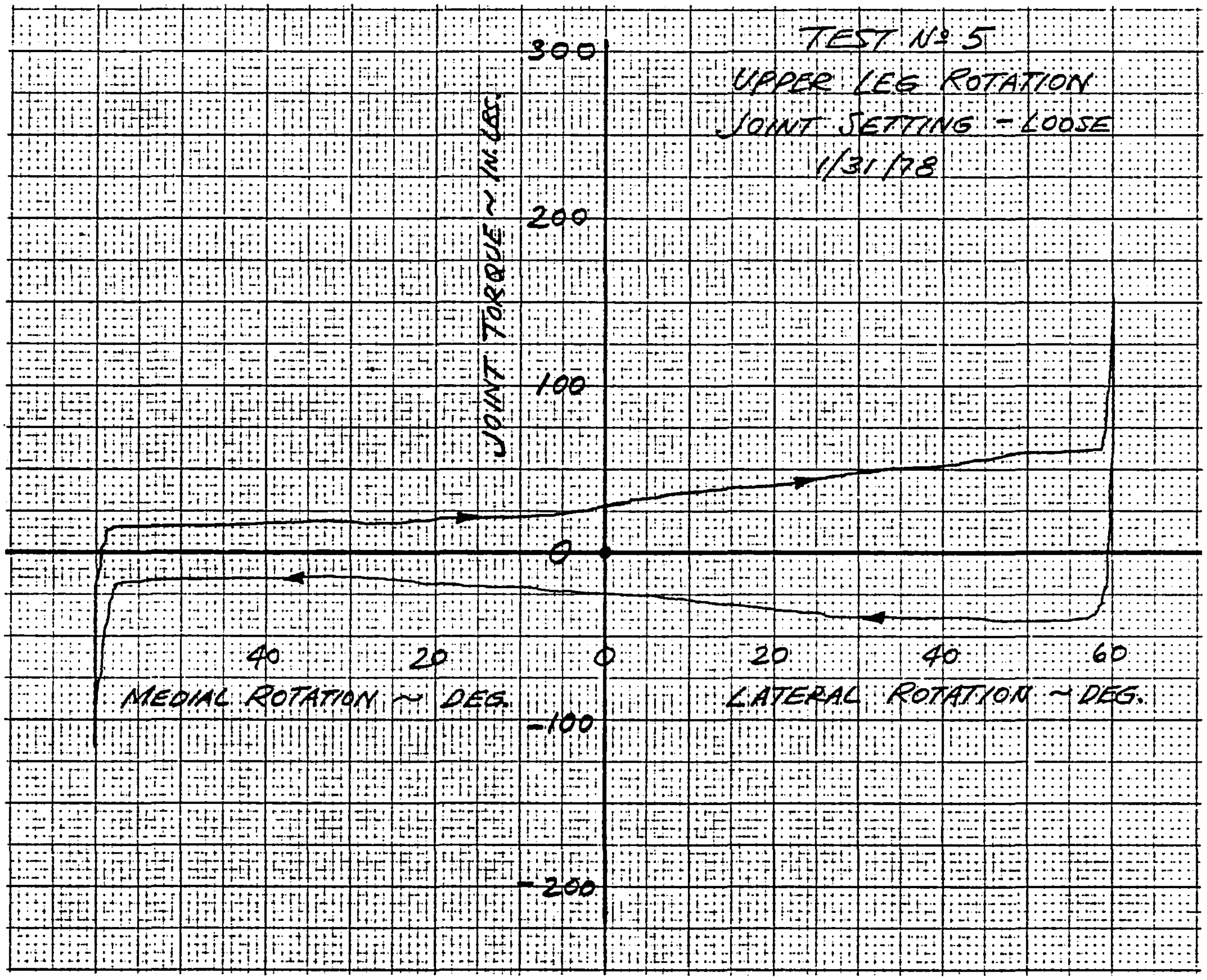

Figure 2-18 THIGH JOINT TORQUE CHARACTERISTICS FOR LATERAL-MEDIAL ROTATION OF THE LOWER LEG

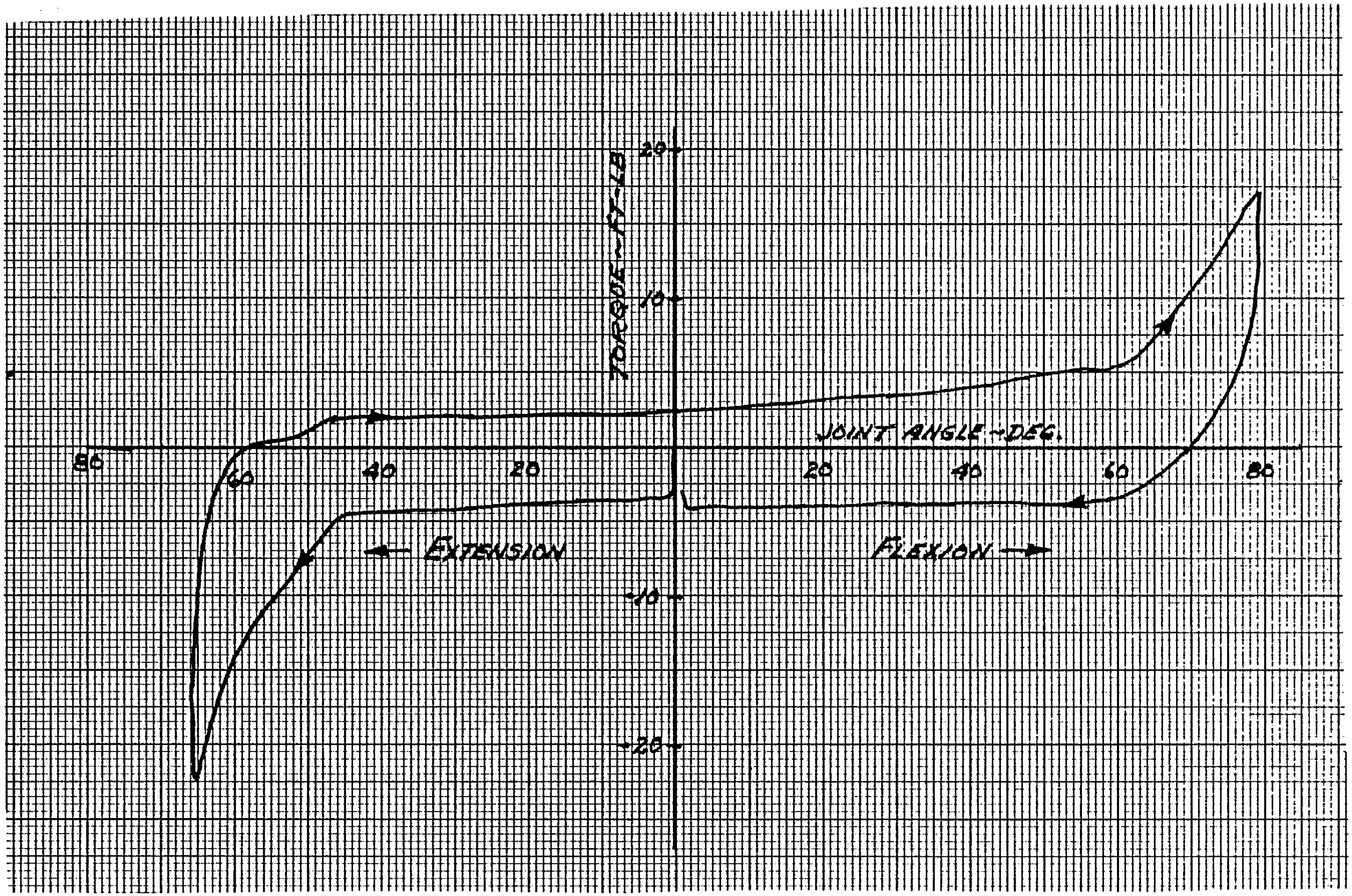

Figure 2-19 KNEE JOINT RESISTIVE TORQUE

Although the reference position of the lower leg for this test was not documented, it is believed that the 65 degree maximum extension angle shown by the curve very nearly corresponds to the position in which the leg was fully extended against the joint stop. The increasing stiffness of the joint observed for flexion angles greater than 60 degrees is probably due to compression of the lower leg against the flesh on the underside of the thigh. The reason for the abrupt torque increase at 45 degrees of extension is not known, but the same result was observed in each of three tests that were performed on the joint.

2.3.6 Ankle

The dummy ankle consists of two pin joints that allow inversion/eversion and dorsiflexion/plantar flexion motions of the foot. These motions and the zero-angle reference orientation of the foot relative to the lower leg are illustrated in Figure 2-20.

The torque characteristics of the joint for inversion/eversion rotations of the ankle are shown in Figure 2-21. The indicated coulomb friction torque for the loose joint setting is about 6 in.-lb. The increase of resistive torque with increasing angle of rotation in each direction results from interference between the skin covering the lower leg and foot. The data indicate hard stops are engaged at approximately 25 degrees of both inversion and eversion motion.

Results of measurements of the other pin joint of the ankle permitting doriflexion/plantar flexion motions of the foot are presented in Figure 2-22. Hard joint stops were engaged at 30 degrees dorsiflexion and at 54 degrees plantar flexion. Here again interference of the skin accounts for most of the torque variation with rotation angle.

2.3.7 Neck

Tests of the flexible rubber neck included measurements of the flexural and torsional resistances for statically applied forces and moments and free oscillation tests for determining damping properties of the neck.

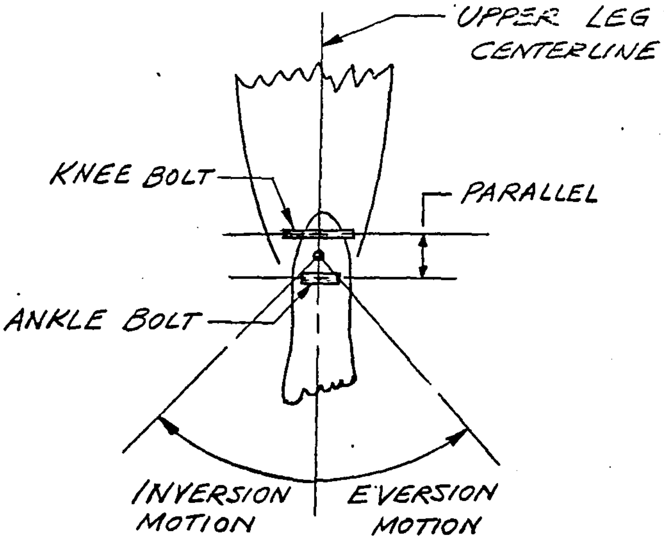

a. Foot Inversion-Eversion Motion

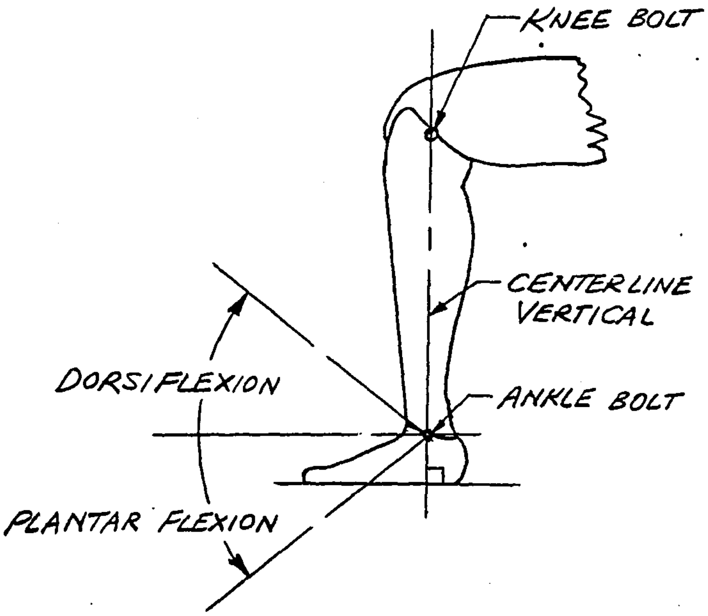

b. Foot Dorsiflexion-Plantar Flexion Motion

Figure 2-20 FOOT REFERENCE ORIENTATION & MOTIONS

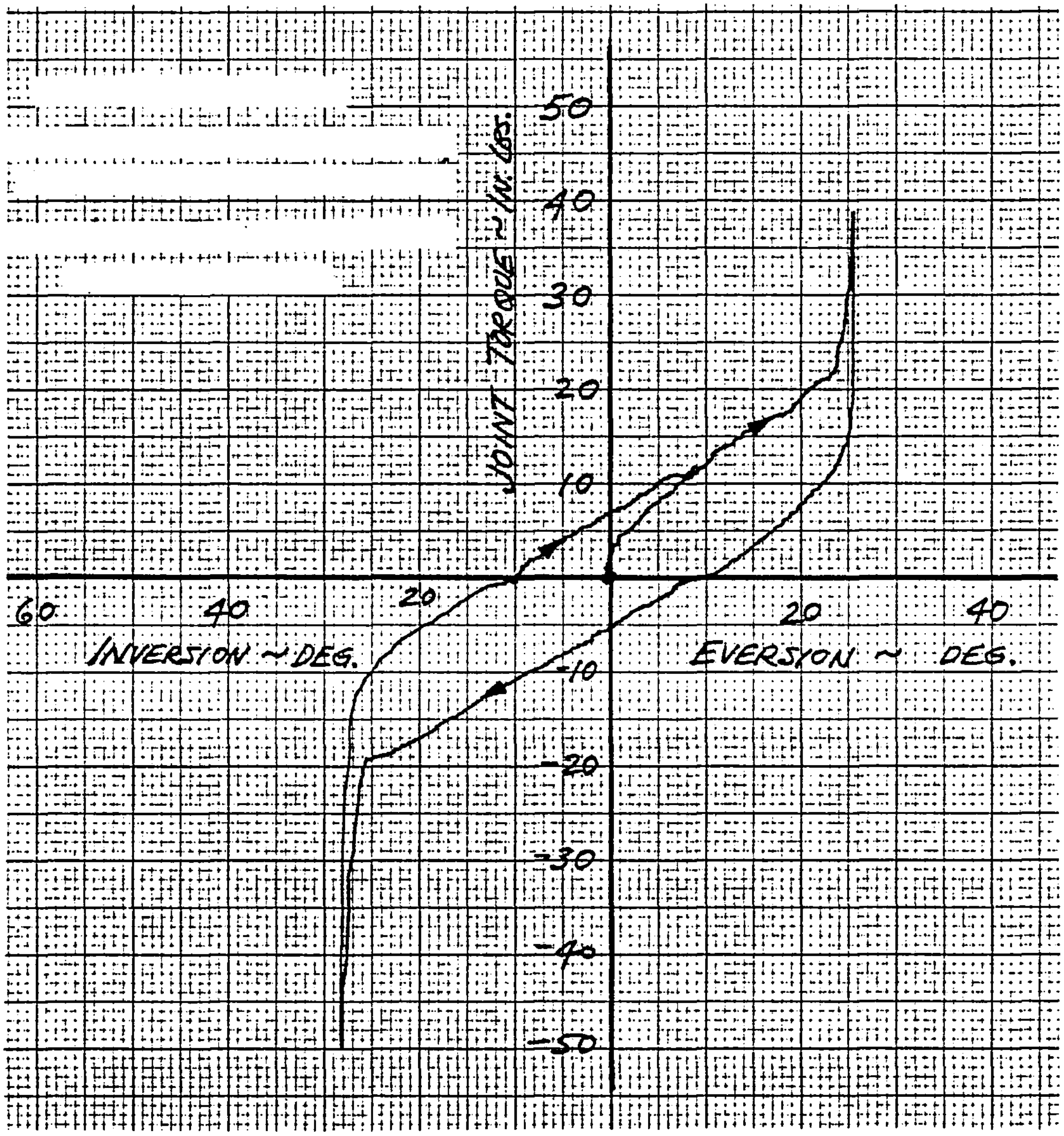

Figure 2-21 ANKLE JOINT TORQUE CHARACTERISTICS FOR EVERSION-INVERSION MOTION OF THE FOOT

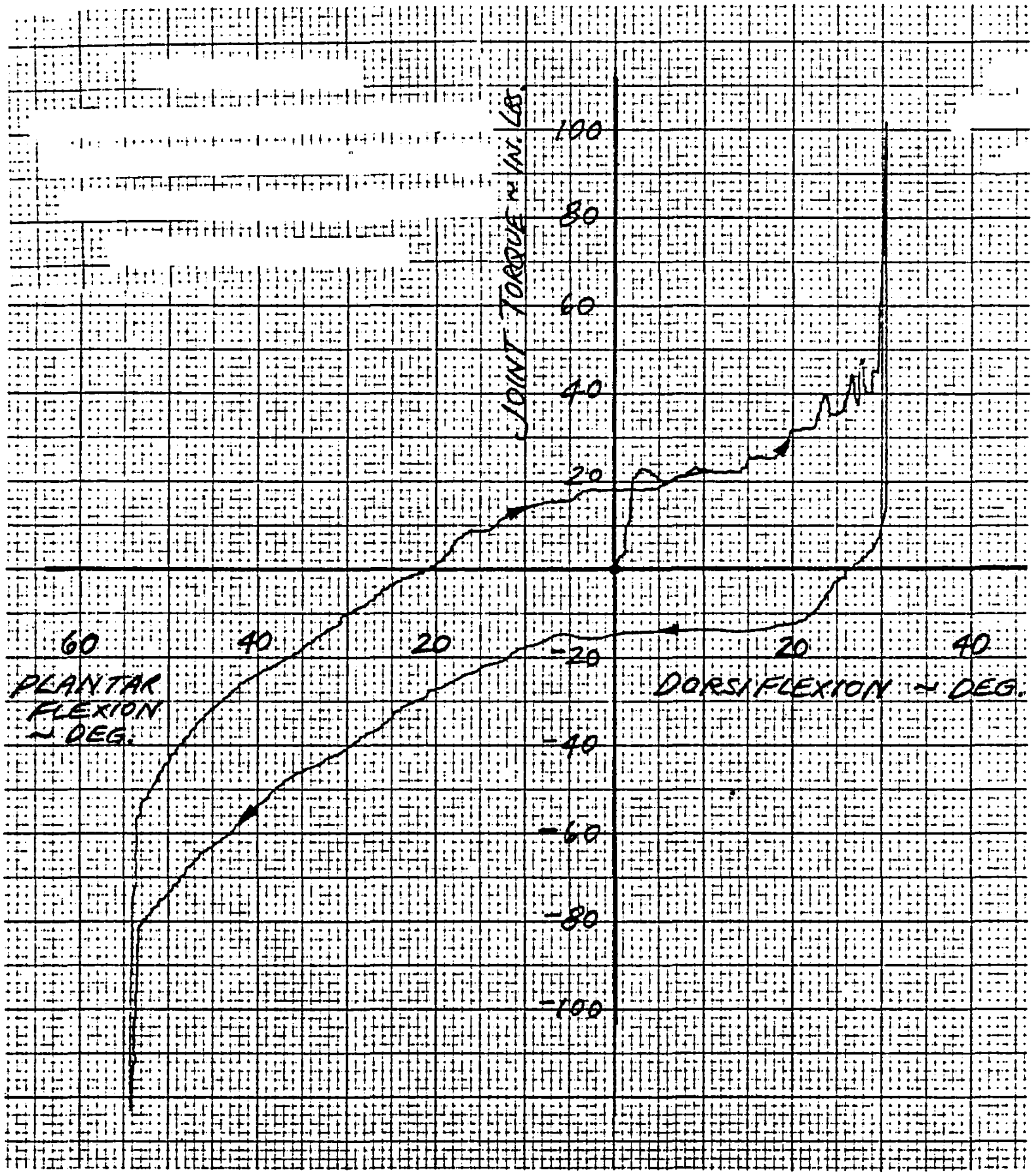

Figure 2-22 ANKLE JOINT TORQUE CHARACTERISTICS FOR DORSIFLEXION-PLANTAR FLEXION MOTION OF THE FOOT

(a) Static Flexion

The head/neck pendulum test apparatus used for determining compliance with the FMVSS 208 dynamic performance requirements was used to obtain static measurements of the flexural stiffness of the neck with the head attached. From the initial position with the pendulum, neck, and head Z axes all vertical, the pendulum was incrementally raised with a winch and the horizontal force, directed through the head C.G., required to maintain vertical alignment of the head was measured with a load cell. In addition, linear and angular potentiometers recorded changes of the head/neck geometry as illustrated in Figure 2-23. The total neck flexion angle ($\phi + \theta$) was verified by separately measuring the pendulum angle from the vertical with an inclinonometer.

Tests were performed with the head/neck assembly mounted on the pendulum so the neck would bend forward, backward, laterally, and in the plane 45 degrees from the sagittal plane. The results of these tests indicated that the flexural resistance of the neck was essentially the same for all bending directions. Typical data measured in the forward flexion test is presented in Figure 2-24 which shows that the total flexion angle and each of the ϕ and θ components of the head rotation vary nearly linearly with the applied force. The distance between the head C.G. and the base of the neck, measured by the radius potentiometer, did not change by more than 0.1 inches when the neck was flexed to the maximum value in any of the tests.

(b) Static Torsion

The static torque characteristics of the neck for twisting of the head with respect to the torso were determined by measuring the twist angle as a function of a moment couple applied to the top of the neck. The results of three tests in which the direction of neck twist was reversed are given in Figure 2-25. The data show a small hysteresis effect for the load-unload cycle in each twist direction.

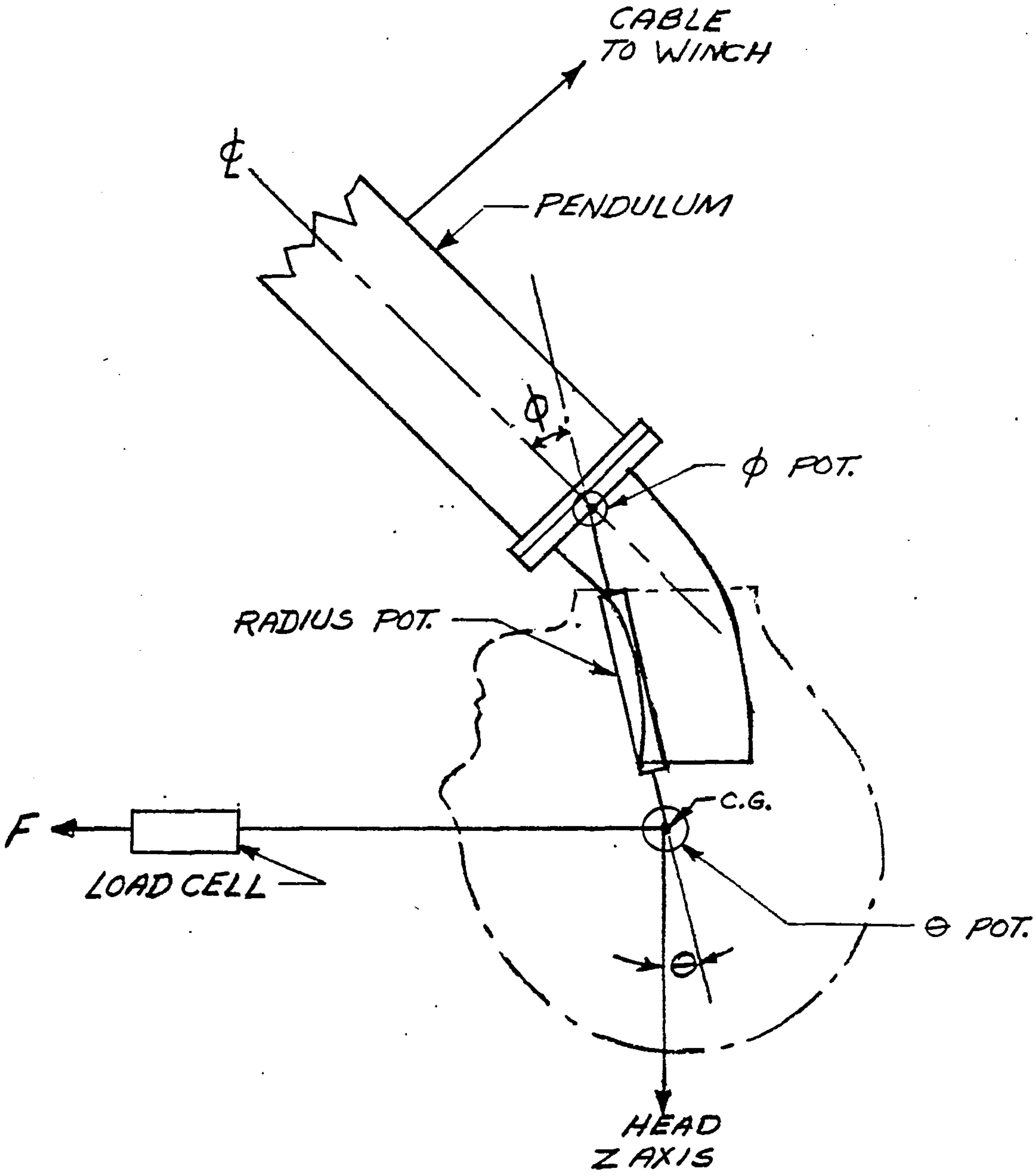

Figure 2-23 NECK STATIC BENDING TEST APPARATUS

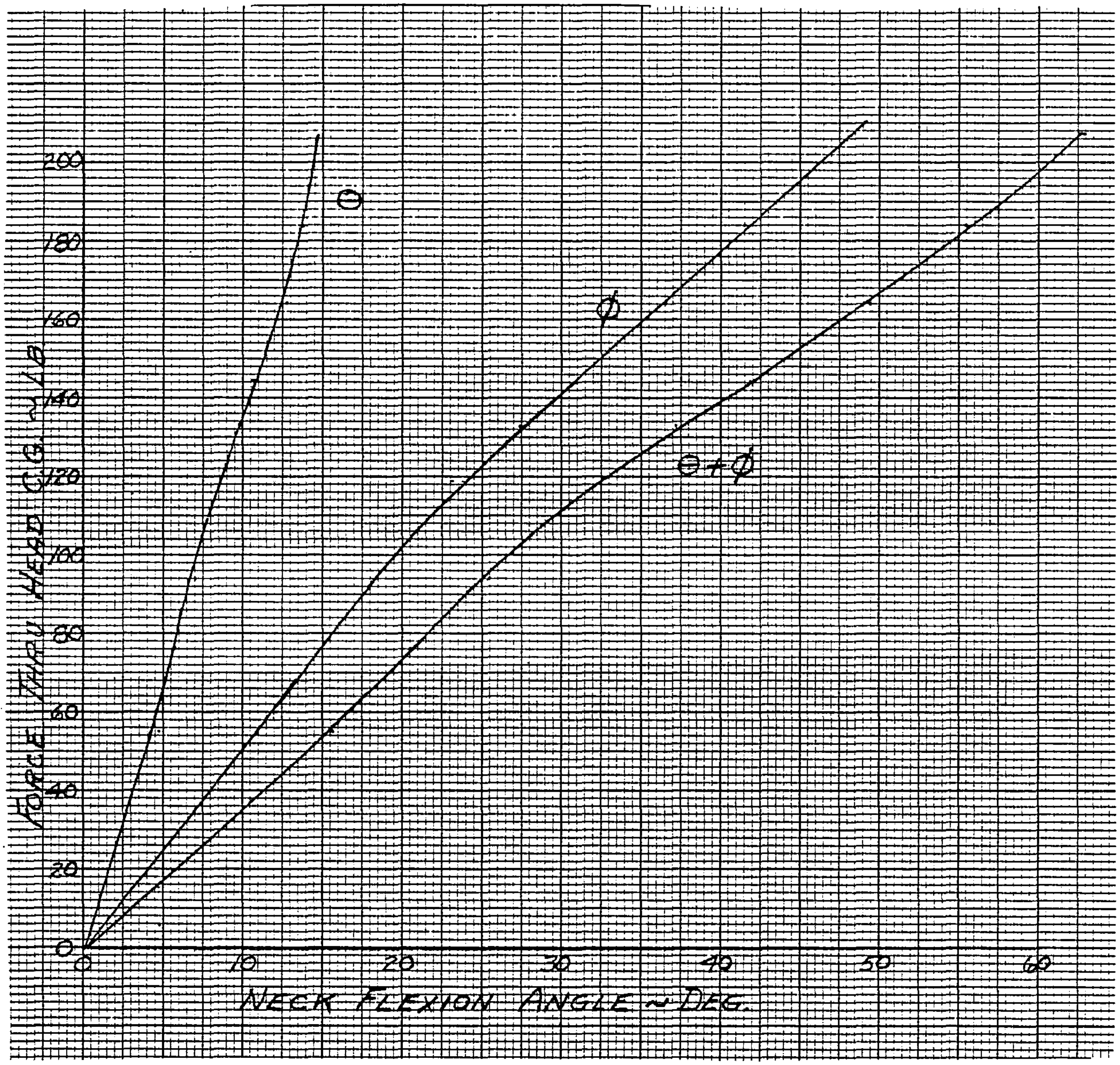

Figure 2-24 NECK STATIC BENDING RESISTANCE

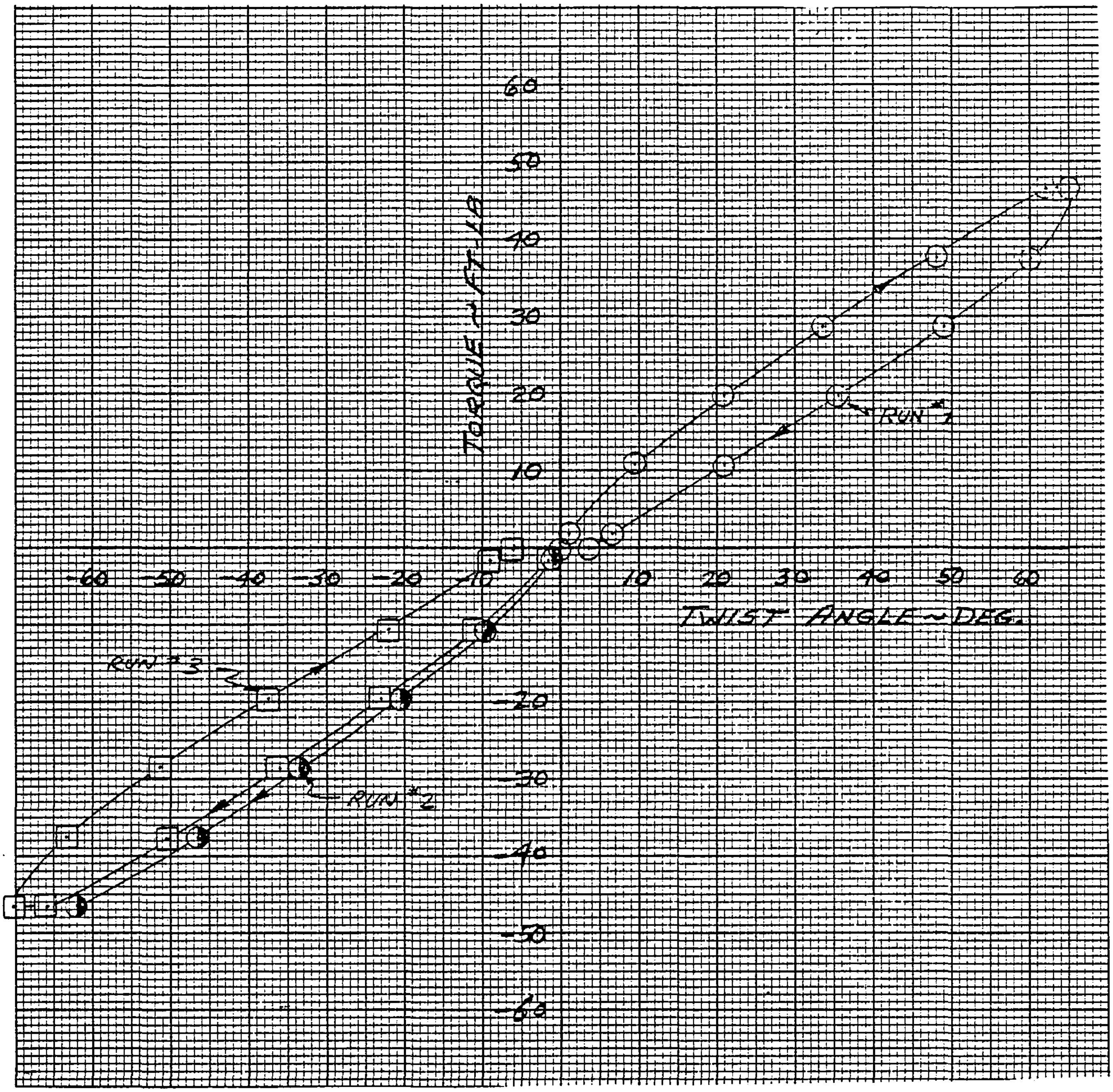

Figure 2-25 NECK TORSIONAL RESISTANCE

(c) Dynamic Free-Oscillation Tests

Information on the damping properties of the rubber neck was obtained from measurements of the decay of flexural and torsional oscillations of the neck. For these tests, the base of the neck was fixed and a fixture whose mass and moment of inertia could be easily varied was attached to the upper end of the neck. The variable inertia feature of the fixture provided the capability for determining joint effective viscous damping coefficients from log-decrement analysis of the measured fixture tangential component of acceleration at several resonant frequencies. The results from the free-oscillation tests of the neck are summarized in Table 2-3.

2.3.8 Lumbar Spine

The flexural and torsional resistances of the dummy rubber lumbar spine was measured in static tests of the upper and lower torso assembly, including the abdominal insert. In addition, the flexural resistance of the torso when the rubber spine was replaced with a single pin joint was also determined in another test.

(a) Static Flexion

The apparatus and procedure for measuring the flexural resistance of the lumbar spine is similar to that employed for the tests of the neck and is illustrated in Figure 2-26. As can be seen in this figure, the horizontal force to maintain the upper torso Z axis vertical as the pendulum was raised was directed through the upper torso center of gravity.

The results of tests in which the upper torso was flexed forward and backward in the sagittal plane are presented in Figure 2-27. At torso angles greater than 15 degrees, the joint resistance for forward bending of the spine is somewhat greater than when the torso is bent backward. This is probably due

TABLE 2-3

RESULTS OF NECK FLEXION AND TORSION FREE-OSCILLATION TESTS

FLEXION

Fixture Weight(1)∿lb.	5.06	14.31	23.56
Fixture I_{yo} ∿lb.-sec.^{2}-in.	0.118	0.765	1.412
Damped Oscillation Frequency∿Hz	9.4	4.0	3.1
Amplitude Decay Factor(2)	0.34	0.29	0.27

TORSION

Fixture Weight(1)∿lb.	5.06	14.31	23.56
Fixture I_{zo}∿lb.-sec.^{2}-in.	0.183	0.810	1.437
Oscillation Frequency∿Hz	10.5	4.7	3.2
Amplitude Decay Factor (2)	0.36	0.29	0.29

Note: (1) Fixture C.G. on neck centerline 1.14 inches above the top of the neck.

(2) Amplitude decay factor = $\frac{1}{n} \ln \frac{A_o}{A_n}$

where: A_o = initial oscillation amplitude

A_n = amplitude of the n^{th} succeeding peak

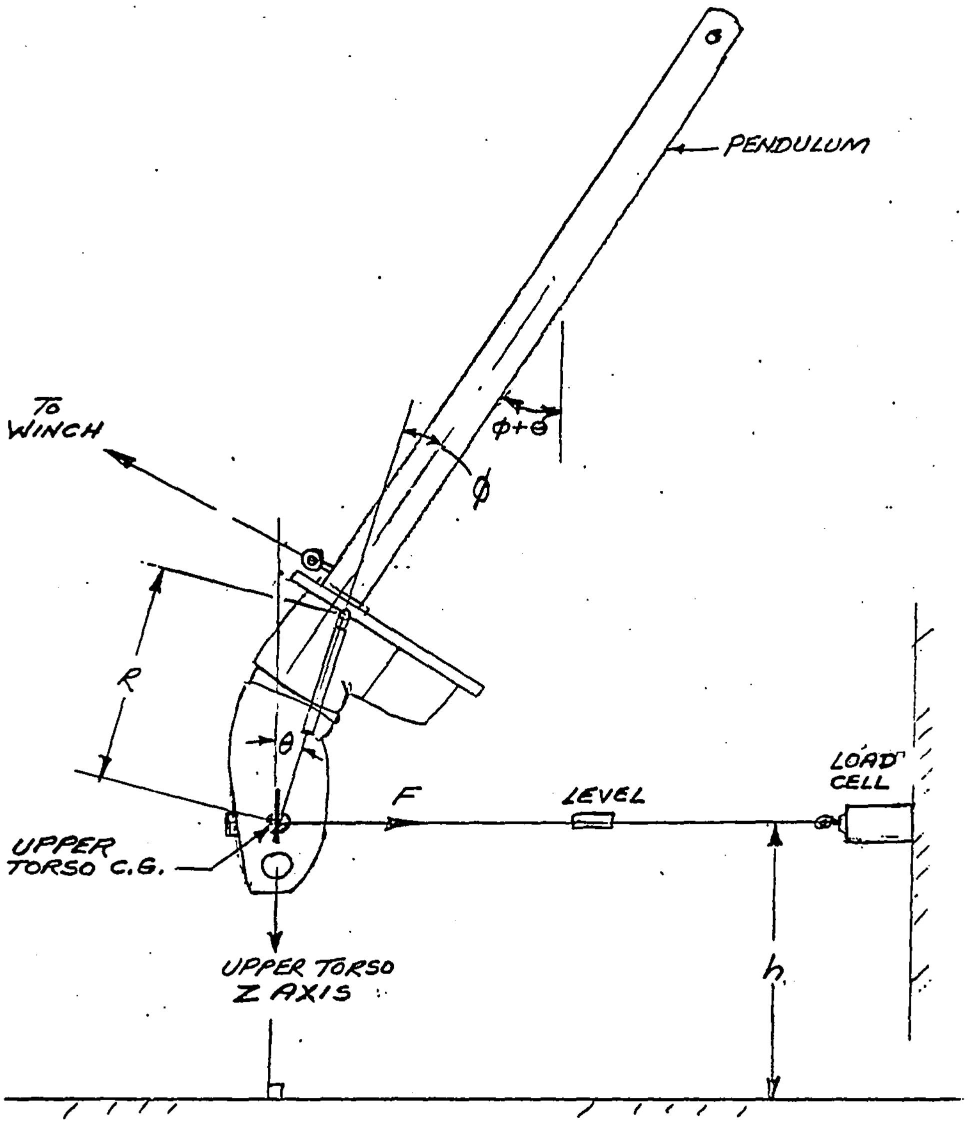

Figure 2-26 LUMBAR SPINE STATIC FLEXION TEST CONFIGURATION

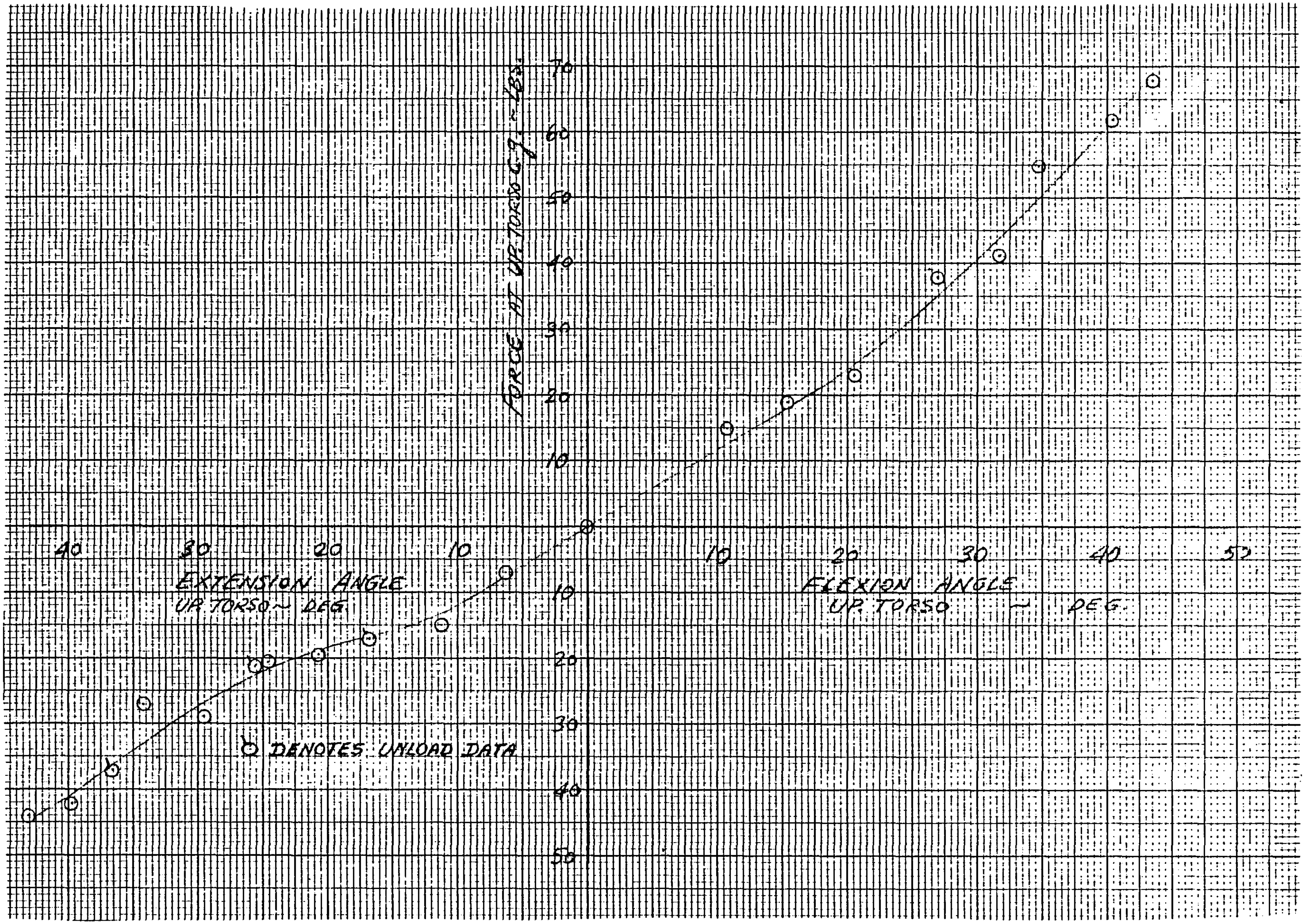

Figure 2-27 LUMBAR SPINE BENDING RESISTANCE

to the difference in the effect of the abdominal insert, which being located ahead of the spine, tends to be squeezed between the upper and lower torso segments during forward flexion.

The degree to which compression of the abdominal insert contributes to the effective resistance of the lumbar spine during forward flexion of the upper torso was investigated by performing a second test in which the rubber spine was replaced by a two-piece steel spine of the same size which contained a single pin joint at the center. Since the center of rotation was fixed and known in this instance, the resistive torque could be calculated from the applied force measurements and is shown in Figure 2-28 as a function of the flexion angle. It should be noted that torque shown in this plot is due almost entirely to compression of the abdominal insert and of the flesh of the upper and lower torsos since the resistance of the pin joint in the spine (i.e., coulomb fiction) was very small.

The force required to rotate the upper torso to a given flexion angle was less with the pin joint* than in the test with the rubber spine due to the bending resistance of the rubber spine. However, a difference in the relative magnitudes of the ϕ and θ angles (see Figure 2-26) was also noted between the two tests. For the rubber spine, the relationship between ϕ and θ was $\theta = 1.05\phi$ compared to $\theta = 1.25\phi$ in the test with the pin joint, thereby indicating that the effective center of rotation is not at the midpoint of the rubber lumber spine.

(b) Static Torsion

Measurements of the static twist characteristics of the dummy's spinal column were made with an assembled torso, including the upper torso skin jacket and abdominal insert. The lower torso was rigidly attached to a base plate and

---

*Note that the applied force in the test with the pin joint can be determined by dividing the torque shown in Figure 2-28 by the 8.95 inch moment arm.

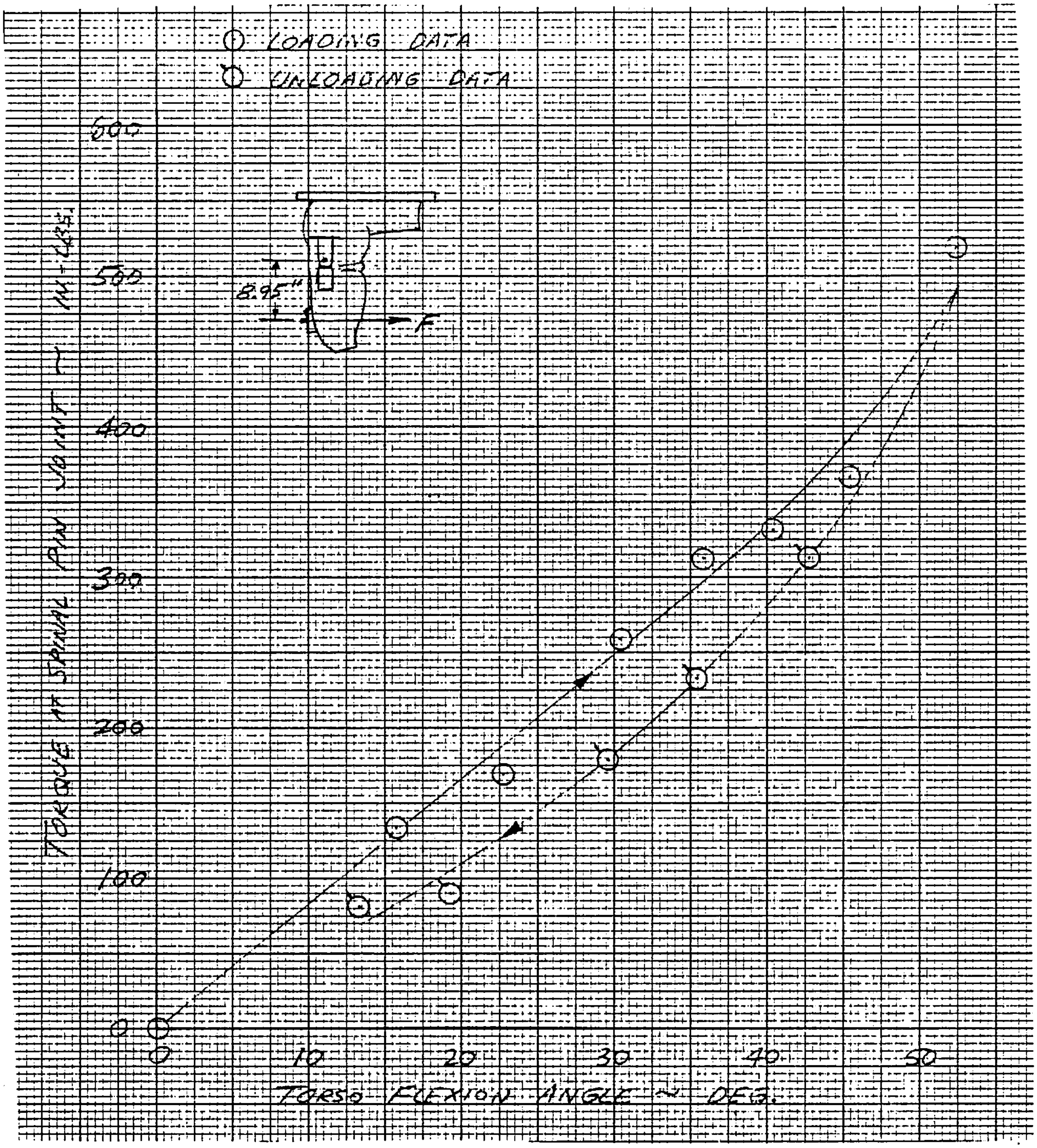

Figure 2-28 UPPER TORSO FLEXURAL RESISTANCE WITH SINGLE PIN LUMBAR SPINE JOINT

a horizontal force couple was applied to the upper torso using a large disc secured at the neck mounting plate. Results of the test in the form of plots of applied torque versus torso twist angle are presented in Figure 2-29. The data indicate somewhat different torsional stiffness for rotations in opposite directions and considerable hysteresis effects. It should be mentioned that the twist angle was noted to drift slowly as the torque was held constant for a period of time. For this reason, measurements of the angle were made within two or three seconds after changing the applied torque.

2.4 Upper Torso Compliance

The compliance of the upper torso loaded by a shoulder belt was investigated in a static test which provides data for estimating how the force-strain properties of belt webbing might be modified to account for the effects of dummy compliance in computer simulations of belt restraint systems. The dummy was supported in a supine position on a rigid surface and the chest was loaded by means of an inextensible steel strap positioned in a typical torso belt configuration as shown in Figure 2-30. Loads were applied by pulling on the upper end of the strap and the force at each end, the corresponding change of belt length between anchor points resulting from the deformation of the torso, and the posterior deflection of the sternum were recorded.

The effective belt stretch due to torso compliance is shown in Figure 2-31. Note that the manner of loading was such that the force at the upper end of the strap was higher than that measured at the lower anchor. Since the loads measured in dynamic sled and full-scale crash tests are usually highest at the upper end of a shoulder belt, the static test results are realistic in that respect. The indication of reduced stiffness evidenced by the curves beginning at about 2 inches of effective belt elongation is probably associated with lateral displacement of the rib cage. The center of the sternum was observed to have displaced nearly 1 inch to the left of the mid sagittal plane when the upper anchor load was 1200 lbs.

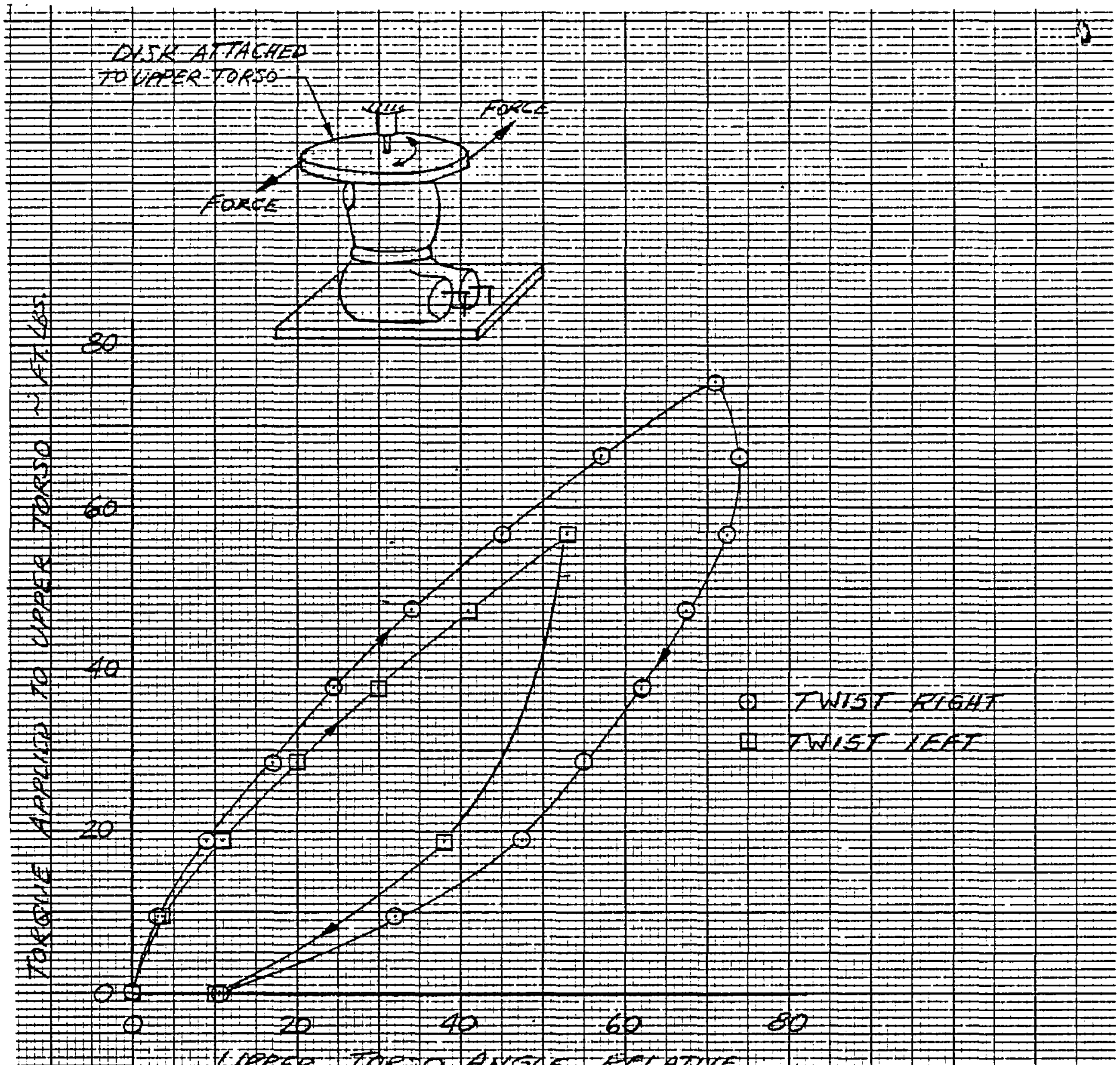

Figure 2-29 TORQUE CHARACTERISTICS OF TORSO FOR TWIST ABOUT LUMBAR SPINE AXIS

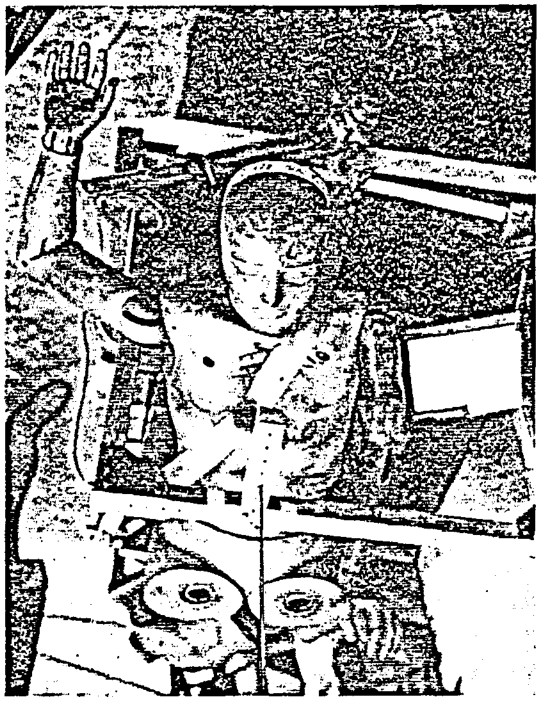

Figure 2-30 TEST SET-UP FOR MEASUREMENT OF DUMMY CHEST COMPLIANCE

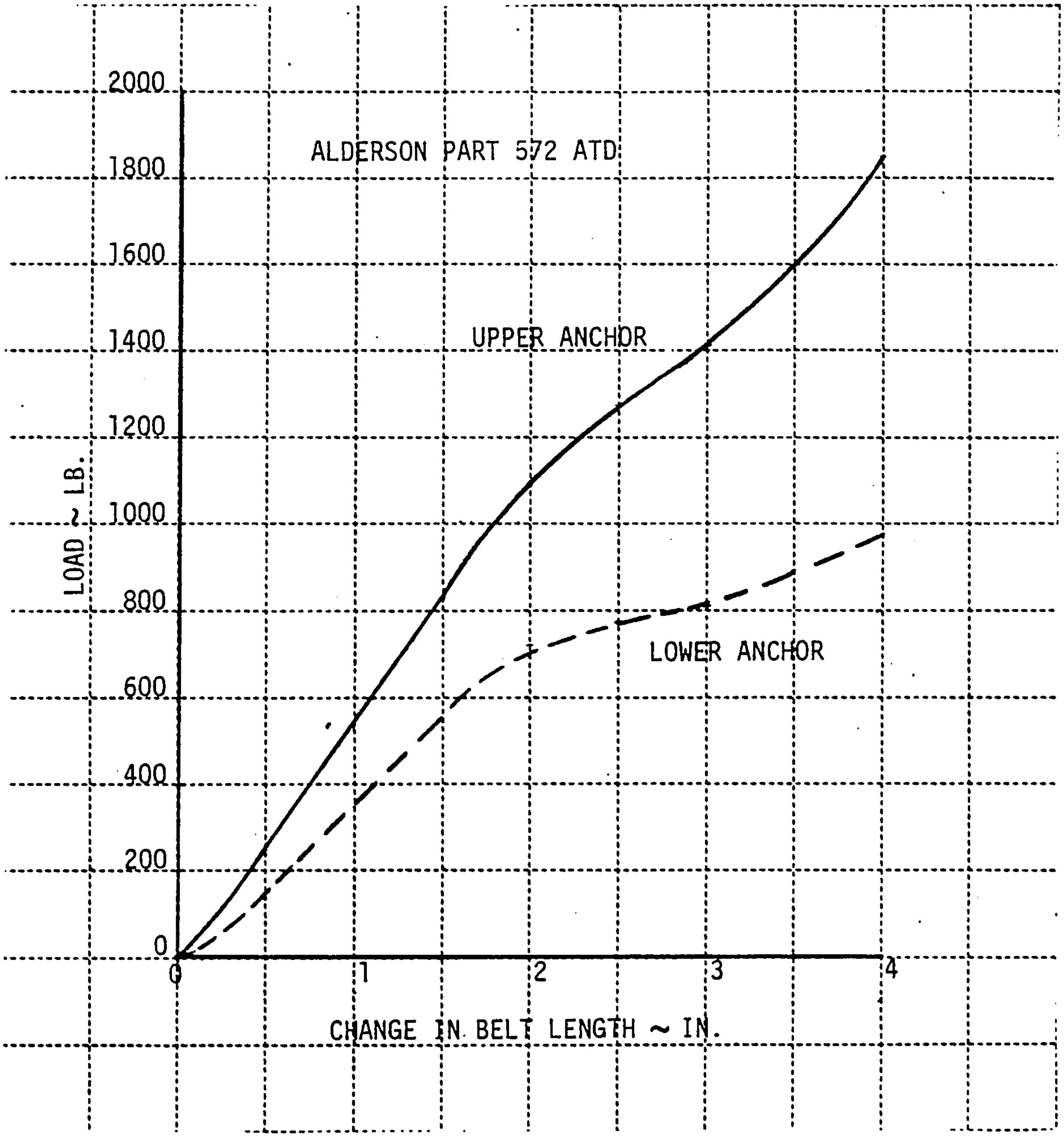

Figure 2-31 EFFECTIVE TORSO BELT STRETCH DUE TO CHEST COMPLIANCE OF 50TH PERCENTILE MALE DUMMY

3.0 CVS MODEL OF DUMMY

The CVS program requires that the dummy be modeled as a collection of rigid segments connected by joints. The Part 572 dummy satisfies this requirement for all of its components except for the neck and the lumbar spine. A fifteen-segment, fourteen-joint model has been selected to describe the dummy. In this model the neck and lumbar spine are assumed to be rigid segments connected by joints to the adjoining segments. The clavicles and associated components of the shoulder are assumed to be part of the upper torso with the shoulder modeled as a single joint connecting the upper torso to the upper arm. The hands are assumed to be part of the lower arms, i.e., the wrist joint is not modeled.

The segments and joints are identified in Table 3-1.

TABLE 3-1
SEGMENTS AND JOINTS OF DUMMY MODEL

SEGMENTS			JOINTS				
No.(i)	Name	Symbol	No.(j)	Name	Symbol	JNT(j)	Connects
1	Lower Torso	LT	1	Pelvis	P	1	LT - CT
2	Center Torso	CT	2	Waist	W	2	CT - UT
3	Upper Torso	UT	3	Neck Pivot	NP	3	UT - NECK
4	Neck	NECK	4	Head Pivot	HP	4	NECK - HEAD
5	Head	HEAD	5	Left Hip	LH	1	LT - LUL
6	Left Upper Leg	LUL	6	Left Knee	LK	6	LUL - LLL
7	Left Lower Leg	LLL	7	Left Ankle	LA	7	LLL - LF
8	Left Foot	LF	8	Right Hip	RH	1	LT - RUL
9	Right Upper Leg	RUL	9	Right Knee	RK	9	RUL- RLL
10	Right Lower Leg	RLL	10	Right Ankle	RA	10	RLL - RF
11	Right Foot	RF	11	Left Shoulder	LS	3	UT - LUA
12	Left Upper Arm	LUA	12	Left Elbow	LE	12	LUA - LLA
13	Left Lower Arm	LLA	13	Right Shoulder	RS	3	UT - RUA
14	Right Upper Arm	RUA	14	Right Elbow	RE	14	RUA - RLA
15	Right Lower Arm	RLA					

In Table 3-1 each segment and joint has been assigned a number and a symbol. The lumbar spine has been called the Center Torso. The column labeled JNT(j) is a connectivity vector which is used by the CVS model to identify the segments connected by a joint. That is, for joint j, the segment j + 1 is connected to the segment JNT(j). For example, joint 13 (Right Shoulder) connects the Right Upper Arm (segment 14) to the Upper Torso (segment 3). The last column labeled "Connects" contains the symbols identifying the segments connected by the joint.

3.1 Segments

This section defines the numerical value of the parameters used by the CVS program for the segments. These values are based on the experimental measurements reported in Section 2.

3.1.1 Segment Weights, Inertias, and Orientation of Principal Axes

Section 2.1 describes the experimental measurements of the weights and Section 2.2 describes the experimental measurements of the inertias. These experimental results are given in Tables 2-1 and 2-2, respectively.

The rotation angles given in Table 2-2 define the orientation of the principal inertial axes of the segments with respect to the geometric reference axes used in the measurements. For input to the CVS program the geometric axes were redefined such that the Z axis was along the long bone axes of the segments where applicable. The Z axis is taken as positive in the downward direction, the X axis as forward, and the Y axis to the right to form a right-handed coordinate system.

The inertial data used to describe the dummy is summarized in Table 3-2. The inertia and the orientation of the principal axes with respect to the geometric axes were computed from the experimental data with the same program that was used to produce Table 2-2. However, the program was modified to ignore

TABLE 3-2

SEGMENT WEIGHTS AND INERTIAS

No.		Segment Weight (lbs.)	Inertia (lb-in-sec^2) Ix	Iy	Iz	Orientation (degrees) yaw	pitch	roll
1	LT	29.04	1.9859	1.3852	1.4802	0.0	23.85	0.0
2	CT	3.00	0.0213	0.0213	0.0087	0.0	0.00	0.0
3	UT	37.87	2.0799	1.5915	1.3362	0.0	0.00	0.0
4	NECK	1.82	0.0118	0.0118	0.0050	0.0	0.00	0.0
5	HEAD	9.67	0.2197	0.2562	0.1638	0.0	42.21	0.0
6	LUL	20.99	0.7723	0.7721	0.1164	0.0	0.00	0.0
7	LLL	7.0	0.5948	0.5907	0.0322	0.0	-3.74	0.0
8	LF	2.76	0.0383	0.0434	0.0132	0.0	0.00	0.0
9	RUL	20.99	0.7723	0.7721	0.1164	0.0	0.00	0.0
10	RLL	7.00	0.5948	0.5907	0.0322	0.0	-3.74	0.0
11	RF	2.76	0.0383	0.0434	0.0132	0.0	0.00	0.0
12	LUA	4.76	0.1378	0.1426	0.0125	0.0	0.00	11.52
13	LLA	4.61	0.2696	0.2614	0.0125	0.0	0.00	0.0
14	RUA	4.76	0.1378	0.1426	0.0125	0.0	0.00	-11.52
15	RLA	4.61	0.2696	0.2614	0.0125	0.0	0.00	0.00

any cross product inertia that was less than 10% of the maximum product of inertia. This procedure can be justified by consideration of the experimental errors of measurement. The data for the Center Torso (lumbar spine) and the Neck were computed by assuming these segments were circular cylinders of uniform density. The weight of some segments was adjusted to account for the addition and/or deletion of components in instances where the model definition was different than the actual segment used in the measurements.

3.1.2 Contact Ellipsoids

The CVS program requires the definition of ellipsoids that are rigidly attached to segments and which are used to compute contact forces resulting from various interactions during the simulation. These primary ellipsoids do not necessarily have to describe the entire body surface; rather they should be defined to best simulate segment interferences for calculation of contact forces. Table 3-3 summarizes the selections made for the baseline model of the dummy. It is the responsibility of the user of the program to redefine these if necessary.*

TABLE 3-3

SEGMENT CONTACT ELLIPSOIDS

Ellipsoid	Length of Semi Axes (in.)			Coordinates of Center (in.)		
	X	Y	Z	X	Y	Z
1	4.90	6.94	6.00	0.00	0.00	-0.27
2	4.10	5.25	4.40	2.15	0.00	0.30
3	4.66	6.78	9.00	0.80	0.00	2.20
4	2.70	2.28	4.00	-0.10	0.00	1.65
5	4.00	3.10	5.00	0.50	0.00	0.40
6	3.30	3.50	11.40	0.15	0.00	-2.20
7	2.36	2.23	9.45	0.00	0.00	0.00
8	1.52	1.60	5.22	0.00	0.00	0.95
9	3.30	3.50	11.40	0.15	0.00	-2.20
10	2.36	2.23	9.45	0.00	0.00	0.00
11	1.52	1.60	5.22	0.00	0.00	0.95
12	2.07	1.64	6.88	0.00	0.00	0.00
13	1.30	1.11	8.38	0.00	0.00	0.00
14	2.07	1.64	6.88	0.00	0.00	0.00
15	1.30	1.11	8.38	0.00	0.00	0.00

3.1.3 Joint Locations

The joint locations are given in this section because they are associated with a particular segment. Detailed descriptions of the joints and the associated parameters are given in Section 3.2.

The CVS program models a joint connecting two segments as a mathematical point fixed in each segment about which one segment may rotate relative to the other. The fixed point in each segment is taken as the origin of the joint coordinate system for the respective segment. These fixed points are assumed

---

*The CVS program allows the user to define additional ellipsoids and/or to redefine the orientation of these primary ellipsoids. If an orientation is not specified, the program assumes the ellipsoid axes are parallel to the geometric axes of the segments to which they are assigned.

to be in the same location in space, i.e., the joints do not pull apart. The joint locations are given with respect to the c.g. (center of gravity) of the segment. The measured locations of the joints were converted to the c.g. reference system and are summarized in Table 3-4. The locations of the joints associated with the neck and the lumbar spine were modified to account for the steel plate located in these rubber joints. Since the neck and the spine are "rubber," the locations of these joints are not well defined.

TABLE 3-4

JOINT LOCATIONS IN ADJOINING SEGMENTS

Joint	Segment	Location (in.)			Segment	Location (in.)		
		X	Y	Z		X	Y	Z
1 P	LT	-1.790	0.000	-2.140	CT	0.000	0.000	2.075
2 W	CT	0.000	0.000	-2.325	UT	-1.131	0.000	6.559
3 NP	UT	1.575	0.000	-6.576	NECK	0.000	0.000	2.185
4 HP	NECK	0.000	0.000	-2.185	HEAD	-0.370	0.000	1.390
5 LH	LT	-0.130	-3.500	1.700	LUL	1.300	0.000	-9.000
6 LK	LUL	-0.043	0.100	6.740	LLL	-0.097	0.000	-7.365
7 LA	LLL	-0.097	0.000	8.835	LF	1.600	-0.130	-2.030
8 RH	LT	-0.130	3.500	1.700	RUL	1.300	0.000	-9.000
9 RK	RUL	-0.043	-0.100	6.740	RLL	-0.097	0.000	-7.365
10 RA	RLL	-0.097	0.000	8.835	RF	1.600	0.130	-2.030
11 LS	UT	-0.161	-7.400	-3.580	LUA	0.047	0.030	-4.690
12 LE	LUA	0.047	0.030	5.610	LLA	-0.120	-0.025	-6.340
13 RS	UT	-0.161	7.400	-3.580	RUA	0.047	-0.030	-4.690
14 RE	RUA	0.047	-0.030	5.610	RLA	-0.120	0.025	-6.340

3.1.4 Details of Segment Data

The basic information used to generate the tables in Sections 3.1.1, 3.1.2 and 3.1.3 is given in the following pages. On these pages the abbreviation c.g. is used for the center of gravity (center of mass).

Segment 1: Lower Torso - LT

Lower torso - pelvis and abdomen assembly (Ref. SA150M060) ATD-7145
Geometric reference: XY plane parallel to lumbar and pelvic adaptor D/02, ATD 7116, X + forward, Y + to right, Z + down.

Segment 1: Lower Torso - LT (continued)

Origin - center of mounting hole for lumbar cable assembly D/05, ATD-7107, Z= 0 at upper surface of D/02 (adjacent to lumbar D/01).

Inertial Properties:

Weight	38.04 lbs.
Inertia (Ix, Iy, Iz)	1.98739, 1.38370, 1.48029 lb-in-sec^2
Yaw, pitch, roll	-3.11, 23.82, -1.08 degrees wrt geometric
c.g. (x, y, z)	1.794, 0.061, 1.576 inches

c.g. is 2.268 in. above leg bone G/02 centerline.
(2.268 + 1.576 = 3.844 location of D/02 above femur centerline)

Weight, inertia and c.g. measurements included:

Abdominal insert	E/04 ATD-3250-2	(viscera sac)
Lumbar	D/01 ATD-7102	3 lbs.
Femur and retainer assembly left	E/05 ATD-3232-1	3.1 lbs.
(includes clamping plate) right	E/06 ATC-3232-2	3.1 lbs.

Adjusted weight (without D/01, E/05 and E/06 but with clamping plates) = 29.04 lbs.

Joint locations:	X	Y	Z	(inches)
1 lower torso - lumbar spine	0.000	0.0000	-0.500	(plate thickness)
5 lower torso - right upper leg	1.656	3.4375	0.905	above leg bone c/l
8 lower torso - left upper leg	1.656	-3.4375	1.095	above leg bone c/l

(c/l - centerline)

Segment 2: Center Torso (Lumbar Spine) - CT

Lumbar spine (Reference SA150M050) ATD-7141
Geometric reference: XY parallel to lumbar and pelvic adapter D/02,
X + forward, Y + right, Z + down
Origin - geometric center

Inertial properties:

Weight	3 lbs.
Inertia (Ix, Iy, Iz)	0.0212581, 0.0222581, 0.0081686 lb-in-sec^2
Yaw, pitch, roll	0, 0, 0 degrees

Segment 2: Center Torso - CT (continued)

Inertia calculation, assuming spine is a cylinder of uniform density:

$$I_x = I_y = M\left(\frac{H^2}{12} + \frac{R^2}{4}\right), \quad I_z = \frac{MR^2}{2},$$

$H = 5.15$ in, $R = 1.45$ in, $G = 386.088$ in/sec^2

Ix, Iy as calculated will be low because of plates in spine (not uniform density).

Iz as calculated will be low because of hole through center.

c.g. taken as the geometric center.

Joint locations with respect to the c.g.

	x y z	inches
2 P - Pelvis	0, 0,. 2.575 - 0.5	(adjusted for
3 W - Waist	0, 0, -2.575 + 0.25	plate thickness)

Segment 3: Upper Torso - UT

Upper torso-Shoulder-Thorax Assembly (Ref. SA150M030) . ATD-7140

Geometric Reference

xy plane parallel to Thoracic and Lumbar Adaptor bottom surface c/14, ATD-7130

x + forward, y + right, z + down

origin - bottom surface c/14, of spine

Inertial Properties

Weight	37.87 lbs			
Inertia (Ix, Iy, Iz)	2.08151	1.59187	1.33425	lb-in-sec^2
Yaw, pitch, roll	-3	-0.84	4.74	degrees wrt geometric
c.g. (x, y, z)	1.131	0	-6.309	inches

Joint Locations

Upper torso-neck-center of mounting surface for neck

x	y	z	inches
2.62 + 1/4 sin 20	0	12.65 - 1/4 cos 20	

(the neck is pitched - 20 degrees with respect to the torso and the joint is moved 1/4 inch into the neck to adjust for the plate).

Segment 3: Upper Torso - UT (continued)

	x	y	z inches
Upper torso-spine	0	0	0.25 (adjusted for plate)
Upper torso-right upper arm*	0.97	7.40	-9.64
Upper torso-left upper arm*	0.97	-7.40	-9.64

*These assume that Shoulder Yokes c/19, c/10, ATD-3056-1,2
and Clavicles c/18, c/17, ATD-3061-1,2
do not move relative to main assembly.

Segment 4: Neck - NECK

Neck B/01 (Ref. SA150M020) ATD-7150

Geometric Reference

xy plane parallel to mounting surfaces, X + forward, y + right
z + down
origin, geometric center

Inertial Properties

Weight	1.82 lbs			
Inertia (x, Iy, Iz)	0.01179,	0.01179,	0.00500	lb-in-sec^2
Yaw, pitch, roll	0	0	0	degrees wrt geometric

Inertia calculation, assuming neck is a cylinder of uniform density.

$$I_y = I_x = M\left(\frac{H^2}{12} + \frac{R^2}{4}\right), \quad I_z = \frac{MR^2}{2}$$

$H = 4.87$ in, $R = 1.45$ in

Joint locations with respect to the c.g.

	x	y	z
3 NP - Neck Pivot	0	0	2.435 - 0.25 (adjusted for
4 HP - Head Pivot	0	0	-2.435 + 0.25 plate thickness)

Segment 5 : Head - HEAD

Head (Ref. SA150-M010)

Segment 5 : Head - HEAD (continued)

Geometric Reference

xy plane parallel to neck mounting surface, x + forward, y + right
z + down (toward neck)
origin - center of mounting hole at junction of head and neck

Inertial Properties

Weight	9.67 lbs			
Inertia (Ix, Iy, Iz)	0.21938,	0.25739,	0.16291	lb-in-sec^2
Yaw, pitch, roll	7.22	42.84	-0.61	degrees wrt geometric
c.g. (x, y, z)	0.37	-0.043	-1.14	inches

Joint Location

	x	y	z	(inches)
4 HP - Head Pivot	0	0	0.25	

Segment 9 : Right Upper Leg - RUL

Right Upper Leg (Ref. SA150M080) ATD-7142-2

Geometric Reference

x + forward (standing)
y + right parallel to knee pin
z + upper leg bone to knee
line through knee pin and center of protruding upper leg bone G/01-ATD-7131-1
center of bone appears to be directly above J/06 on ATD-7100
origin - center of knee joint pin. F/14 ATD3773 - center of upper leg bone G/01-ATD-7131-1

Inertial Properties

Weight	17.99 lbs.			
Inertia (Ix, Iy, Iz)	0.77409,	0.77147,	0.11530	lb-in-sec^2
Yaw, pitch, roll	-42.180	-0.16	2.33	degrees wrt geometric
c.g. (x, y, z)	0.0434	0.10	-6.74	inches

(Weight, Inertia and c.g. without Femur Assembly E/06)

Segment 9: Right Upper Leg - RUL (continued)

Joint Locations	x	y	z	inches
8 RH - Right Hip	0.7	-0.525	-16.20	
9 RK - Right Knee	0	0	0	

Segment 6: Left Upper Leg - LUL

Left Upper Leg (Ref. SA150M081) ATD-7142-1

Assume mirror symmetry with respect to right upper leg

Inertial Properties

Weight	17.99 lbs.			
Inertia (Ix, Iy, Iz)	0.77409,	0.77147,	0.11530	lb-in-sec^2
Yaw, pitch, roll	42.18	-0.16	-2.33	degrees wrt geometric
c.g. (x, y, z)	0.0434	-0.10	-6.74	inches

Joint Locations	x	y	z	inches
5 LH - Left Hip	0.7	0.525	-16.20	
6 LK - Left Knee	0	0	0	

Segment 10: Right Lower Leg - RLL

Right Lower Leg F/07 (Ref. SA150M080) ATD-7142-2
ATD-3738-2

Geometric Reference

z axis knee pin, ankle pin

x axis + forward y axis + right

origin - center of knee pin

Inertial Properties

Weight	7.00 lbs			
Inertia (Ix, Iy, Iz)	0.59504,	0.59083	0.03184	lb-in-sec^2
Yaw, pitch, roll	11.85	-3.94	0.58	degrees wrt geometric
c.g. (x, y, z)	0.097	0	7.365	inches (y not measured)

Segment 10: Right Lower Leg - RLL (continued)

Joint Locations	x	y	z	inches
9 RK - Right Knee	0	0	0	
10 RA - Right Ankle	0	0	16.20	

Segment 7: Left Lower Leg - LLL

Left Lower Leg G/07 (Ref. SA150M081) ATD-7142-1
ATD-3738-1

Same as Right Lower Leg
mirror symmetry on inertia

Segment 11: Right Foot - RF

Right Foot F/09 (Ref. SA150M080) ATD-7142-2
ATD-3141-2

Geometric Reference

z axis parallel to floor plane (+ heel to toe)
y parallel to ankle pin
x + toward top
origin, center of ankle pin

Inertial Properties

Weight 2.76 lbs
Inertia error in measurement

	x	y	z	inches
c.g.	-1.6	-0.13	2.03	

Joint Locations	x	y	z
10 RA - Right Ankle	0	0	0

Segment 8: Left Foot - LF

Left Foot G/09 (Ref. SA150M081) ATD-7142-1
ATD-3141-1

Same as Right Foot - mirror symmetry

Segment 14 : Right Upper Arm - RUA

Right Upper Arm (Ref. SA150M070) ATD-7143-2

Geometric Reference

z axis + center of shoulder pivot toward center of elbow pivot
x + forward, parallel to J07 bolt
y + toward right parallel to elbow joint
origin - center of shoulder pivot

Inertial Properties

Weight	4.59 lbs + 0.17 lbs bolt (elbow)			
Inertia (Ix, Iy, Iz)	0.13774	0.14269	0.01249	lb-in-sec^2
Yaw, pitch, roll	5.46	1.27	-11.45	degrees wrt geometric
c.g. (x, y, z)	-0.047	0.03	4.69	inches

(Measurements without elbow pivot bolt)

Joint Locations	x	y	z	inches
13 RS - Right Shoulder	0	0	0	
14 RE - Right Elbow	0	0	10.30	

Segment 12 : Left Upper Arm - LUA

Left Upper Arm (Ref. SA150M071) ATD-7143-1

Same as Right Upper Arm
mirror symmetry on inertia and c.g.

Segment 15 : Right Lower Arm and Hand - RLA

Right Lower Arm and Hand (Ref. SA150M010) ATD-7143-2
(Forearm) ATD-3145-2, MD 403-2, ATD-3142-2

Measurements made with wrist locked and wrist pivot 90° to elbow pivot

Segment 15: Right Lower Arm and Hand - RLA (continued)

Geometric Reference

z + from center of Elbow pivot to center of wrist pivot
y + toward right parallel to elbow pivot
x + toward thumb
origin - center of elbow pivot

Inertial Properties

Weight	4.61 lbs			
Inertia (Ix, Iy, Iz)	0.27271	0.25852	0.01237	lb-in-sec^2
Yaw, pitch, roll	27.10	0.90	1.26	degrees wrt geometric
c.g. (x, y, z)	0.120	-0.025	6.34	inches

Joint Location	x	y	z	inches
14 RE - Right Elbow	0	0	0	

Segment 13: Left Lower Arm and Hand - LLA

Left Lower Arm and Hand (Ref. SA150M071)	ATD-7143-1
(Forearm)	ATD-3145-1, MD-403-1, ATD-3142-1

Same as Right Lower Arm and Hand
Mirror symmetry on inertia and c.g.

3.2 Joint Coordinate Systems and Joint Parameters

The Part 572 dummy is modeled using three types of joints:

1) Ball Joints, used for the neck and the lumbar spine,
2) Pin Joints, used for the knees, and
3) Euler Joints, used for the hips, ankles, shoulders, and elbows.

The wrist joints were not modeled; the hands were considered part of the lower arms. The parameters that must be determined to describe the joint are:

A) Joint location: All joints are modeled as if the relative angular motion between the segments connected by the joint occurs about a fixed point in each segment. The position of this fixed point is taken as the origin of the joint coordinate system and is specified in the description of the segments. Joint locations are summarized in Section 3.1.3, Table 3-4.

B) Joint orientation: A local coordinate system is defined in each segment at the joint. The relative orientations of these coordinate systems are used to compute the torques developed at the joints. The orientation of the local coordinate system at the joint relative to the geometric coordinate system of the segment is specified in terms of three angles, usually the yaw, pitch and the roll of the joint reference relative to the segment reference. The joint orientations selected for the CVS model of the Part 572 dummy are listed in Table 3-5.

C) Center of symmetry: The standard joint routines in the CVS program assume that the torques are symmetric functions of the relative angles at the joints. The center of symmetry for ball and pin joints is controlled by proper orientation of the joint coordinate systems. The center of symmetry for an Euler Joint is specified for each axis (precession, nutation and spin). The values selected for each Euler Joint of the dummy model are also given in Table 3-5.

D) Spring parameters for each free axis, shown in Table 3-6.

E) Viscous and friction characteristics: The standard joint routines in the CVS program use seven parameters for which values are listed in Table 3-7.

The location of the joints and the orientation of the joint coordinate systems are taken from the experimental measurements and/or the engineering drawings. The locations (Item A) are given in the description of the segments.

TABLE 3-5

JOINT ORIENTATIONS FOR THE PART 572 DUMMY MODEL

	Joint			Principal Axis Segment JNT(J)			Principal Axis Segment J + 1			Center of Symmetry		
J	Symbol	JNT	PIN	Yaw	Pitch	Roll	Yaw	Pitch	Roll	Prec.	Nuta.	Spin
					(degrees)			(degrees)			(degrees)	
1	P	1	-2	0	0	0	0	0	0	-	-	-
2	W	2	-2	0	0	0	0	0	0	-	-	-
3	NP	3	-2	0	-20	0	0	0	0	-	-	-
4	HP	4	-2	0	0	0	0	0	0	-	-	-
5	LH	1	-4	-90	90	0	0	4.76	0	27	-70	0
6	LK	6	1	0	0	0	0	43.0	0	-	-	-
7	LA	7	-4	90	0	-0.6	90	0	0	0	79	0
8	RH	1	-4	90	90	0	0	4.76	0	-27	70	0
9	RK	9	1	0	0	0	0	43	0	-	-	-
10	RA	10	-4	90	0	-0.6	90	0	0	0	79	0
11	LS	3	-4	0	0	90	0	0	0	55	-65	0
12	LE	12	-4	90	0	0	90	0	0	8	-70	0
13	RS	3	-4	0	0	-90	0	0	0	55	65	0
14	RE	14	-4	90	0	0	90	0	0	-8	70	0

Column	Entries in Table
1	Joint Number
2	Joint Symbol
3	Joint Vector JNT(J) defines connectivity, i.e., PIN 1 Pin or hinge joint, initially unlocked -2 Ball joint, initially locked -4 Euler Joint, initially locked
5, 6, 7	Yaw, Pitch and Roll of the axis system of the joint with respect to the geometric axis system of segment JNT(J). (YPR1)
8, 9, 10	Yaw, Pitch and Roll of the axis system of the joint with respect to the geometric axis system of segment J + 1. (YPR2)
11, 12, 13	Center of Symmetry. This is only required for the Euler Joints, hence, is entered as the center of symmetry on the precession, nutation, and spin axes respectively. (YPR3)

TABLE 3-6

JOINT SPRING PARAMETERS

Joint	Symbol	1	2	3	4	5	Axis
1	P	50.000	0	0	0	90	flexure
		34.383	0	0	0	170	torsion
2	W	50.000	0	0	0	90	flexure
		34.383	0	0	0	170	torsion
3	NP	31.200	0	0	0	90	flexure
		15.000	0	0	0	170	torsion
4	HP	31.200	0	0	0	90	flexure
		15.000	0	0	0	170	torsion
5	LH	7.500	75	75	0	77	precession
		7.500	75	75	0	35	nutation
		16.000	160	160	0	60	spin
6	LK	0.000	10	0	0	53	flexure
7	LA	1.000	10	10	0	26	precession
		1.000	10	10	0	42	nutation
8	RH	7.500	75	75	0	77	precession
		7.500	75	75	0	35	nutation
		16.000	160	160	0	60	spin
9	RK	0.000	10	0	0	53	flexure
10	RA	1.000	10	10	0	26	precession
		1.000	10	10	0	42	nutation
11	LS	0.000	100	100	0	125	precession
		0.000	100	100	0	60	nutation
12	LE	0.000	20	20	0	52	precession
		5.000	50	50	0	70	nutation
13	RS	0.000	100	100	0	125	precession
		0.000	100	100	0	60	nutation
14	RE	0.000	20	20	0	52	precession
		5.000	50	50	0	70	nutation

Column:
1) Linear spring coefficient, (in.-lbs per degree).
2) Quadratic spring coefficient, (in.-lbs per degree squared).
3) Cubic spring coefficient, (in.-lbs per degree cubed).
4) Energy dissipation coefficient, (1 for no loss, 0 for full loss).
5) Joint stop, location with respect to the center of symmetry.

For the ball joint two sets of spring parameters must be specified, one for the flexure axis and the other for the torsion axis.

For the pin joint, only the flexure axis is specified.

For the Euler Joint a set of parameters must be specified for each free axis.

TABLE 3-7

JOINT VISCOUS AND FRICTION PARAMETERS

Joint	Symbol	1	2	3	4	5	6	7	Axis
1	P	1.20	122.4	30	500	0	0	0	
2	W	1.20	122.4	30	300	0	0	0	
3	NP	0.15	100.0	30	15	0	0	0	
4	HP	0.15	100.0	30	10	0	0	0	
5	LH	1.00	100.0	30	150	0	0	0	precession
		1.00	200.0	30	300	0	0	0	nutation
		1.00	100.0	30	150	0	0	0	spin
6	LK	1.00	20.0	30	30	0	0	0	
7	LA	0.50	20.0	30	30	0	0	0	precession
		0.50	20.0	30	30	0	0	0	nutation
		0.00	0.0	30	0	0	0	0	spin
8	RH	1.00	100.0	30	150	0	0	0	precession
		1.00	200.0	30	300	0	0	0	nutation
		1.00	100.0	30	150	0	0	0	spin
9	RK	1.00	20.0	30	30	0	0	0	
10	RA	0.50	20.0	30	30	0	0	0	precession
		0.50	20.0	30	30	0	0	0	nutation
		0.00	0.0	30	0	0	0	0	spin
11	LS	0.10	50.0	30	100	0	0	0	precession
		0.10	50.0	30	100	0	0	0	nutation
		0.00	0.0	30	0	0	0	0	spin
12	LE	0.10	20.0	30	30	0	0	0	precession
		0.10	20.0	30	30	0	0	0	nutation
		0.00	0.0	30	0	0	0	0	spin
13	RS	0.10	50.0	30	100	0	0	0	precession
		0.10	50.0	30	100	0	0	0	nutation
		0.00	0.0	30	0	0	0	0	spin
14	RE	0.10	20.0	30	30	0	0	0	precession
		0.10	20.0	30	30	0	0	0	nutation
		0.00	0.0	30	0	0	0	0	spin

Column:
1) Viscous coefficient (in.-lbs per degree per second).
2) Coulomb friction (in.-lbs).
3) Relative angular velocity for full Coulomb (degrees per second).
4) Maximum torque for a locked joint (in.-lbs).
5) Minimum torque for an unlocked joint (in.-lbs).
6) Minimum angular velocity for an unlocked joint (degrees per second).
7) Coefficient of restitution, $e = (1 + \mu)/2$ where μ is the classical coefficient of restitution.

The ball and pin joints use only one set of viscous parameters; the Euler Joint requires a set for each axis.

The center of symmetry and the spring characteristics (Items C and D) were derived from static measurements of all the joints except the neck and the lumbar spine. The neck and lumbar spine are basically rubber cylinders which are not rigid bodies and hence are not well defined. They are modeled as separate segments connected by ball joints to the adjoining segments. The spring and viscous characteristics were determined from special static and dynamic tests which are described later in Sections 3.3, 3.4, and 3.5.*

Since no dynamic tests were made for the joints other than the neck and spine, the viscous coefficients could not be determined. Therefore, arbitrary values were assumed which are shown in Table 3-7. The Coulomb friction can be preset on the dummy, a default value sufficient to hold the segment in static equilibrium is tabulated. It was assumed that the maximum torque for a locked joint was 150 percent of the Coulomb friction, and the minimum torque and the minimum angular velocity for an unlocked joint were both zero. The relative angular velocity for full Coulomb friction was arbitrarily set at 30 degrees per second for all joints. This controls the ramp function. A zero value for coefficient of restitution of all joints was also assumed in the model.

The following pages contain illustrations of the joint reference systems with respect to the geometric reference systems of the segments connected by each joint.

---

*Final values for the two joints of the neck and of the spine were determined by "tuning" to achieve acceptable correlation with results of pendulum impact tests.

(a) Lower Spine (Pelvis) Joint - Ball Joint

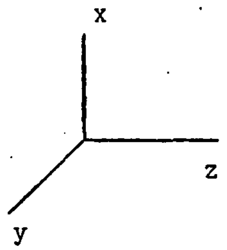

Geometric ref.
in lower torso

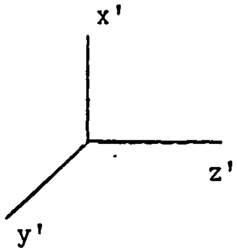

Joint ref.
in lower torso

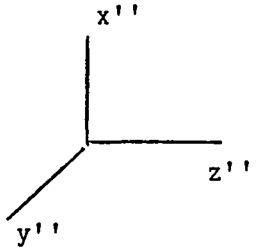

Joint ref.
in spine

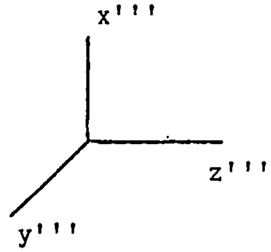

Geometric ref.
in spine

YPR1:	yaw	0.0 degrees	YPR2:	yaw	0.0 degrees
	pitch	0.0 degrees		pitch	0.0 degrees
	roll	0.0 degrees		roll	0.0 degrees

(b) Upper Spine (Waist) Joint - Ball Joint

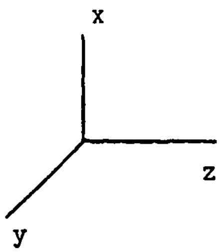

Geometric ref.
in spine

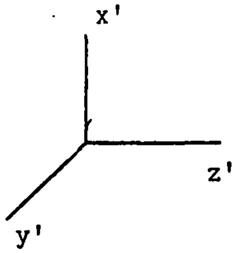

Joint ref.
in spine

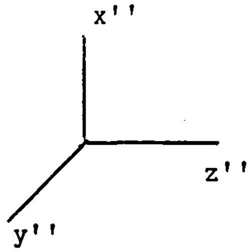

Joint ref.
in upper torso

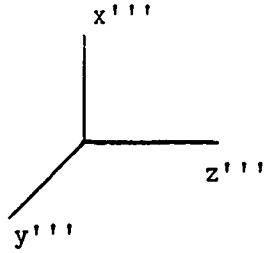

Geometric ref.
in upper torso

YPR1:	yaw	0.0 degrees	YPR2:	yaw	0.0 degrees
	pitch	0.0 degrees		pitch	0.0 degrees
	roll	0.0 degrees		roll	0.0 degrees

(c) Lower Neck Joint (Neck Pivot) - Ball Joint

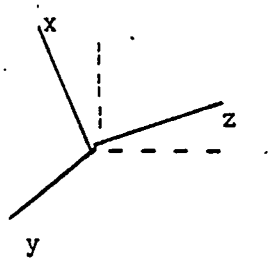

Geometric ref.
in upper torso

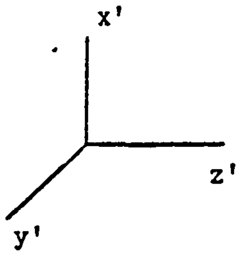

Joint ref.
in upper torso

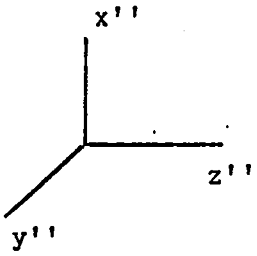

Joint ref.
in neck

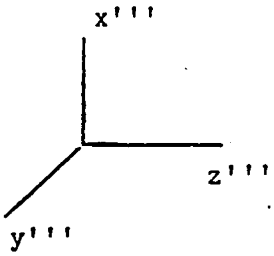

Geometric ref.
in neck

YPR1: yaw 0.0 degrees
pitch -20.0 degrees
roll 0.0 degrees

YPR2: yaw 0.0 degrees
pitch 0.0 degrees
roll 0.0 degrees

(d) Upper Neck Joint (Head Pivot) - Ball Joint

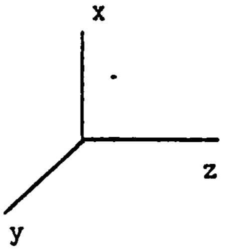

Geometric ref.
in neck

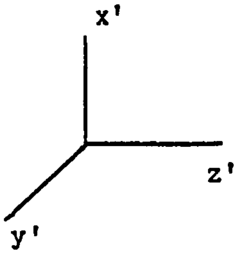

Joint ref.
in neck

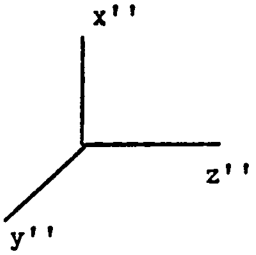

Joint ref.
in head

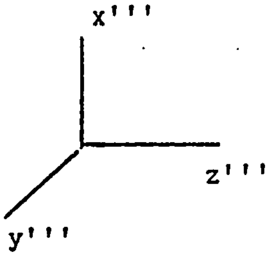

Geometric ref.
in head

YPR1: yaw 0.0 degrees
pitch 0.0 degrees
roll 0.0 degrees

YPR2: yaw 0.0 degrees
pitch 0.0 degrees
roll 0.0 degrees

(e) Left Hip - Euler Joint

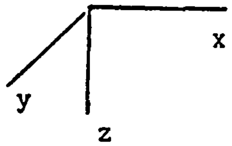

Geometric ref.
in lower torso

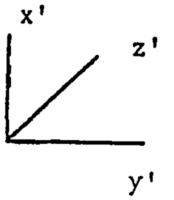

Joint ref.
in lower torso

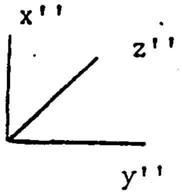

Joint ref.
in upper leg

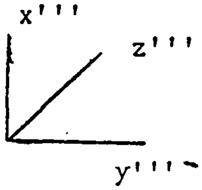

Geometric ref.
in upper leg

YPR1:	yaw	-90.0 degrees	YPR2:	yaw	0.0 degrees
	pitch	90.0 degrees		pitch	4.76 degrees
	roll	0.0 degrees		roll	0.0 degrees

Note: z' along y because of the pin in the femur
x' along -z because of the slot in the ball

Center of Symmetry:
YPR3: precession 27 degrees, soft stop due to flesh, hard stop due to plate
nutation -70 degrees, hard stop due to slot in ball
spin - hard stop due to slot in leg bone

Typical Values:

precession	nutation	spin	
0	-90	0	sitting with leg forward
90	-90	0	standing
0	0	0	impossible because of slot in ball (leg horizontal to the left)

This representation of the hips as Euler Joints assumes that the axis through the leg bone z" coincides with the axis of the pin z' at 0 degrees nutation, which is incorrect. A more accurate representation would require the definition of the Femur Assemblies E05 and E06 as separate segments with an Euler Joint at the hip with the spin axis locked and a pin joint at the leg bone; however, this refinement is not deemed necessary.

(f) Right Hip - Euler Joint

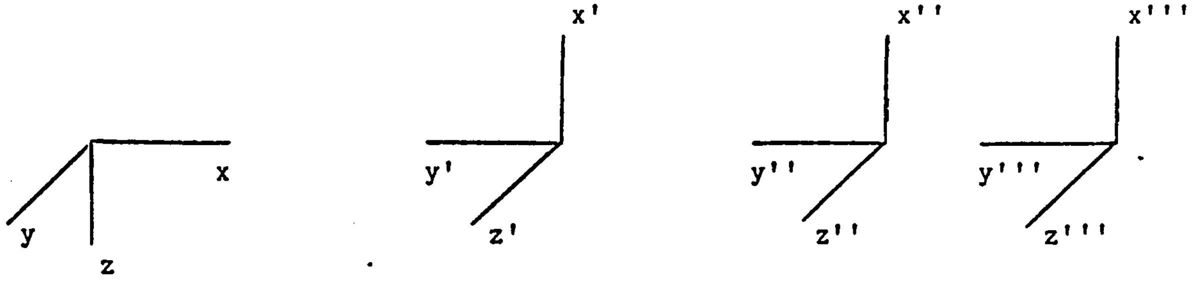

Geometric ref. in lower torso — Joint ref. in lower torso — Joint ref. in upper leg — Geometric in upper leg

YPR1:	yaw	90.0 degrees	YPR2:	yaw	0.0 degrees
	pitch	90.0 degrees		pitch	4.76 degrees
	roll	0.0 degrees		roll	0.0 degrees

Note: z' along y because of the pin in the femur
x' along -z because of the slot in the ball

Center of Symmetry:
YPR3: precession 27 degrees, soft stop due to flesh, hard stop due to plate
nutation 70 degrees, hard stop due to slot in ball
spin - hard stop due to slot in leg bone

Typical Values:

precession	nutation	spin	
0	90	0	sitting with leg forward
-90	90	0	standing
0	0	0	impossible because of slot in ball (leg horizontal to the right)

(g) Right Knee, Left Knee - Pin Joints

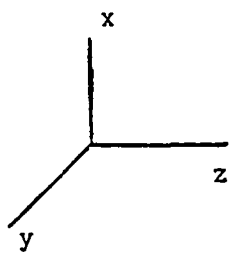

Geometric ref.
in upper leg

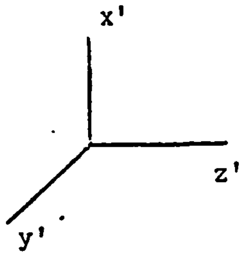

Joint ref.
in upper leg

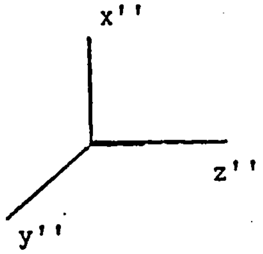

Joint ref.
in lower leg

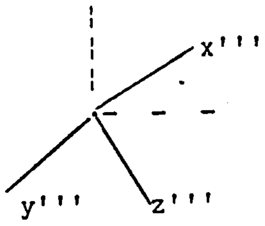

Geometric ref.
in lower leg

YPR1:	yaw	0.0 degrees	YPR2:	yaw	0.0 degrees
	pitch	0.0 degrees		pitch	43.0 degrees
	roll	0.0 degrees		roll	0.0 degrees

Center of Symmetry:

Pitch set to 43.0 degrees for center of symmetry.

Note that since the joint references are illustrated as aligned, the lower leg is pitched 43 degrees with respect to the upper leg. (The z axes of the geometric reference systems are parallel to the long bones of the legs.)

(h) Right Ankle, Left Ankle - Euler Joints, Spin Axes Locked

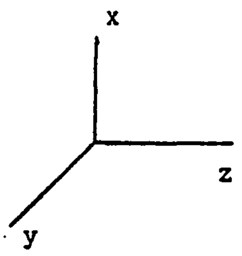

Geometric ref.
in lower leg

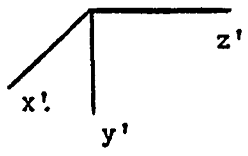

Joint ref.
in lower leg

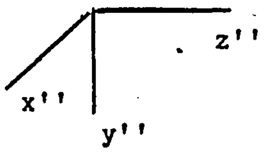

Joint ref.
in foot

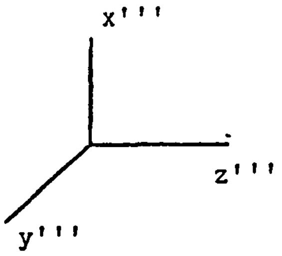

Geometric ref.
in foot

YPR1:	yaw	90.0 degrees	YPR2:	yaw	90.0 degrees
	pitch	0.0 degrees		pitch	0.0 degrees
	roll	-0.6 degrees		roll	0.0 degrees

Note: This representation assumes that the centerline of the pin allowing lateral motion of the foot intersects the centerline of the ankle pin allowing up-down motion. Positive precession characteristics for the left ankle should be like negative precession characteristics for the right ankle.

Center of Symmetry:

YPR3: precession 0.0 degrees, hard stop due to slot and bolt
nutation 79.0 degrees, hard stop due to slot and bolt
spin - axis locked

The z axes of the geometric reference systems are parallel to the long bones of the legs and the feet. The nutation axis of the Euler Joint (x' or x") is the flexure axis of the ankle, normally this is about 90.0 degrees, note that the center of symmetry for nutation is 79 degrees.

(i) Left Shoulder - Euler Joint, Spin Axis Locked

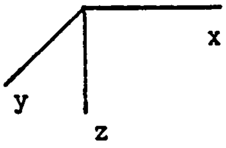

Geometric ref.
in upper torso

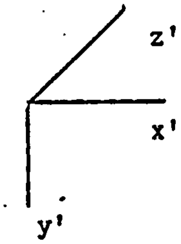

Joint ref.
in upper torso

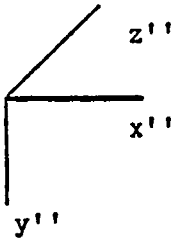

Joint ref.
in upper arm

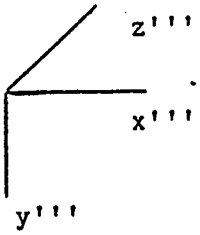

Geometric ref.
in upper arm

YPR1:	yaw	0.0 degrees	YPR2:	yaw	0.0 degrees
	pitch	0.0 degrees		pitch	0.0 degrees
	roll	90.0 degrees		roll	0.0 degrees

Note: This representation ignores the motion of the shoulder yoke C/10 and the clavicle C/17.

Center of Symmetry:

YPR3: precession 55.0 degrees, hard stop due to slot and bolt
nutation -65.0 degrees, limited by upper torso and clavicle
spin - permanently locked

Typical Values:

precession	nutation	spin	
0	-90	0	arm down along torso, z''' down, x''' forward
-90	-90	0	arm horizontal, z''' forward, x''' up
0	0	0	arm horizontal, z''' left, x''' forward

(j) Right Shoulder - Euler Joint, Spin Axis Locked

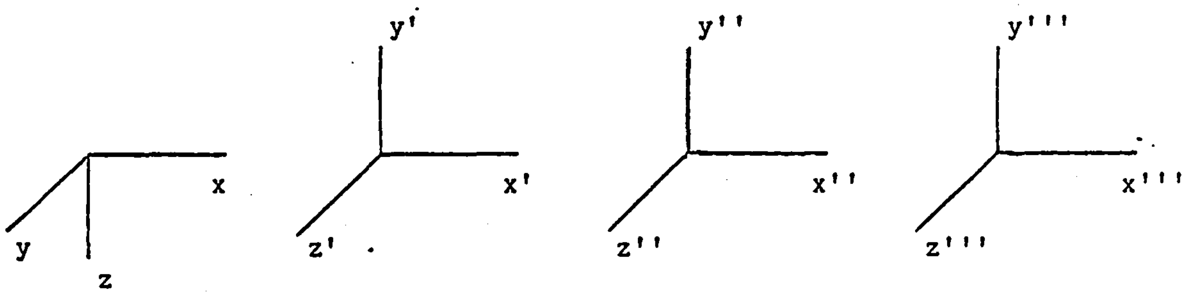

Geometric ref. in upper torso

Joint ref. in upper torso

Joint ref. in upper arm

Geometric ref. in lower arm

YPR1:	yaw	0.0 degrees	YPR2:	yaw	0.0 degrees
	pitch	0.0 degrees		pitch	0.0 degrees
	roll	-90.0 degrees		roll	0.0 degrees

Note: This representation ignores the motion of the shoulder yoke C/10 and the clavicle C/17.

Center of Symmetry:

YPR3: precession 55.0 degrees, hard stop due to slot and bolt
nutation 65.0 degrees, limited by upper torso and clavicle
spin - permanently locked

Typical Values:

precession	nutation	spin	
0	90	0	arm down along torso, z''' down, x''' forward
90	90	0	arm horizontal, z''' forward, x''' up
0	0	0	arm horizontal, z''' right, x''' forward

(k) Right Elbow, Left Elbow - Euler Joints, Spin Axes Locked

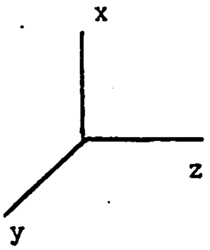

Geometric ref.
in upper arm

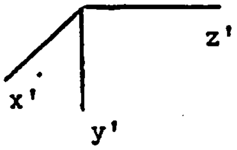

Joint ref.
in upper arm

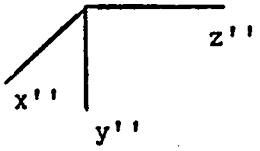

Joint ref.
in lower arm

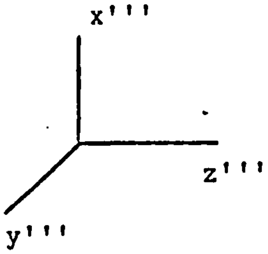

Geometric ref.
in lower arm

YPR1: yaw 90.0 degrees
pitch 0.0 degrees
roll 0.0 degrees

YPR2: yaw 90.0 degrees
pitch 0.0 degrees
roll 0.0 degrees

Center of Symmetry:

YPR3: precession -8.0 degrees, hard stop due to slot and bolt
nutation 70.0 degrees, hard stop due to slot and bolt
spin - axis locked

The z axes of the geometric reference systems are parallel to the long bones in the arms. The nutation axis of the Euler Joint (x' or x'') is the flexure axis of the elbow.

3.3 Analytical Model of Neck Using Two Joints

Dynamic resonance tests were performed on the neck to estimate the spring and viscous parameters for use in the CVS program. The neck is modeled as a single rigid segment connected to the head and the torso by ball joints. To model the behavior of such a system consider the system shown in Figure 3-1.

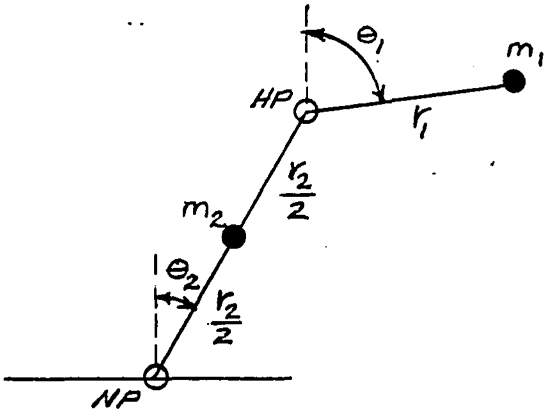

Figure 3-1 TWO-JOINT MODEL OF THE NECK

where: r_1 = distance from head-neck joint to c.g. of head,

r_2 = distance from head-neck pivot to neck-torso pivot (neck length),

m_1, m_2 = mass of head and neck, respectively,

I_1, I_2 = respective inertias about c.g. of segments,

k = linear spring coefficient,

v = linear viscous coefficient,

θ_1, θ_2 = respective angular displacements from vertical of the head pivot and neck pivot joints.

The linearized equations of motion of this sytem, ignoring gravity and the centrifugal forces are:

$$\begin{aligned} I_{11}\ddot{\theta}_1 + I_{12}\ddot{\theta}_2 &= k(\theta_2 - \theta_1) + v(\dot{\theta}_2 - \dot{\theta}_1) \\ I_{12}\ddot{\theta}_1 + I_{22}\ddot{\theta}_2 &= -k(2\theta_2 - \theta_1) - v(2\dot{\theta}_2 - \dot{\theta}_1) \end{aligned} \tag{3.1}$$

where: $I_{11} = I_1 + m_1(r_1)^2$

$I_{12} = m_1 r_1 r_2 \cos(\theta_2 - \theta_1)$

$I_{22} = I_2 + 0.25 m_2 (r_2)^2 + m_1 (r_2)^2$

Although this is a fourth-order system, the response to an initial angular displacement may be approximated by considering only the dominant mode of oscillation. This response is given by the equation:

$$\theta_1(t) = \theta_0 e^{-at}[\cos(bt) + \frac{a}{b}\sin(bt)] \tag{3.2}$$

where: $a = \frac{v}{2I}$

$b^2 = \frac{k}{I} - a^2$

$I = I_{11} + I_{12} + 0.5I_{22} + \sqrt{(I_{11} + I_{12})^2 + (I_{12} + 0.5I_{22})^2}$

θ_0 = initial angular displacement of the head.

The response as given by equation 3.2 is a damped sinusoid. The value of a and b may be estimated from the experimental data by measuring the frequency and the amplitudes of the peaks. The peaks (positive and negative) occur when $bt = k\pi$ and a is proportional to the logarithm of the ratio of the peaks, i.e.,

$$a = \frac{b}{\pi} \ln\left(\frac{P_k}{P_{k+1}}\right)$$

The numerical data used in the computations is:

$r_1 = \sqrt{(0.37)^2 + (1.39)^2} = 1.438$ inches

$r_2 = 4.37$ inches

$m_1 = 9.67$ lbs.

$m_2 = 1.82$ lbs.

$I_1 = 0.2562$ lb-in-sec^2

$I_2 = 0.01179$ lb-in-sec^2

Using this data the value of I is computed as 1.3445 lb-in-sec^2. From the experimental data the frequency was estimated as 5.656 Hertz and the peak amplitudes were as follows:

k	peak amplitude	ratio
0	20.0	
		1.408
1	14.2	
		1.352
2	10.5	
		1.312
3	8.0	
		1.454
4	5.5	
		1.375
5	4.0	
	AVERAGE RATIO	1.380

Using the numerical data in the formulas yields the estimates:

$b = 2(5.656)\pi = 35.538$

$a = 2(5.656)\ln(1.380) = 3.6434$

$v = 0.171$ in-lb per degree per second

$k = 29.95$ in-lb per degree

3.4 Estimate of the Flexure Spring Function for the Lumbar Spine

Static loading tests of the lumbar spine are described in Section 2.3.8, and the results are plotted in Figure 2.27. Representing the spine as a single segment connected to the upper torso and to the lower torso by ball joints, the geometry of the system is illustrated in Figure 3.2 below.

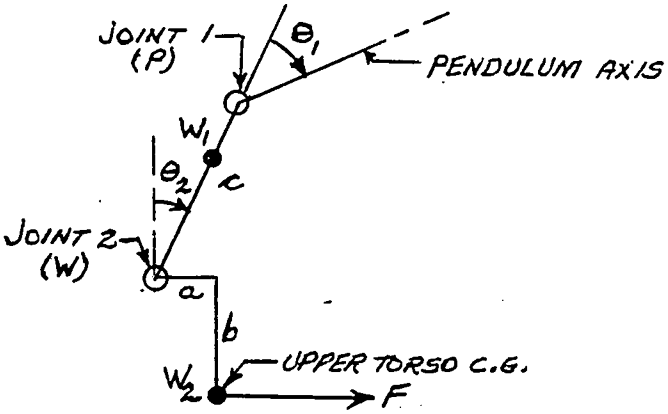

Figure 3-2 TWO-JOINT MODEL OF THE SPINE

where: c = distance between joint 1 and joint 2 (length of spine)

b = vertical distance from joint 2 to c.g. of upper torso

a = horizontal distance from joint 2 to c.g. of upper torso

w_1 = weight of spine

w_2 = weight of upper torso

θ_1 = angle at joint 1

θ_2 = angle at joint 2

F = measured force (horizontal and through c.g. of upper torso).

The static balance equations of the system are:

$$T_1 = -aw_2 + (w_2 + 0.5w_1)c \sin \theta_2 + F(b + c \cos \theta_2)$$

$$T_2 = -aw_2 + bF$$

It is reasonable to assume that the characteristics at each of the joints are the same. It is also assumed that the torque versus angle relation of each of the joints can be expressed as a cubic function of the angle as follows:

$$T(\theta) = A_1\theta + A_2\theta^2 + A_3\theta^3$$

In the experiment the force F required to hold the torso was measured as a function of the total flexure angle θ where:

$$\theta = \theta_1 + \theta_2 - \theta_0$$

The angle θ_0 is introduced in this expression to account for the fact that the angle θ was set to zero when the force was zero.

Using the experimental data of F versus θ, the values of the coefficients, A_j, were determined by a least square fit procedure for four cases. The results are given below.

		COEFFICIENT		
Case No.		A_1 in-lb/rad.	A_2 in-lb/rad.^{2}	A_3 in-lb/rad.^{3}
1	(Cubic fit to all of the data)	1175	985	1435
2	(Linear fit to all of the data)	1205	0	0
3	(Cubic fit to positive data only)	1198	1014	1035
4	(Linear fit to positive data only)	1526	0	0

3.5 Dynamic Torsion Model of the Neck or Spine

Section 2.3.7 describes torsional tests of the neck and the results are tabulated in Table 2.3. Consider the sketch of the test setup shown in Figure 3-3 below where the neck is modeled as a rigid body with two joints.

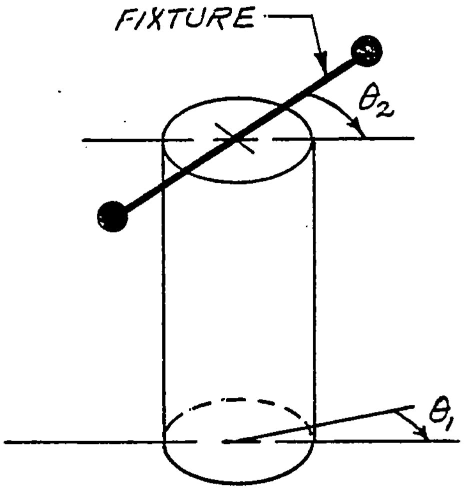

Figure 3-3 MODEL OF DYNAMIC NECK TORSION TEST

The torsional equations of motion for this system are:

$$I_2\ddot{\theta}_2 = k(\theta_1 - \theta_2) + v(\dot{\theta}_1 - \dot{\theta}_2)$$
$$I_1\ddot{\theta}_1 = -k(\theta_1 - \theta_2) - v(\dot{\theta}_1 - \dot{\theta}_2) - k\theta_1 - v\dot{\theta}_1$$

where: I_1 = inertia of the neck

I_2 = inertia of the fixture

θ_1 = angle of the rigid neck

θ_2 = angle of the fixture

k = torsional spring constant at the joints

v = viscous constant at the joints

The characteristic equation of this linearized system is a quartic which may be factored into the two quadratics:

$$s^2 + \frac{(sv + k)}{I}$$
$$s^2 + (sv + k)\,\frac{I}{I_1 I_2}$$

where: $I = I_2 + 0.5I_1 + \sqrt{I_2^2 + (0.5I_1)^2}$

When the inertia of the neck is small compared to the inertia of the fixture, the value of I is approximately twice the inertia of the fixture and the dominant mode of oscillation is given by the first of the two quadratics above. The values of k and v may be estimated from the formulas:

$$k = I\,(2\pi f)^2$$
$$v = 4Idf$$

where: d = amplitude decay factor = natural logarithm of the ratio of successive peaks

f = oscillation frequency

Using the experimentally measured values shown in Table 2-3, the values of k and v are:

Fixture Inertia lb-in-sec^2	f Hertz	d	k lb-in/radian	v lb-in-sec/radian
0.183	10.5	0.36	1593	5.5
0.810	4.7	0.29	1413	8.8
1.437	3.2	0.29	1162	10.7

Since the inertia of the head about the z axis was measured as 0.164, the values calculated from the data obtained with the smallest fixture inertia (i.e., 0.183 lb-in-sec^2) are perhaps the best to use for the model. The large variation of these results suggests that the neck cannot be simply modeled as a rigid body with two joints having linear characteristics.

4.0 SUBSYSTEMS TESTS AND SIMULATIONS

The predictive capability of the CVS computer program was first investigated by simulating dynamic pendulum impact tests performed on the head/neck and the upper torso/lower torso subassemblies of the dummy. The program subroutines associated with the computation of forces produced from contacts with an air bag were also checked in simulations of static tests of a small pre-inflated air bag of ellipsoidal shape. In this section, the various tests are briefly described and results from simulations of these relatively simple physical systems are presented for comparison with measured responses.

4.1 Head/Neck Pendulum Impact

4.1.1 Description of Tests

Dynamic tests of the dummy head/neck subassembly were performed with the compound pendulum impact apparatus used for determining compliance of the head response with FMVSS 208 Part 572 requirements. A sketch of the test configuration showing the principal components and dimensions is given in Figure 4-1. In the physical experiment, the pendulum was released from a pre-determined height so as to achieve the desired velocity upon contact with the honeycomb arresting block. Crushing of the honeycomb absorbed-most of the system energy as the pendulum was stopped and then moved in the reverse direction slightly during unloading of the honeycomb. The head/neck assembly, however, continued to swing forward and backward in an arc which resulted in multiple load/unload cycles of the pendulum against the crushed face of the honeycomb.

The test matrix included replicate tests with the head oriented at 0 (facing forward), 45, 90 and 180 degrees. The pendulum impact velocity was nominally 23 ft./sec. for most of the tests, but response data for the zero degree head orientation were also obtained in impacts at 14.9 ft./sec. Data

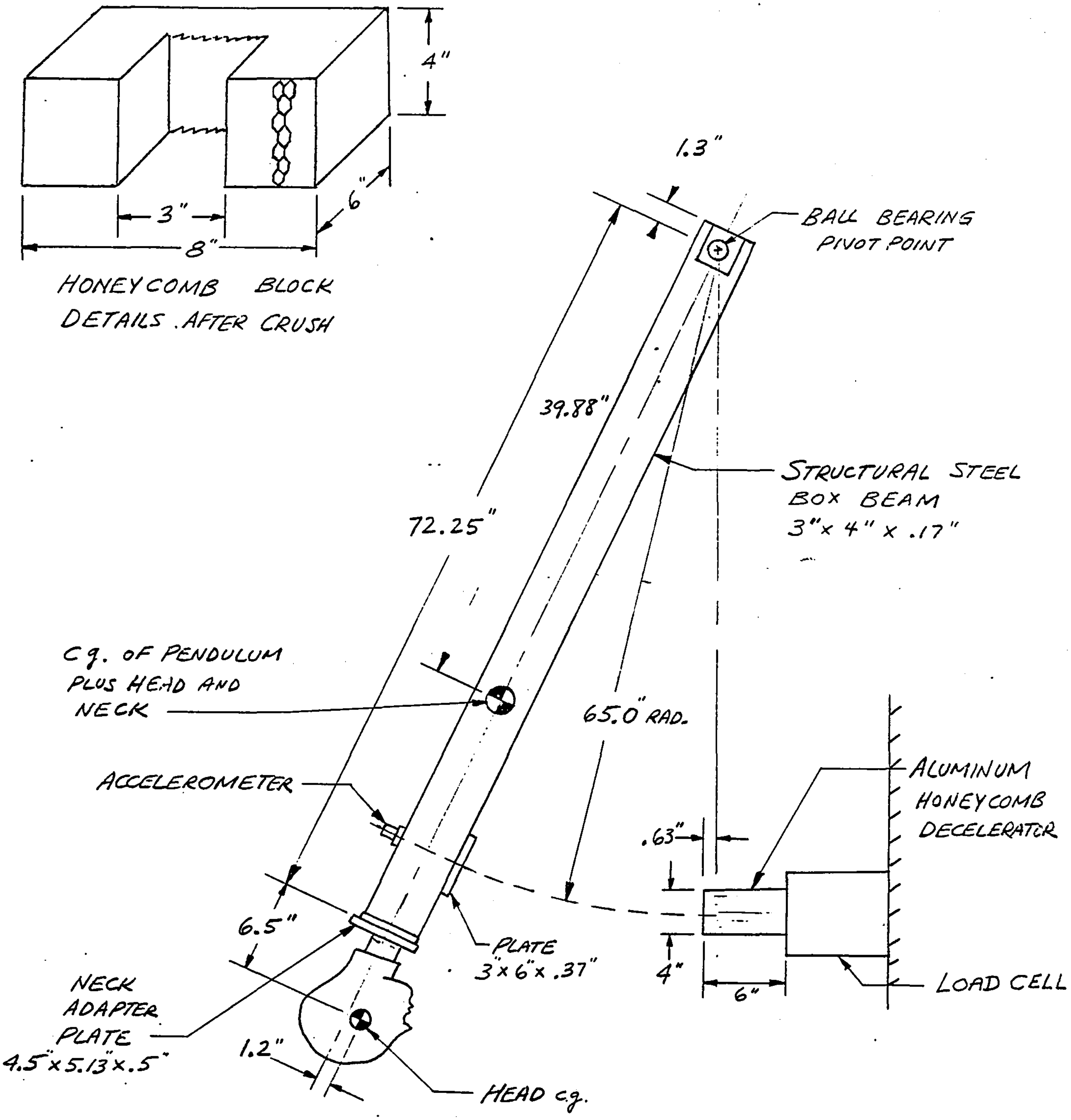

Figure 4-1 HEAD-NECK DYNAMIC TEST CONFIGURATION

recorded in the tests included time histories of the pendulum X component of linear acceleration, honeycomb reaction force, X, Y and Z components of head acceleration and the head motion as measured by the ϕ, θ and radius potentiometers illustrated in Figure 2-23. Typical data from tests performed with the head oriented at the various angles are contained in Appendix A. The motion of the head in these tests may be seen in the photographs of Figure 4-2 which were obtained with a sequence camera.

4.1.2 Simulation of Tests

The purpose of the CVS simulations of the head-neck pendulum tests was to verify the measured parameters of the head-neck configuration and the modelling assumptions used to simulate the rubber neck structure of the Part 572 dummy. The program input required to simulate the head-neck pendulum test can be divided into four categories:

1) Control Information
    - Date, run number, and identification.
    - Time duration and integrator controls to produce a simulation time of 120 msec.
    - Basic configuration of 3 segments, 3 joints and no vehicle deceleration.
    - Segment symmetry input to restrict all motion to X-Z plane.
    - Tabular time history control of angular acceleration, velocity and position of all 3 segments, and of joint parameters for all 3 joints.

2) Measured experimental geometrical data
    - One plane surface input describing contact surface of honeycomb structure such that initial contact occurs when the pendulum is in its vertical position.
    - Honeycomb force deflection function.

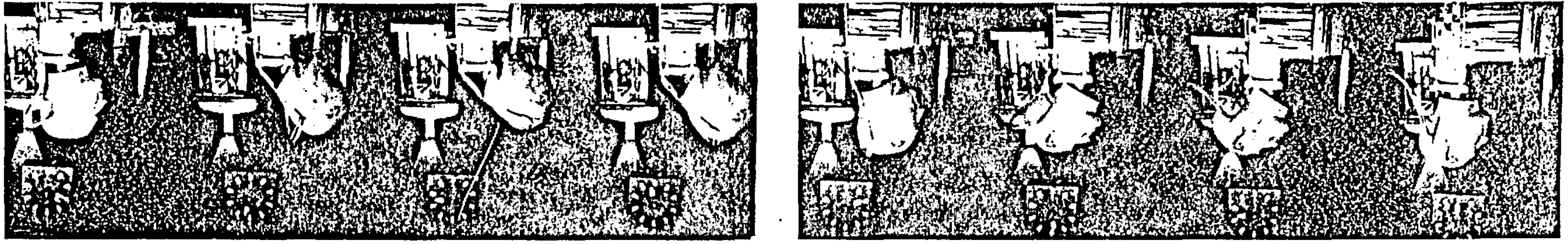

HEAD ORIENTED AT 0°

HEAD ORIENTED AT 45°

HEAD ORIENTED AT 90°

HEAD ORIENTED AT 180°

Figure 4-2 HEAD MOTION IN PENDULUM IMPACT TESTS

- One segment-plane contact between the pendulum segment and honeycomb plane.
- Initial conditions for zero time (pendulum in vertical position) assuming inertial origin is at pendulum pivot point requires Z-component of linear position and X-component of linear velocity for the pendulum (reference segment), 180 degree roll for the neck and head, and Y-component of angular velocity of all 3 segments. All other values are zero.
- Tabular time history control of linear acceleration, velocity and position of the accelerometer on the pendulum, and neck c.g. and of the accelerometer in the head.

3) Measured experimental data of dummy segments
    - Segment weights, moments of inertia, contact ellipsoid semiaxes and center locations.
    - Joint location and angular orientation with respect to adjacent segments.

4) Variable or unmeasurable experimental data to be determined
    - Joint flexural and torsional spring characteristics.
    - Joint viscous characteristics.
    - Coefficient of friction of pendulum against honeycomb structure.
    - R and G factors controlling the unloading and reloading characteristics of the force-deflection for the pendulum and honeycomb structure.

Two types of simulations were performed. The first were full-drop simulations where time zero represents initial release of the pendulum. These require a simulation time of 750 to 1250 msec, depending on the drop height and resulting striking velocity, of which only about the final 150 msec are of primary interest. The second type were simulation of only the impact phase where time zero is the time of initial impact of the pendulum against the aluminum honeycomb. Most of the initial input parameters for the second type were determined from the geometry of the test apparatus. However, the full-drop simulations were used to determine the relative angular orientation and velocity of the head and neck with respect to the pendulum at initial impact. For the pendulum itself, the initial angular orientation is determined by the geometry of the test apparatus and the initial striking velocity is obtained experimentally by measuring the time necessary for the pendulum accelerometer to traverse a fixed distance just prior to impact. The full-drop simulations showed that the increase in velocity while traversing this small fixed distance was about 2 in./sec.

It was discovered that the time to impact and the initial striking velocity could be varied considerably by changing the joint viscous coefficient of the pendulum pivot. The value used in early simulations was found to be too high and hence was reduced by a factor of 10 as a result of full-drop simulations.

All further simulations were of the shorter-impact-only type, where time zero represents the time of initial impact. The inputs to these simulations fall into various categories as follows:

1. The geometry of the test apparatus as depicted in Figure 4-1. The initial pitch of the pendulum was determined (both analytically and experimentally) to be 2.7°.

2. The initial segment orientations and velocities determined from the experimentally-measured striking velocity and from the full-drop simulations.

3. The force-deflection characteristics of the aluminum honeycomb decelerator. The initial loading and assumed constant force vs. deflection portions were determined from the graphical output of the component tests. The abrupt unloading and reloading characteristics, the R (energy absorption) and G (deflection) factors,

are difficult to measure experimentally and, therefore, were examined in the matrix of simulation runs performed.

4. The characteristics of the head and neck segments consisting of:

   a) Those that can be measured experimentally and
   b) Those modeling assumptions to simulate the rubber neck structure.

Several simulations were run to establish the proper values of the R (energy absorption) and G (deflection) factors to define the unloading force-deflection function used for the pendulum contact with the aluminum honeycomb. The CVS program is based on the assumption that this unloading function is a non-negative, concave quadratic between the point of maximum delfection, d_{max}, and the point of complete unloading, d_g, determined by R and G. Inconsistent input values for R and G can cause this unloading function to default to a straight line between d_{max} and d_g or a quadratic with zero slope at d_g. In both cases the value of G is preserved, but the value of R may be changed (higher or lower) from that specified by input.

For simulations of tests performed at a pendulum impact velocity of 23 ft./sec., an input value of $R = 0.01$ constrained the value of G to lie between 0.973 for a zero slope quadratic and 0.982 for the straight line to satisfy the value of R. CVS simulations produced highly non-linear variations of the resulting impact force of the pendulum against the honeycomb structure for varying values of the G factor within this tight range.

Results of computer simulations are presented in Figure 4-3 where they are compared with responses measured in a test with the head oriented at zero degrees (see Figure 4-2 and Appendix A). Figure 4-3(a) presents plots of the pendulum force exerted upon the aluminum honeycomb in the experimental component test and for simulations that used values of 0.970, 0.973 and 0.982 for the G factor. Figure 4-3(b) presents a comparison of experimental and

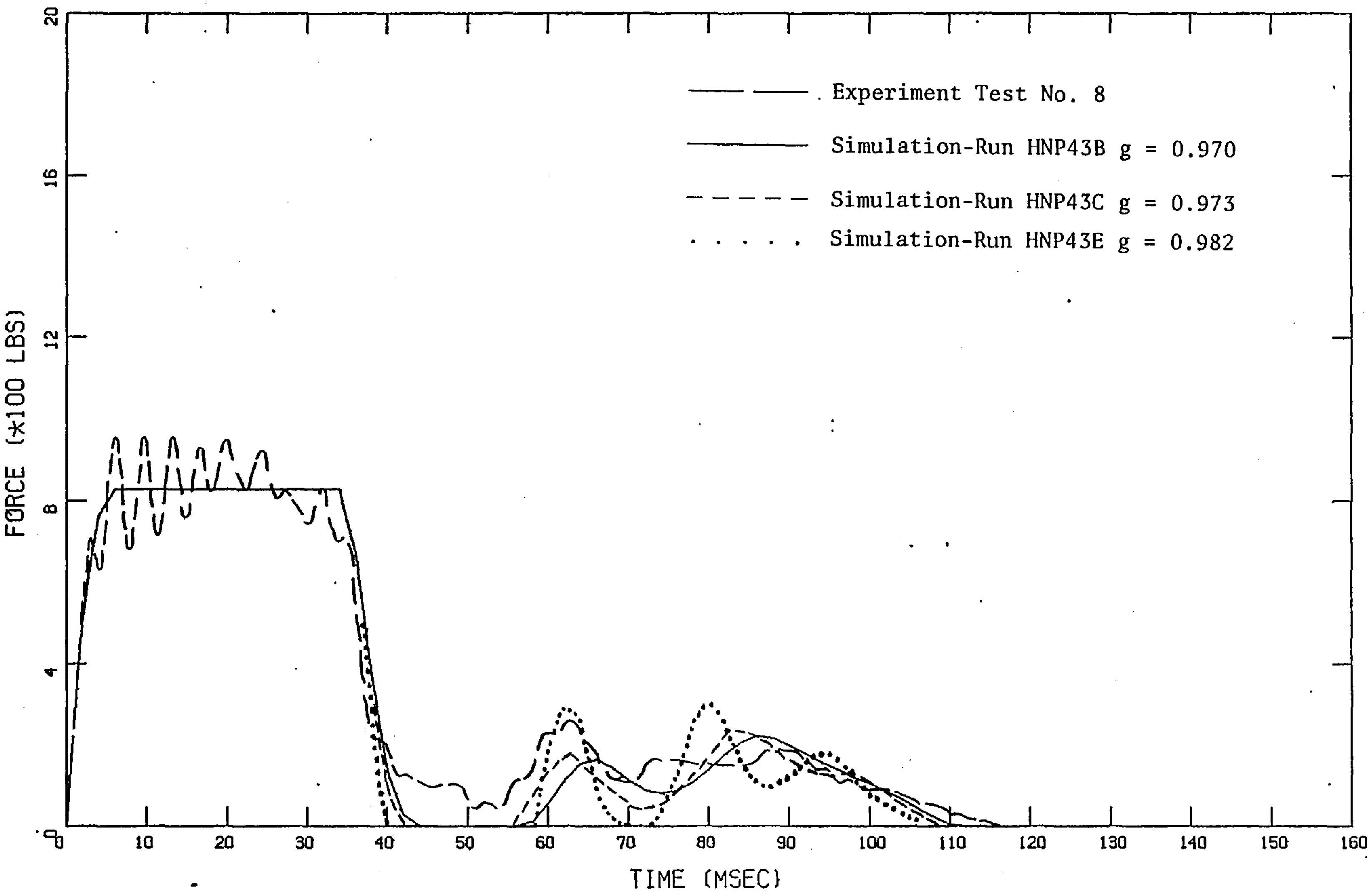

(a) HONEYCOMB TARGET FORCE

Figure 4-3 COMPARISON OF MEASURED AND SIMULATED RESPONSES - HEAD/NECK PENDULUM IMPACT TEST

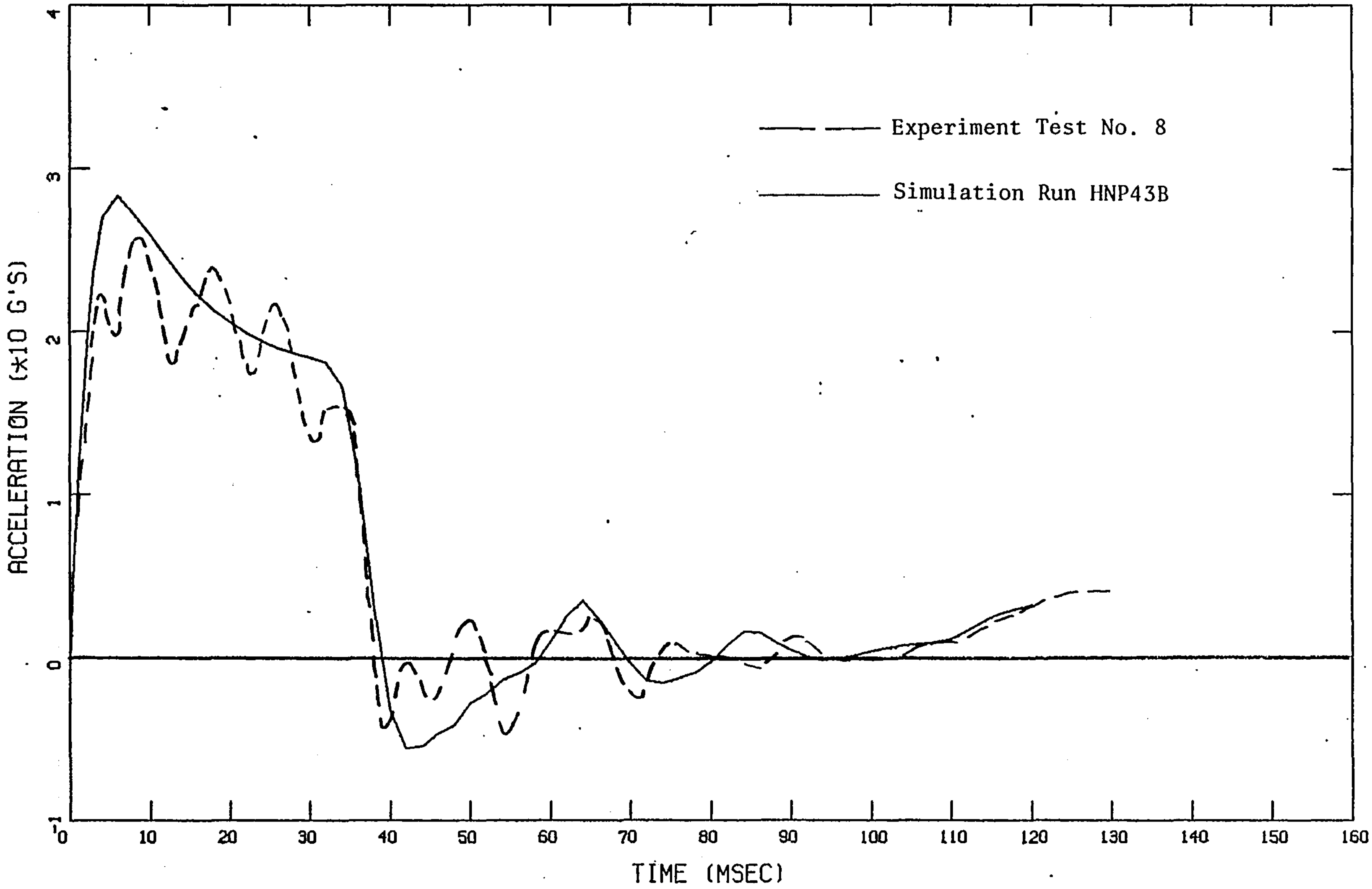

(b) PENDULUM X ACCELERATION

Figure 4-3 (cont'd)

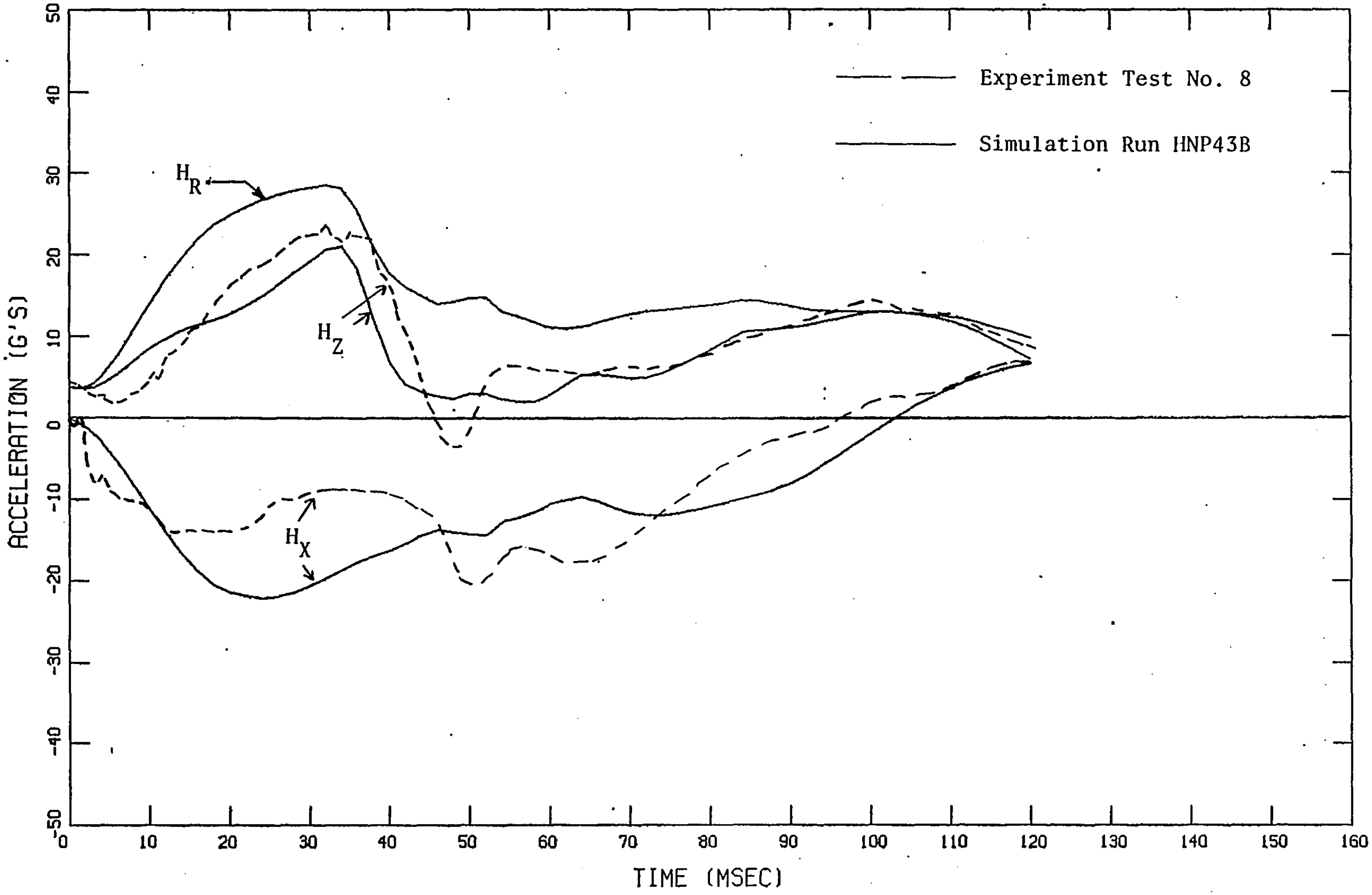

(c) HX,HZ AND HR ACCELERATIONS

Figure 4-3 (cont'd)

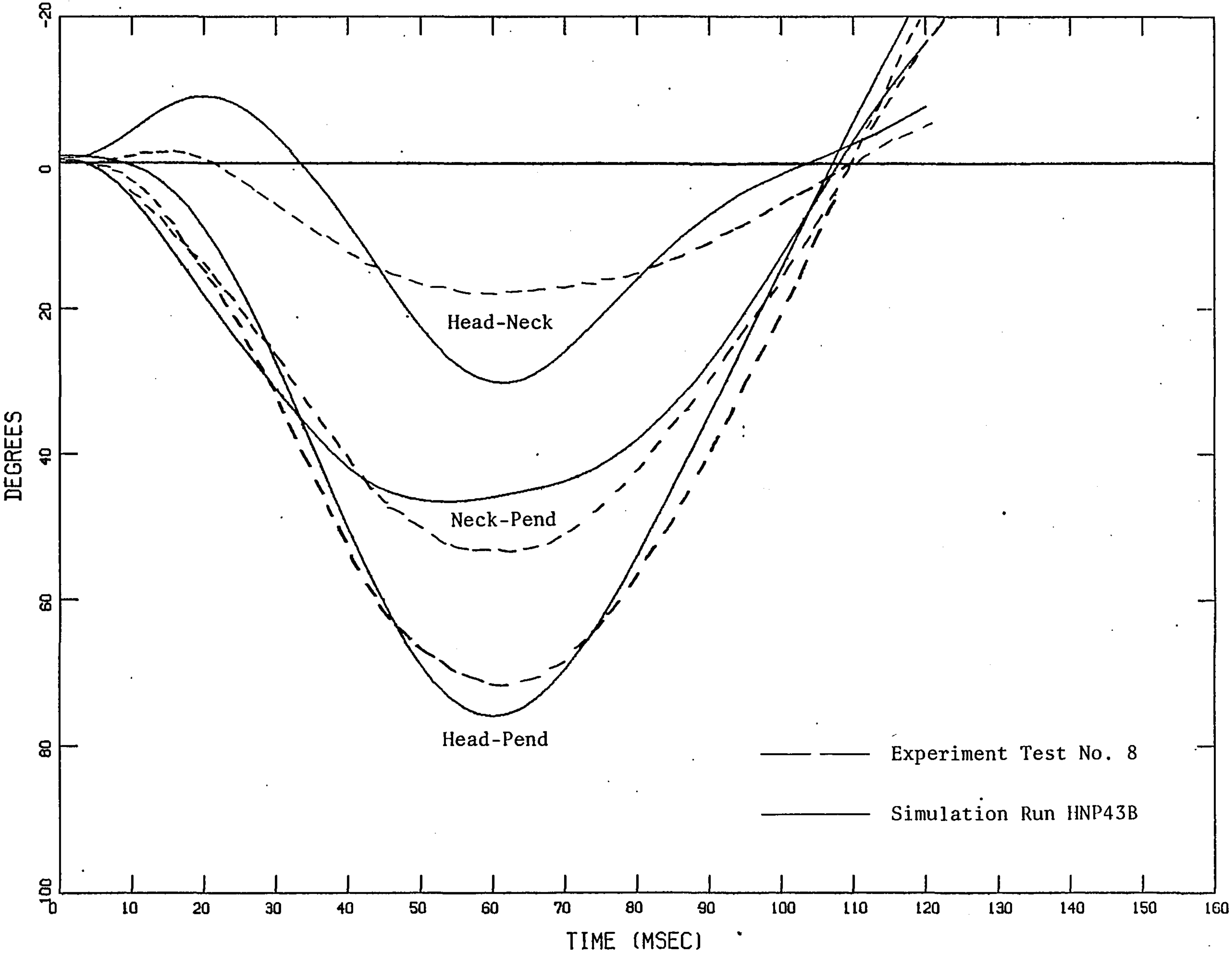

(d) ANGLES

Figure 4-3 (cont'd)

simulation results (with G = 0.970) for the pendulum X acceleration. The 400 Hertz oscillation that may be noted in the first 30 milliseconds of the experimental data is probably due to a mechanical oscillation of the test apparatus which was not modeled, hence does not appear in the simulations which had a load limit of about 800 pounds for the honeycomb. The 100 Hertz oscillation that appears in the experimental data is due to the mechanical vibration of the six foot pendulum. The simulation treated the pendulum as a rigid body so this vibration did not occur in the simulations.

Figure 4-3(c) compares the experimental and simulated X and Z components of head acceleration, and Figure 4-3(d) presents the relative pitch of the neck with respect to the pendulum, the head to the neck and the head to the pendulum. An examination of these figures shows some differences between the measured and simulated head and neck motions. Part of this difference is undoubtedly due to improper modeling assumptions for the rubber neck structure of the Part 572 dummy, i.e., the rubber neck is modeled as a single rigid segment with ball joints connecting it to the head and upper torso. Another part of the difference in Figure 4-3(d) is because of a difference in the geometry of the instrumentation and the simulation, i.e., the angles θ and ϕ (illustrated in Figure 2-23) are not precisely the same as the angles between the head and the neck and between the neck and the torso for the single segment, two-joint rigid body model of the neck used in the simulation.

4.2 Torso Pendulum Impact

4.2.1 Description of Tests

The methodology and apparatus for measurement of the torso response as influenced by the dynamic flexion behavior of the lumbar spine was similar to that used for the head/neck tests. The test configuration consisted of the upper torso, lower torso (including the abdominal insert) and part of the upper legs mounted in an inverted position on an aluminum adapter plate attached to the lower end of the pendulum. The lower torso was rigidly fastened to the adapter plate with bolts through the end of both femur shafts and at the attachment to the pelvis accelerometer cavity flange. The hip joints were also tightened to further prevent movement of the lower torso which could influence the motion of the upper torso. The abdominal insert was secured with a small cord to maintain it properly positioned in the lower torso. The test configuration is shown in the photographs of Figure 4-4 and dimensional information is given in Figure 4-5.

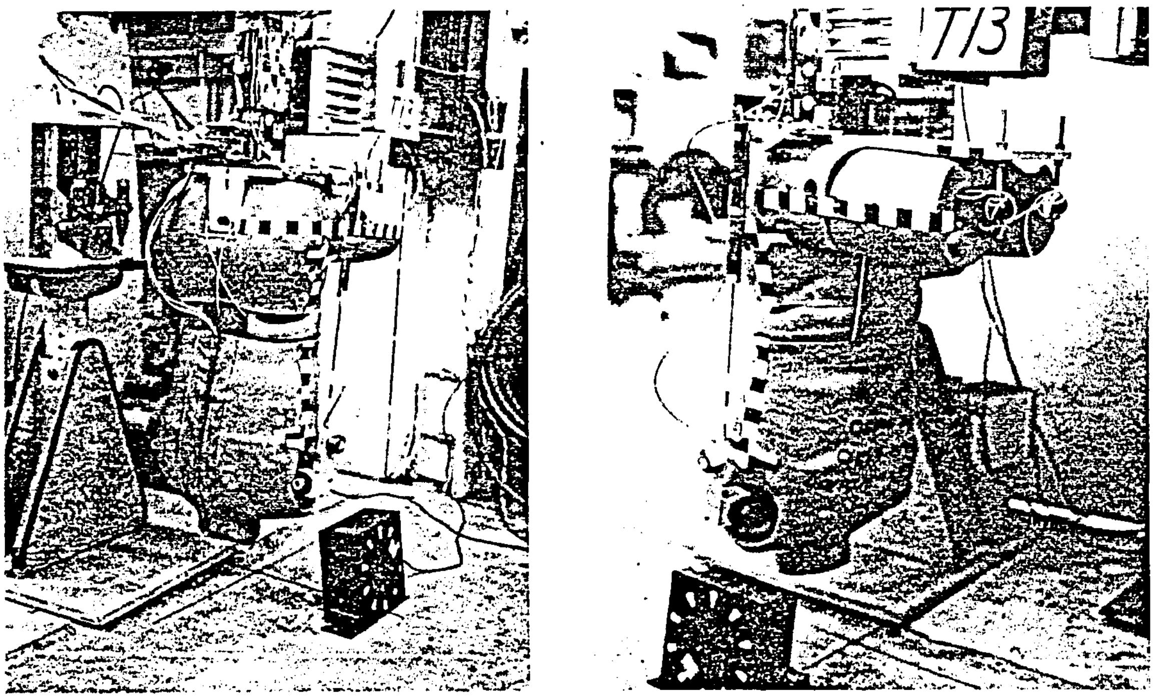

Figure 4-4 TORSO PENDULUM IMPACT TEST APPARATUS

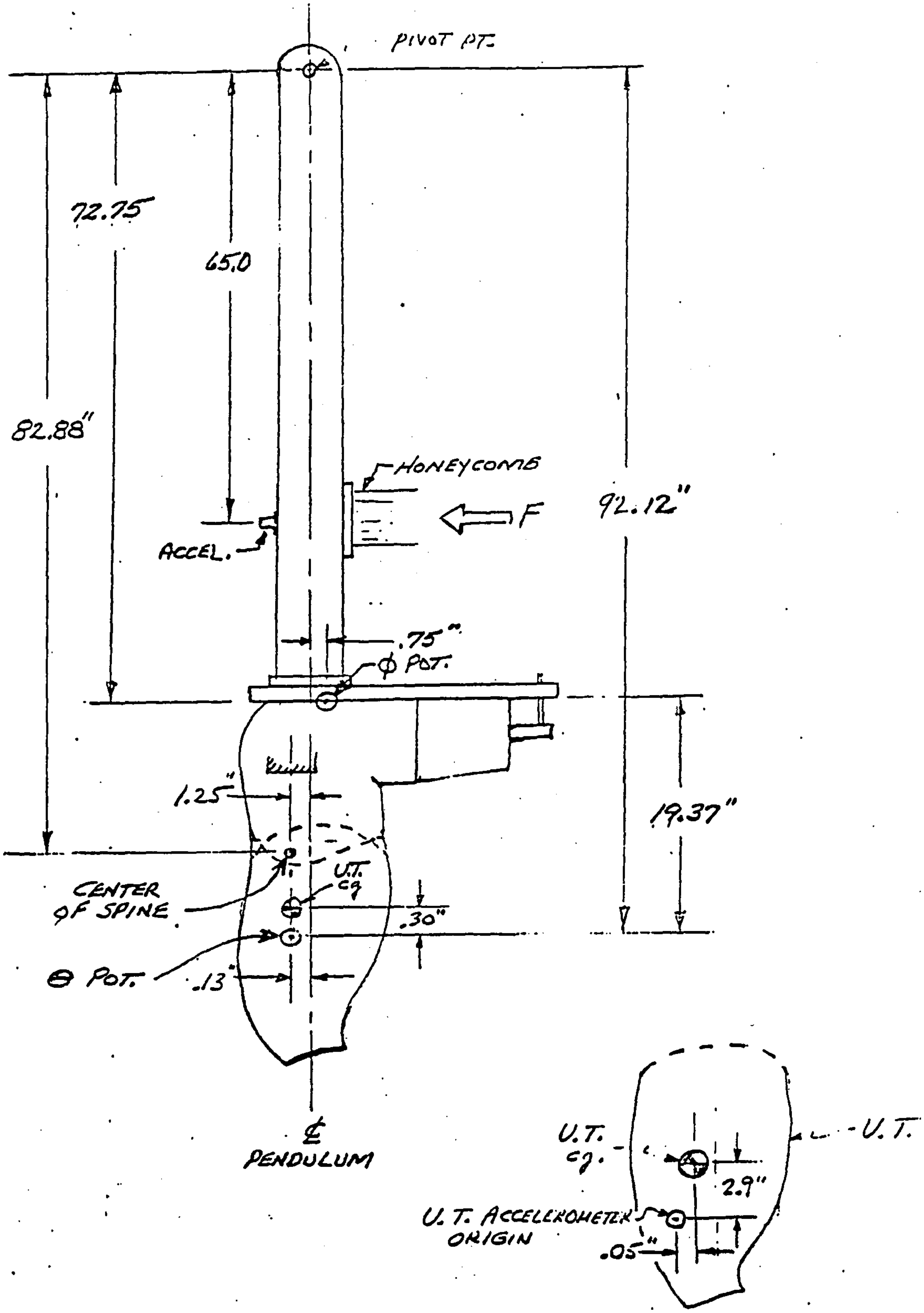

Figure 4-5 GEOMETRY OF TORSO DYNAMIC FLEXION TEST CONFIGURATION

Data measured in the tests included the pendulum acceleration, honeycomb energy absorber reaction force, X, Y and Z components of the upper torso acceleration, and the motion of the upper torso relative to the pendulum measured by the θ and ϕ rotary potentiometers and another linear potentiometer that recorded changes of the distance between the rotary potentiometers. Replicate tests were performed at each of three nominal impact velocities (7, 12 and 13.5 ft./sec.) obtained by varying the height from which the pendulum was released.* The motion of the torso during impact of the pendulum at a velocity of 13.6 ft./sec. is shown in the sequence photos of Figure 4-6.

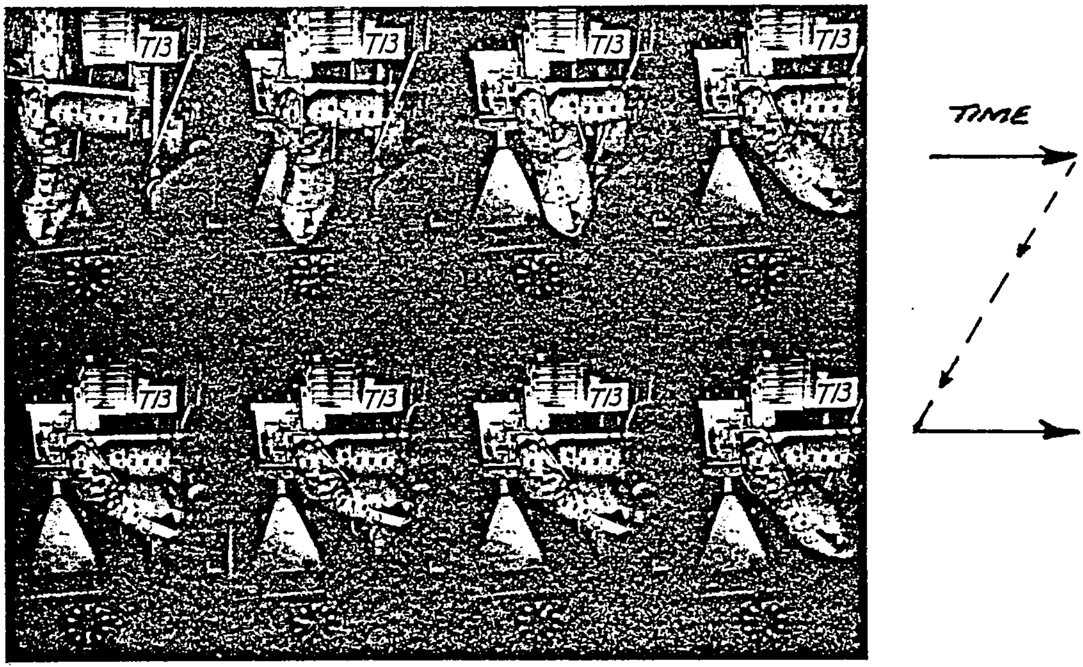

Figure 4-6 UPPER TORSO FLEXION DURING PENDULUM IMPACT AT 13.6 FT./SEC.

A second series of dynamic torso tests was performed in which the rubber lumbar spine was replaced with a tubular steel member of the same size and which was provided with a single pin joint at the midpoint. Thus, in contrast with the rubber spine, the location of the spine joint was accurately

---

*Different honeycomb configurations were also used for each group of tests to accommodate the different energy absorption requirements.

known and remained fixed in these tests which facilitated modeling of the physical system. The pin-joint spine was slightly heavier (4.25 lb.) than the rubber spine and permitted the upper torso to rotate up to 76 and 81 degrees in flexion and hyperextension, respectively, before engaging hard metal-to-metal stops.

Responses measured in the torso pendulum impact tests are presented in the following subsections where they are compared with results obtained from computer simulations of the experiments.

4.2.2 Simulations of Tests with Rubber Spine

To simulate the torso pendulum tests using the CVS program the model illustrated in Figure 4-7 was used.

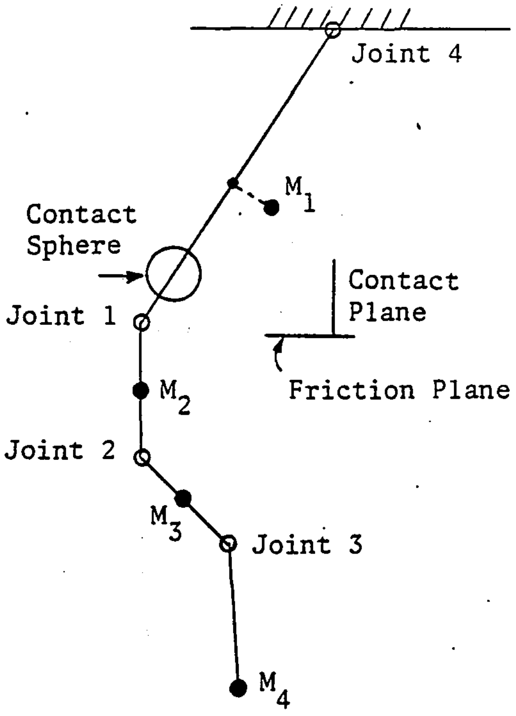

Figure 4-7 MODEL OF TORSO-PENDULUM TEST

The model consists of four segments and four joints where:

Segment	
1	Pendulum
2	Lower Torso
3	Center Torso (Lumbar Spine)
4	Upper Torso

Joint	
1	Connects Lower Torso to Pendulum, a locked joint
2	Connects Lower Torso to Center Torso
3	Connects Center Torso to Upper Torso
4	Connects Pendulum to inertial reference, a pinned joint

A sphere with a radius of 2.5 inches was attached to the pendulum and allowed to contact a plane attached to inertial reference. A force-deflection characteristic based on the measured characteristics of the honeycomb material was assigned to this contact. An R (energy absorption) factor of 0.01, a G (deflection) factor of 0.954, and a friction coefficient of 0.25 were used. The characteristics of the honeycomb are plotted in Figure 4-8.

The success of the simulation is dependent on the proper modeling of the lumbar spine which is a flexible rubber cylinder about 3 inches in diameter and 5.4 inches long. It was modeled by two joints located equidistant from the geometric center of the spine segment and having identical characteristics. In the sequence of simulations that were performed several runs were made to determine an appropriate value of the linear spring constant. In the tests the total angular motion of the upper torso had a magnitude of 60° and a period of about 1/2 second. These values are directly related to the spring constant. Increasing the spring constant will decrease the magnitude and shorten the period. For a simple oscillation we have $\theta + (k/\phi)\theta = 0$ where k is the spring constant and ϕ is the inertia. The solution for an initial angular velocity of θ_0 is:

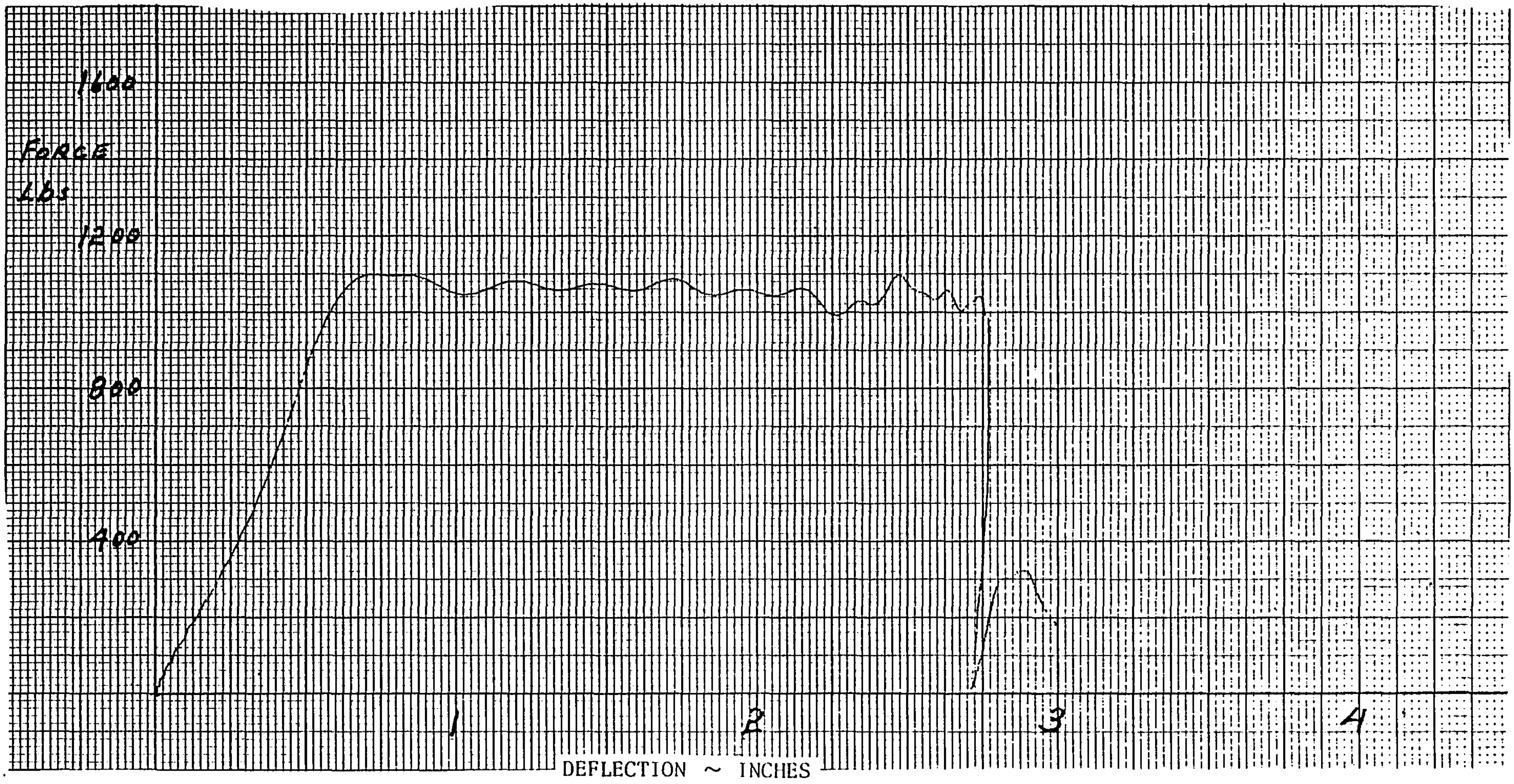

Figure 4-8 FORCE-DEFLECTION CHARACTERISTIC OF ALUMINUM HONEYCOMB

$$\theta = \dot{\theta}_o \frac{\sin \Omega t}{\Omega}$$

where $\Omega = \sqrt{k/\phi}$

Thus, one would expect the magnitude and the period to vary as $1/\sqrt{k}$. A small amount of viscous damping and coulomb friction was assumed.

Initial Conditions

Initially all segments were pitched -54° with zero velocity. The system then was allowed to swing about the pivot. Contact with the honeycomb occurred when the pendulum (segment 1) was pitched -2.6° at a time of 747 ms. If there were no such contact, zero pitch would have occurred at 750 ms. This may be calculated by considering the equation of a pendulum.

$$(\phi + mr^2)\ \ddot{\theta} = -mrg \sin \theta$$

where
ϕ inertia
m mass
r position of cg relative to pivot
g gravity

The solution of this equation is an elliptic function. The period T is given by the equation:

$$T = \frac{1}{\Omega} \int_0^{\pi/2} \frac{d\phi}{\sqrt{1 - \sin^2 \frac{\theta_o}{2} \sin^2 \phi}}$$

where θ_o is the initial angle and

$$\Omega = \sqrt{\frac{mrg}{\phi + mr^2}}$$

The four-segment model has the following values.

$w = mg = 180.37$ lbs.
$\phi = 389.55$ lb-in-sec^2
$r = 62.60$ in.
$\theta_o = 54°$

Thus, $\Omega = 2.2549$ rad/sec
$K = 1.663$ (from tables of Elliptic Integrals)
$T = K/\Omega = 738$ ms.

The computer run had a value of 750 ms. The difference is due to the fact that the simulation model is a compound pendulum. The position and velocity of the segments at 740 ms (just prior to impact) were used as initial conditions for the subsequent parameter studies. All of the model input values are given in the computer printout presented in Appendix B.

Discussion of Results

The following experimental measurements are compared to the simulation results in Figure 4-9 through 4-14:

1 Load cell force
2 Pendulum x acceleration
3 Chest X acceleration
4 Chest Z acceleration
5 Total angle of chest (upper torso) relative to pendulum

The following points are worth noting in these figures:

- Figure 4-9 - Load Cell Force for Runs 16 and 17

G (deflection) factors of 0.954 and 0.934 were used in Runs 16 and 17, all other parameters were the same. Note the difference in timing of the first rebound. Run 16 peaked at 108 ms. and run 17 at 118 ms. A change in G affects the loading and unloading behavior of the force deflection function used to approximate the honeycomb.

The most obvious discrepancy is the magnitude of the peaks which is about 700 lbs. for the predictions compared to 300 lbs. in the experiment. It was obvious that there was some energy loss that we were not representing in the simulation. To simulate an additional loss of energy, a friction plane which would contact the sphere attached to the pendulum was added to the model. This contact was specified to have a constant normal force of 0.01 lbs. and a friction coefficient of 10000 to produce a friction force of 100 lbs. The results of two simulation runs (Runs 24 and 25) are discussed in the ensuing paragraphs.

- Figure 4-10 - Load Cell Force for Runs 24 and 25

Run 24 used a force-deflection function for the honeycomb that produced a constant force of 1060 lbs. This combined with the 100 lbs. friction produced a total deceleration force of 1160 lbs.

The force-deflection function used for Run 25 was modified by subtracting 100 lbs. from the constant portion of the function to produce a total force of 1060 lbs.

Note that the magnitudes of the first rebound peak in these runs are more in agreement with the experiment than the results of earlier simulations. The timing is better for Run 25 than it is for Run 24. However, the second rebound which occurs at 180 ms. and the third rebound which occurs at 230 ms. are not simulated. The factor controlling the timing of these rebounds is not known, but it appears that the length of the center torso (segment 3) may have a significant effect since the high frequency mode of oscillation of the compound pendulum will be most directly affected by the length.

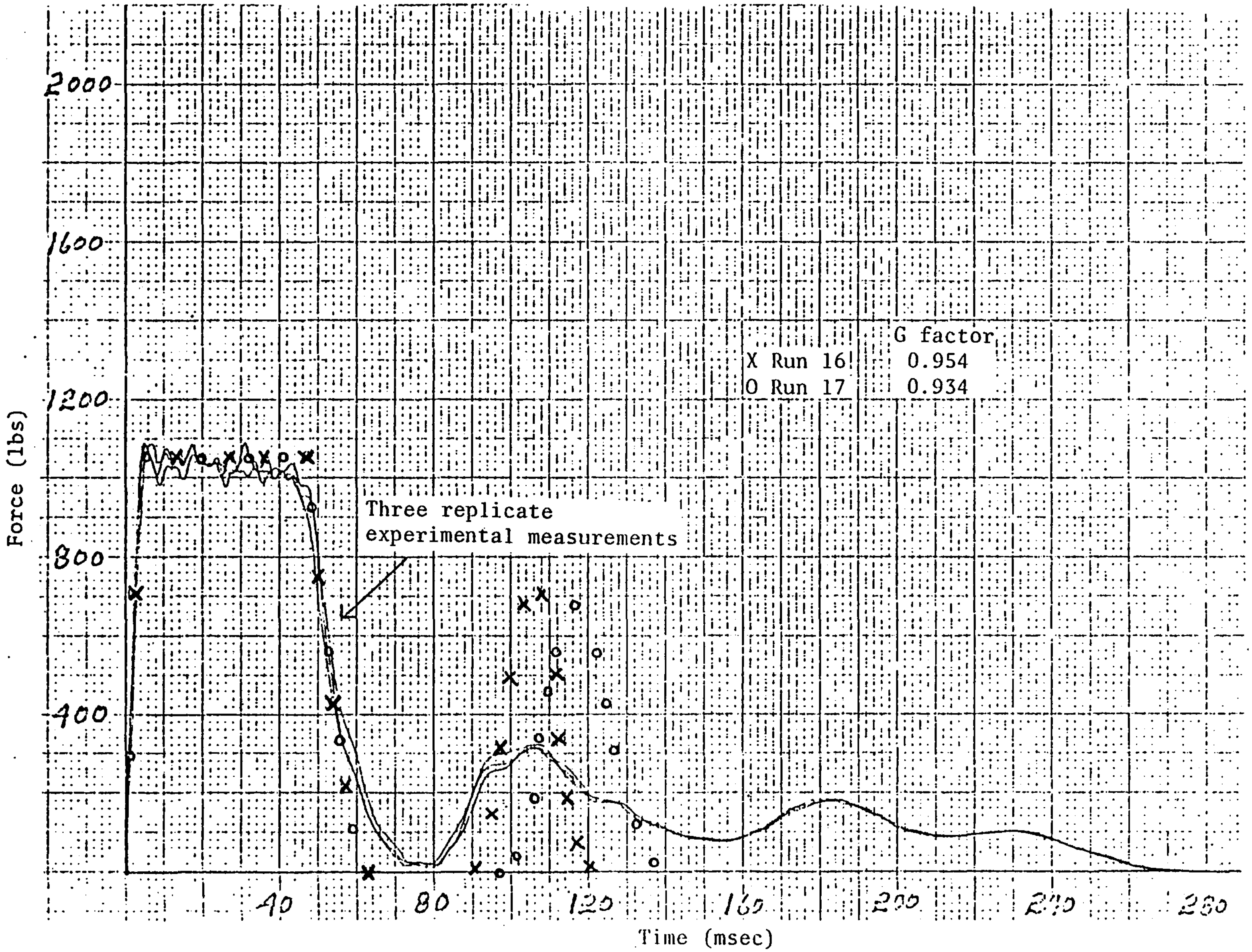

Figure 4-9 LOAD CELL FORCE COMPARISON FOR SIMULATION RUNS 16 AND 17

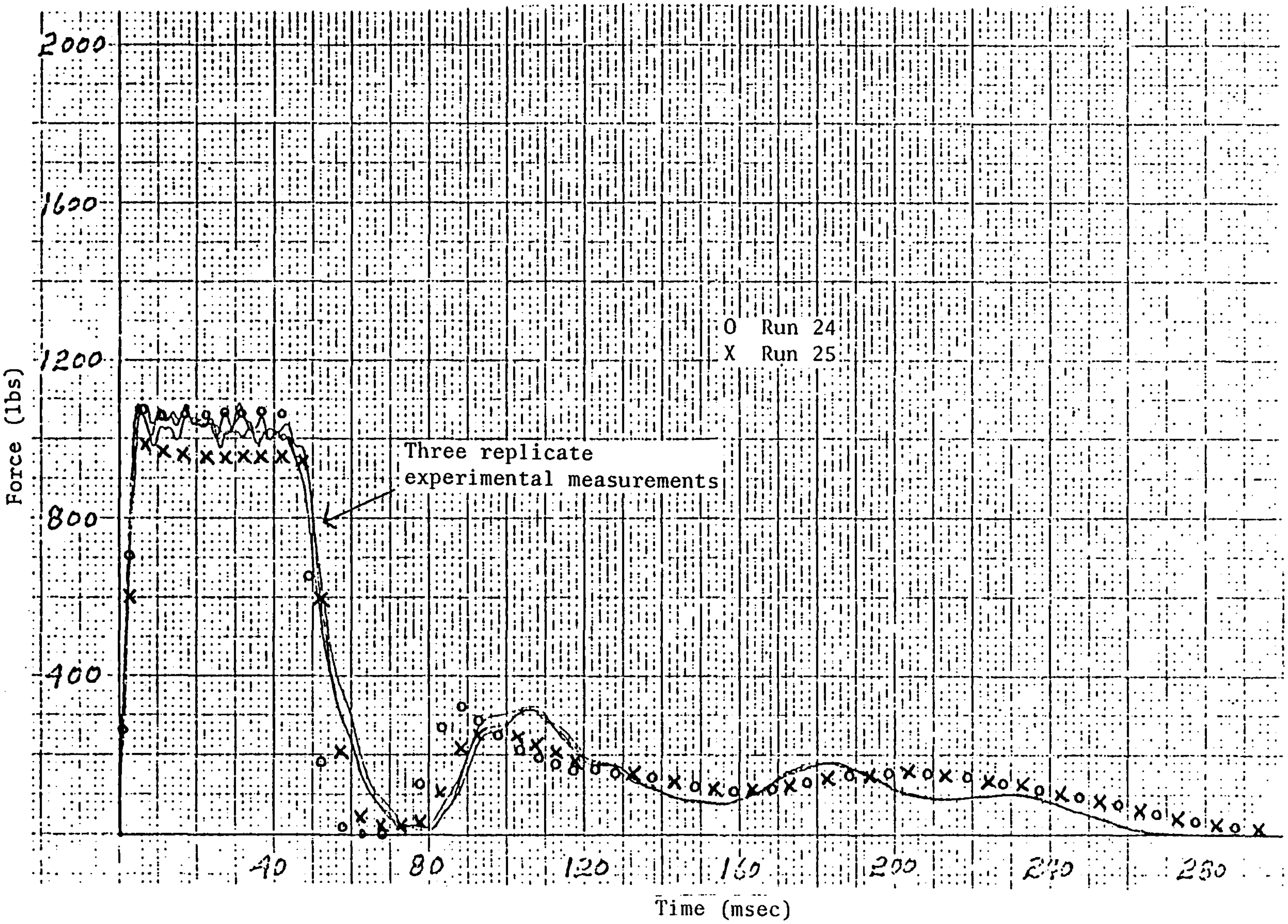

Figure 4-10 LOAD CELL FORCE COMPARISON FOR SIMULATION RUNS 24 AND 25

Although this friction absorbed approximately the correct amount of energy we are not sure that it is the explanation. If it were truly a friction component normal to the surface of the honeycomb caused by the pendulum contacting the deformed side surfaces of the honeycomb, it should produce a negative force at the load cell when the pendulum is moving out of the honeycomb. This is not apparent in the experimental results.

- Figure 4-11 - Pendulum X Acceleration for Runs 24 and 25

The most noticeable difference between the runs is the timing of the first unloading (at about 50 ms.). Run 25 is better than Run 24, but neither of the simulations showed the high frequency oscillation that is apparent in the experimental data. This is to be expected since it is believed that this oscillation is the first bending mode of the pendulum which is not modeled in the simulations where the pendulum is considered a rigid body.

- Figure 4-12 - Chest X Acceleration for Runs 24 and 25

The results for these runs are essentially identical on this plot. The high frequency oscillation in the first 40 ms. of the experimental data is thought to be due to a resonance in the chest cavity of the dummy.

It is apparent that the experimental results between 30 and 70 ms., 0-70 ms. and after 140 ms. are not simulated properly. The reason for this is not known, but it may be related to the length of the center torso.

- Figure 4-13 - Chest Z Acceleration for Runs 24 and 25

Oscillation in the chest cavity is very noticeable at the start of this plot. In the 40 to 70 ms. interval, Run 25 is definitely better than Run 24. From 100 to 180 ms. the simulation is in excellent agreement with the experiment. The reason for the discrepancy in the interval between 70 and 100 ms. and also beyond 180 ms. is not known.

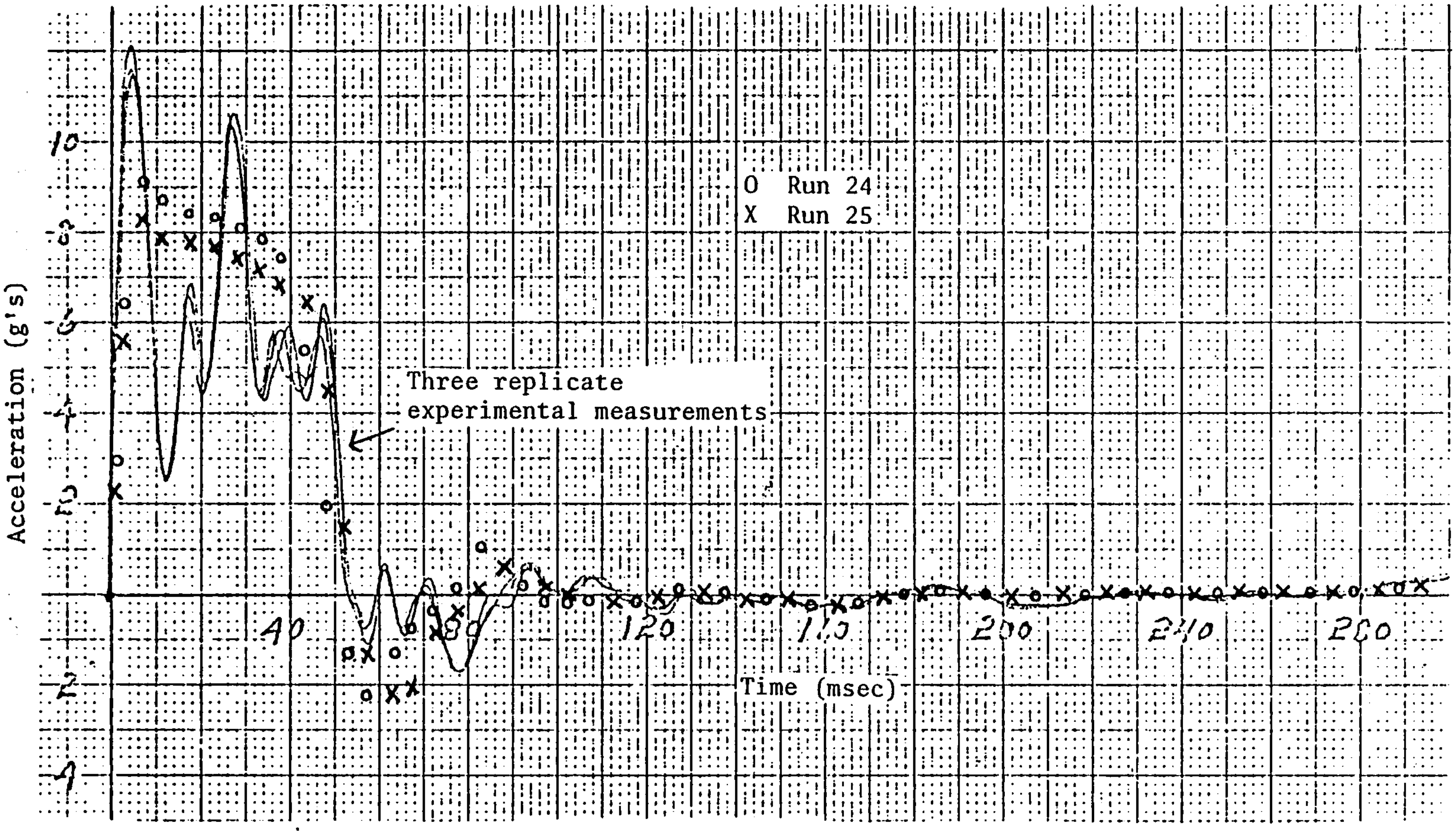

Figure 4-11 PENDULUM X ACCELERATION

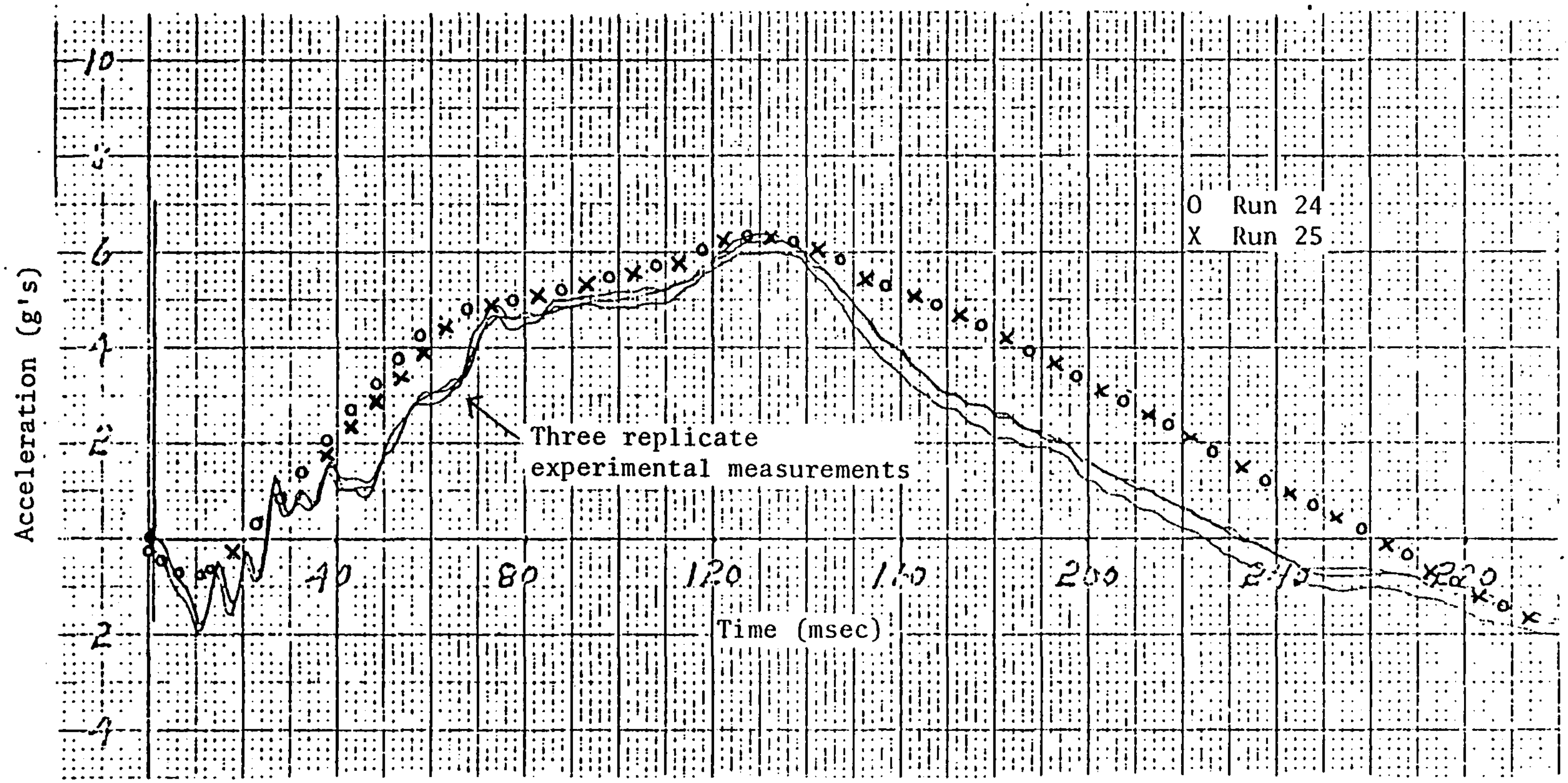

Figure 4-12 CHEST X ACCELERATION

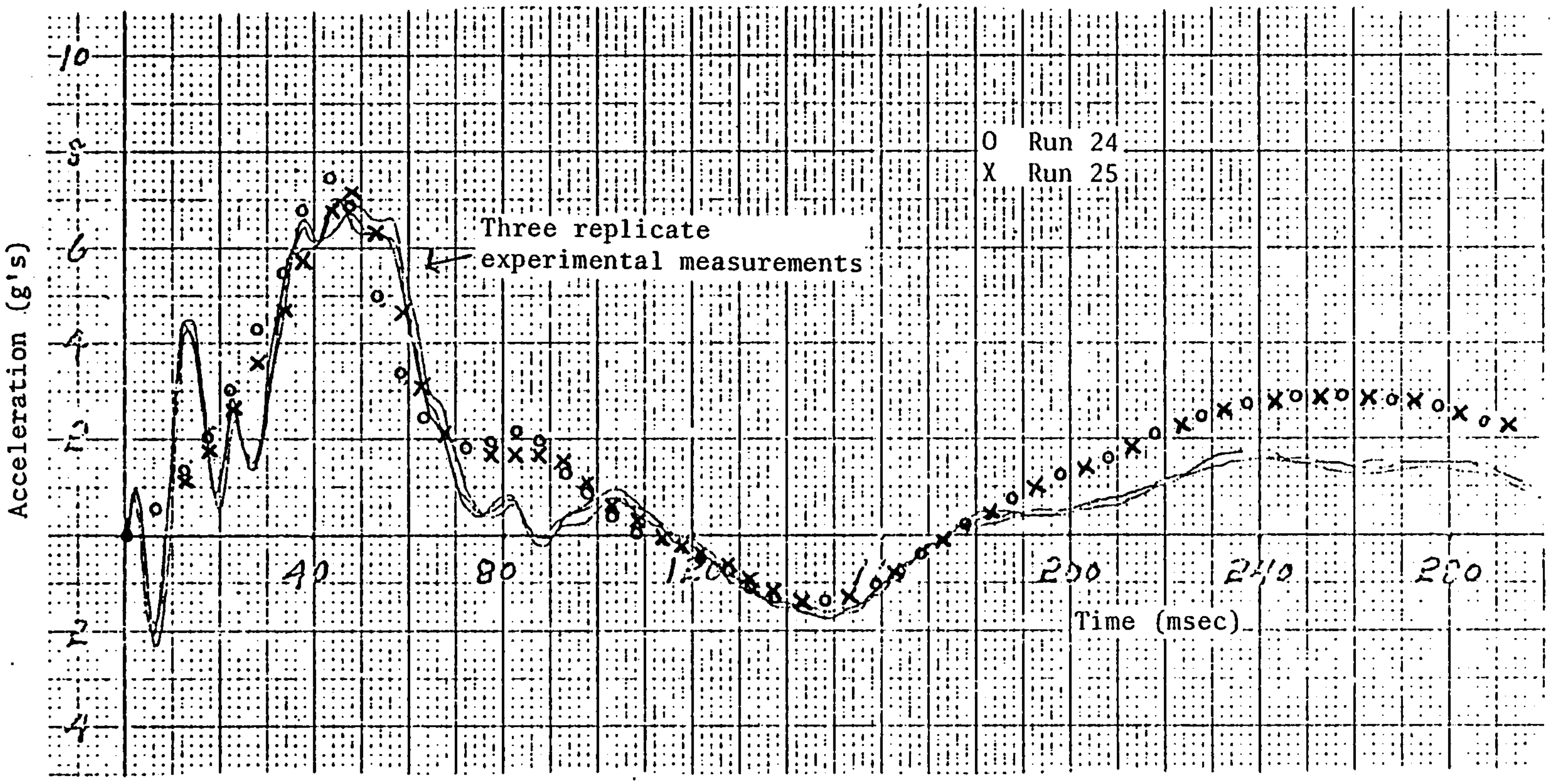

Figure 4-13 CHEST Z ACCELERATION

- Figure 4-14 - Total Angle Chest Relative to Pendulum for Runs 24 and 25

The agreement between the experiment and the simulations is quite good. There is no appreciable difference in the two runs. Perhaps an even better correlation could be achieved by tuning the spring constant, the viscous friction and the coulomb friction at the joints.

Examination of the first 40 ms. shows the existence of a higher mode of oscillation in the experiment that does not appear in the simulation. This may be affected by the length of the center torso or may be an indication that the center torso must be modeled with more than one segment and two joints.

4.2.3 Simulation of Tests With Single Pin Spine

Although data were obtained in tests of the pin joint spine at three different pendulum impact speeds (4, 6.5 and 8.1 ft./sec.), only the 6.5 ft./sec. velocity test condition was simulated with the CVS in a series of eight computer runs. The model and values of the input parameters used to characterize the physical system were developed by a researcher independent of those who simulated the tests of the torso with the rubber spine. Hence, even though the test hardware, except for the dummy spine, was the same for all tests, the inputs for the simulation runs differ due to differences in certain assumptions that were necessary in modeling the system. For example, computations of the inertial properties of the pendulum to correct for hardware added for mounting the dummy, and of the lower torso segment to account for the effects of including part of the upper legs, involved assumptions that could lead to different values of the input parameters by the different investigators.

The test configuration was modeled as a system of three segments and three joints for all but the last computer run as follows:

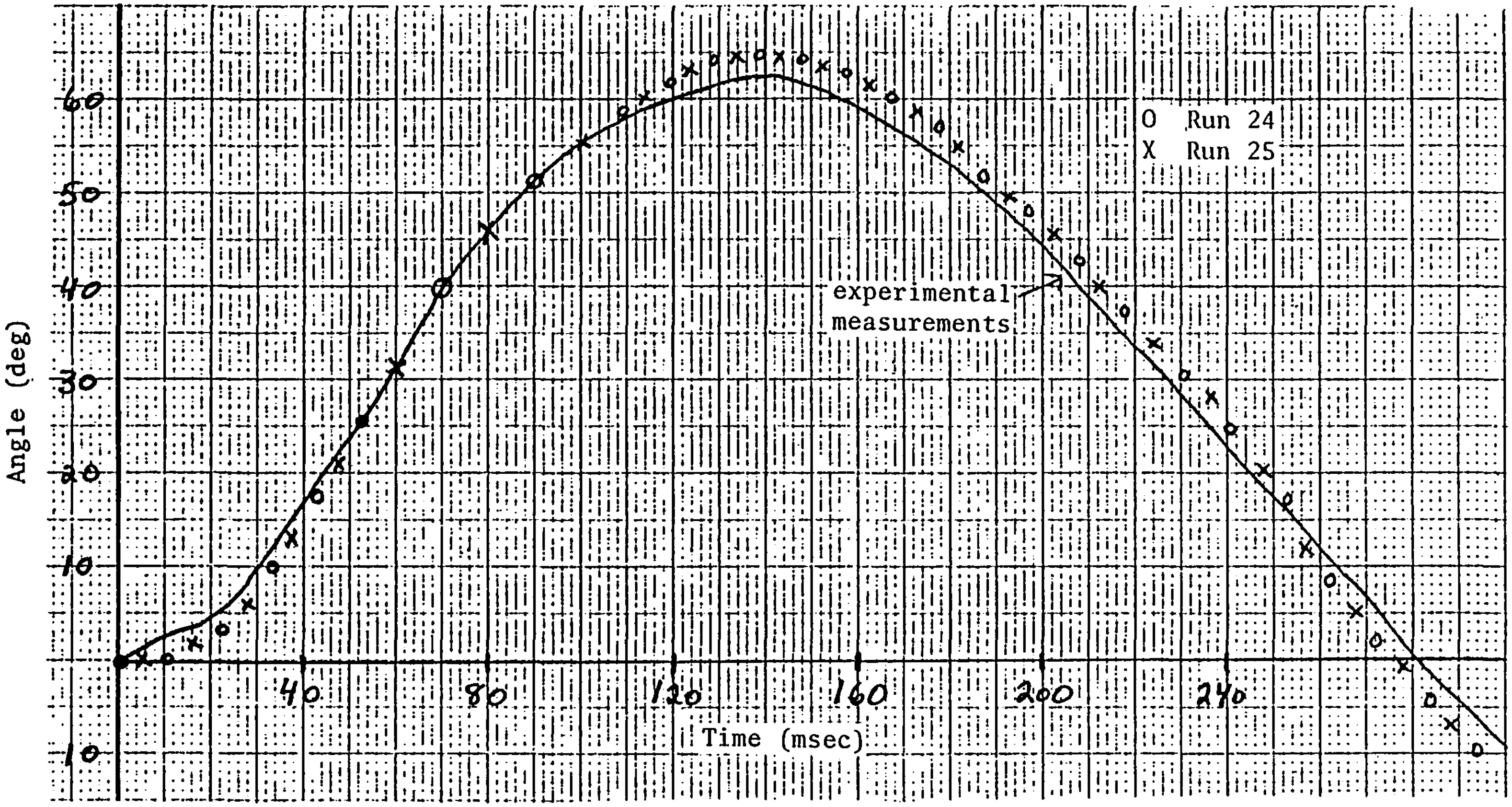

Figure 4-14 TOTAL CHEST ANGLE RELATIVE TO PENDULUM

SEGMENT	JOINT
1 Pendulum	1 Locked pin joint connecting lower torso to pendulum
2 Lower torso	2 Pin joint connecting upper and lower torsos
3 Upper torso	3 Pin joint connecting pendulum to ground

In the final simulation, an additional segment of negligible mass was connected to the upper torso via a locked pin joint. This segment was used to permit monitoring of the upper torso linear accelerations along the same axes as the X and Z accelerometers installed in the dummy chest which, due to the design of the dummy, actually are rotated (pitched) about six degrees with respect to the upper torso geometric reference axes. The pendulum pivot was assumed to have zero rotational resistance. Data from the static test of the dummy with the pin joint spine (Figure 2-28) were used to define certain of the inputs for the model, but the values of some of the joint parameters were assumed. For example, a soft joint stop was assumed to be engaged at 40 degrees of flexion so the resistive torque increased to 1000 in.-lb. at 60 degrees with 84 percent energy dissipation during unloading. All of the inputs for a typical simulation run are given in Appendix C.

The first few computer runs were concerned mainly with simulating the dynamics of the system during the free fall of the pendulum prior to impact. Results of two of the simulations are presented in Table 4-1 for comparison with measured test data. As may be seen from the table, the responses obtained in simulation run No. 4 show very good correlation with the experimental data.

TABLE 4-1

SUMMARY OF MEASURED AND SIMULATED RESPONSES
PRIOR TO IMPACT OF TORSO PENDULUM SYSTEM

	TEST NO.		SIMULATION RUN NO.	
PARAMETER	18	19	2	4
Time to impact, msec.	706	706	708	704
Max. spine rearward flexion, deg.	(-)25	(-)31.5	(-)5.4	(-)30.8
Spine flexion angle at impact, deg.	6	(-)0.5	(-)4.2	(-)1
Upper torso angular velocity at impact, deg./sec.	157	153	4.6	155

The improved predictions of Run No. 4 over those of Run No. 2 resulted from the following changes of inputs:

(1) The viscous coefficient of the spine pin joint was changed from 1 in.-lb/deg./sec. in Run No. 2 to zero for Run No. 4.

(2) The linear spring coefficient of the spine pin joint was decreased from 8.25 in.-lb./deg. in Run No. 2 to zero for Run No. 4.

(3) The initial pitch angle of the upper torso with respect to the lower torso was changed from zero in Run No. 2 to 11. degrees (pitched forward) for Run No. 4 which was the initial angle recorded in test 18.

Thus, except for an assumed coulomb friction of 10 in.-lb., the pin joint as simulated in Run No. 4 developed no other resistive torque. However, this is not an altogether unreasonable representation of the dummy spine in this instance for which the motion of the upper torso is predominantly in the hyperextension (i.e. rearward) range. Unlike the case of forward flexion where the effective resistive torque of the joint results primarily from squeezing of the abdominal insert between the upper and lower torso segments, there is little or no such interference between segments during rearward rotation of the upper torso. Since the CVS model is based on the assumption of symmetry of the joint torque characteristics as a function of the flexure angle, simulation of both the pre- and post-impact phases of the experiment in a single computer run would not be expected to show as good overall agreement with the measured test responses as when simulated separately using the joint properties more appropriate to each phase.

Results of three simulations of the system dynamics after contact of the pendulum with the honeycomb energy absorber are displayed in Figure 4-15 together with the measured responses. It is well to point out that Runs 5 and 8 simulated only the portion of the test subsequent to impact of the pendulum

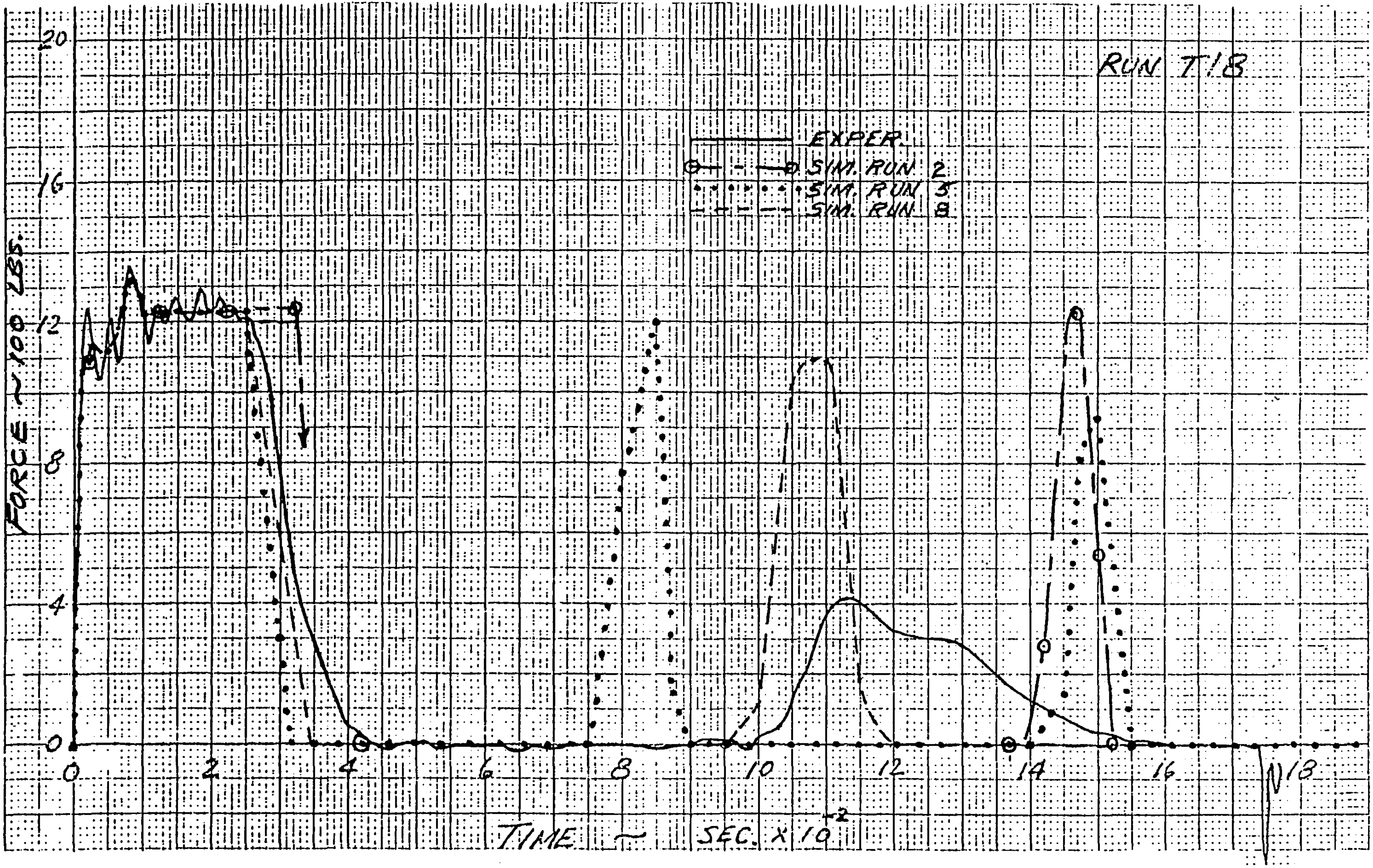

(a) PENDULUM FORCE

Figure 4- 15 COMPARISON OF SIMULATED AND MEASURED RESPONSES FOR PENDULUM TEST OF DUMMY TORSO WITH PIN JOINT SPINE

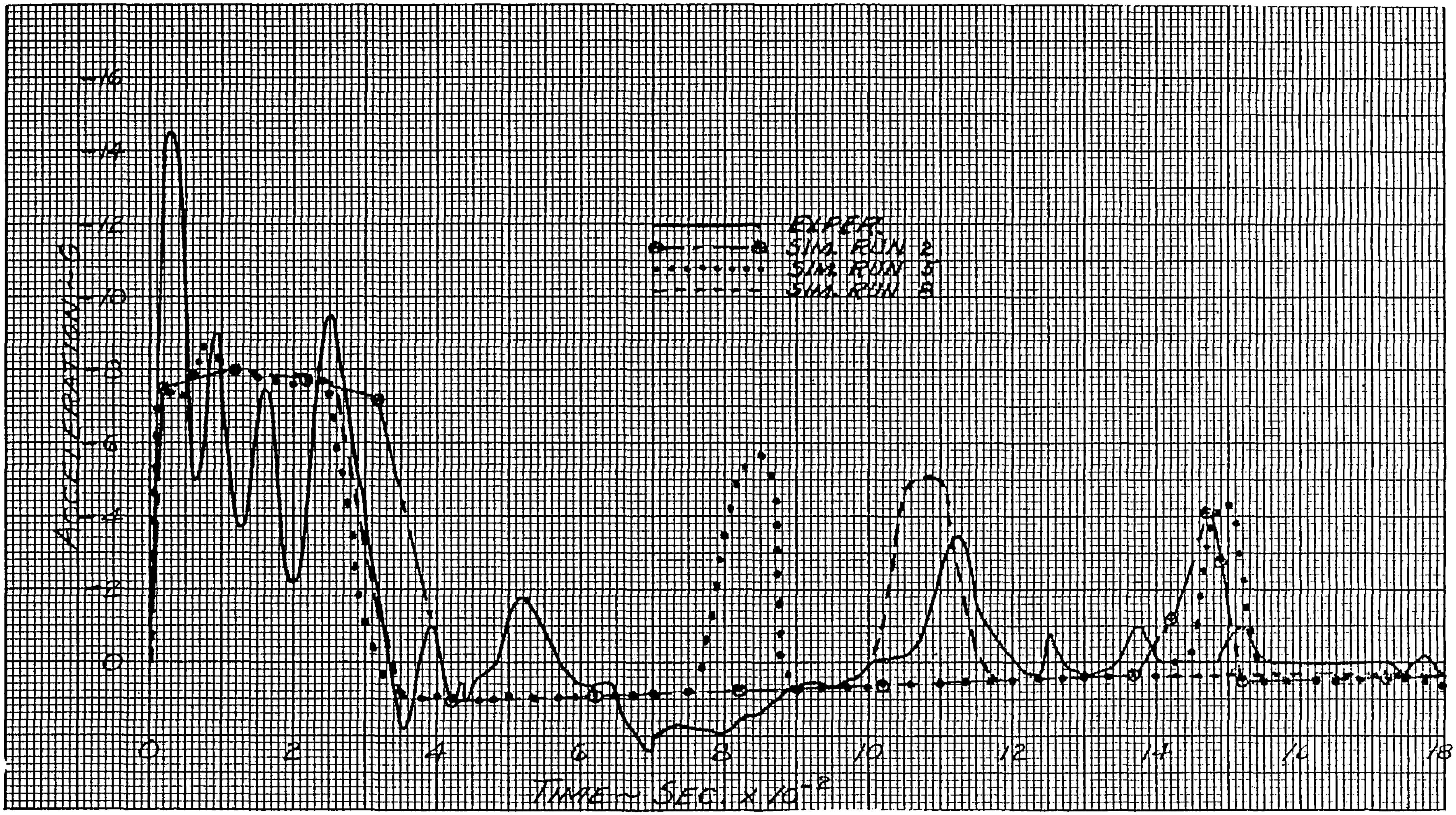

(b) PENDULUM ACCELERATION

Figure 4-15 (CONT'D.)

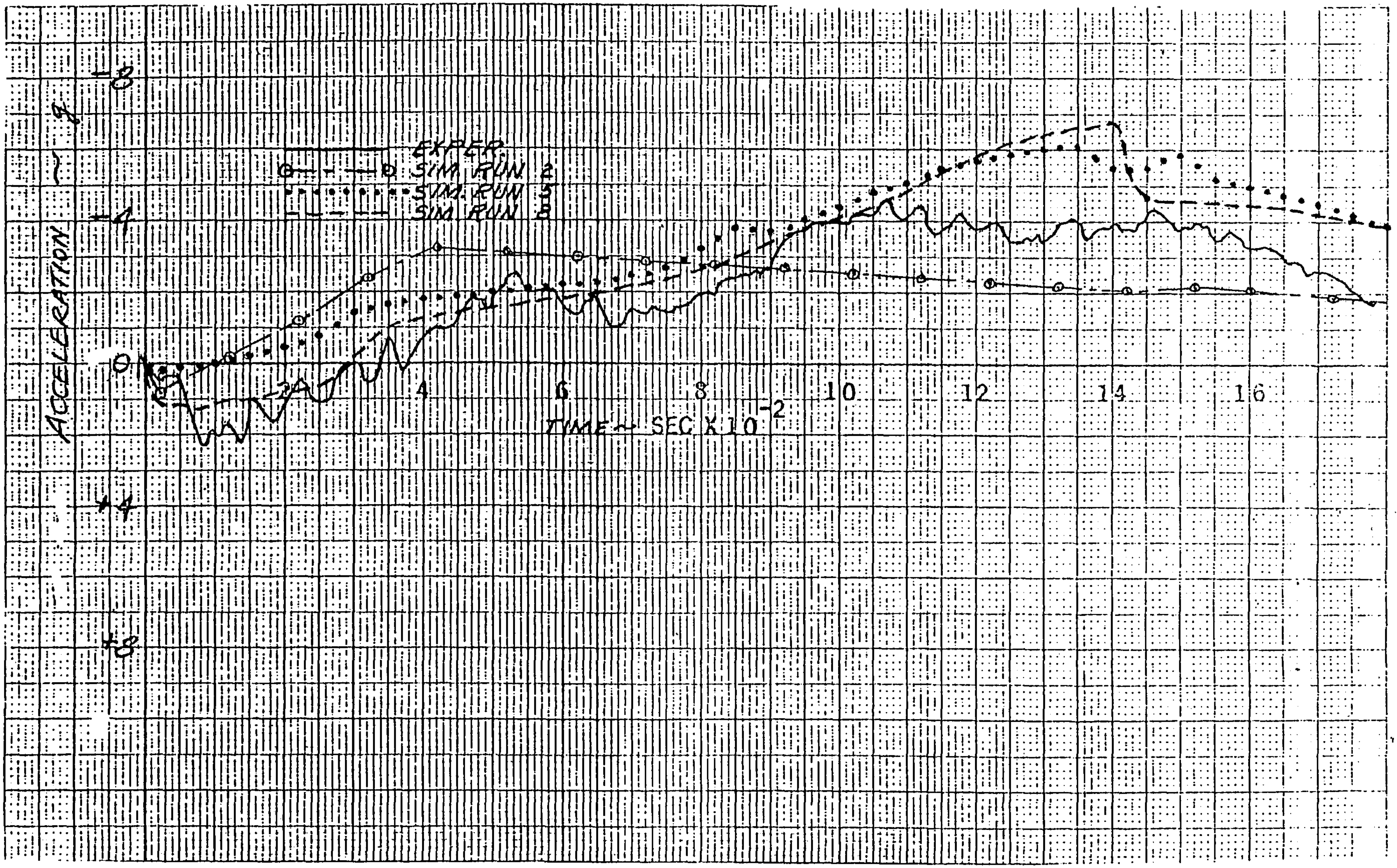

(c) CHEST X ACCELERATION

Figure 4-15 (CONT'D.)

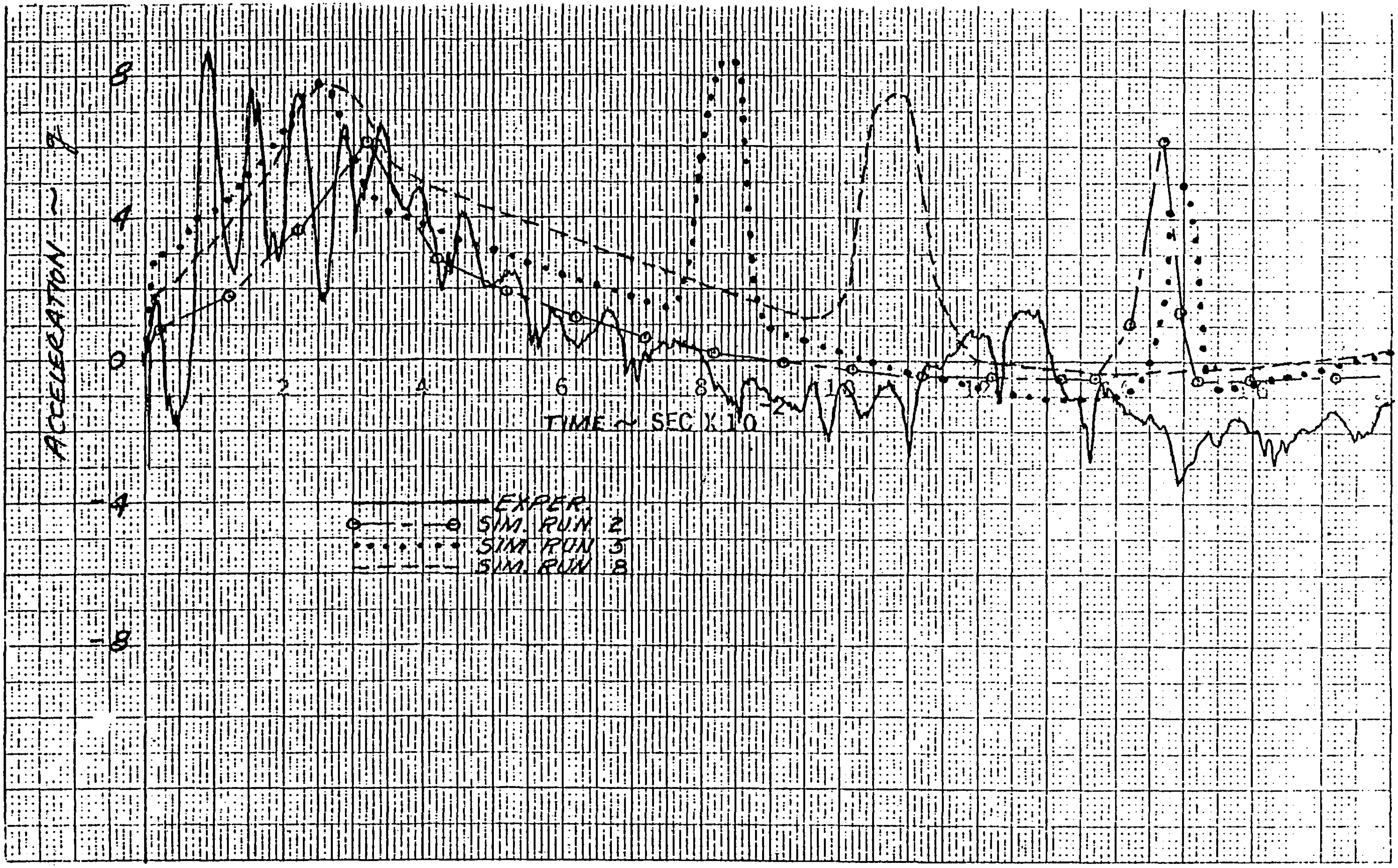

(d) CHEST Z ACCELERATION

Figure 4-15 (CONT'D.)

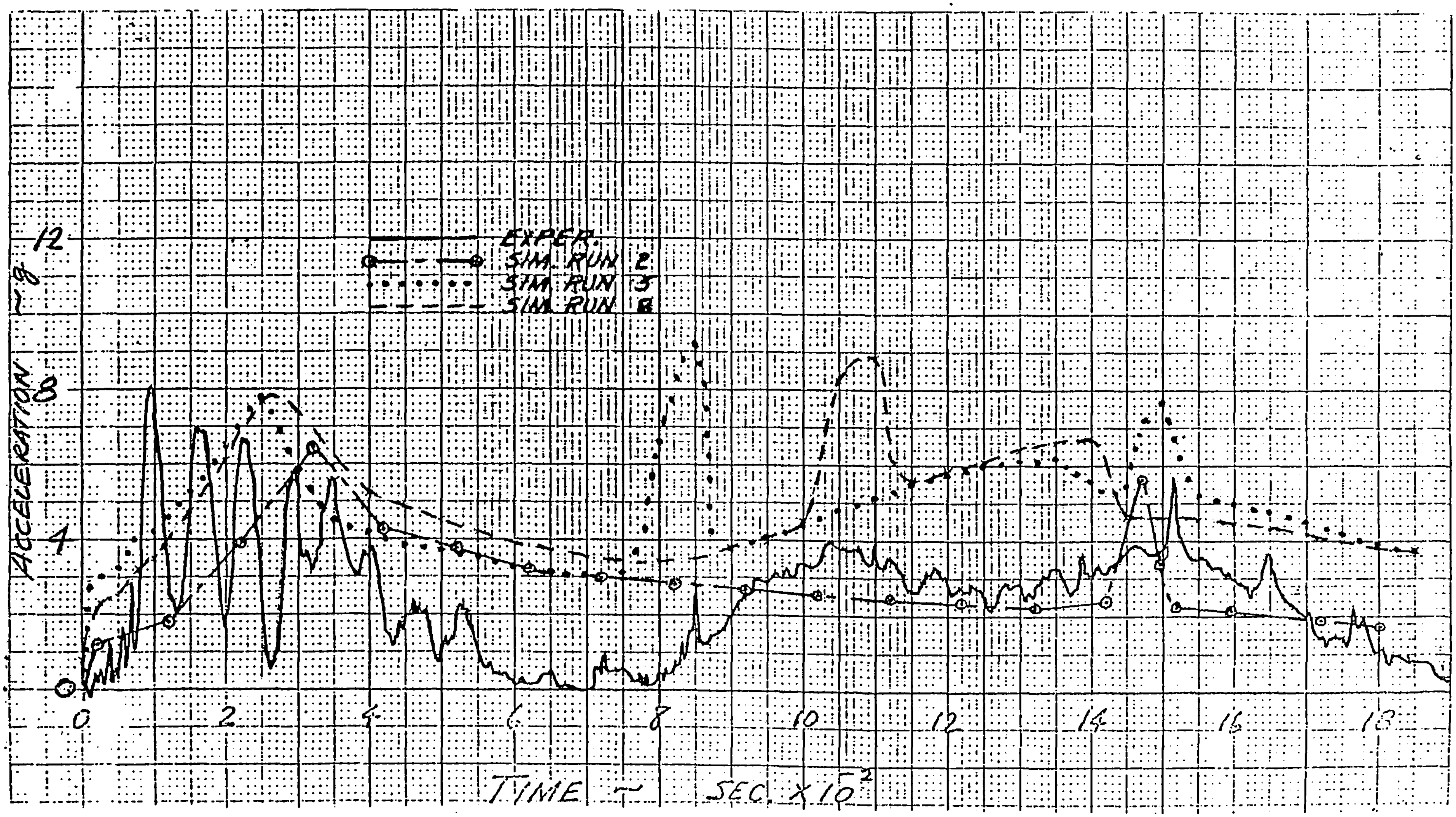

(e) CHEST RESULTANT ACCELERATION

Figure 4-15 (CONT'D.)

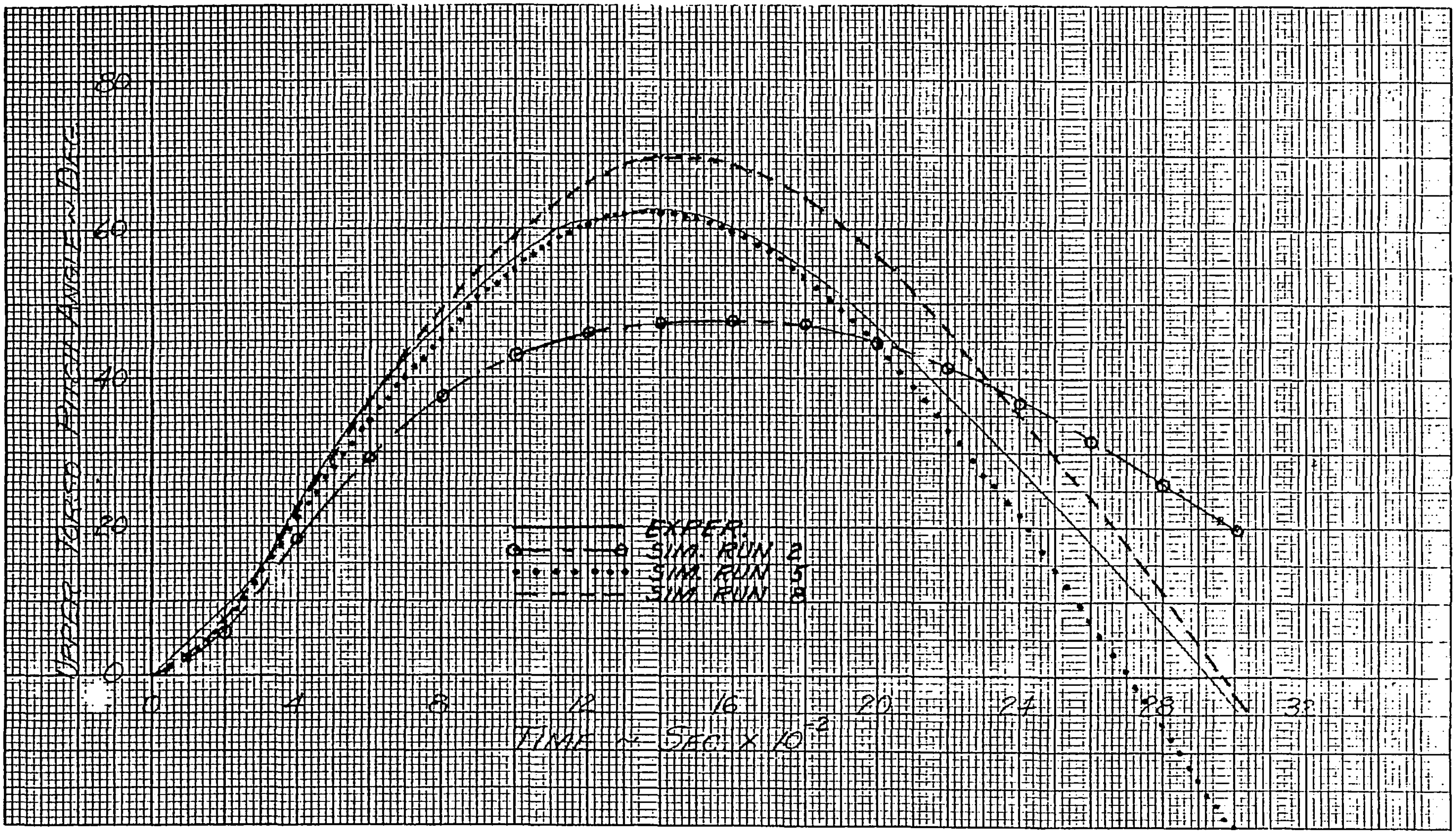

(f) SPINE PIN JOINT FLEXION ANGLE

Figure 4- 15 (CONT'D.)

with the energy absorber whereas Run 2 also included the free-fall phase of the pendulum. Since, as discussed earlier, the conditions at the time of impact were not predicted very accurately in Run No. 2, the correlation with the post-impact test data is not as good as the results obtained in the other two simulation runs. For Run No. 5, the values of the upper torso angle and angular velocity at the time of impact measured in test No. 18 (see Table 4-1) were input to the model. Compared to Run No. 2, the two most notable effects of these changes (and the change of the spine joint viscous coefficient from 1.0 to 0.0) were: (1) greatly improved agreement between the predicted and measured time histories of the upper torso angle (Figure 4-15 (f)), and (2) secondary impact of the pendulum with the energy absorber occurred earlier (Figure 4-15 (a)). Although the test data indicate that the pendulum also reloaded the energy absorber at about t = 100 msec, the recontact was not simulated well by the model since the predicted force level not only was too large but also now occurred too early.

The inputs to the model for Run No. 8, listed in Appendix C, included the following changes from values used for Run No. 5:

Parameter	Run No. 5	Run No. 8
Energy absorber recovered energy factor "R"	0.001	0.01
Energy absorber permanent set factor "G"	0.975	0.92
Spine joint stop energy dissipation coefficient	0.84	0.45
Spine joint initial flexion angle	-6° (UT fw'd)	0°
Orientation of chest accelerometer axes	0°	-6° Pitch

As may be seen in Figure 4-15(a), the timing of the second contact of the pendulum with the honeycomb energy absorber is much better but the force pulse is still too high in magnitude and of too short duration. In terms of the pendulum acceleration, however, the effect of the difference between the predicted and measured forces is less obvious. It is of interest to note that the reloading of the pendulum is clearly reflected in the Z component of the predicted dummy chest acceleration but is much less discernible in the experimental results which show a high frequency oscillation superimposed on the basic acceleration response. In general, the correlation between the predicted and measured chest Z accelerations is not as good in Run No. 8 as in the previous simulations. However, the X component of the chest acceleration agrees much more closely with the experimental data, particularly during the first 110 milliseconds when the acceleration initially is slightly positive and then reverses sign. The reduction of the predicted chest X acceleration at t = 140 msec. results from the small value assumed for the energy dissipation coefficient of the spine joint which reduced the torque sharply upon unloading of the joint stop.

The predicted maximum flexion of the spine pivot in Run No. 8 was about 7 degrees more than that measured in the test but the time at which the pitch angle of the upper torso returned to zero was in better agreement for Run No. 8 than for the other simulations. Since the angle of the torso at impact of the pendulum was zero for Run No. 8, compared to 6 degrees in Run No. 5, the resistive torque at a given time was less and the soft joint stop was engaged later in Run No. 8. As a result, the maximum pitch angle and the time at which it occurred were increased slightly in Run No. 8.

Better overall agreement with the experimental results could probably be achieved by changing the values of the various input parameters for the spine joint torque characteristics. For example, decreasing the flexure angle at which the joint stop is engaged would reduce the overshoot of the torso pitch angle since higher torques would be generated earlier. Moreover, parameters could be adjusted so that energy would be dissipated during unloading to cause the upper torso to return to zero pitch angle at the proper rate. However, further simulations were not deemed warranted in view of the limited information that was available for estimating the effective torque characteristics of the spine over the range of flexion angle that occurred in the dynamic tests.

4.3 Simulation of Air Bag Static Tests

Several static tests of a specially designed pre-inflated air bag were performed to provide data for checking the CVS program algorithms used to calculate the bag shape, pressure and force resulting from contact by an object. The bag was designed as an ellipsoid having semi-axes 10 in., 10 in. and 15 in. long, which resulted in a bag volume of 6283 in^3 (3.64 ft^3). The bag was fabricated from 24 warp by 24 fill, 1/4 in. ripstop neoprene coated nylon. A meteorological weather balloon was used as a liner to pre-inflate the bag and to prevent any leakage of air through the fabric or seams.

Data were obtained for two bag contact configurations. In the first, a 6.5 in. diameter hemispherical penetrator was pressed into the bag along a vertical minor semi-axis and the bag was supported by a flat reaction surface. For the second loading configuration, illustrated in Figure 4-16, the bag was centrally supported by an 8 in. diameter hemispherical penetrator and again was loaded by forcing an identical penetrator into the top of the bag along the vertical minor axis. The force and the bag pressure were recorded as the upper penetrator was moved downward in 0.5 in. increments to a maximum stroke of 6 inches. It should be noted that, because of the symmetry of this configuration, the penetrations of the hemispheres into the bag were always equal. Hence, the maximum bag penetration by each contacting surface was 3 inches.

Experimental and simulation results for the test of the first configuration (flat reaction surface) in which the bag was initially inflated to a pressure of 0.31 psi are presented in Figure 4-17 for comparison. The curves of the experimental volume change and the force predicted by the model are based on the assumption of an isothermal compression process (exponent $\eta = 1$). It may be seen that the model increasingly overpredicts the force with increasing penetrator stroke. This results primarily because the volume change calculated by the model is too large, although the effective area on which the pressure acts is also slightly greater than that indicated by the test data. Analysis of data from another test performed with the bag inflated to 0.70 psi initial pressure also showed similar discrepancies.

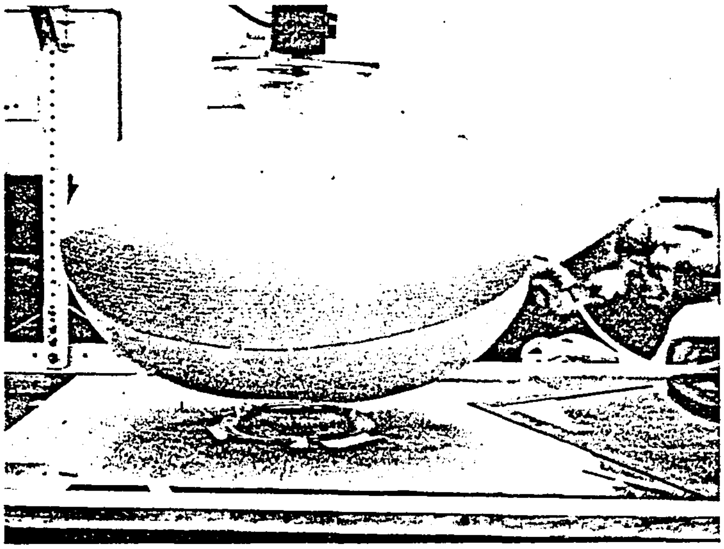

Figure 4-16 STATIC TEST OF AIR BAG CONTACTED BY TWO IDENTICAL HEMISPHERES

It is believed that stretching of the bag fabric on the bias as the bag was loaded resulted in smaller changes of the actual bag volume than those computed by the model, and mainly accounts for the differences between the predicted and measured forces. This conclusion is based on observations of the bag shape and distortions of the fabric weave pattern in the vicinity of the hemispherical penetrator. However, detailed checkout of the CVS air bag algorithms was made difficult because of the assymmetry of the bag deformation resulting from the contacts with surfaces of different shape.

Results of simulations of two tests of the air bag loaded along the minor axis of the ellipsoid by two identical hemispheres (see Figure 4-16) are compared with test data in Figure 4-18. The tests were performed with the bag initially pressurized to 0.31 and 0.57 psi, respectively. Again, both the change of bag volume calculated from the measured pressures in the test and the force predicted by the model are based on the assumption of an isothermal compression of the air in the bag. It may be seen that, like the results discussed earlier,

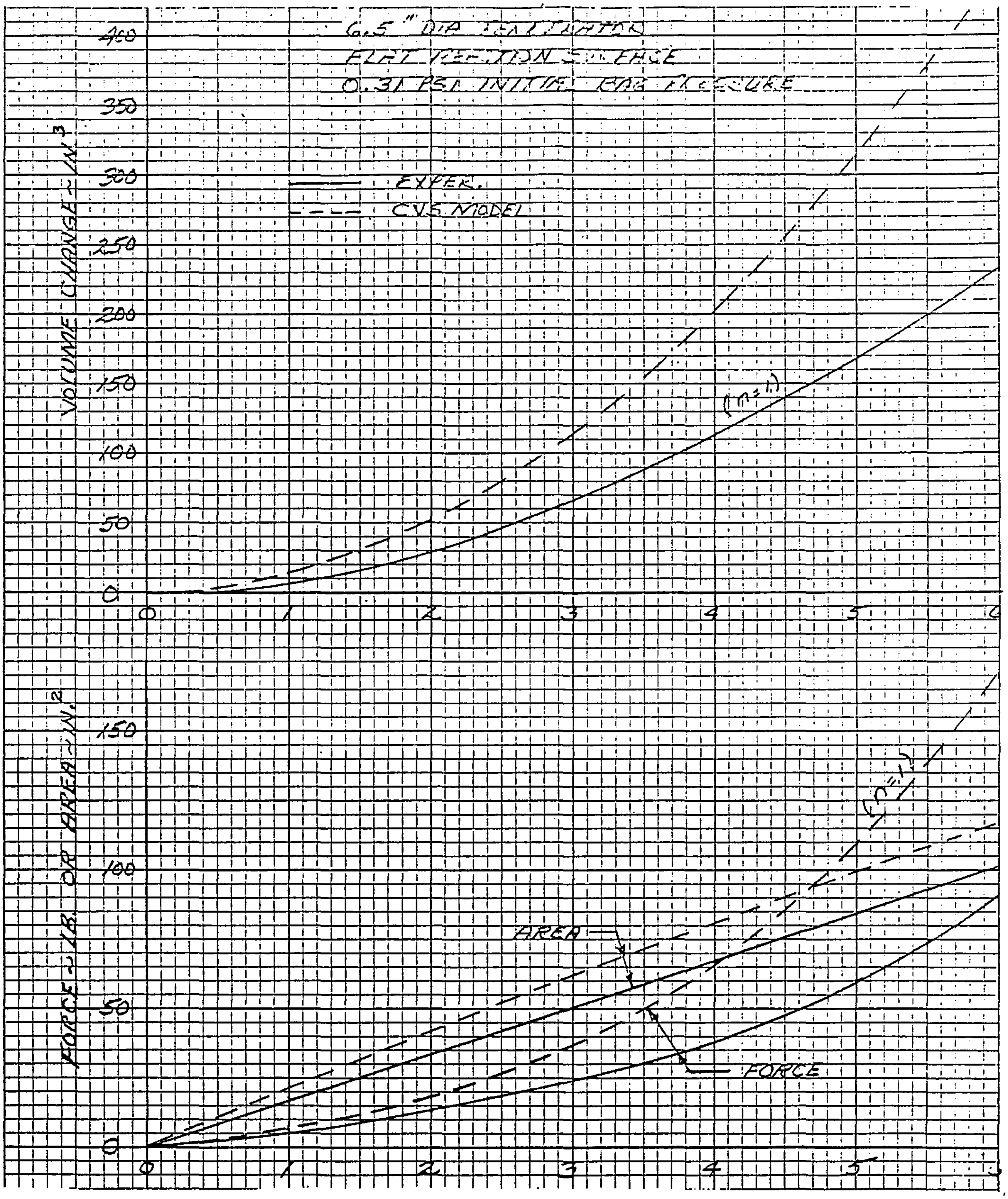

PENETRATOR STROKE - IN.

Figure 4-17 COMPARISON OF MEASURED AND SIMULATED RESULTS - AIR BAG STATIC TEST CONFIGURATION NO. 1

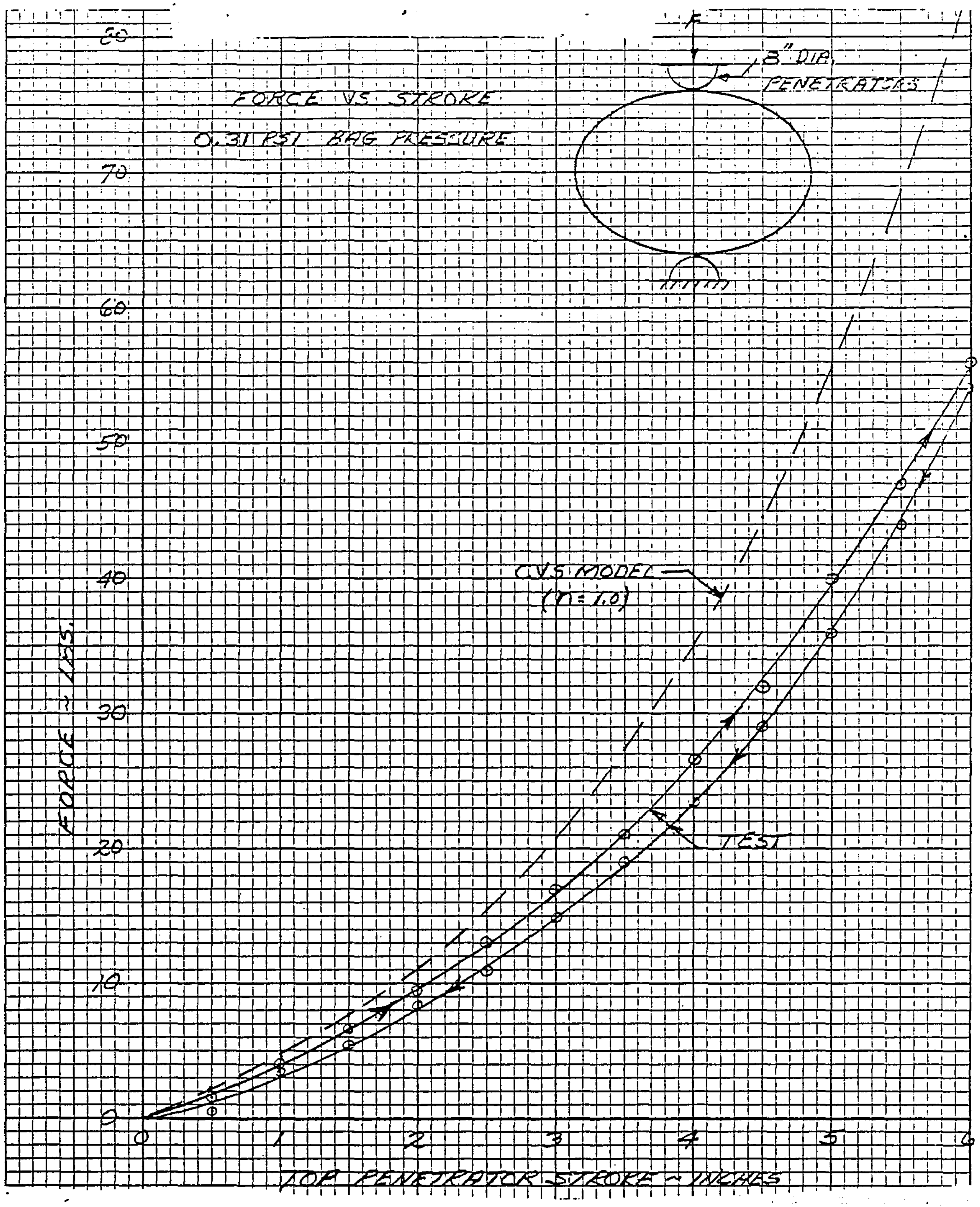

Figure 4-18 COMPARION OF MEASURED AND SIMULATED RESULTS - AIR BAG STATIC TEST CONFIGURATION NO. 2

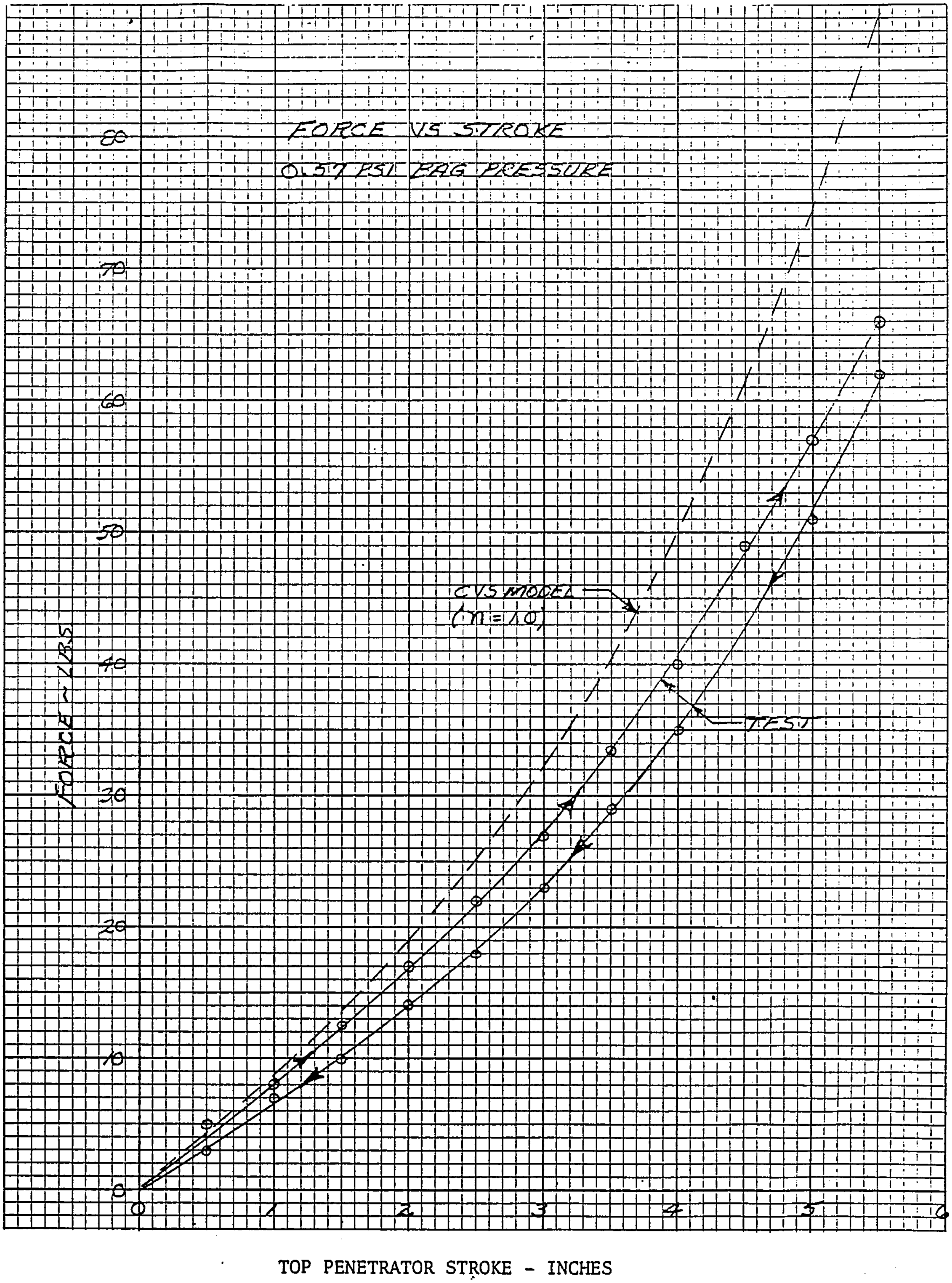

Figure 4-18(CONT'D.)

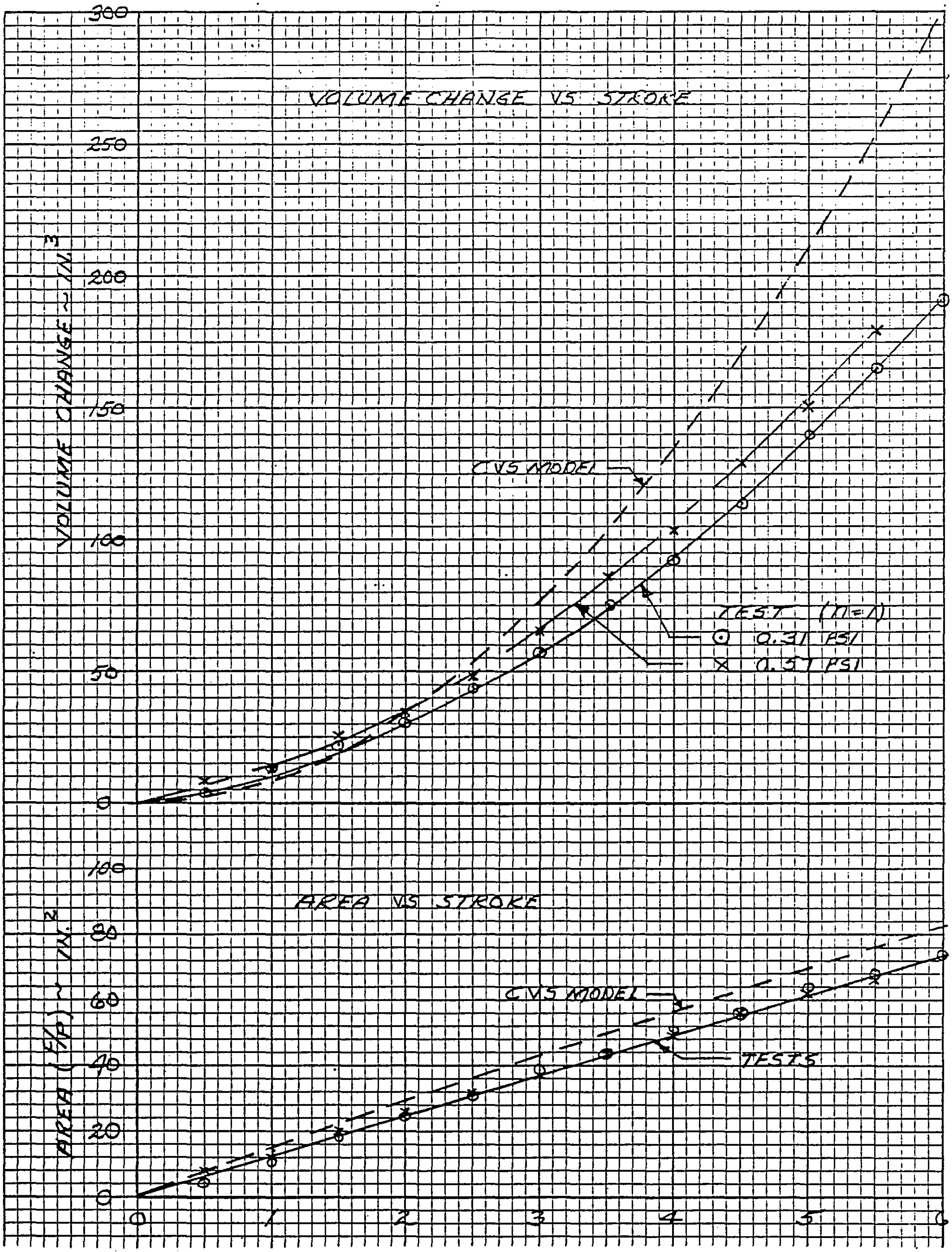

TOP PENETRATOR STROKE - INCHES

Figure 4-18 (CONT'D.)

the model overpredicted the force primarily because of the difference between the bag volumes as calculated by the simulation algorithm and as deduced from the test data. It should be noted that the percent reduction of bag volume was not very great in the tests (less than 5 percent for the maximum penetration). Thus, only a slight violation of the model assumption that the bag does not stretch would be expected to produce significant discrepancies between the simulated and experimental results.

For each of the configuration 2 tests, it is of interest to note that lower forces and pressures were measured during unloading of the bag. However, no leaks were detected and the bag pressure returned to the initial inflation pressure upon complete unloading. Since the maximum loading of the bag was maintained for several minutes before unloading was begun, it is possible that slight additional stretching of the fabric occurred during that time which would account for the lower forces recorded during the subsequent unloading portion of the tests.

5.0 SIMULATIONS OF WHOLE DUMMY SLED TESTS

Results of replicate sled tests that were performed for the specific purpose of providing comprehensive and reliable data for validating CVS predictions of whole dummy responses in realistic vehicle crash situations are documented in Reference 9. In these tests, which simulated 30 mph frontal impacts, the Part 572 dummy was restrained either by a lap and shoulder belt system that included a force limiting device at each of the three anchor points or by a preinflated air bag. The results from simulations of the tests of each configuration are presented and discussed in the following subsections.

5.1 Simulation of Belt Restraint Tests

The belt restraint test configuration was simulated first, using inputs for the dummy model developed from the data presented in Section 3. The contact plane descriptions, sled acceleration pulse and contact force-deflection functions were derived from the data measured in the sled tests.

It must be emphasized that the purpose and design of this initial effort was not to perform simulations for validating the model of the sled tests but rather to:

(1) Verify the input deck for the Alderson Part 572 dummy.

(2) Establish those levels of sophistication and simplification of the CVS program capabilities deemed necessary and sufficient to perform the validation of the full-scale system tests.

(3) Establish adequate CVS simulations that can be used as baseline or benchmark models for the sensitivity studies required for Contract No. DOT-HS-6-01410, "Development of Approximating Solutions for the CVS Program and Dummy Design Information."

(4) Further verify the newly developed features of the CVS program that will be required by these validation and sensitivity studies.

(5) Establish basic CVS input decks that can be used for full-scale simulations.

It is estimated that approximately 120 computer simulations were executed over a three-month period consisting of the following:

(1) Short (time zero only) simulations designed to check out the basic format and contents of the CVS program input deck.

(2) Short (time zero only) simulations to determine the initial positions and angular orientation input parameters to agree with experimentally measured data and to produce acceptable low initial accelerations.

(3) Long (200 msec.) simulations that attempted to model the three-point belt system using the standard two-point belt algorithm of the CVS program.

(4) Long (140 msec.) simulations modeling the three-point belt system components with one-sided (tension only) linear spring functions.

(5) Long (140 msec.) simulations modeling the three-point belt system by utilizing the elaborate harness-belt algorithm that was developed by Calspan (Reference 6) and which is now included in the CVS-IV program.

In the initial trial runs, temporary force-deflection characteristics for the belts and panels contacting the body segments from other CVS simulations of similar sled runs were included in this basic input deck.

Only the data from sled Run 2049 was used for comparison with the output of these simulations because the responses measured in the three replicate sled tests performed are very similar.

During all of the above effort, once the basic CVS input deck and initial positioning were established, no input changes were made except in the model of the three-point belt system that was employed in the sled runs. Although some satisfactory intermediate results were obtained, the overall kinematics were always incorrect due to an inability to match the timing and general characteristics of the initial loading of the individual belt components. In addition, the majority of the simulations experienced computational difficulties due to geometric limitations imposed by the CVS program; namely, the location of the fixed point falling outside of the tangent points in the runs that used the standard two-point belt algorithm. Because of this problem with tangent points and because the standard belt routines were not designed to model a three-point belt system, a series of simulations were made that used the harness-belt algorithms.

Figure 5-1 compares photographs obtained from the south movie camera for sled Run No. 2049 with the AFAMRL Program VIEW plots obtained from the results of CVS Run R2049K for times of zero to 120 smec. at 20 msec. intervals. Run R2049K used the standard belt routines to model the three-point belt restraint.

It was obvious that unless the loading characteristics of the three individual belt components were adequately simulated by the CVS program, no useful comparisons could be made between the simulations and experimentally measured results. Since no dynamic loading characteristics of the belts were available at the time the runs were made, the necessary force-deflection characteristics required by the CVS program were determined by a trial and error procedure. In this procedure force-deflection characteristics were modified until a reasonable match of the measured loading (force vs. time) of the individual belt components was obtained between the simulation and the sled test. The trial and error procedure concentrated primarily on the loading phase of the belt system. (Subsequent studies have shown that the force-deflection loading characteristics derived from the experimental data are very close to those actually used, as indeed one could expect.) Again, it should be emphasized that the overall purpose of this effort was not to validate the full-scale system tests but to achieve those goals listed at the beginning of this subsection.

All of the simulations that modeled the three-point belt system with the newly developed harness-belt algorithm of the CVS program used a coefficient of friction of 0.1 for the belt points contacting the body segments along the belt line and 1.0 perpendicular to the belt line. These simulations produced poor results during the loading phase of the simulations due to excessive slippage of the belt and erratic behavior of the tie point. As a last resort, the coefficient of friction along the belt line was increased from 0.1 to 0.5 and lowered for the tie point from 1.0 to 0.5. The results of this simulation (CVS Run R2050G, 6/12/80) appear to be very satisfactory and are shown superimposed onto the plots of data measured in the sled test in

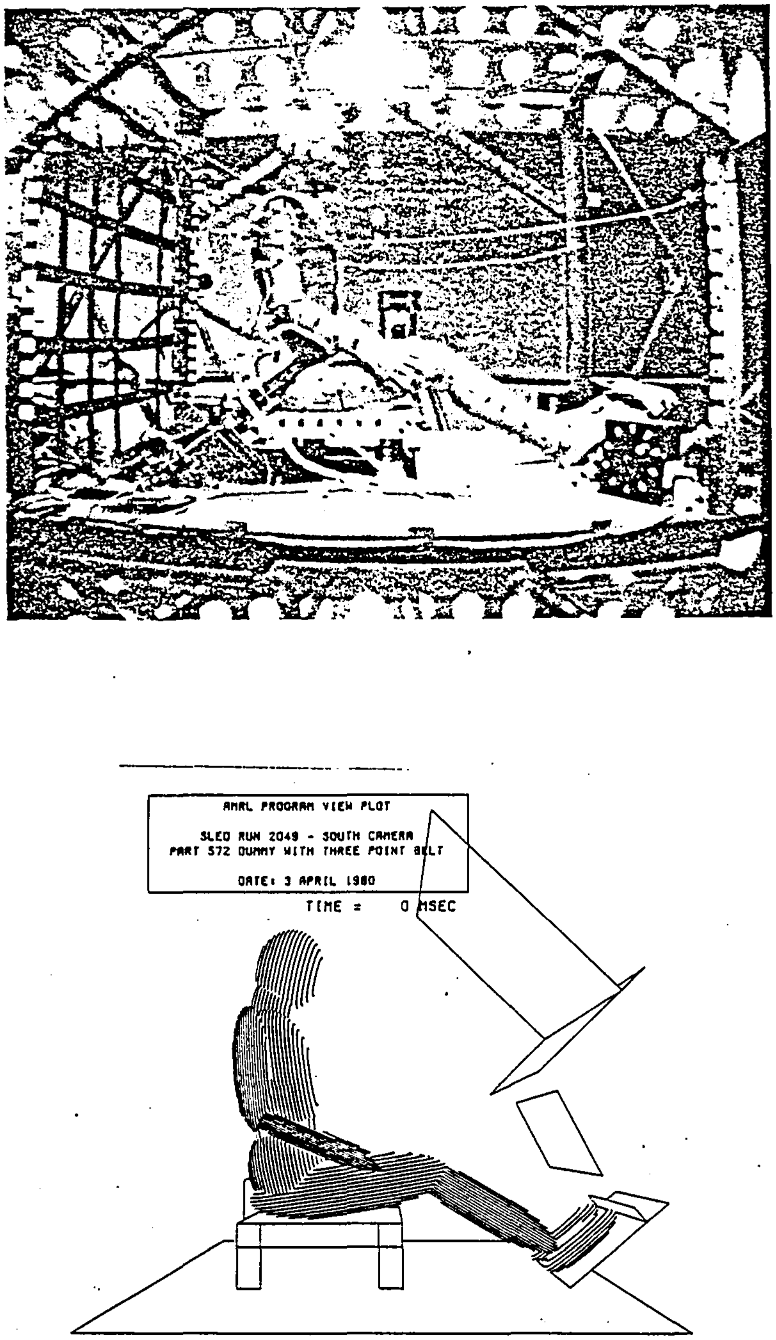

(a) t = 0

Figure 5-1 COMPARISON OF CALSPAN SLED RUN 2049 AND CVS RUN R2049K

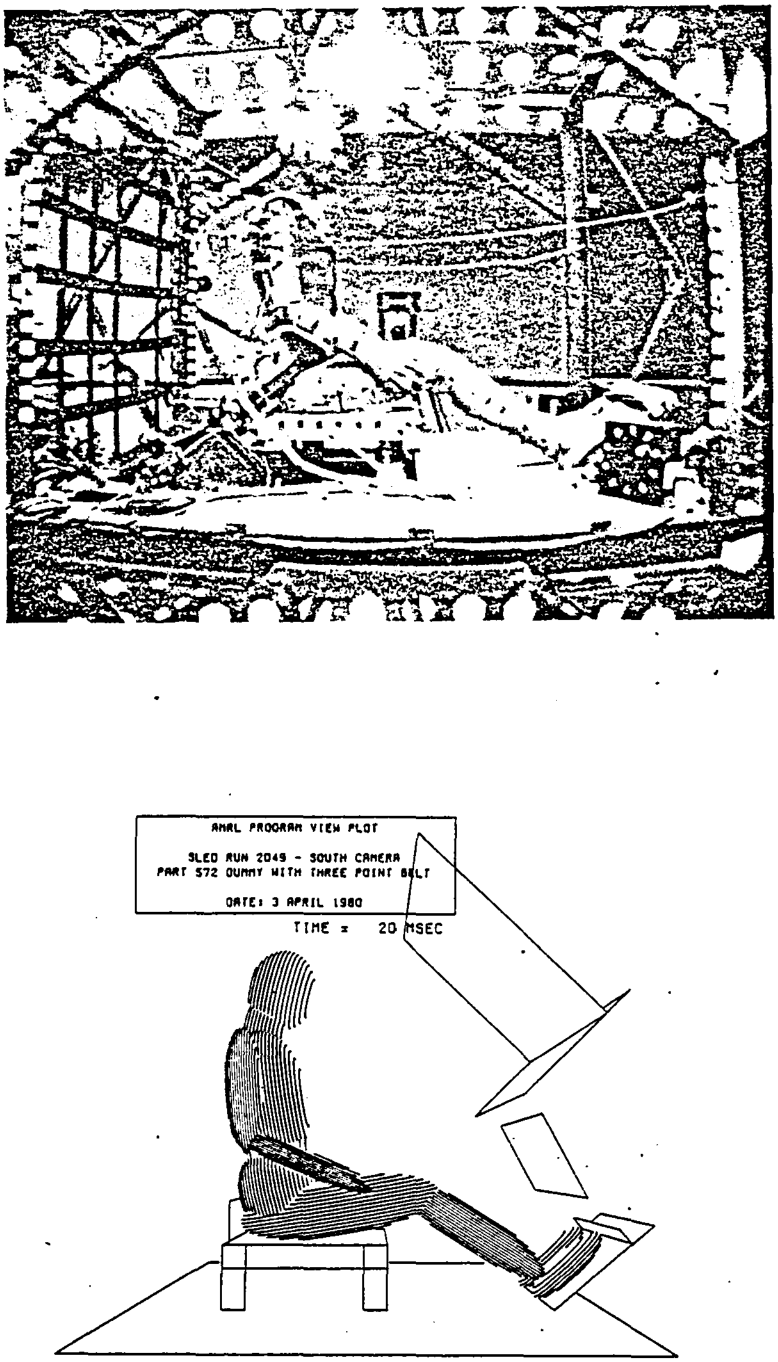

Figure 5-1 (b) t = 20 msec.

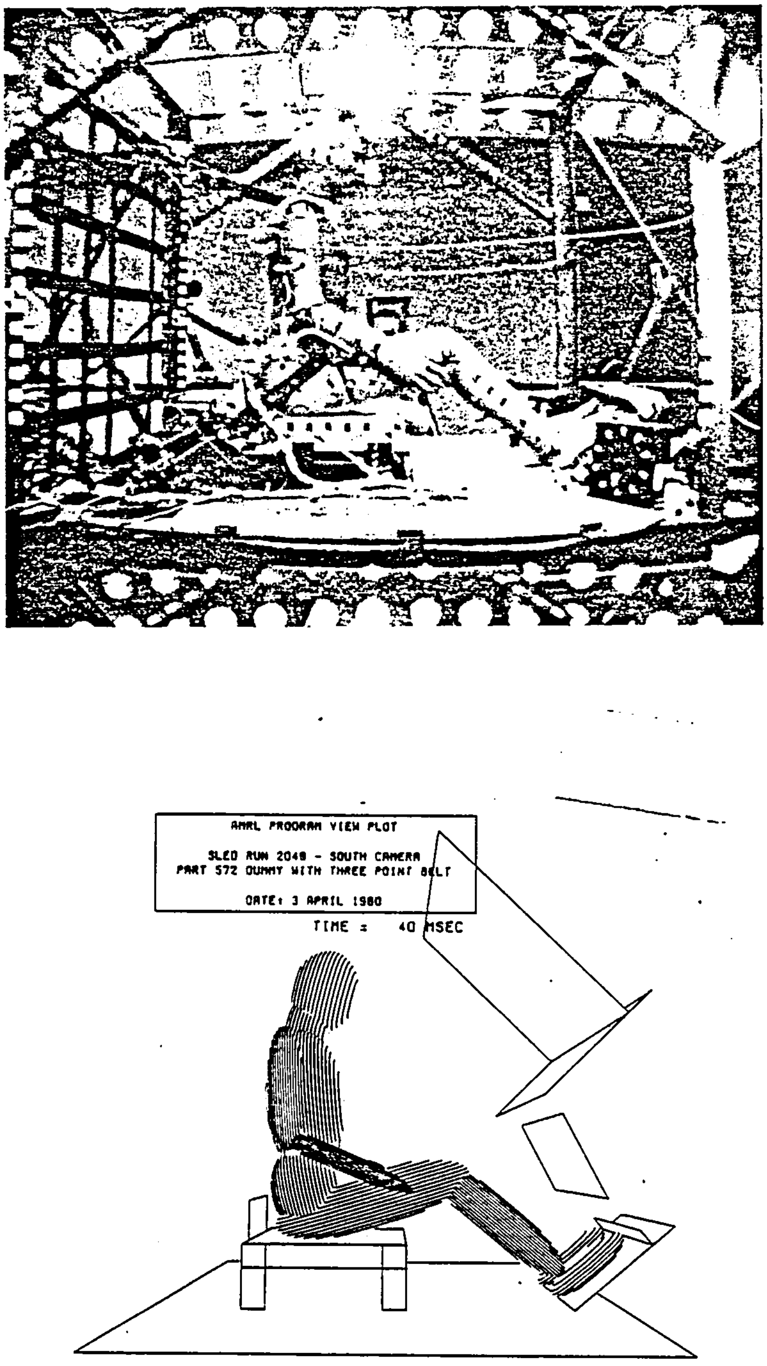

Figure 5-1 (c) t = 40 msec.

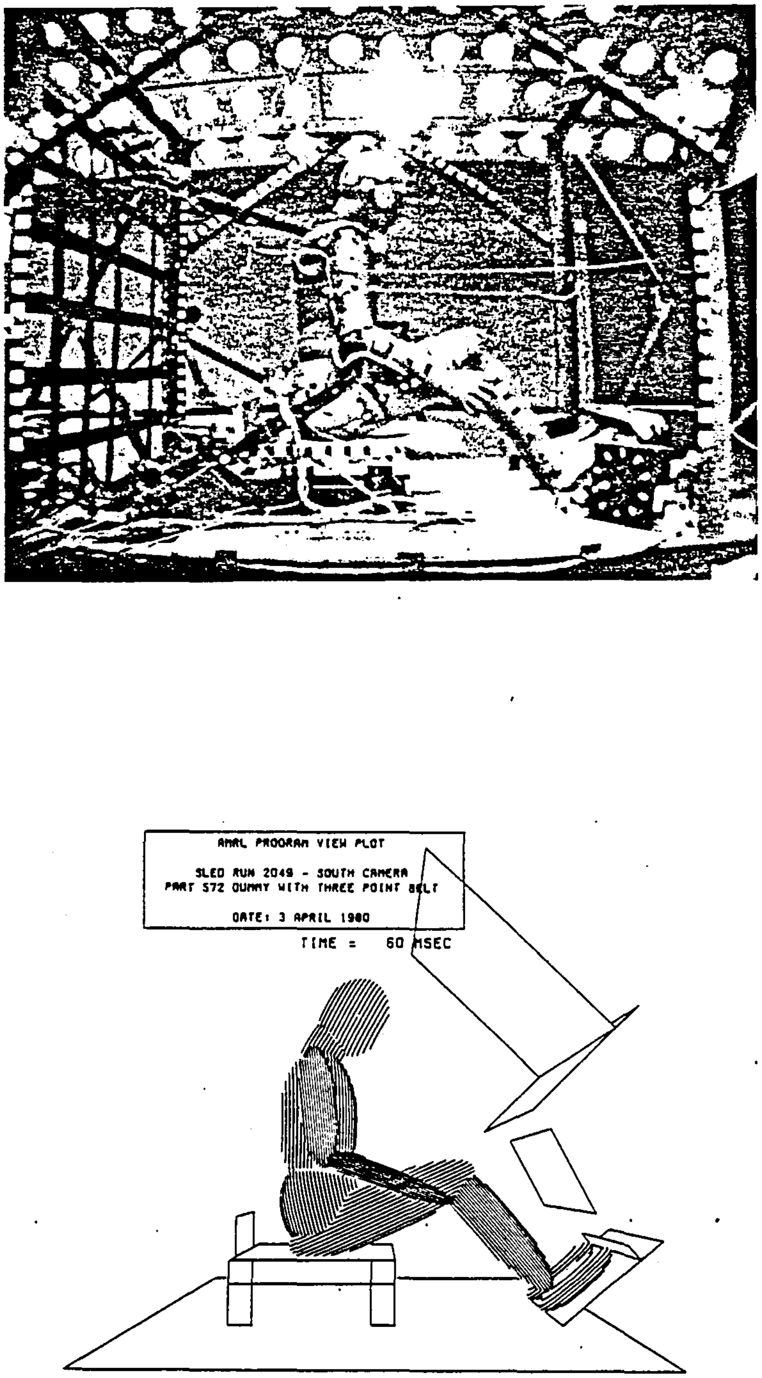

Figure 5-1 (d) t = 60 msec.

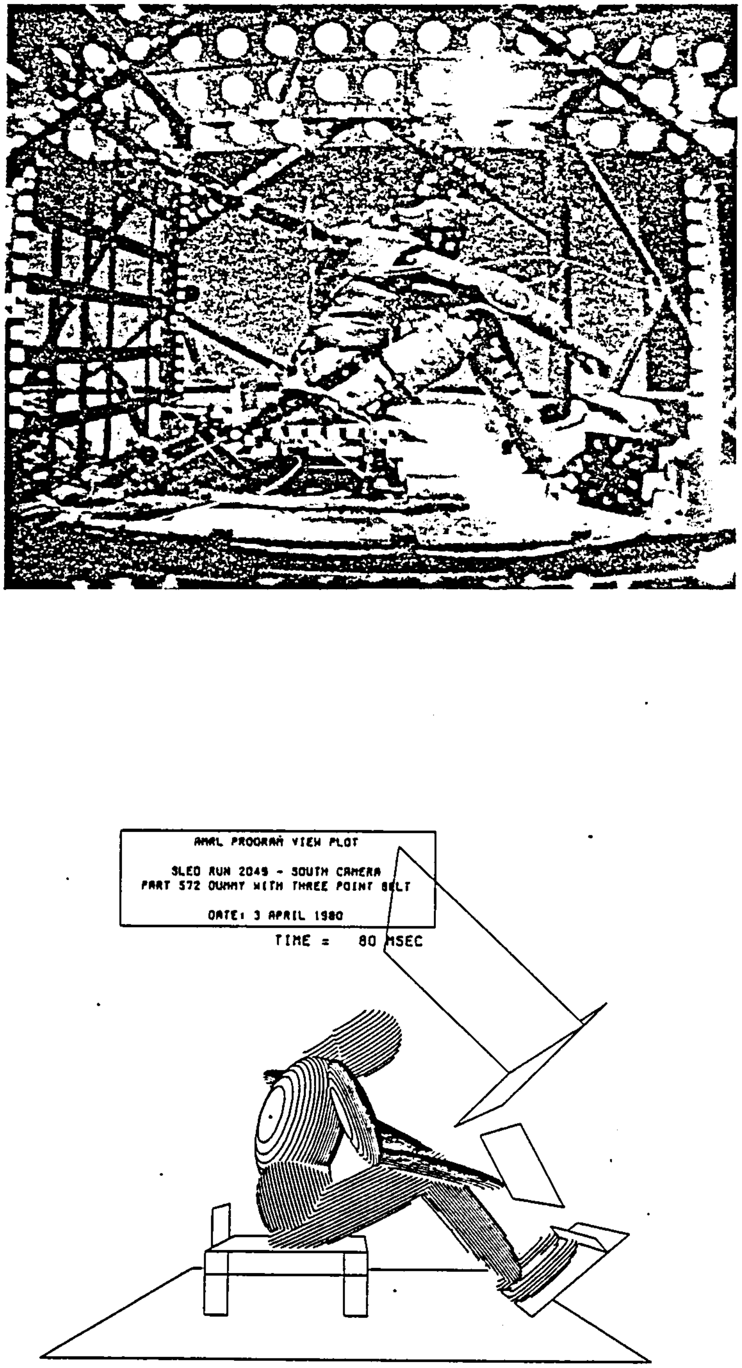

Figure 5-1 (e) t = 80 msec.

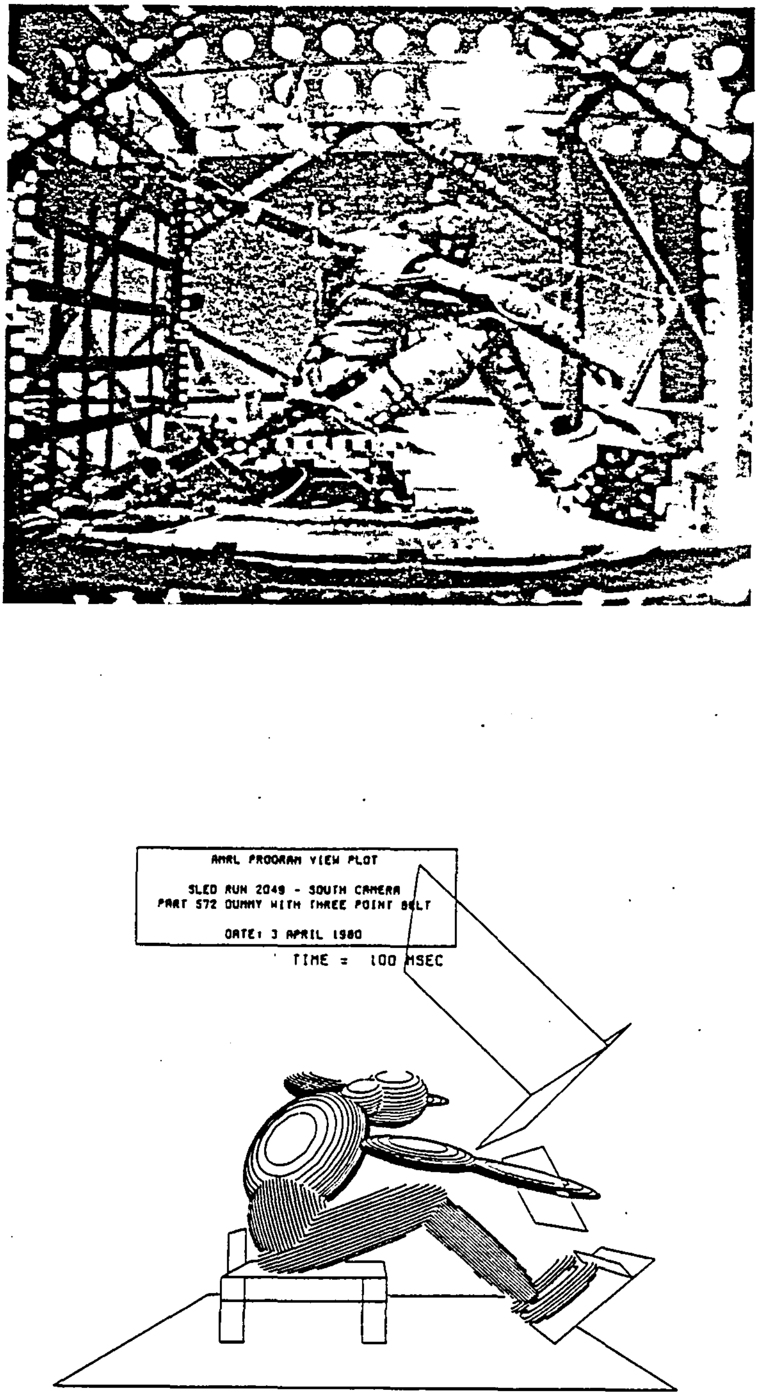

Figure 5-1 (f) t = 100 msec.

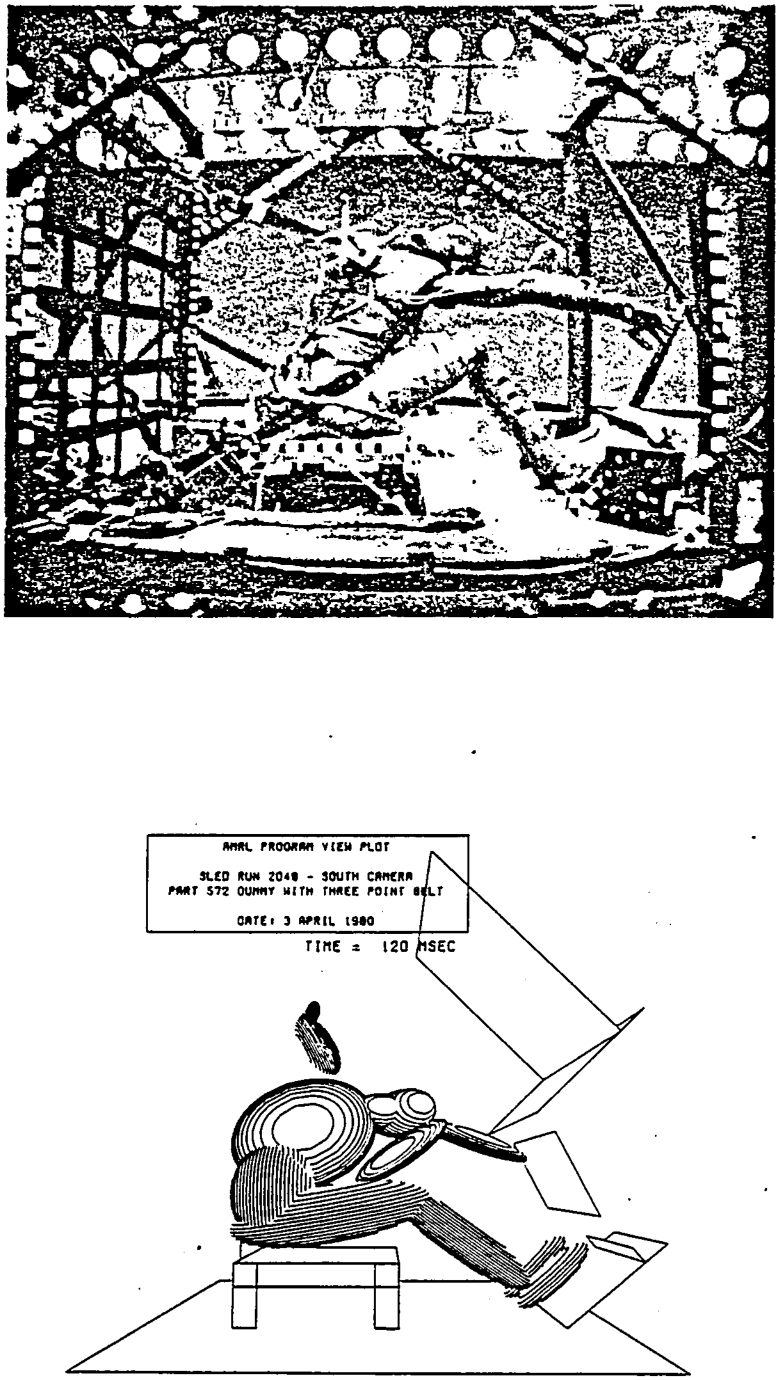

Figure 5-1 (g) t = 120 msec.

Figure 5-2. The actual and predicted kinematics of the dummy are shown for comparison in the several photographs and corresponding computer graphics displays of Figure 5-3.

The complete computer output of CVS Run R2050G input, time zero results, and tabular time histories are included in the User's Manual, Volume III of this report.

5.2 Simulation of Air Bag Restraint Tests

Simulations of the air bag restraint test configuration were performed using the same values for all of the inputs as were used for simulating the belt restraint tests except, of course, those inputs associated with the different restraint systems. The preinflated air bag employed in the tests was a cylinder 28 inches in diameter and 30 inches wide. Since air bags are modeled as ellipsoids in the CVS, the selection of the ellipsoid semi-axes dimensions that would provide a satisfactory idealization of the cylindrical air bag was necessarily based on judgment. In the interest of at least simulating the correct geometry in the vertical longitudinal plane of the contact by the dummy, the minor axes of the ellipsoidal air bag were each assumed to be equal to the 28 inch diameter of the test air bag. The width of the ellipsoidal bag (45 in.) was then determined on the basis of matching the internal volume of the cylindrical bag.

Due to time and funding limitations, only a few preliminary computer runs of the air bag restraint configuration were possible. All but one of these were short-duration runs to determine suitable values for the bag inflation parameters so the bag would be fully inflated and generate forces on the occupant at about the same time as that indicated by the experimental data. In addition, it was required that the supply gas be essentially exhausted at that time so there would be no significant inflow to the bag subsequent to full inflation. Since no data were available to define the force-deflection characteristics of the knee bolster contacted by the legs of the dummy, the

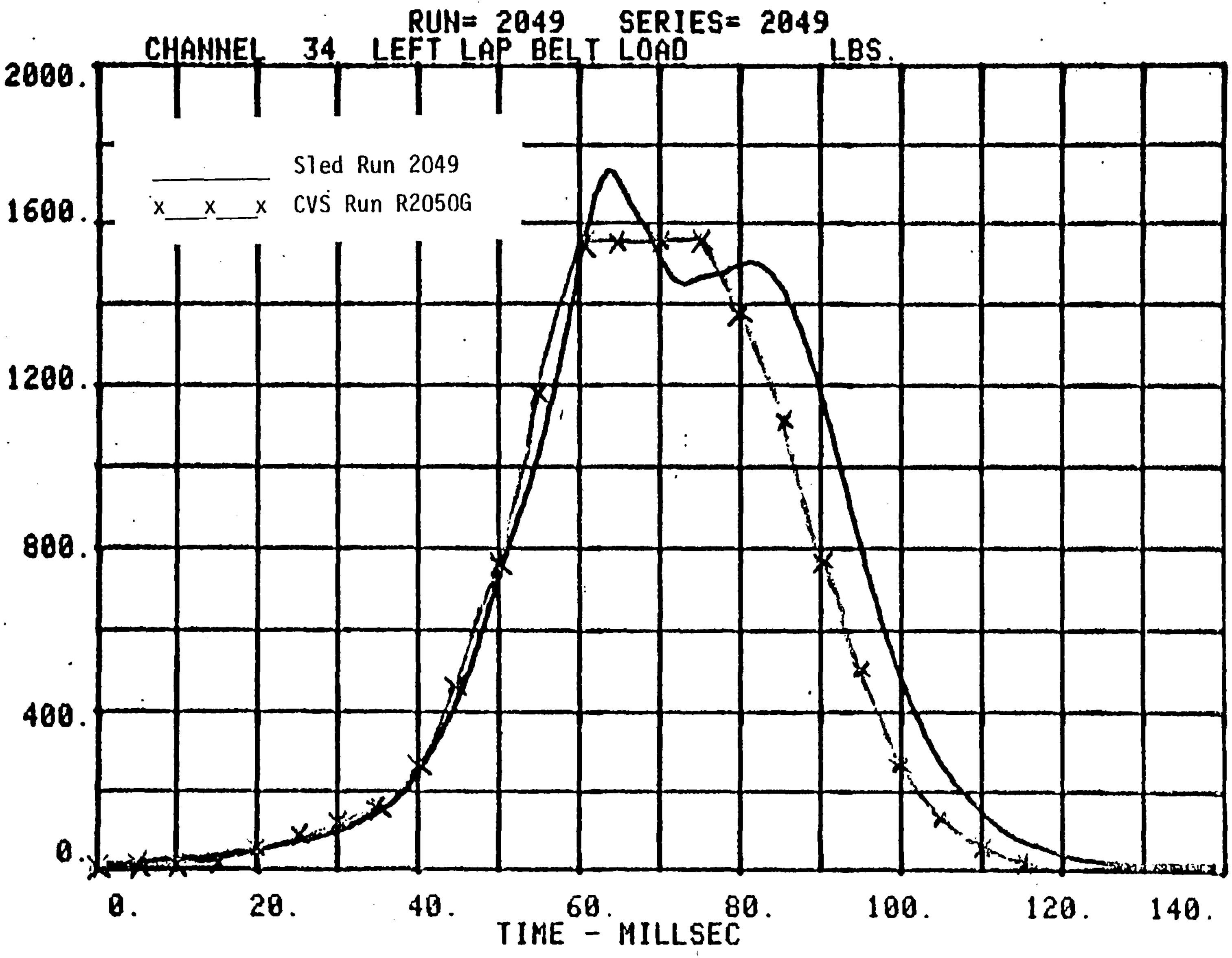

(a) Left Lap Belt Load

Figure 5-2 COMPARISON OF CVS MODEL AND MEASURED RESPONSES FOR BELT RESTRAINT CONFIGURATION

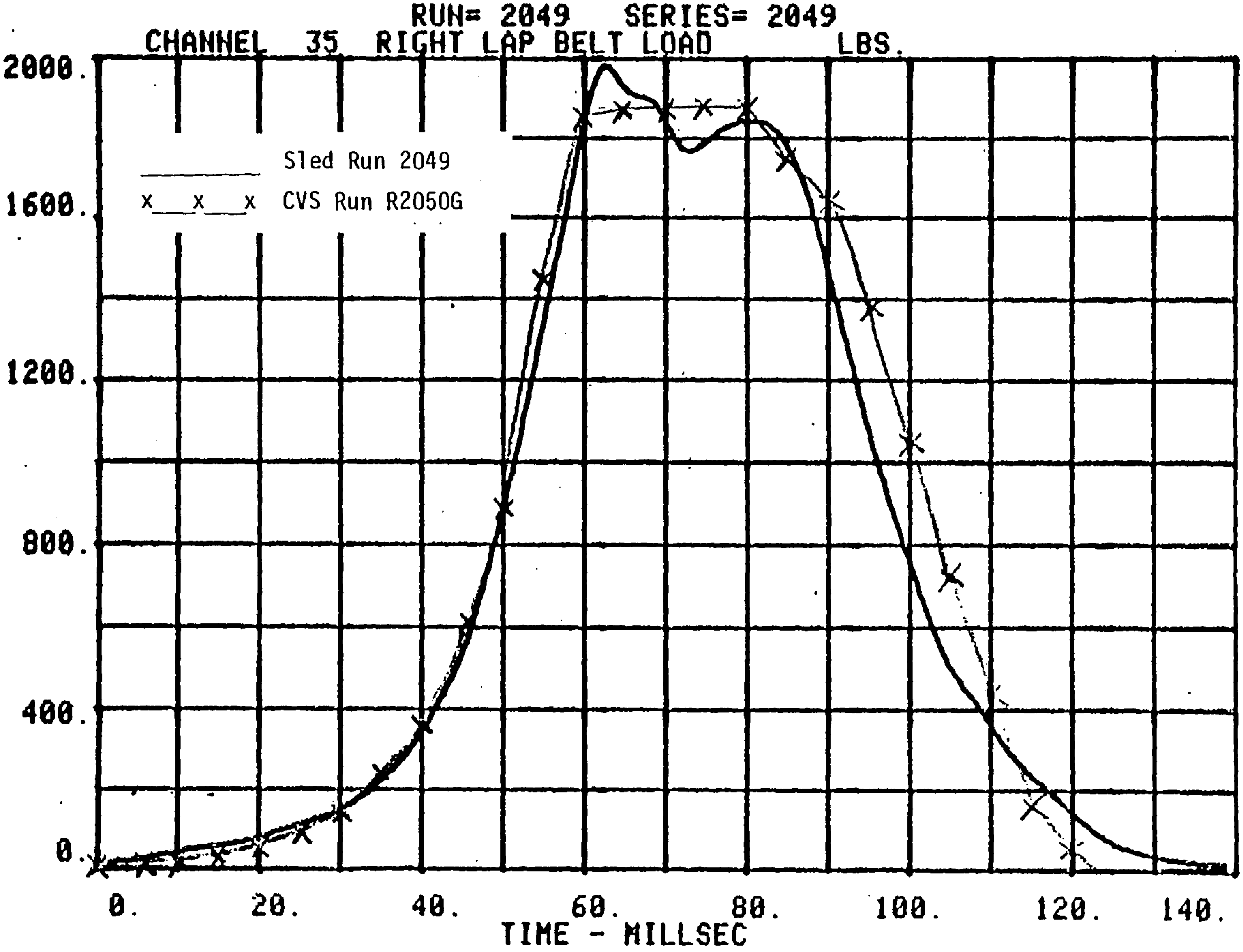

(b) Right Lap Belt Load

Figure 5-2 COMPARISON OF CVS MODEL AND MEASURED RESPONSES FOR BELT RESTRAINT CONFIGURATION (CONT'D.)

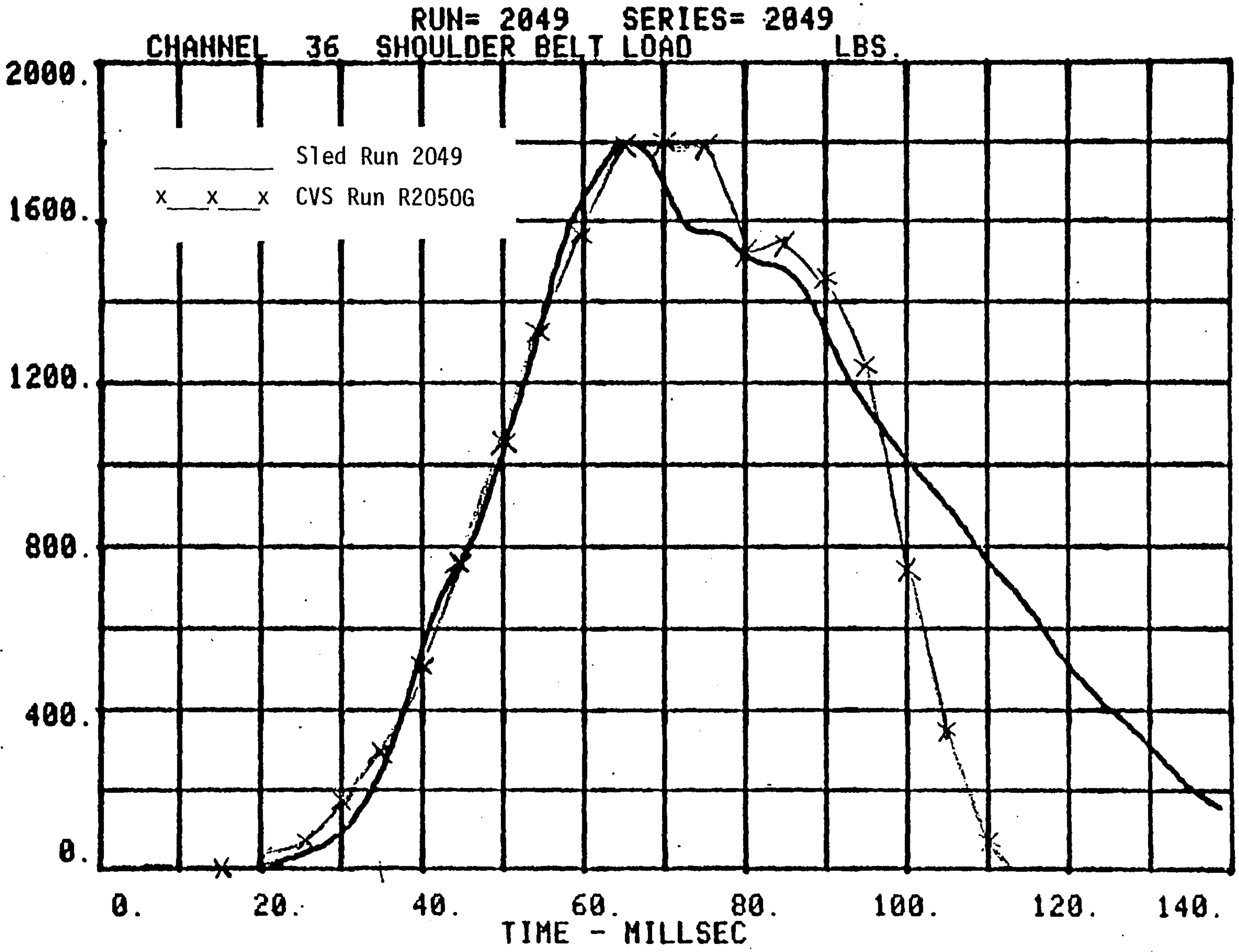

(c) Shoulder Belt Load

Figure 5-2 COMPARISON OF CVS MODEL AND MEASURED RESPONSES FOR BELT RESTRAINT CONFIGURATION (CONT'D.)

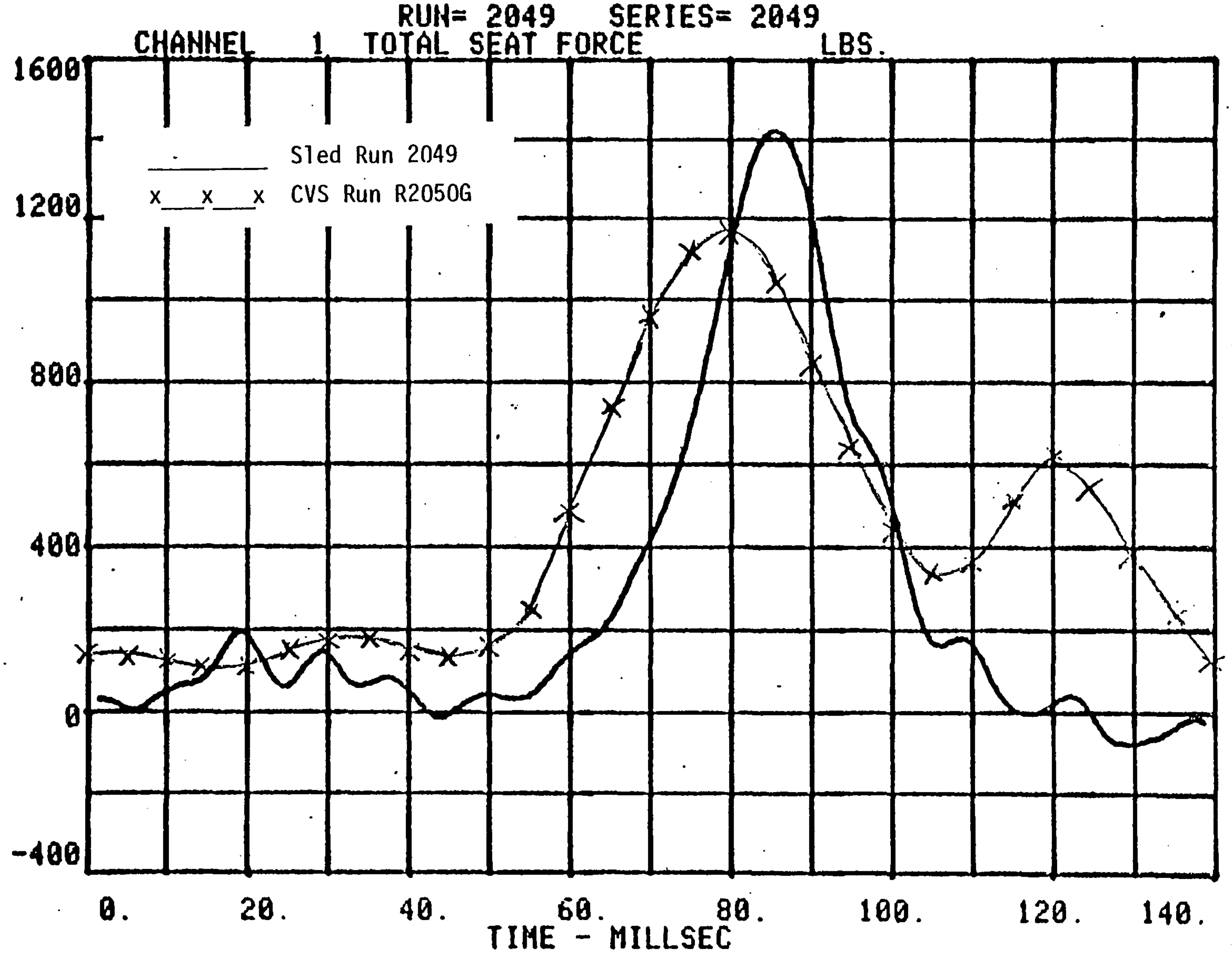

(d) Total Seat Force

Figure 5-2 COMPARISON OF CVS MODEL AND MEASURED RESPONSES FOR BELT RESTRAINT CONFIGURATION (CONT'D.)

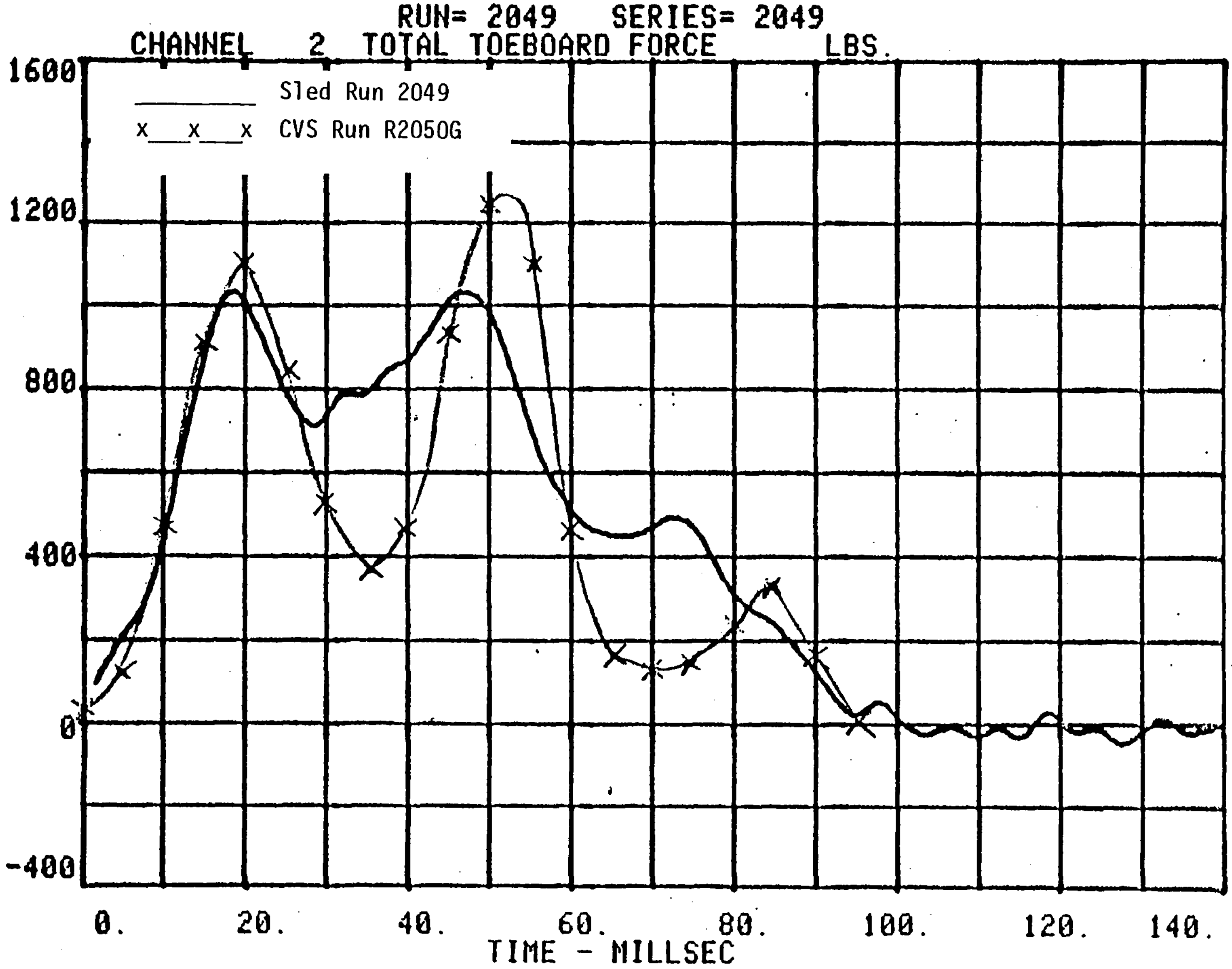

(e) Total Toeboard Force

Figure 5-2 COMPARISON OF CVS MODEL AND MEASURED RESPONSES FOR BELT RESTRAINT CONFIGURATION (CONT'D.)

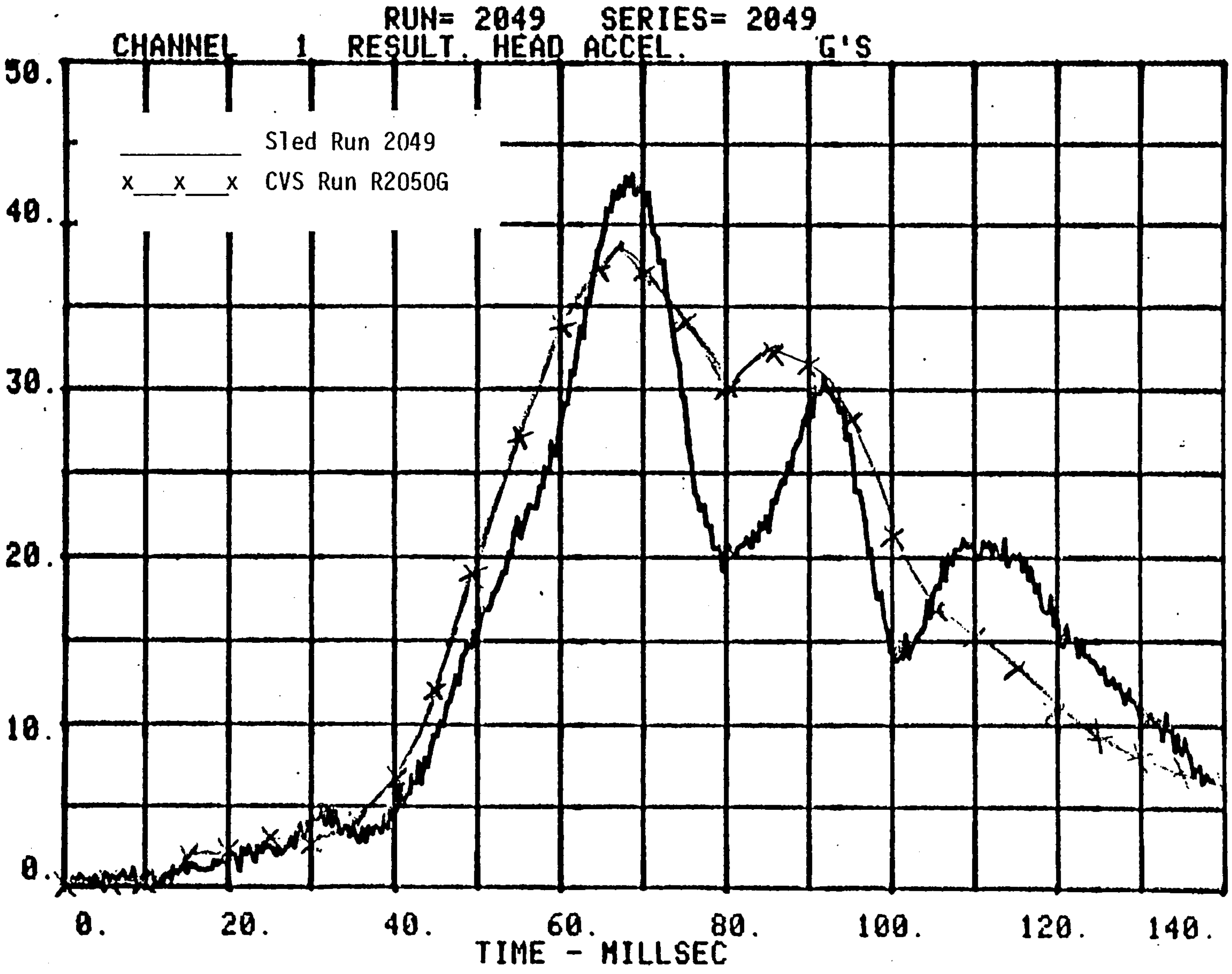

(f) Resultant Head Acceleration

Figure 5-2 COMPARISON OF CVS MODEL AND MEASURED RESPONSES FOR BELT RESTRAINT CONFIGURATION (CONT'D.)

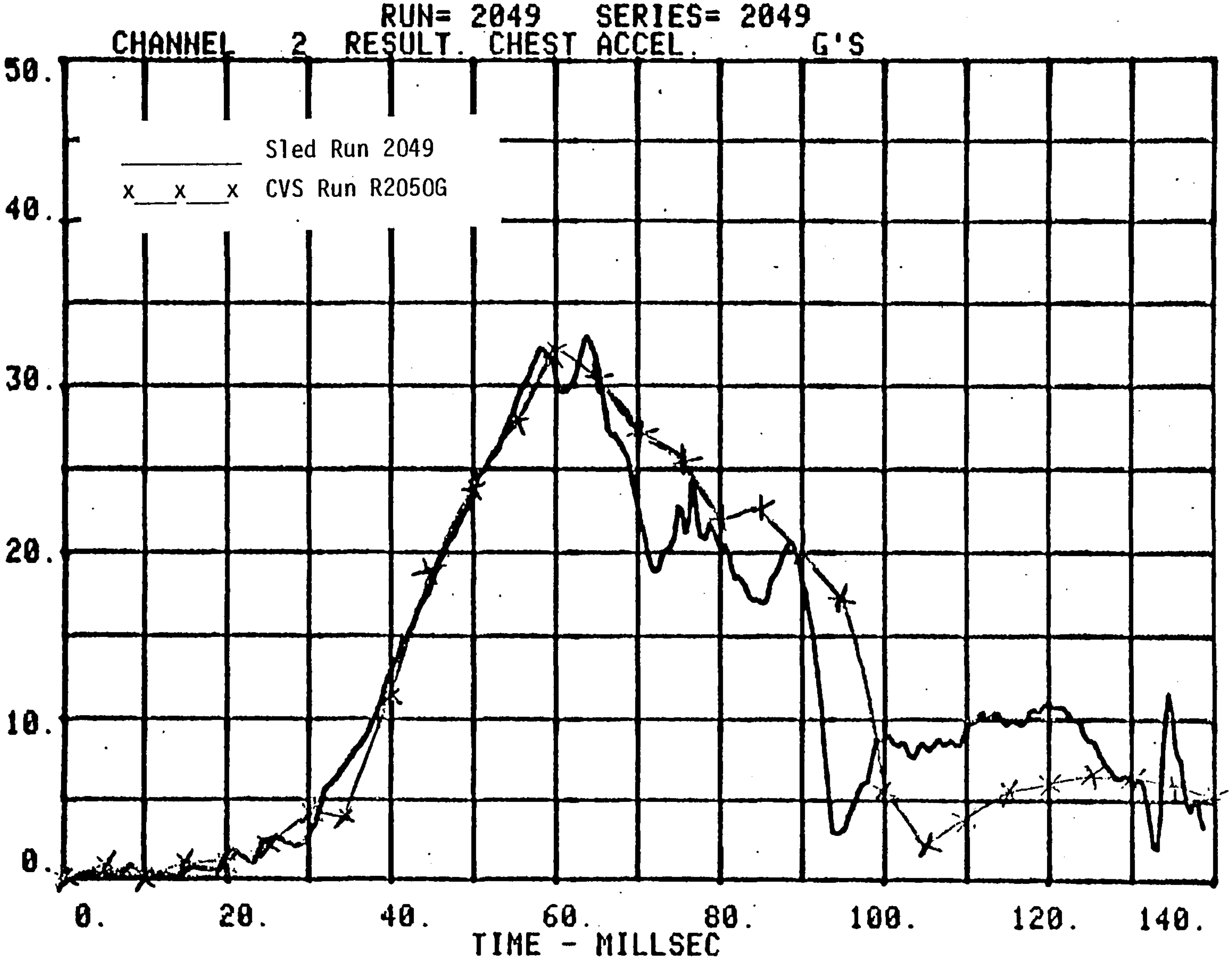

(g) Resultant Chest Acceleration

Figure 5-2 COMPARISON OF CVS MODEL AND MEASURED RESPONSES FOR BELT RESTRAINT CONFIGURATION (CONT'D.)

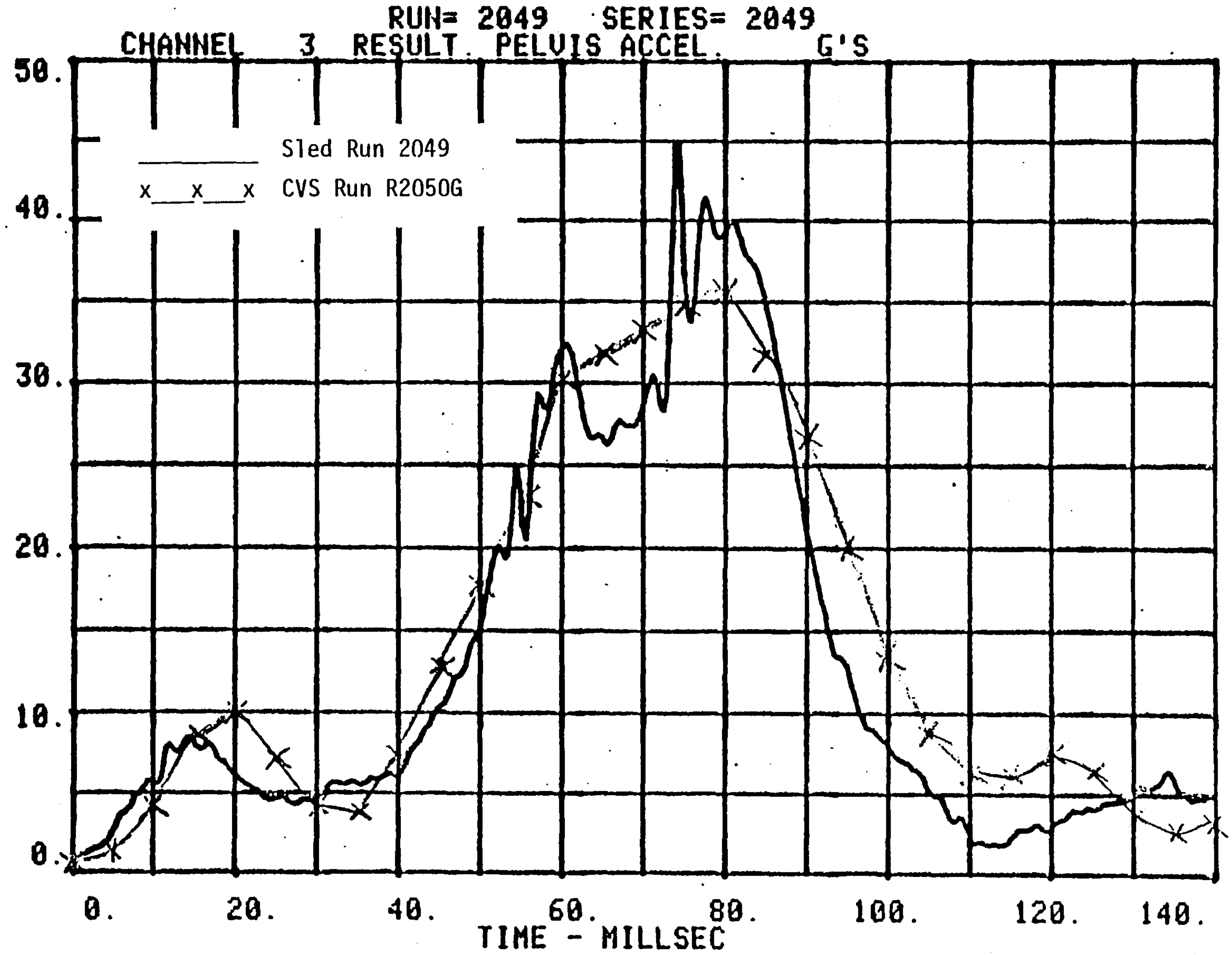

(h) Resultant Pelvis Acceleration

Figure 5-2 COMPARISON OF CVS MODEL AND MEASURED RESPONSES FOR BELT RESTRAINT CONFIGURATION (CONT'D.)

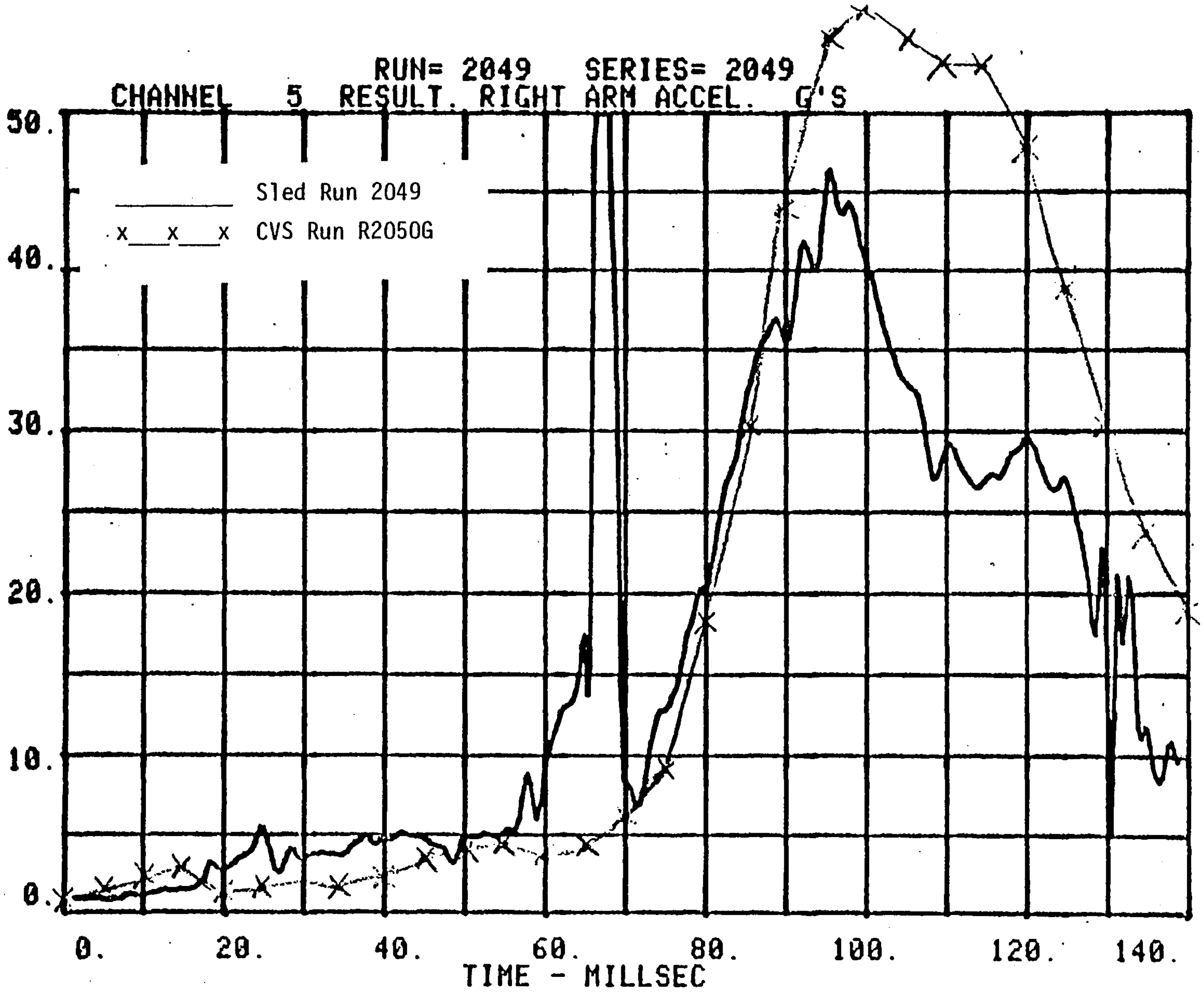

(i) Right Arm Resultant Acceleration

Figure 5-2 COMPARISON OF CVS MODEL AND MEASURED RESPONSES FOR BELT RESTRAINT CONFIGURATION (CONT'D.)

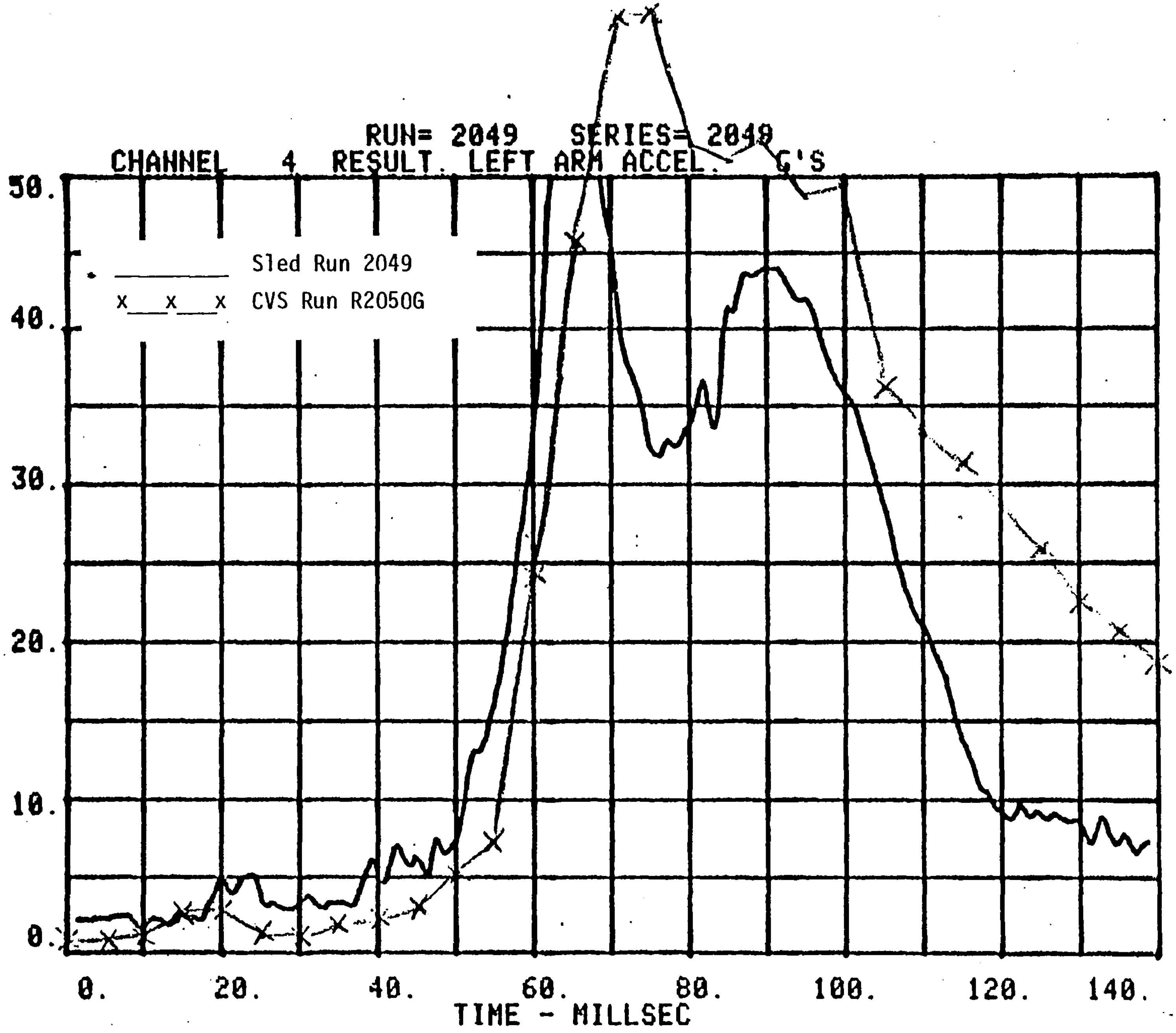

(j) Left Arm Resultant Acceleration

Figure 5-2 COMPARISON OF CVS MODEL AND MEASURED RESPONSES FOR BELT RESTRAINT CONFIGURATION (CONT'D.)

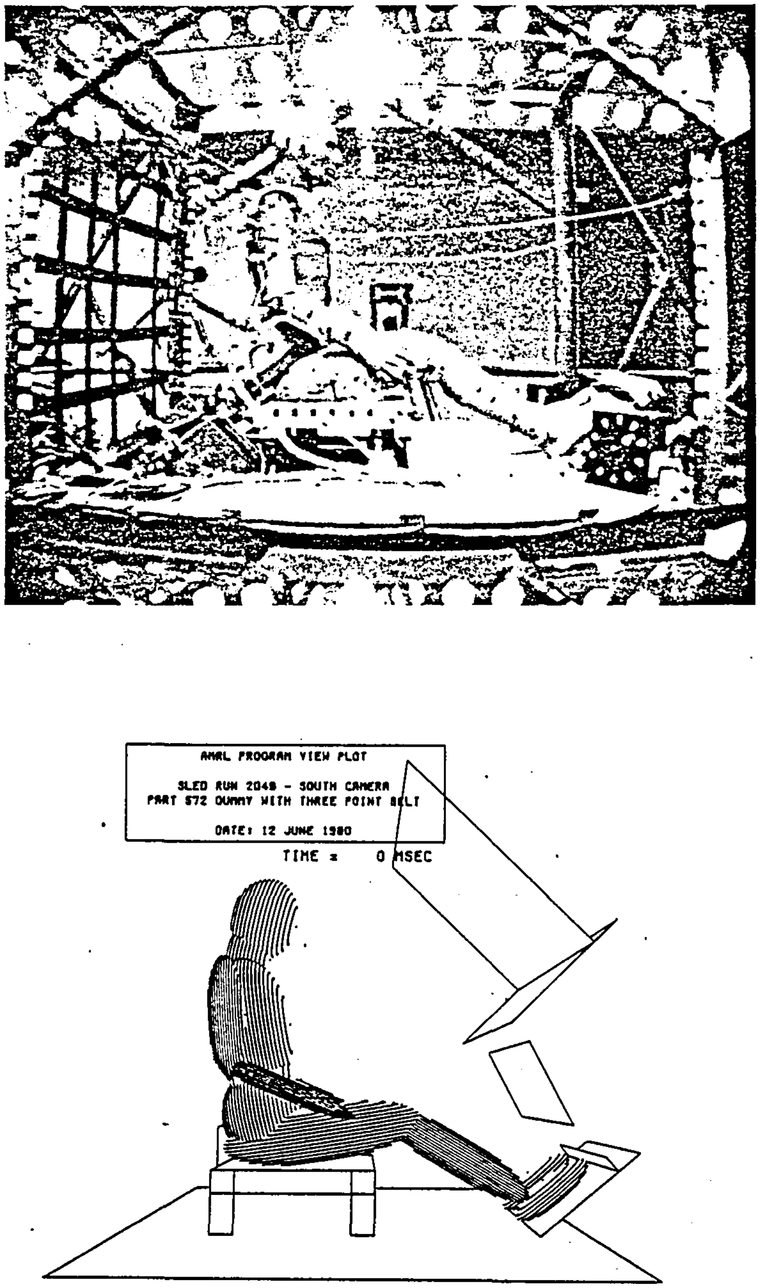

(a) t = 0 msec.

Figure 5-3 COMPARISON OF CALSPAN SLED RUN 2049 AND CVS RUN R2050G

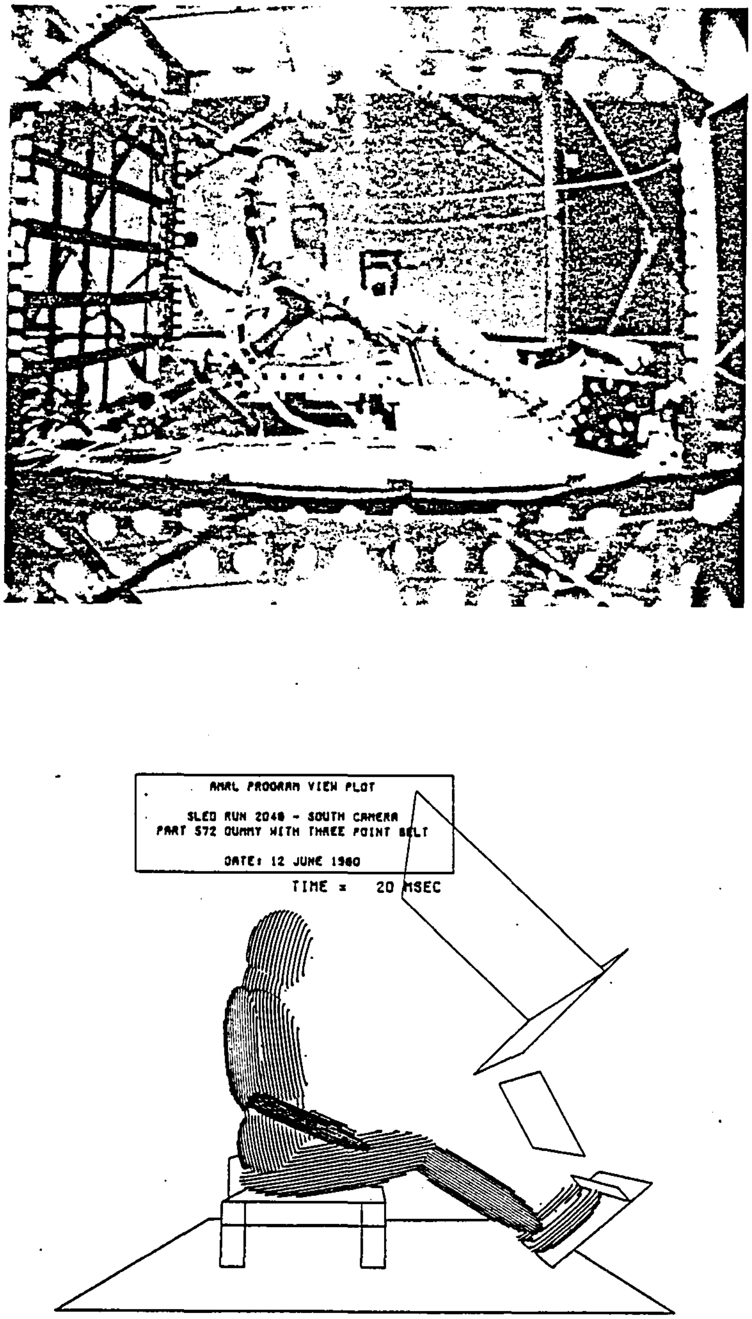

Figure 5-3 (b) t = 20 msec.

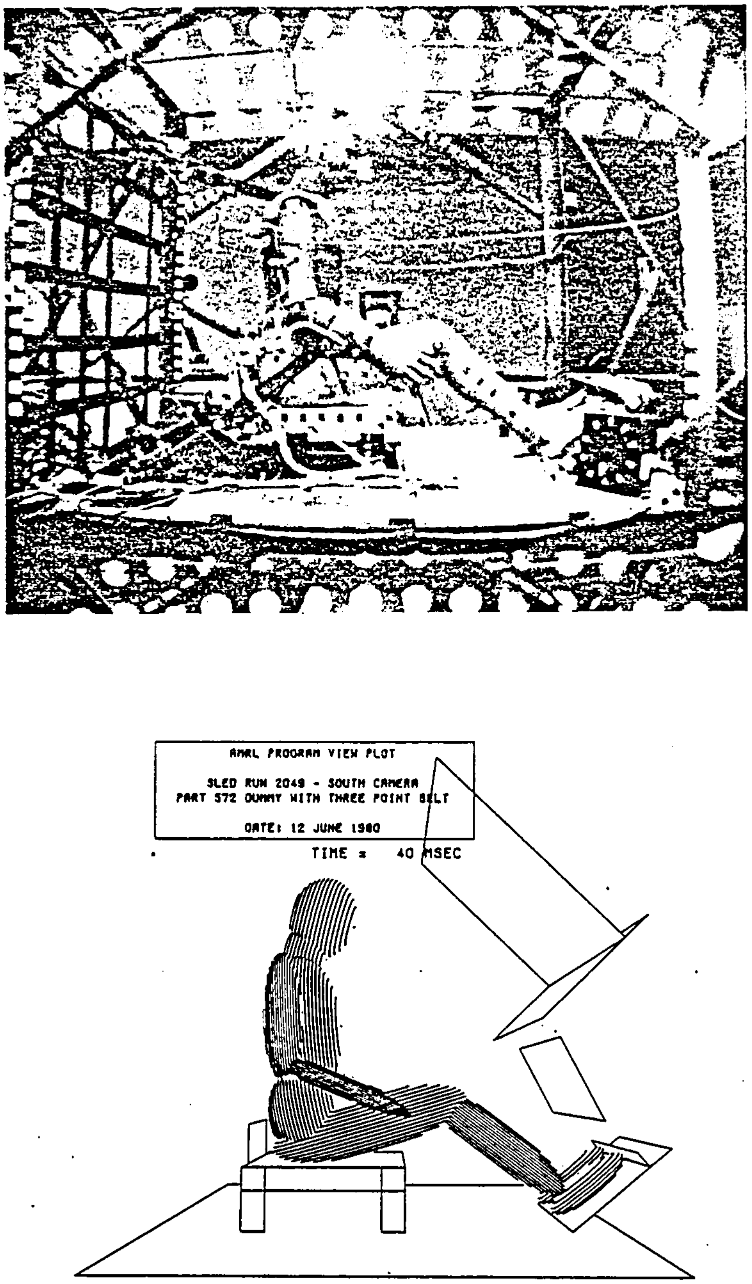

Figure 5-3 (c) t = 40 msec.

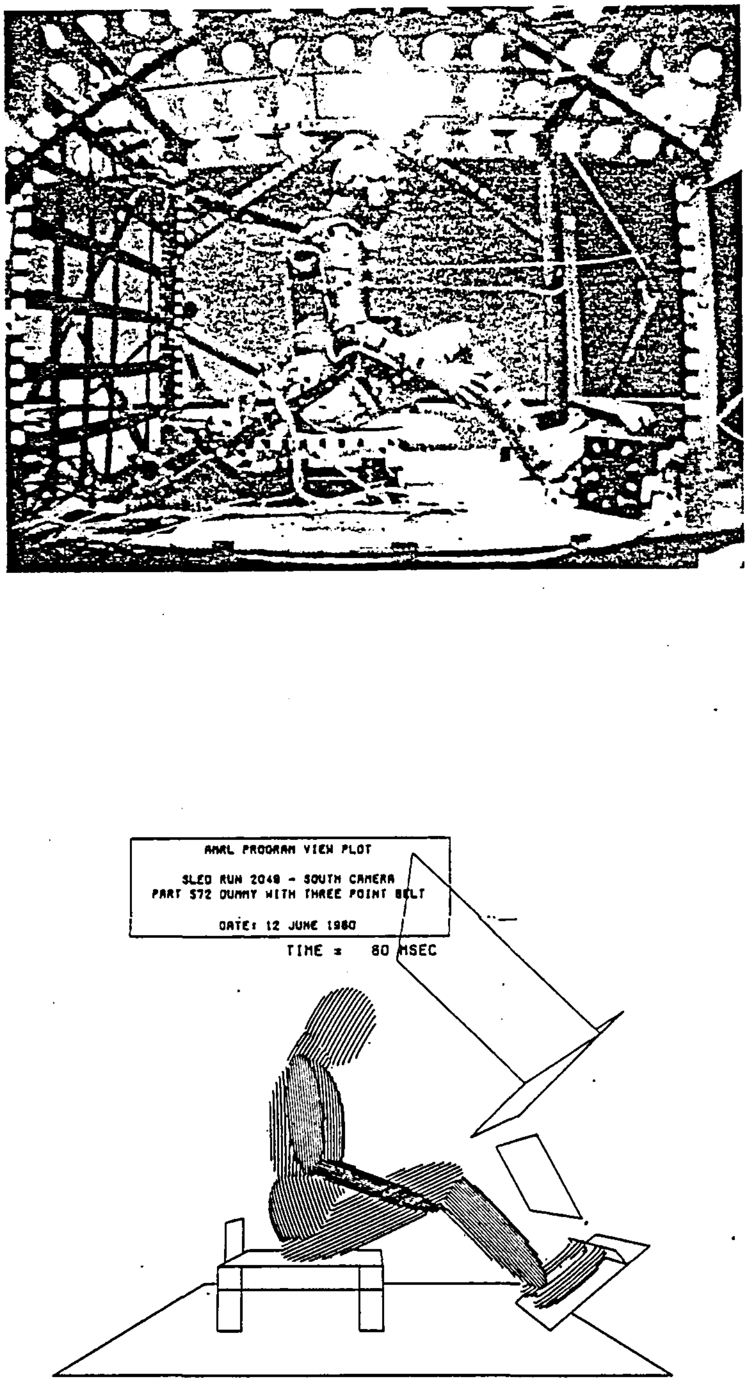

Figure 5-3 (d) t = 60 msec.

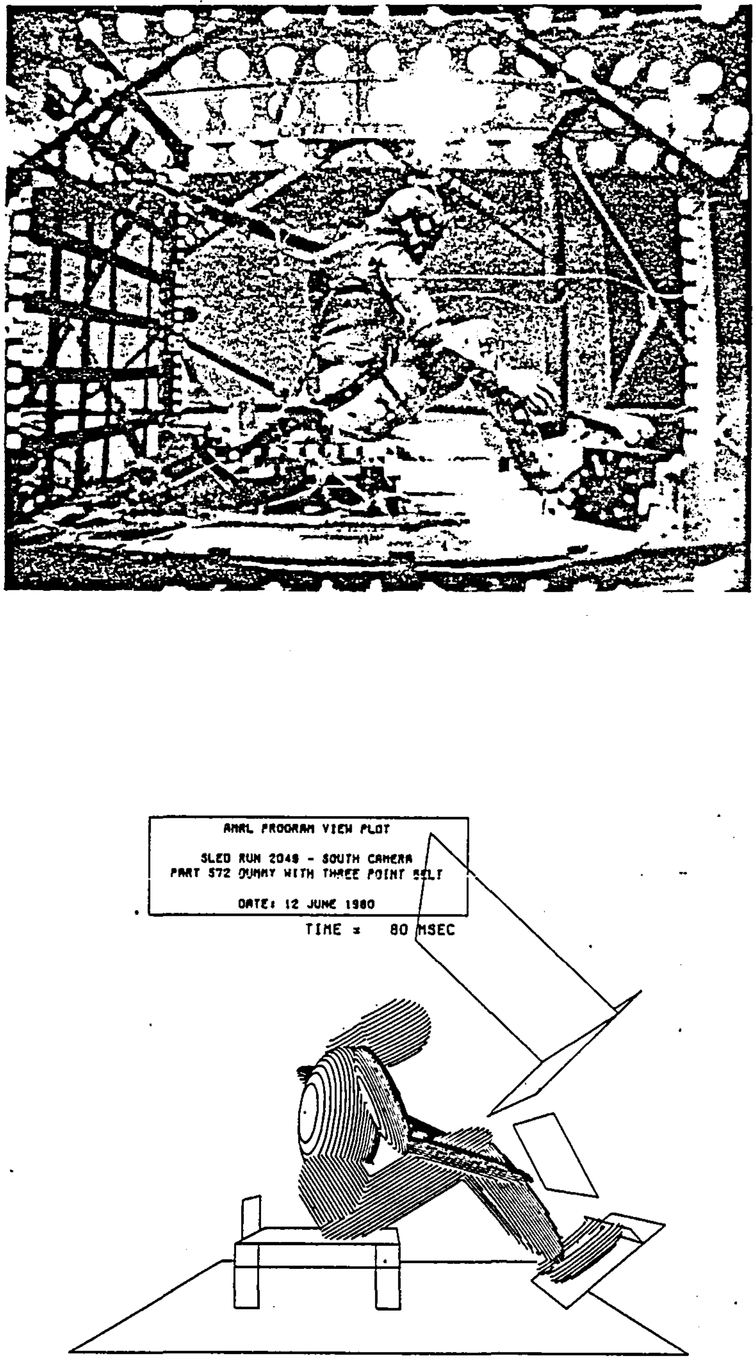

Figure 5-3 (e) t = 80 msec.

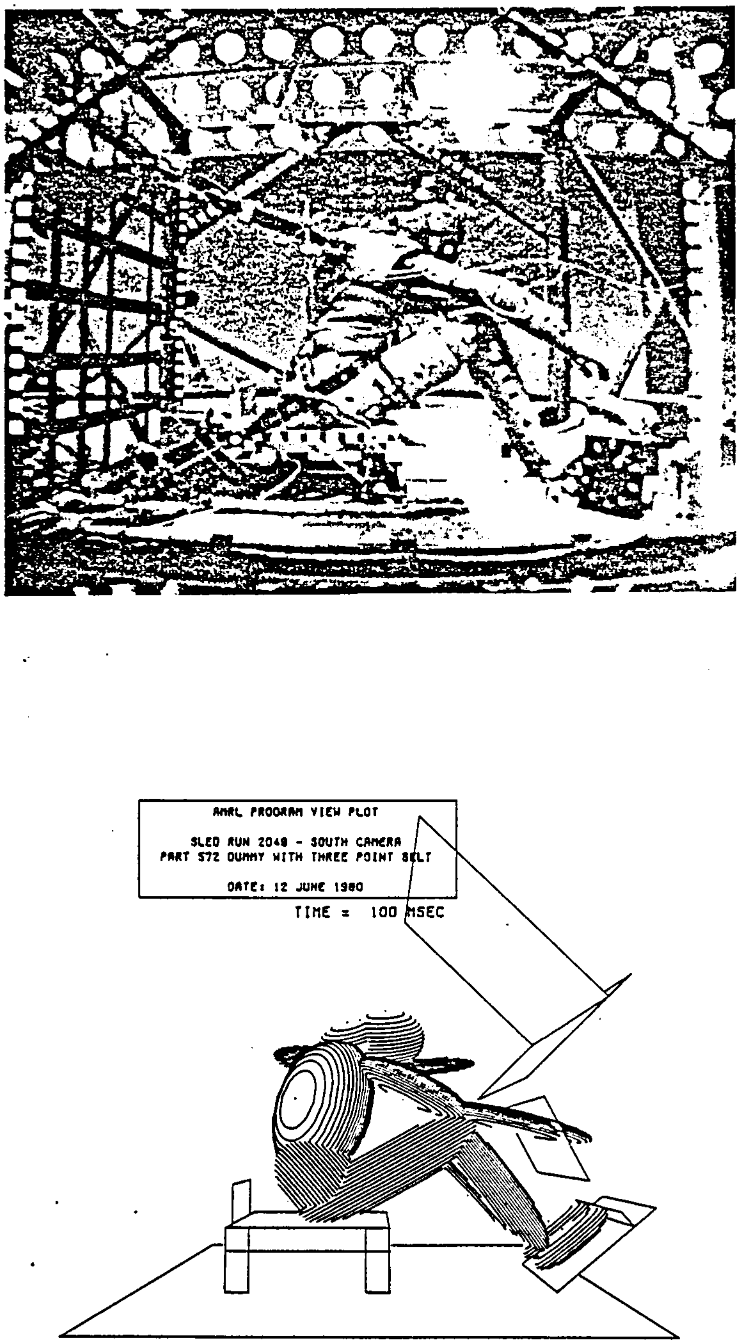

Figure 5-3 (f) t = 100 msec.

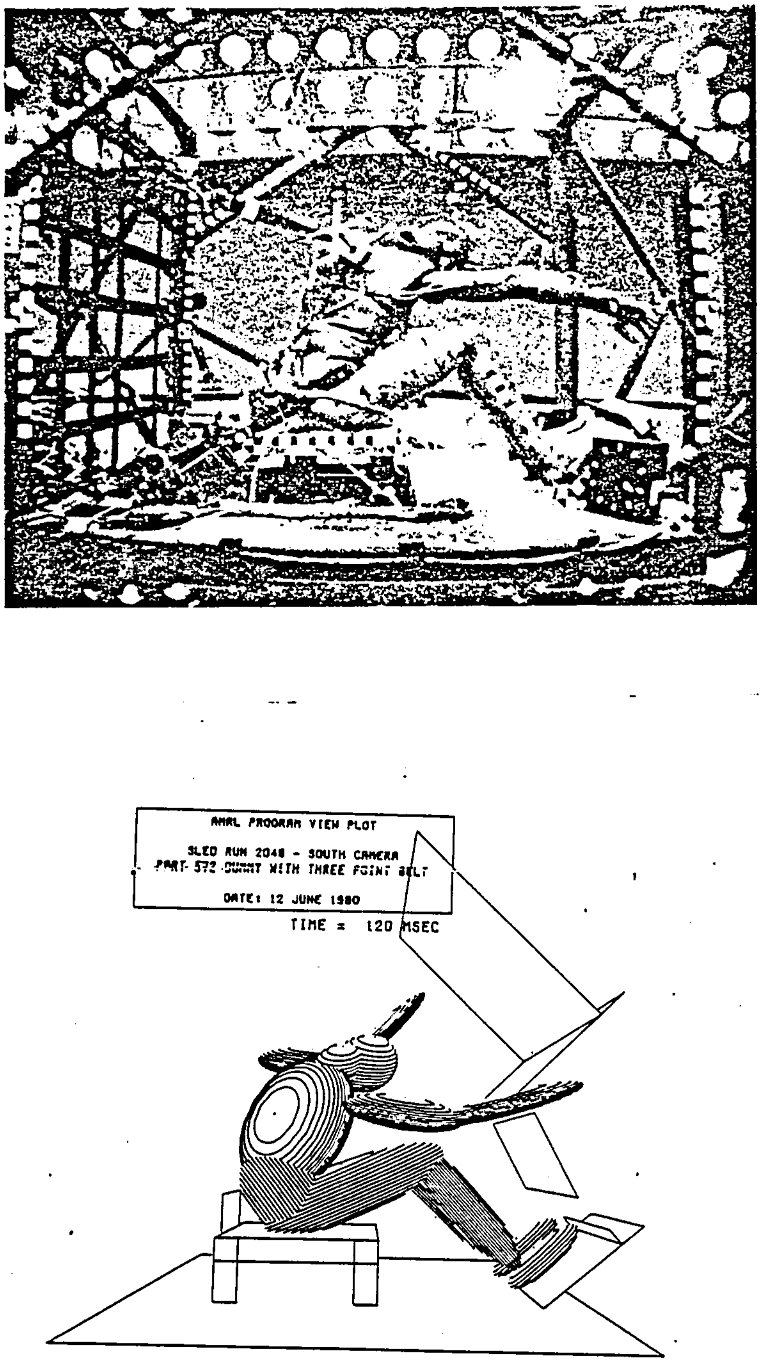

Figure 5-3 (g) t = 120 msec.

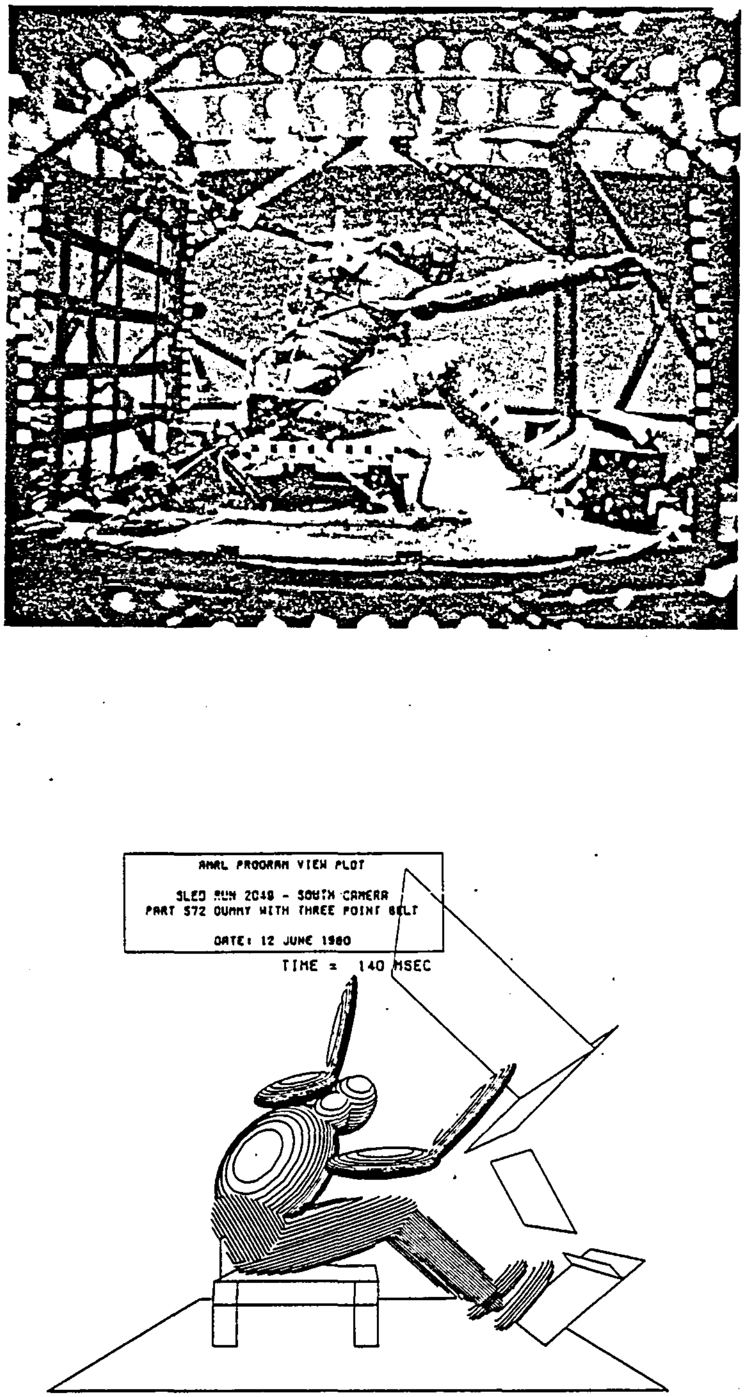

Figure 5-3 (h) t = 140 msec.

values of the input parameters for that panel were also adjusted in the early simulation runs in attempts to achieve better agreement with the sled test measurements.

Results from the simulation model are shown in Figure 5-4 for comparison with response time histories measured in the sled tests. Although the model results are deemed quite favorable with respect to approximating the magnitude and general shape of the waveform of many of the measurement variables, several large discrepancies may be observed that are noteworthy. From the plots of the head accelerations, it may be seen that the peak value of the x component and the large and rapid change from positive to negative of the Z component of acceleration were not accurately predicted by the model. As a result of these differences, the predicted value of the Head Injury Criterion (HIC) was 2120 compared to 1109 computed from the head accelerations measured in the test. Somewhat better agreement is shown by the results for the chest accelerations, but the duration of the predicted pulse is shorter. Note that the x component of the predicted head and chest acceleration responses increase abruptly at about 66 milliseconds. The reason for this is that the pressure in the bag suddenly increased from zero to 1.3 psi in 2 milliseconds when the simulated bag became fully deployed and at which time the occupant had already moved forward several inches so as to penetrate the bag. The buildup of forces in the sled test was initially delayed and then was more gradual partly because of the presence of voids between the (spherical) weather balloon liner and the bag itself. Thus, it was not until the liner had stretched sufficiently to fully contact the interior surface of the bag that pressure started to rise and produce significant restraining forces on the dummy. As may be seen in Figure 5-4 (n), the model overpredicted the peak bag pressure slightly, but, for the most part, the experimental measurements were matched quite closely.

Among the loads imposed on the various contact panels, the normal force on the rigid seat pan was least accurately predicted by the model. In the actual test the dummy lower torso was forced downward against the seat by

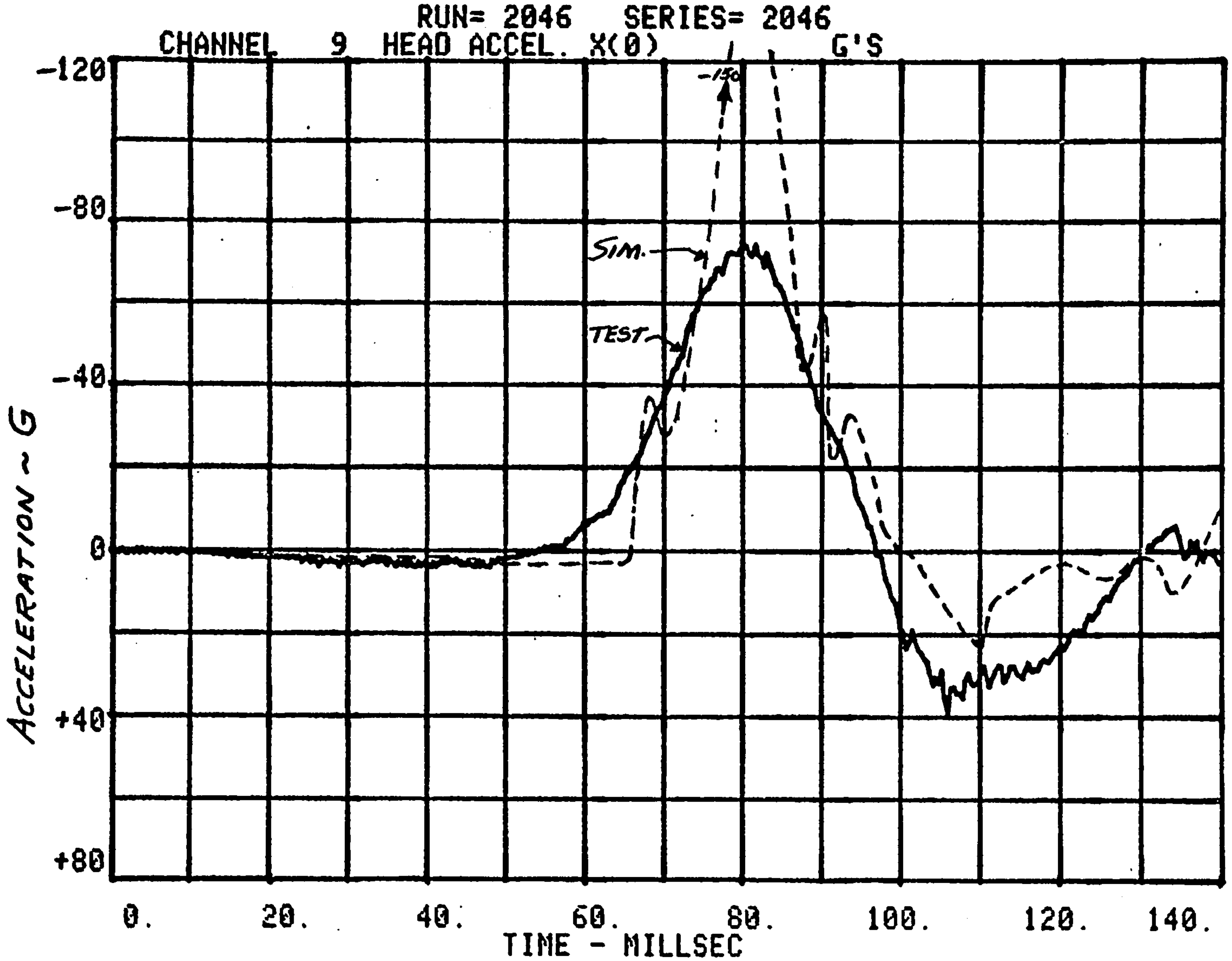

(a) Head X Acceleration

Figure 5-4 COMPARISON OF CVS MODEL AND MEASURED RESPONSES FOR AIR BAG RESTRAINT CONFIGURATION

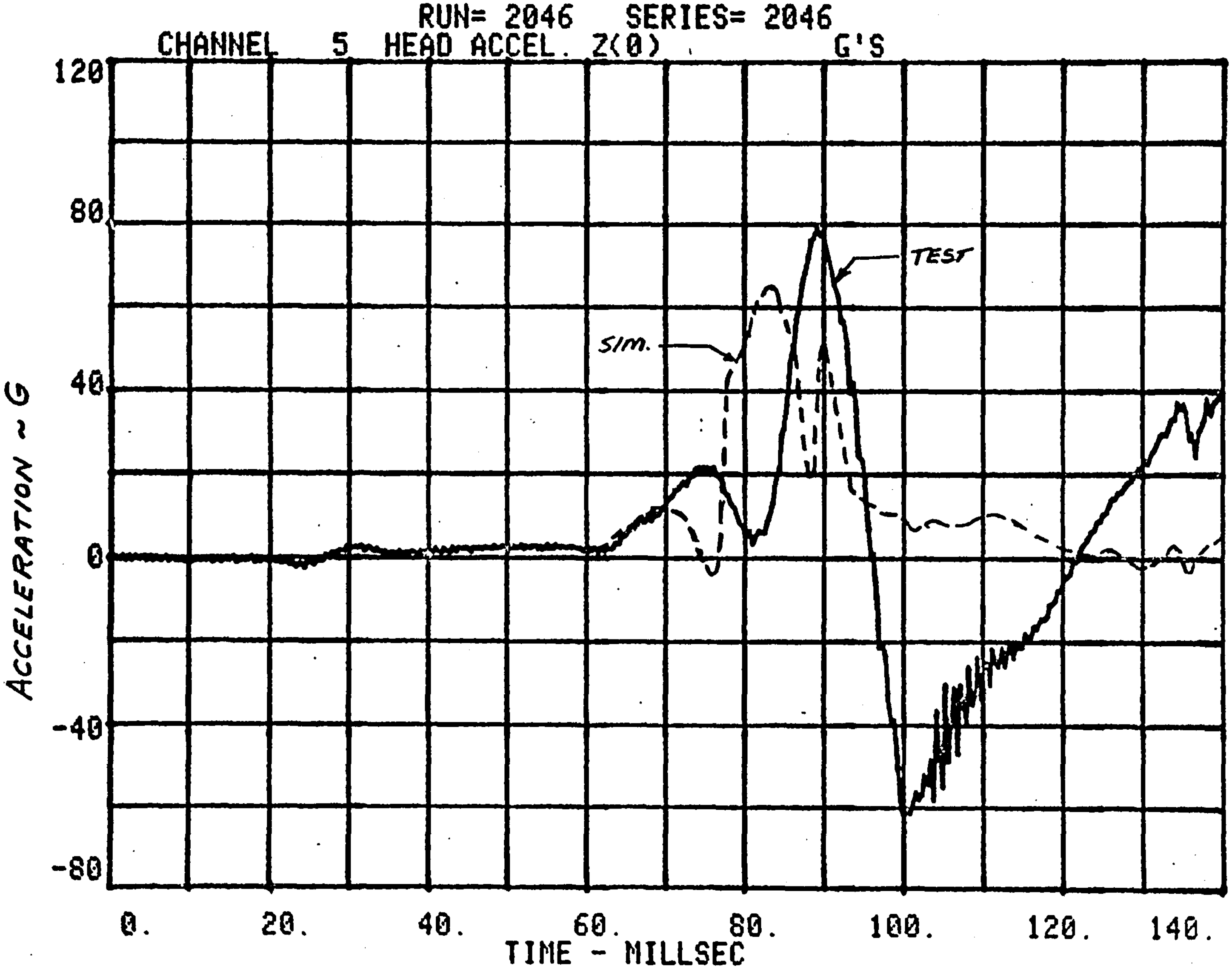

(b) Head Z Acceleration

Figure 5-4 COMPARISON OF CVS MODEL AND MEASURED RESPONSES FOR AIR BAG RESTRAINT CONFIGURATION (CONT'D.)

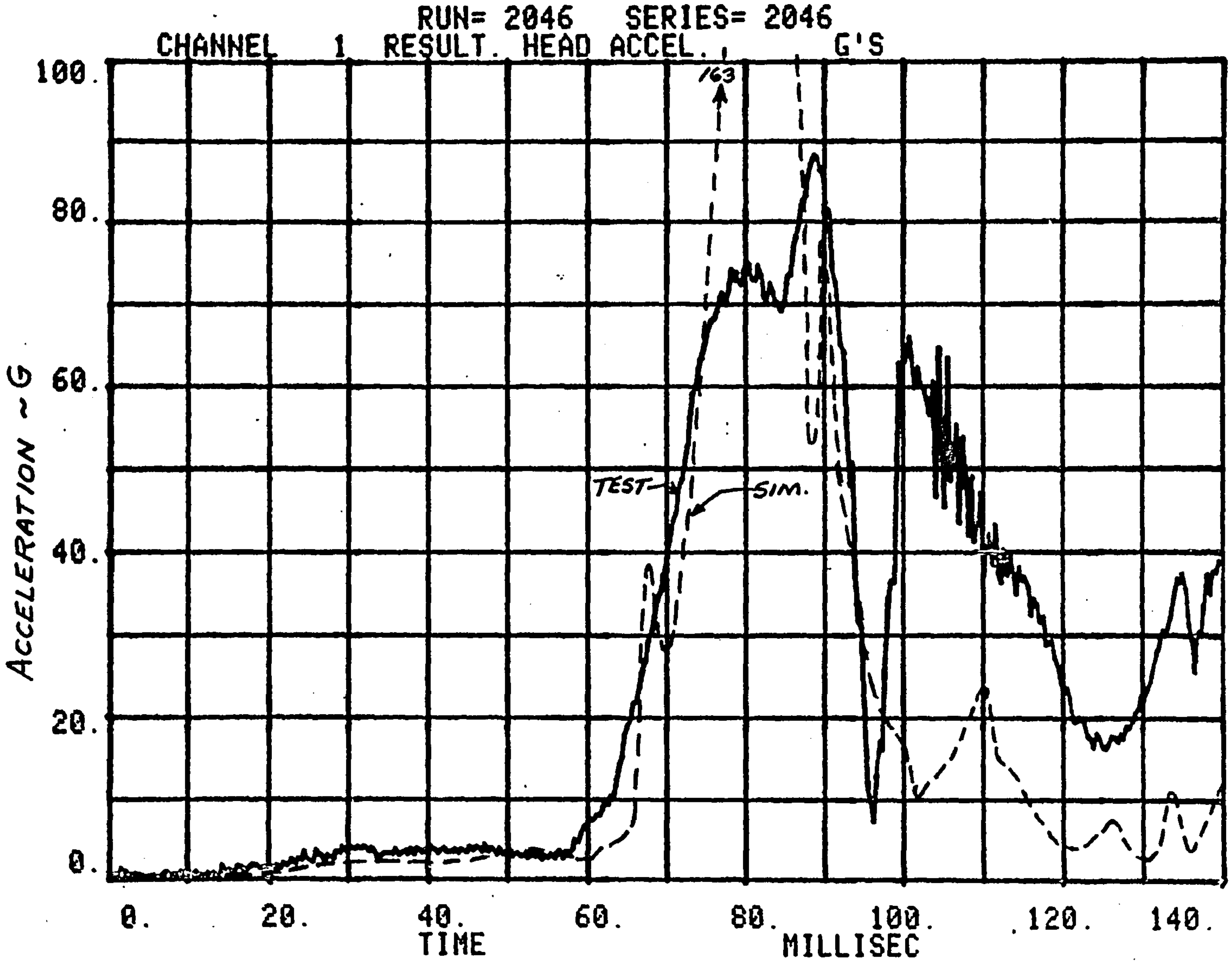

(c) Head Resultant Acceleration

Figure 5-4 COMPARISON OF CVS MODEL AND MEASURED RESPONSES FOR AIR BAG RESTRAINT CONFIGURATION (CONT'D.)

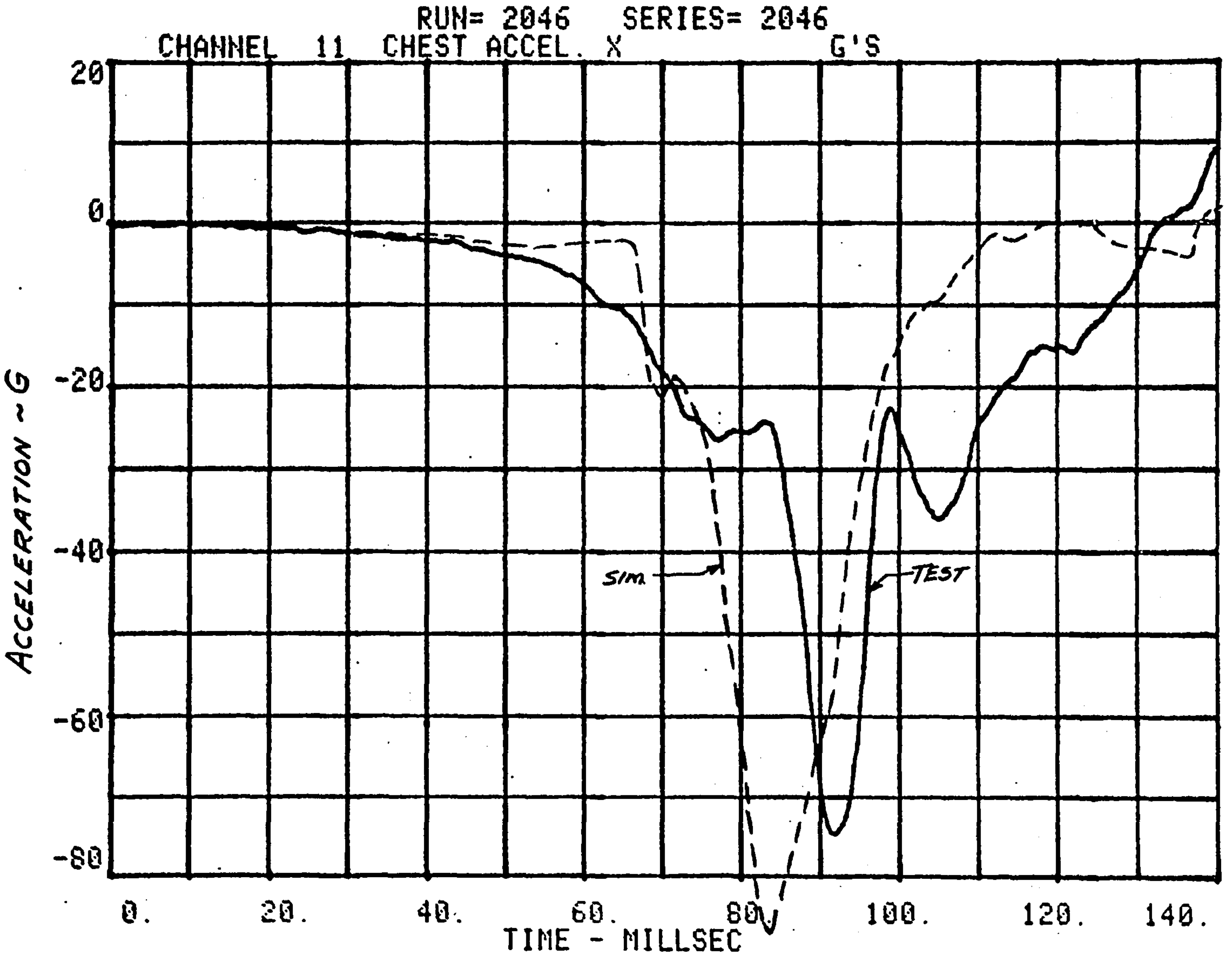

(d) Chest X Acceleration

Figure 5-4 COMPARISON OF CVS MODEL AND MEASURED RESPONSES FOR AIR BAG RESTRAINT CONFIGURATION (CONT'D.)

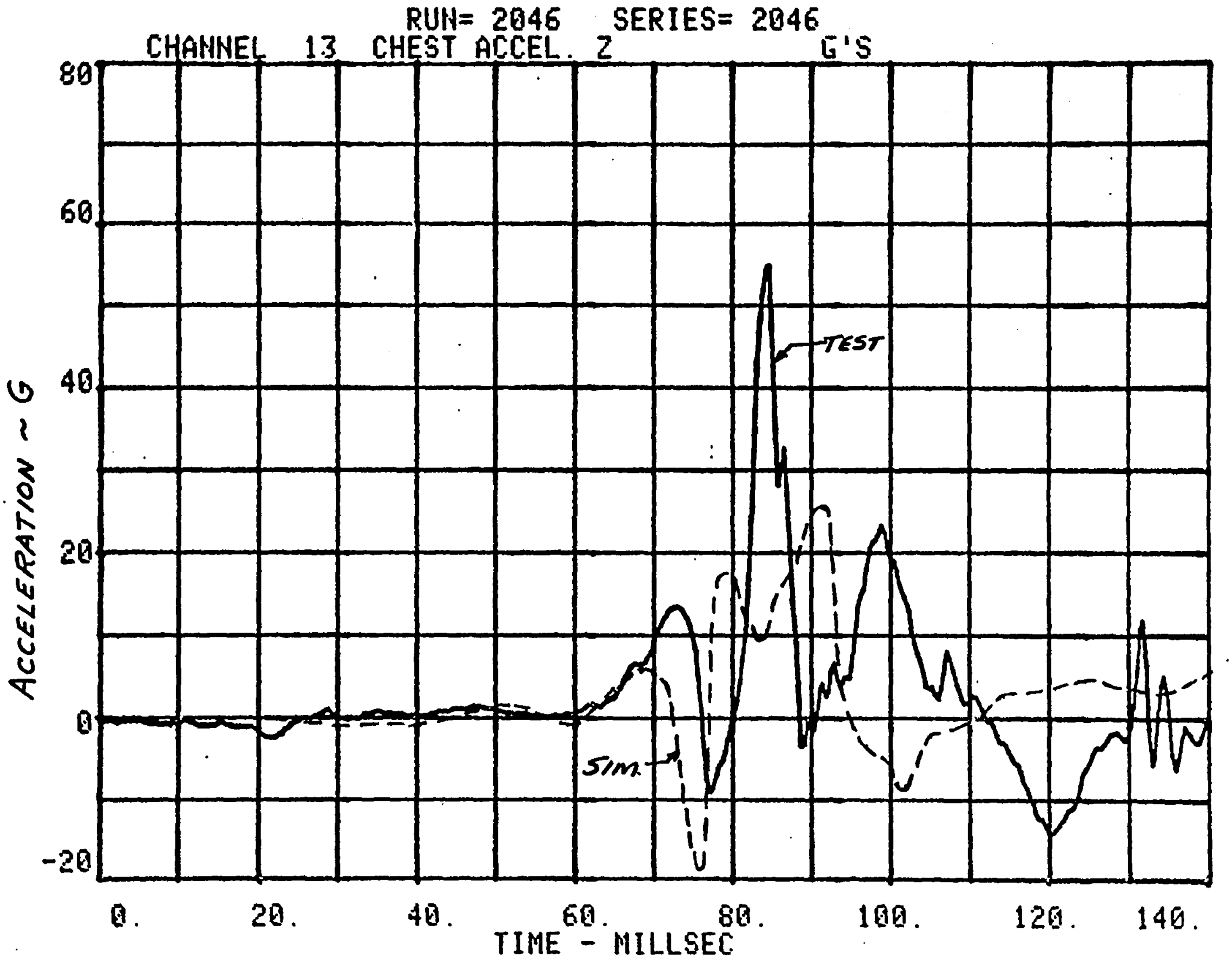

(e) Chest Z Acceleration

Figure 5-4 COMPARISON OF CVS MODEL AND MEASURED RESPONSES FOR AIR BAG RESTRAINT CONFIGURATION (CONT'D.)

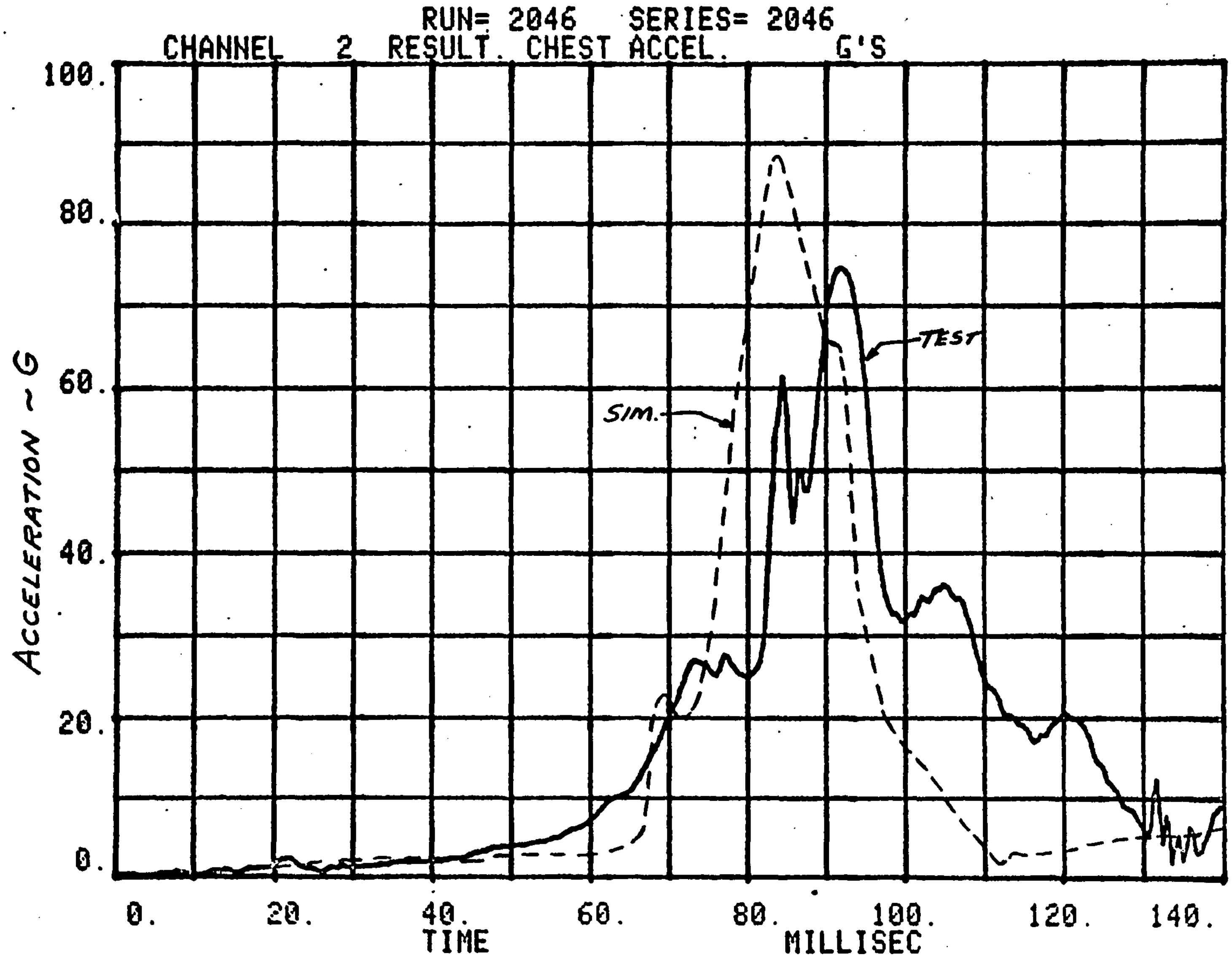

(f) Chest Resultant Acceleration

Figure 5-4 COMPARISON OF CVS MODEL AND MEASURED RESPONSES FOR AIR BAG RESTRAINT CONFIGURATION (CONT'D.)

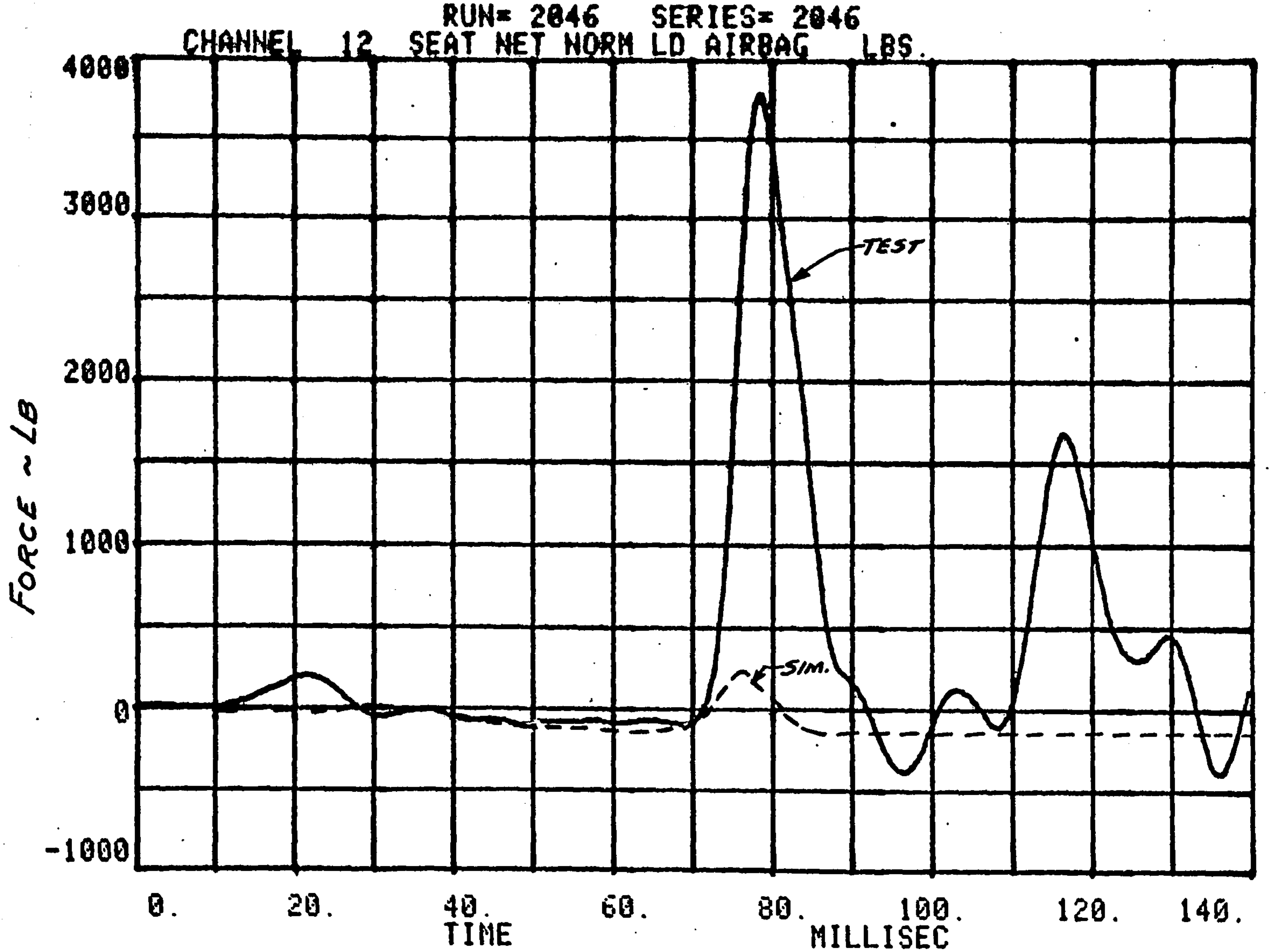

(g) Seat Normal Load

Figure 5-4 COMPARISON OF CVS MODEL AND MEASURED RESPONSES FOR AIR BAG RESTRAINT CONFIGURATION (CONT'D.)

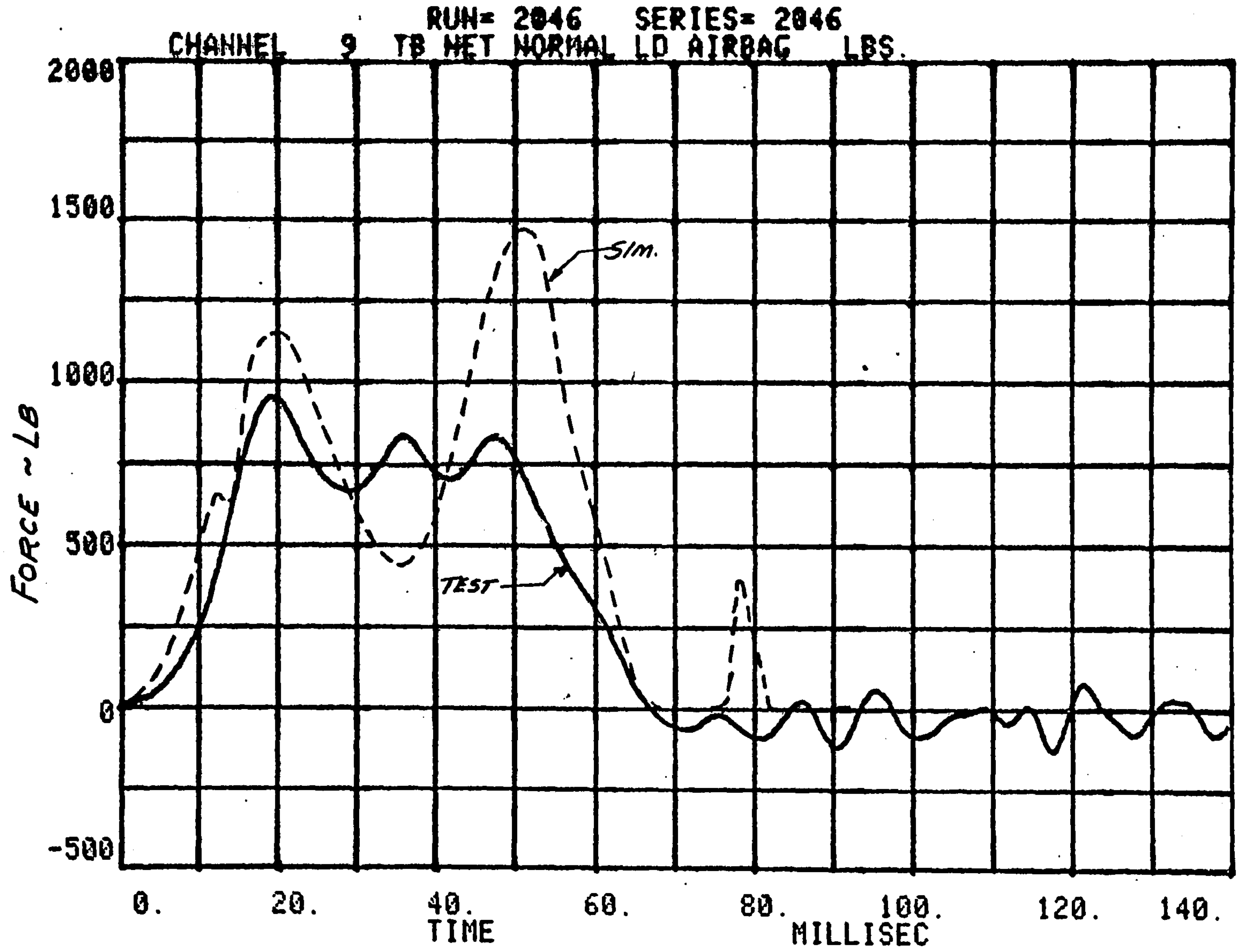

(h) Toeboard Normal Load

Figure 5-4 COMPARISON OF CVS MODEL AND MEASURED RESPONSES FOR AIR BAG RESTRAINT CONFIGURATION (CONT'D.)

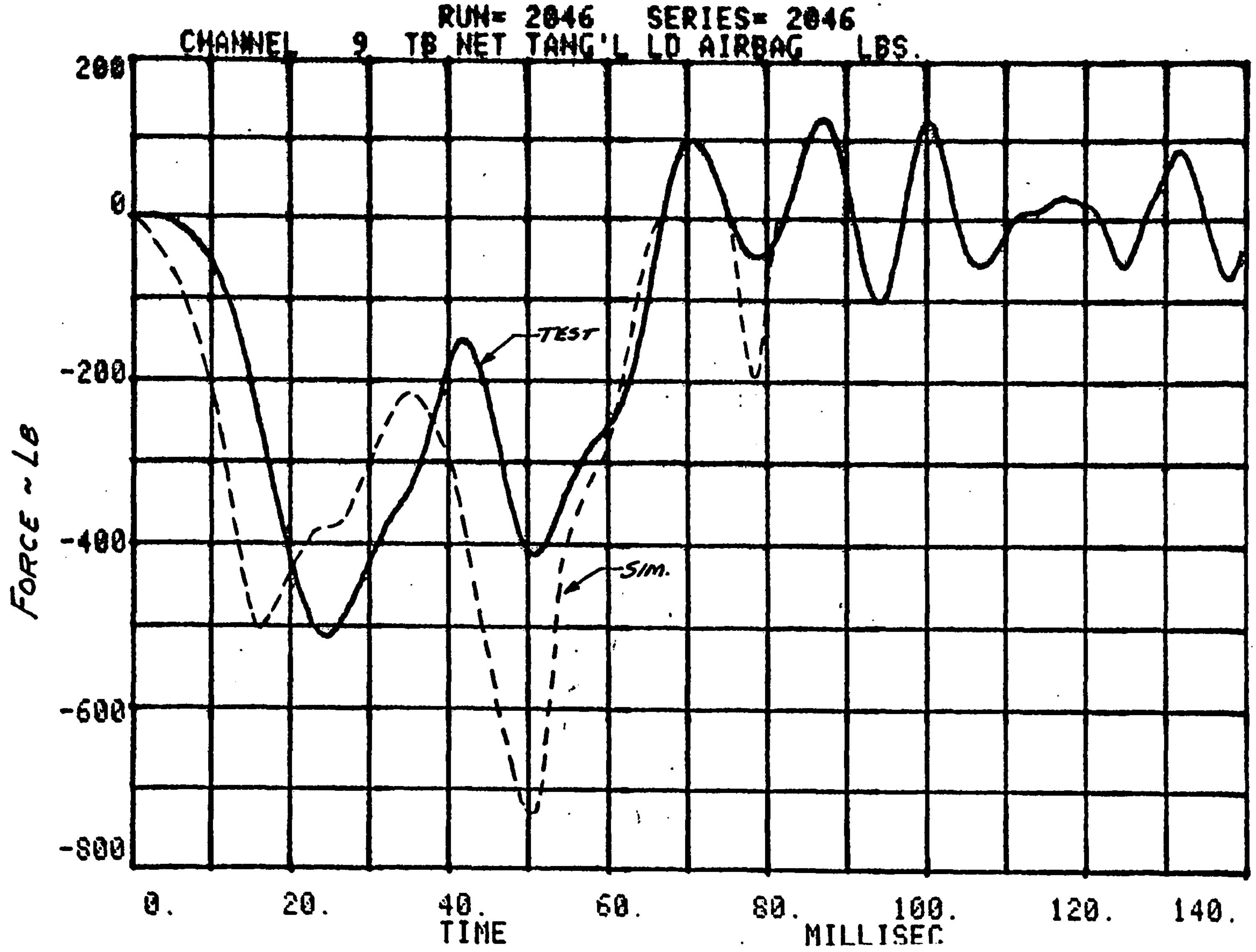

(i) Toeboard Tangential Load

Figure 5-4 COMPARISON OF CVS MODEL AND MEASURED RESPONSES FOR AIR BAG RESTRAINT CONFIGURATION (CONT'D.)

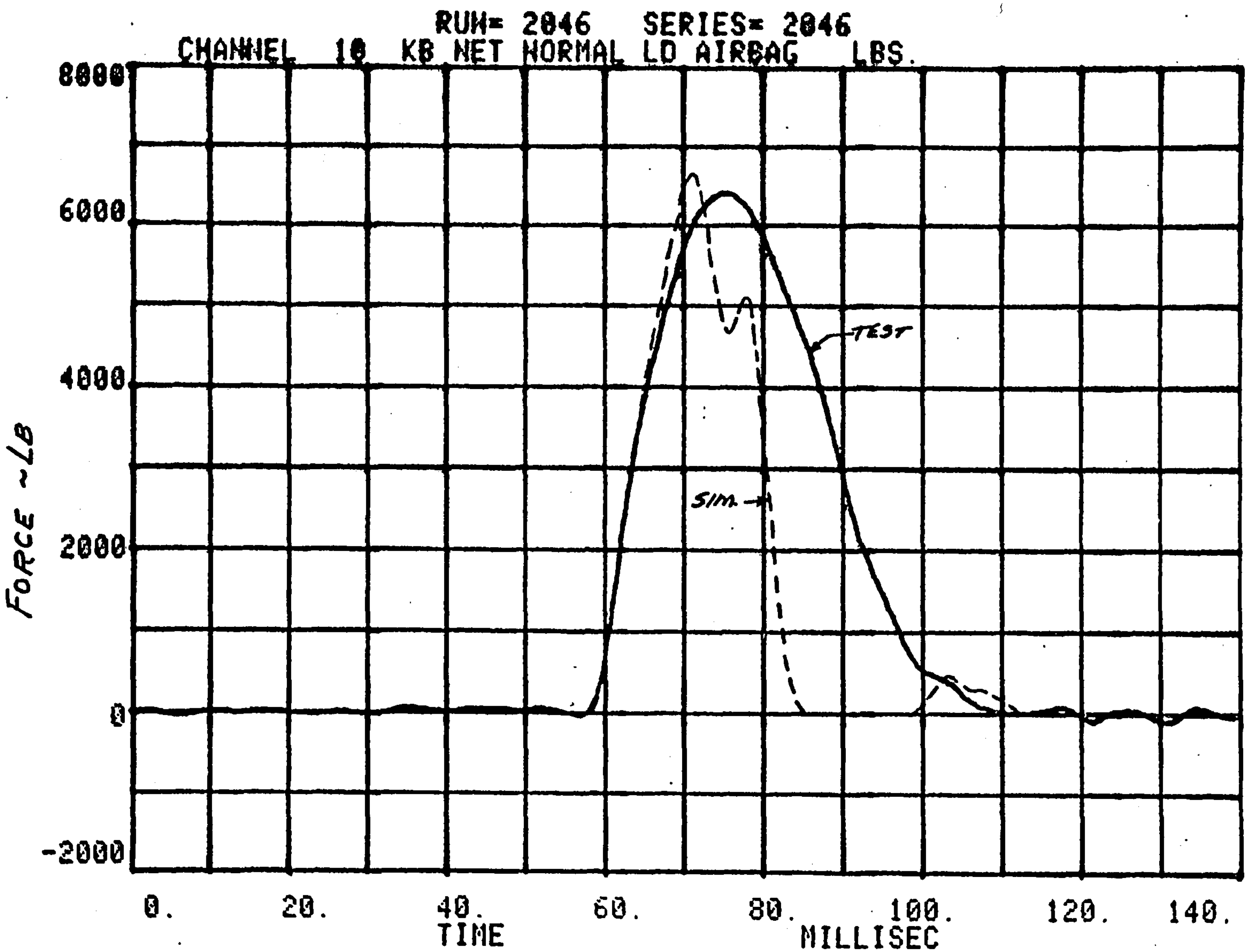

(j) Knee Bolster Normal Load

Figure 5-4 COMPARISON OF CVS MODEL AND MEASURED RESPONSES FOR AIR BAG RESTRAINT CONFIGURATION (CONT'D.)

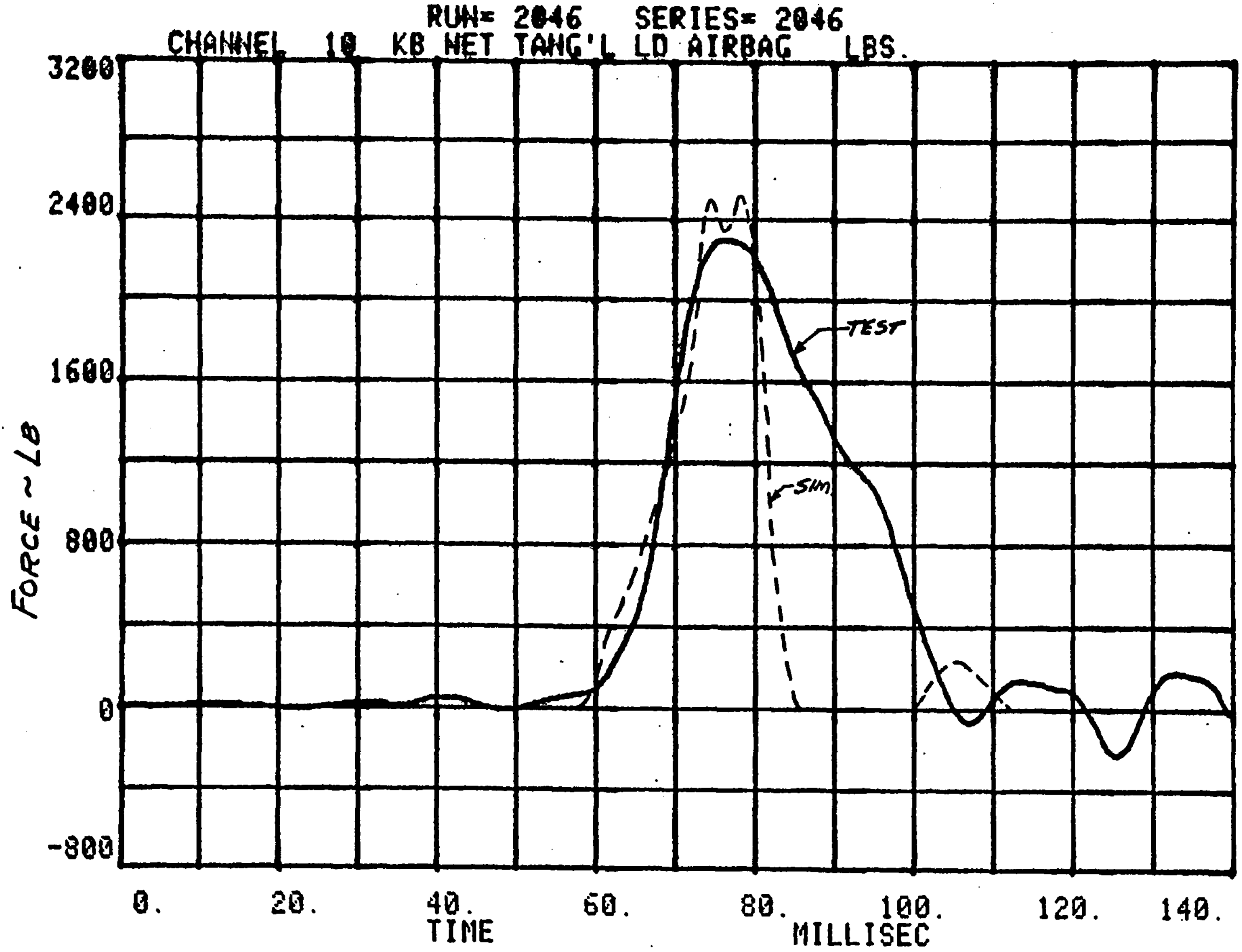

(k) Knee Bolster Tangential Load

Figure 5-4 COMPARISON OF CVS MODEL AND MEASURED RESPONSES FOR AIR BAG RESTRAINT CONFIGURATION (CONT'D.)

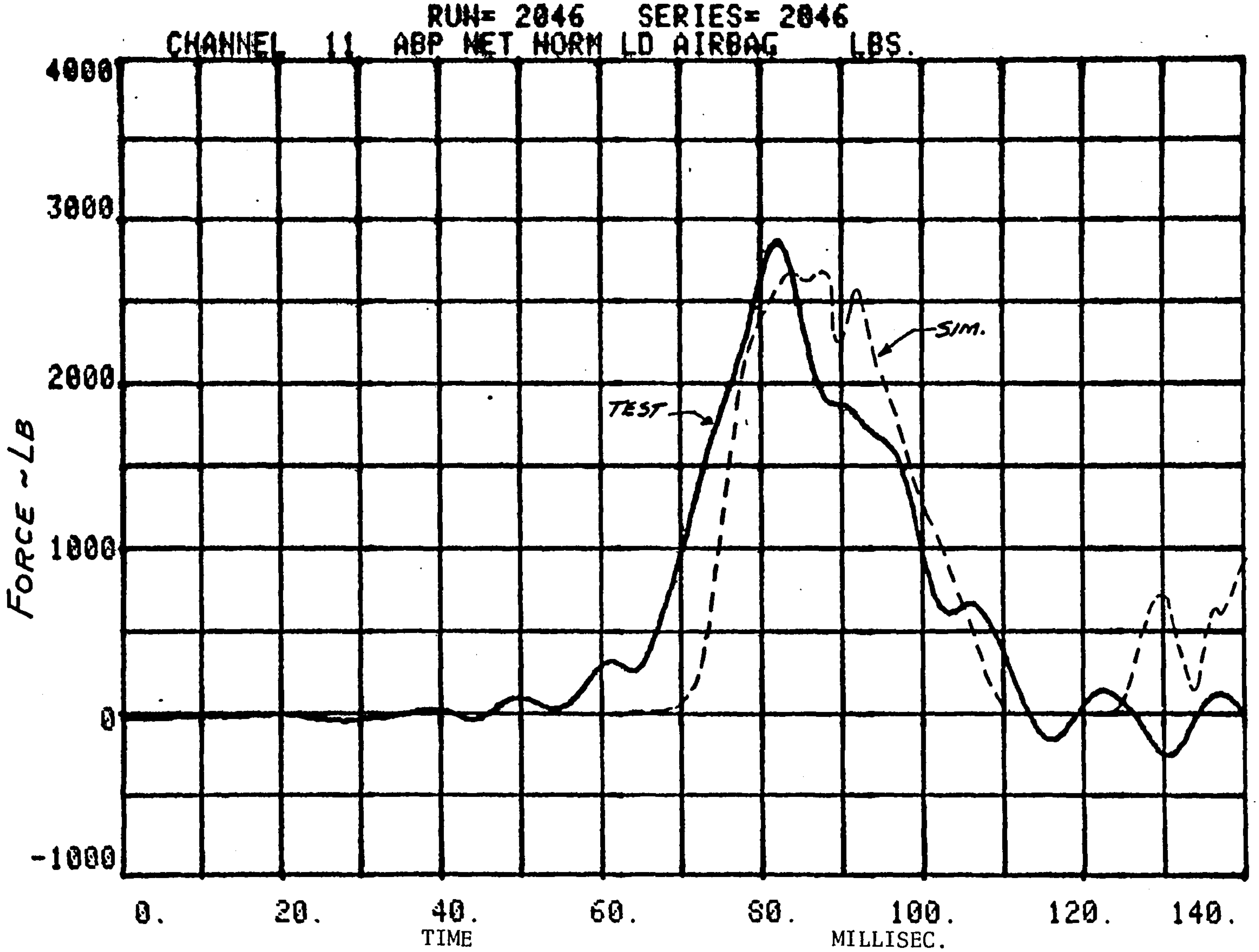

(1) Air Bag Panel Normal Load (Windshield)

Figure 5-4 COMPARISON OF CVS MODEL AND MEASURED RESPONSES FOR AIR BAG RESTRAINT CONFIGURATION (CONT'D.)

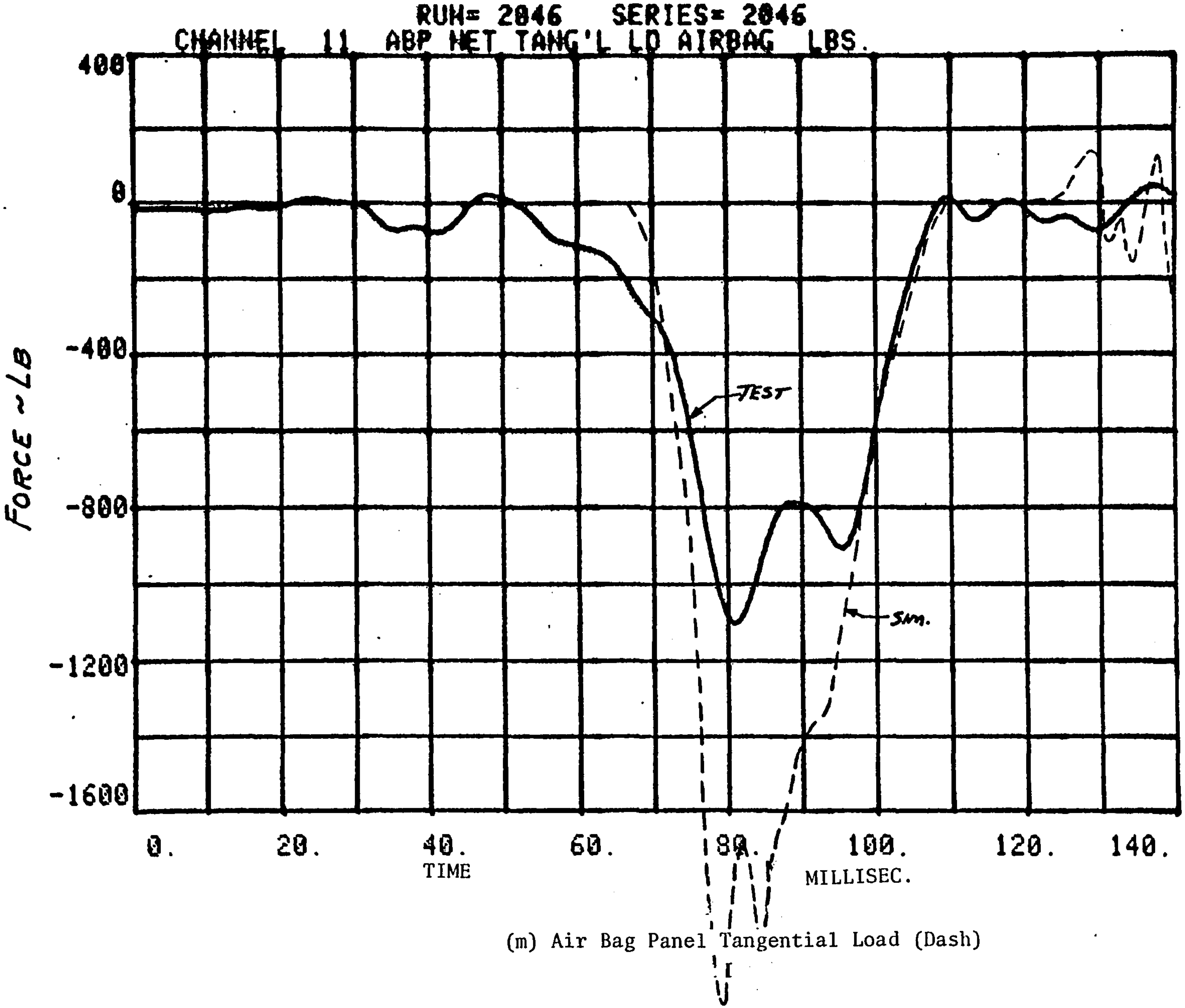

(m) Air Bag Panel Tangential Load (Dash)

Figure 5-4 COMPARISON OF CVS MODEL AND MEASURED RESPONSES FOR AIR BAG RESTRAINT CONFIGURATION (CONT'D.)

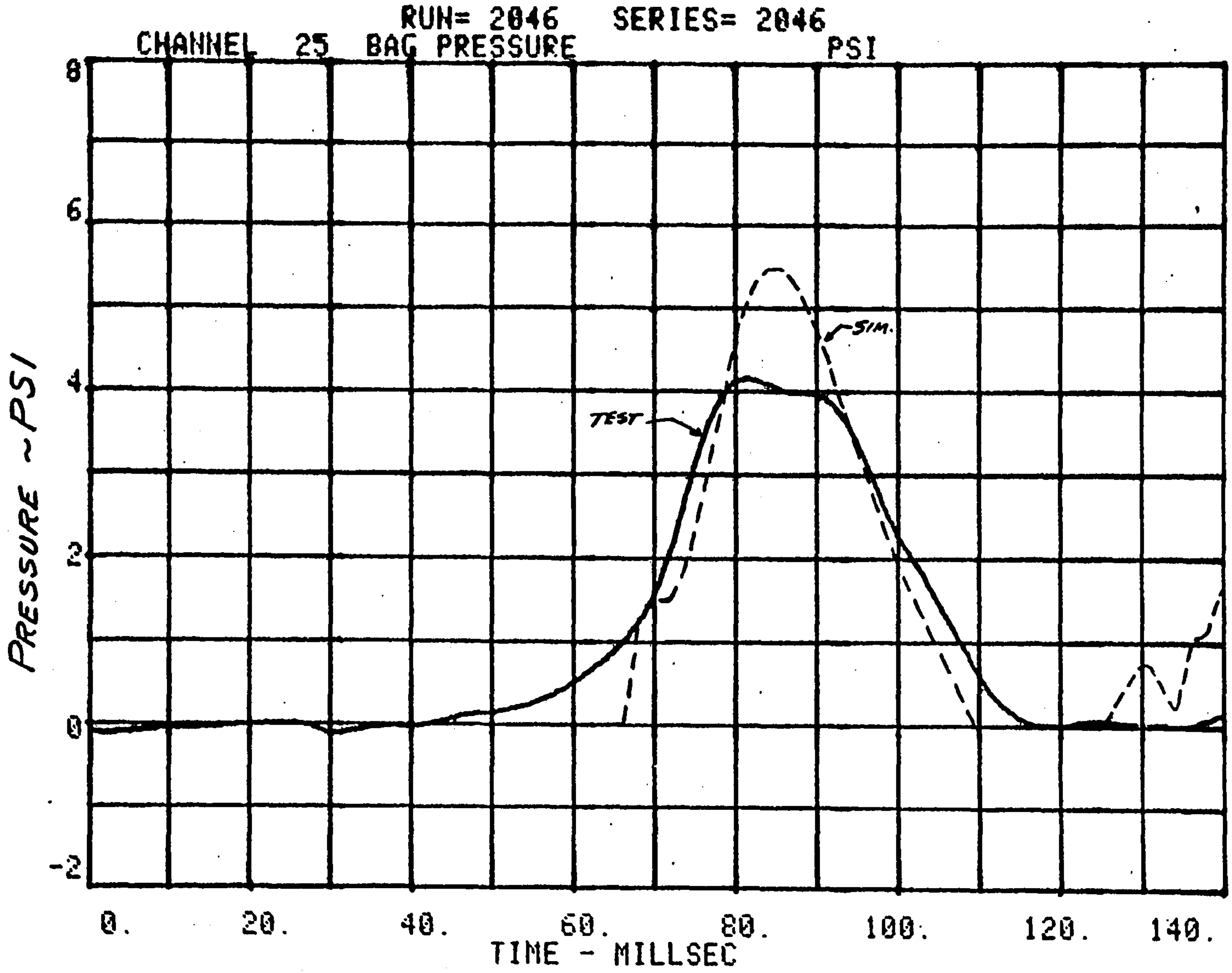

(n) Air Bag Pressure

Figure 5-4 COMPARISON OF CVS MODEL AND MEASURED RESPONSES FOR AIR BAG RESTRAINT CONFIGURATION (CONT'D.)

the high forces resulting from contact of the lower legs with the knee bolster which were transmitted through the femurs. It appears that the orientation of the torso and legs was sufficiently different in the simulation that the contact with the knee bolster caused the occupant to load the seat by only a very small amount before being lifted upward off the seat. Comparison of the shapes of the waveforms for the other contact panels clearly shows a correlation between the model and experimental responses although the magnitudes of the force peaks differ considerably in some instances.

It is of interest to note that the air bag reaction forces against the panel representing the windshield were much better predicted than those stemming from reacting against the dash panel. The fact that the measured forces on the windshield were higher than those on the smaller size dash whereas the predicted forces were nearly the same magnitude for both panels suggests that the difference is due to an edge effect that is not accounted for in the simulation. The high-speed films of the test showing that the bag was fully supported by the windshield but not by the dash panel which, because of its much shorter length, allowed the bag to "droop" over the forward edge, reinforces the plausibility of such a hypothesis.

6.0 CONCLUDING REMARKS

An input data set for a CVS computer program model of a Part 572 50th percentile male anthropomorphic dummy was developed in this research program. In this model the dummy is idealized as an assembly of 15 rigid segments connected by 14 joints. Values for most of the input parameters which describe the physical characteristics of the dummy are based on data obtained from measurements and tests of components and subassemblies, but it was also necessary to estimate some of them.

It should be recognized that rarely, if ever, is it possible to model a given system in toto because of practical considerations of model complexity, lack of information on the physical system or processes involved, or even difficulty in manipulation or use of the information. Hence, every model is an approximation of the physical system it represents and, of necessity, is based on simplifying assumptions concerning the various aspects of the nature and behavior of the real system. For this reason, differences between predicted and observed responses of an actual system are to be expected, the disparities depending in part on the adequacy of the assumptions and approximations for the particular operating environment of the system. It is believed that the correlations between simulated and actual system responses shown by the detailed comparisons presented in this report are indicative of the general level of accuracy that can be expected in typical applications of the CVS computer program.

One of the difficulties in speaking of validating a model lies in defining what is meant by "validation." Although at first thought it would appear to be relatively easy to define the term "validation" in relation to computerized mathematical models, a cursory review of some of the published literature on this subject indicates that there is no uniformly accepted definition of the term "validation." Various technical disciplines choose widely differing definitions for their specific purposes. Furthermore, "verification" is often used as a synonym for "validation," which is in general accord with standard dictionary definitions of these two terms.

Fishman and Kiviat (Reference 10) describe three principal problem areas relating to statistical analysis of computer simulation results: verification, validation, and problem analysis. According to their definitions, verification determines whether a model with a particular mathematical structure and data base actually behaves as an investigator assumes it does. Validation tests whether a simulation model reasonably approximates a real system. Problem analysis seeks to insure the proper execution of the simulation and the handling of its results; consequently, it deals with a host of matters: the concise display of solutions, efficient allocation of computer time, proper design of tests of comparisons, and correct estimates of sample sizes needed for specified levels of accuracy. In other words, verification and validation insure that a model is properly designed; only after a model has been verified and validated can an experimenter justifiably use a model to probe system behavior. Problem analysis mainly deals with the results of this probing.

Validating a model therefore means establishing that it resembles the actual system reasonably well and, if so, we expect that its simulated response to an input should exhibit behavior similar to that observed for the real system. In the view of VanHorn (Reference 11) validation is the process of building an acceptable level of confidence that an inference about a simulated process is a correct or valid inference for the actual process. These two views on the definition of "validation" are seen to be quite consistent.

Naylor and Finger (Reference 12) assert that to verify or validate any kind of model means to prove the model to be true. But to prove that a model is "true" implies that one has established a set of criteria for differentiating between those models which are "true" and those which are "untrue" and that one has the ability to apply these criteria to any given model. No criteria exist either for selecting the critical output variables for comparison or for defining the level of agreement required for validity.

Schrank and Holt (Reference 13) propose that the criterion of the usefulness of the model be adopted as the key to its validation, thereby shifting the emphasis from a conception of its abstract truth or falsity to the question of whether the errors in the model render it too weak to serve the intended purposes. Since this involves a judgment on the part of the individual investigator, it appears that validity of a model, like beauty, "lies in the eyes of the beholder."

In view of the fact that assumptions are inherent in any mathematical model, it is clear that a given model may yield better predictions for one situation than for another, i.e., validation is problem dependent. However, the agreement achieved between predictions and observed responses of a system ("validity") is also user dependent. As an example, an air bag restraint is represented in the CVS as having an ellipsoidal shape. If an air bag as part of a physical system being simulated is not ellipsoidal, the user must decide on a set of model input values for the ellipse semi-axes that, in his estimation, is most representative of the real air bag for the particular situation. Inasmuch as the "best" choice of inputs often is not obvious, or indeed may even be indeterminable, different users may select different values in simulating the same physical system. The model in this case is the same for all users (i.e., the air bag modeled as an ellipsoid), but the resulting predictions, and hence the indication of validity, are user dependent.

Model validity is also seen to be user dependent in another way when it is recognized that the CVS program is not a singular model. Indeed, generality and flexibility of the computer program has been an objective throughtout its development. Features such as the ability to vary the number of segments and joints, to disjoin sets of segments, to employ various options (e.g., position constraints, sliding or rolling constraints, etc.) allow, in effect, the creation of many models. Again, because the "correct" or "best" model that can be created from the available options for simulating a given real system is not known a priori, various users may select different options with consequent different predictions of system behavior and indications of validity.

In view of the foregoing discussion, the authors have drawn no conclusions concerning the validity of the CVS model that is demonstrated by the results obtained in this study.

7.0 REFERENCES

1. Bartz, John A., "A Three-Dimensional Computer Simulation of a Motor Vehicle Crash Victim, Phase I - Development of the Computer Program", Calspan Report No. VJ-2978-V-1, July, 1971.

2. Bartz, John A. and Butler, Frank E., "A Three-Dimensional Computer Simulation of a Motor Vehicle Crash Victim, Phase 2 - Validation Study of the Model", Calspan Report No. VJ-2978-V-2, December, 1972.

3. Bartz, John A., Butler, Frank E. and Ryan, Charles T., "A Three-Dimensional Computer Simulation of a Motor Vehicle Crash Victim, Further Development - Mutual Force-Deflection Characteristics and Comprehensive 'Debug' Facility", Calspan Report No. ZQ-5326-V-2, September, 1974.

4. Fleck, J. T., Butler, F. E., and Vogel, S. L., "An Improved Three-Dimensional Computer Simulation of Motor Vehicle Crash Victims", Volumes I-IV, Report Nos. DOT-HS-801507, -508, -509, -510, July, 1974.

5. Fleck, J. T. and Butler, F. E., "Development of an Improved Computer Model of the Human Body and Extremity Dynamics", Report No. AMRL-TR-75-14, July, 1975 (AD A-014816).

6. Butler, F. E. and Fleck, J. T., "Advanced Restraint System Modeling", Report No. AFAMRL-TR-80-14, May, 1980.

7. Federal Motor Vehicle Safety Standard 208, Part 572, "Anthropomorphic Test Dummy".

8. "Development of Approximating Solutions for CVS Program and of Dummy Design Information", Contract No. DOT-HS-01418 (in progress).

9. DeLeys, Norman J., "Data For Validation of Crash Victim Simulator", Calspan Report No. 6197-V-1, August, 1981.

10. Fishman, George, S. and Kiviat, P. J., "Digital Computer Simulation: Statistical Considerations," the RAND Corporation, Santa Monica, California, RM-5287-PR, 1967.

11. Van Horn, R., "Validations," The Design of Computer Simulation Experiments, Duke University Press, Durham, North Carolina, 1969.

12. Naylor, T. H. and Finger, J. M., "Verification of Computer Simulation Models," Management Science XIV, October 1969, pp. 92-101.

REFERENCES (cont'd)

13. Schrank, W. E. and Holt, C. G., "Critique of: Verification of Computer Simulation Models," Management Science XIV, October 1967, pp. 104-106.

APPENDIX A

Head/Neck Pendulum Impact Data Plots

Data records from four head/neck pendulum impact tests with the head oriented at yaw angles of 0, 45, 90 and 180 degrees are contained herein. The data are presented in the following sequence for each test.

- Honeycomb reaction (pendulum) force
- Pendulum X acceleration
- Head x, y, z and resultant accelerations
- θ, ϕ and total ($\theta + \phi$) head rotation angles
- Radius length, R, as a function of angle ϕ

The measured impact velocity of the pendulum for each test is tabulated below.

Test No.	Head Orientation	Pendulum Impact Velocity ft/sec.
8	0°	23.31
4	45°	22.12
9	90°	22.83
11	180°	22.88

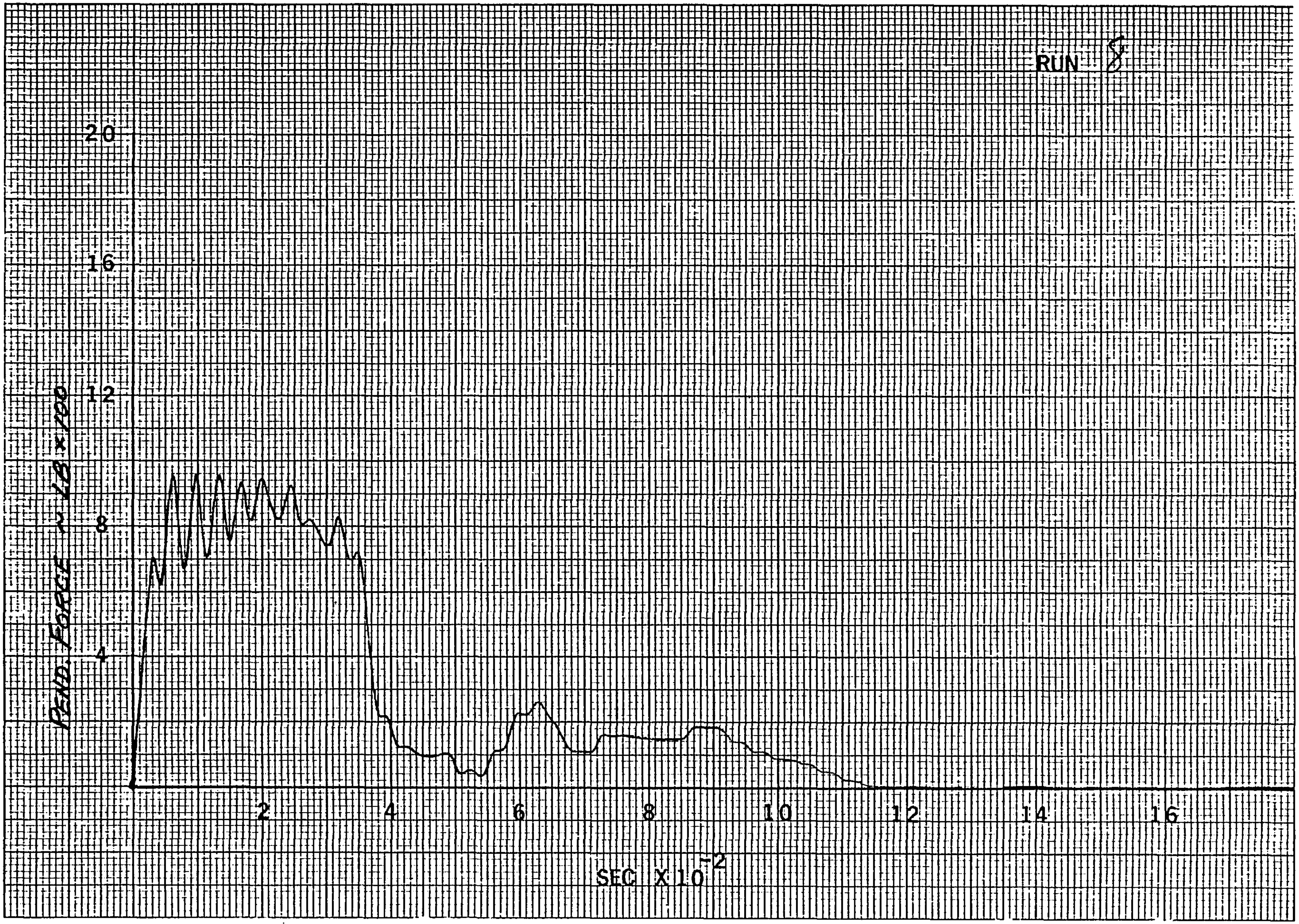

Figure A-1 H/N TEST NO. 8 RESPONSES, 0° HEAD ORIENTATION

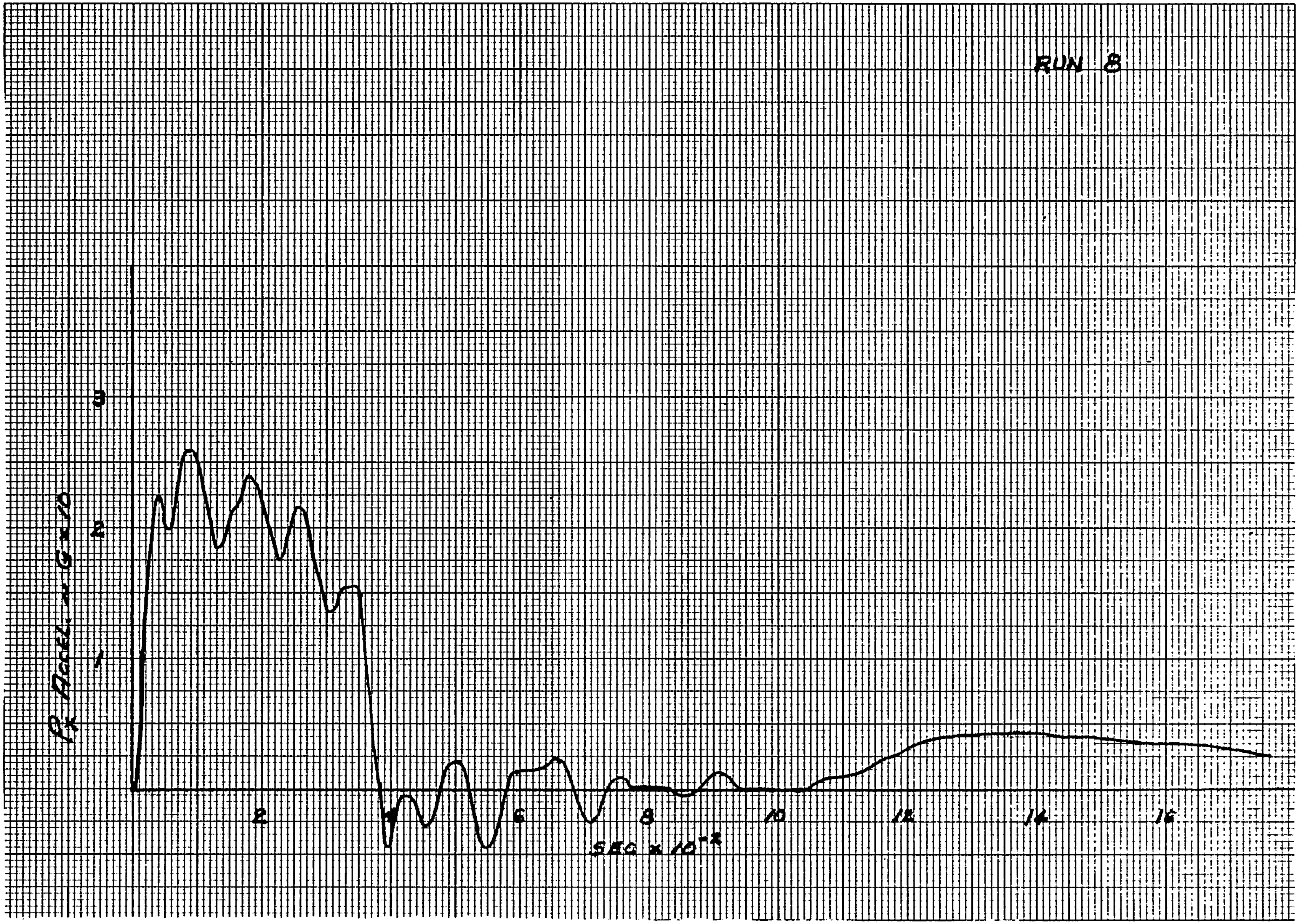

Figure A-1 (Cont'd)

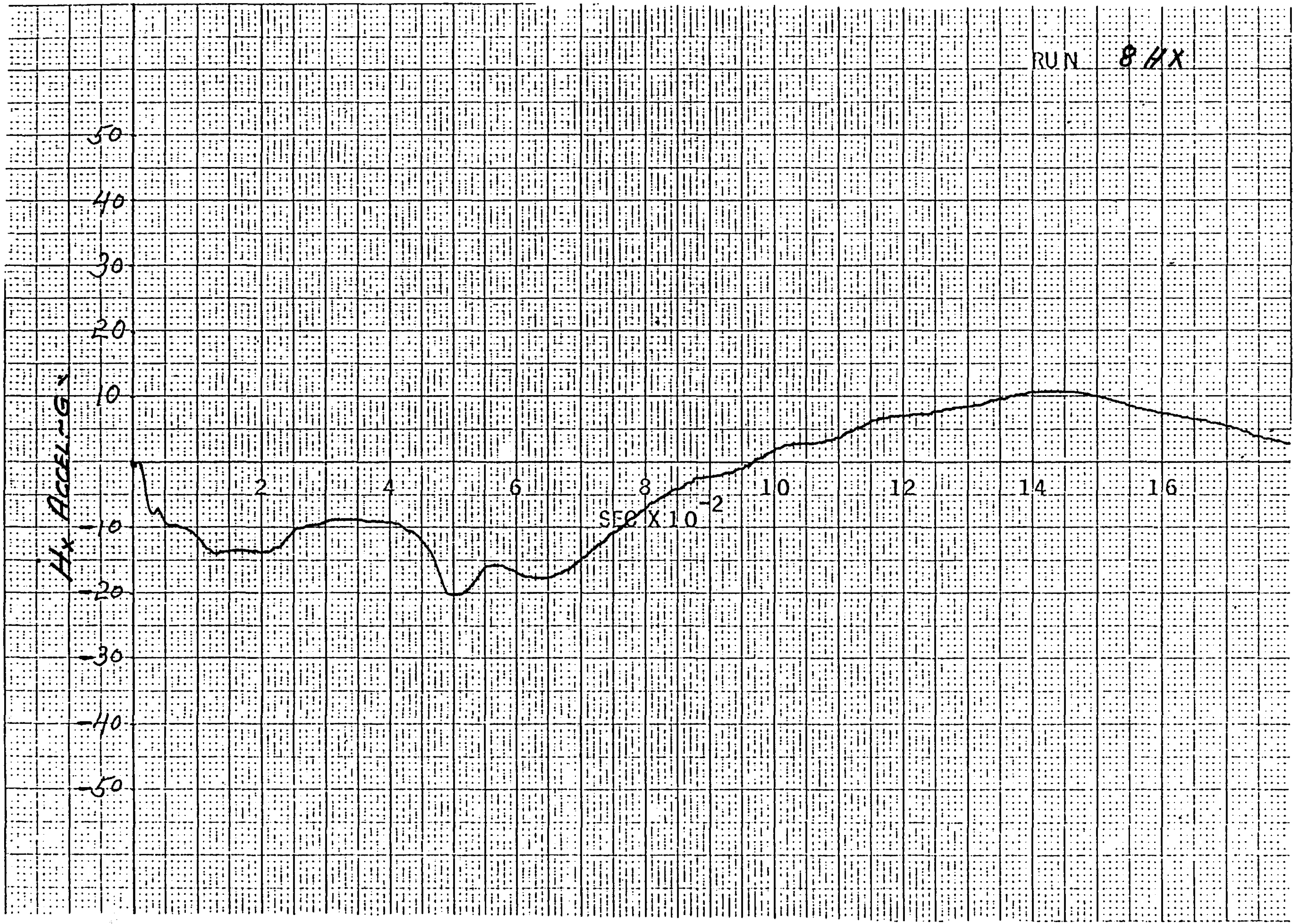

Figure A-1 (Cont'd)

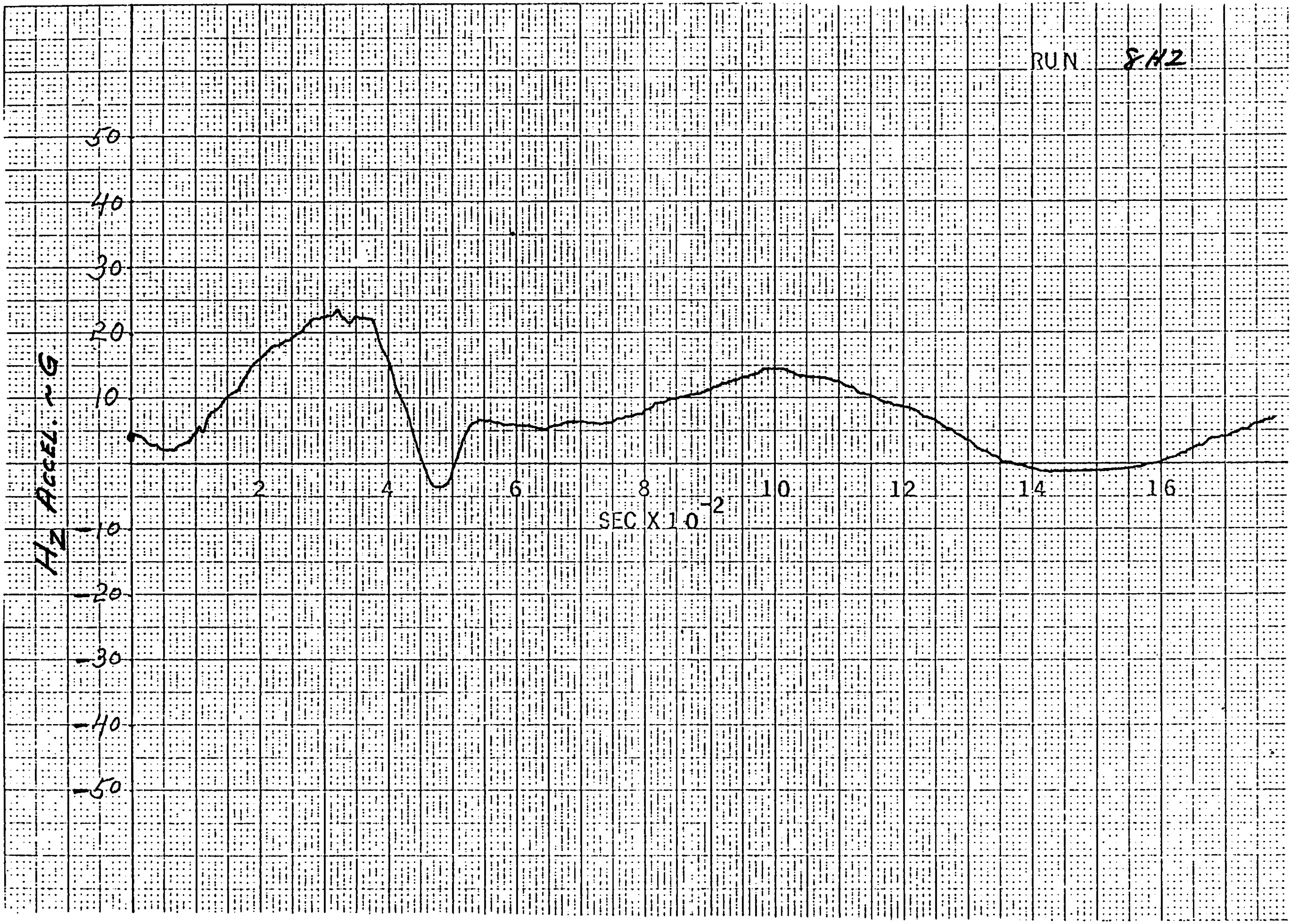

Figure A-1 (Cont'd)

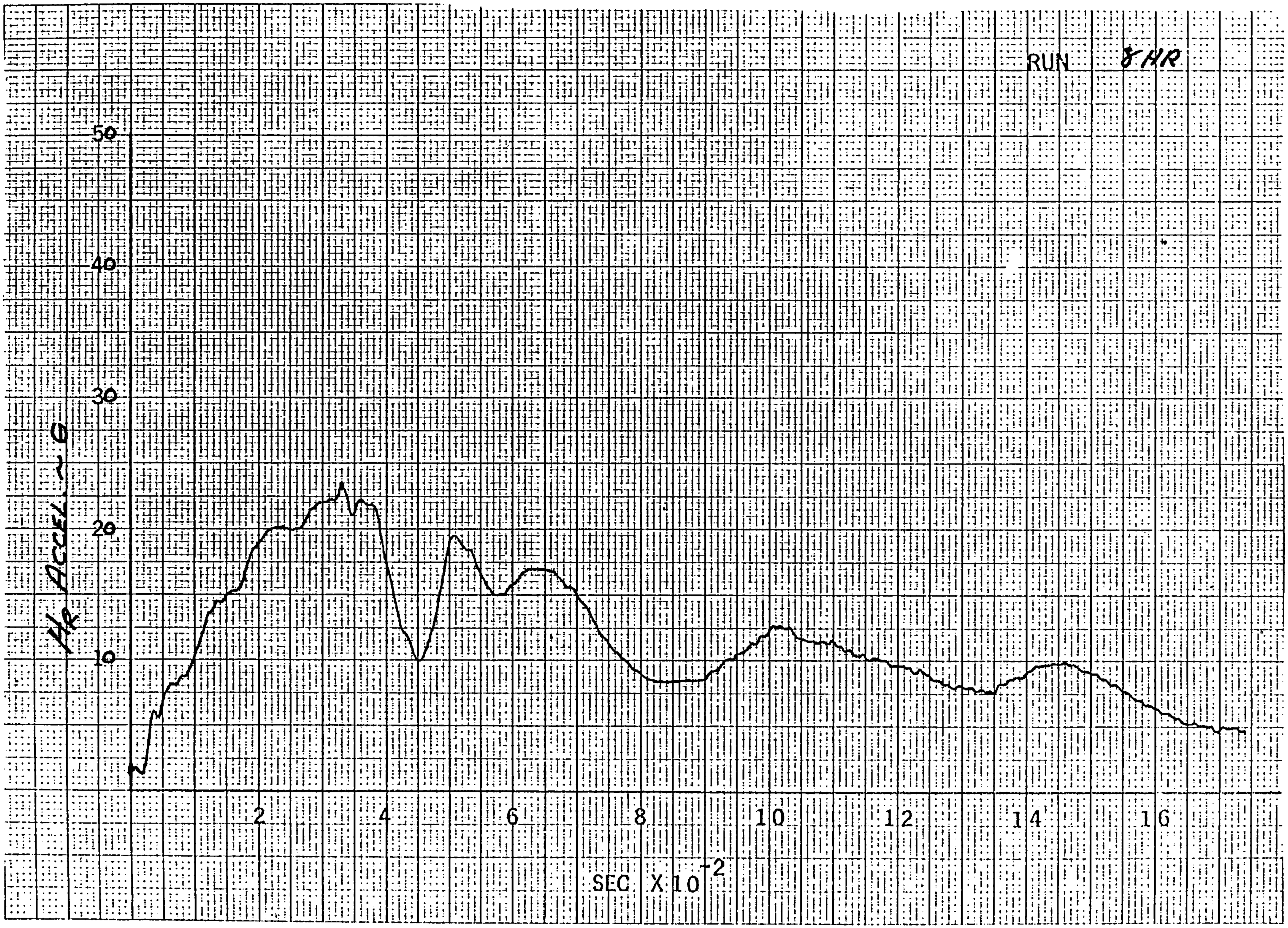

Figure A-1 (Cont'd)

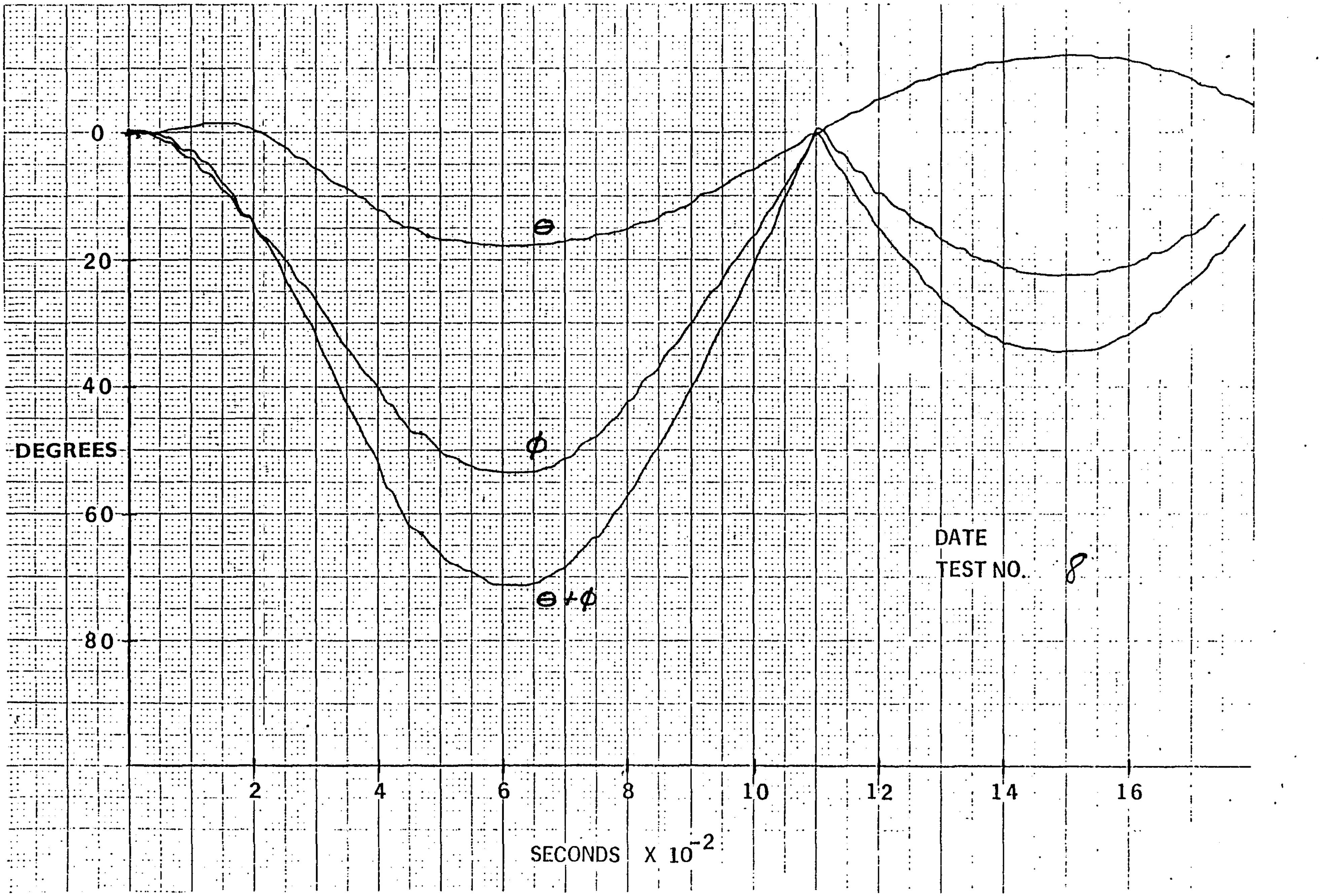

Figure A-1 (Cont'd)

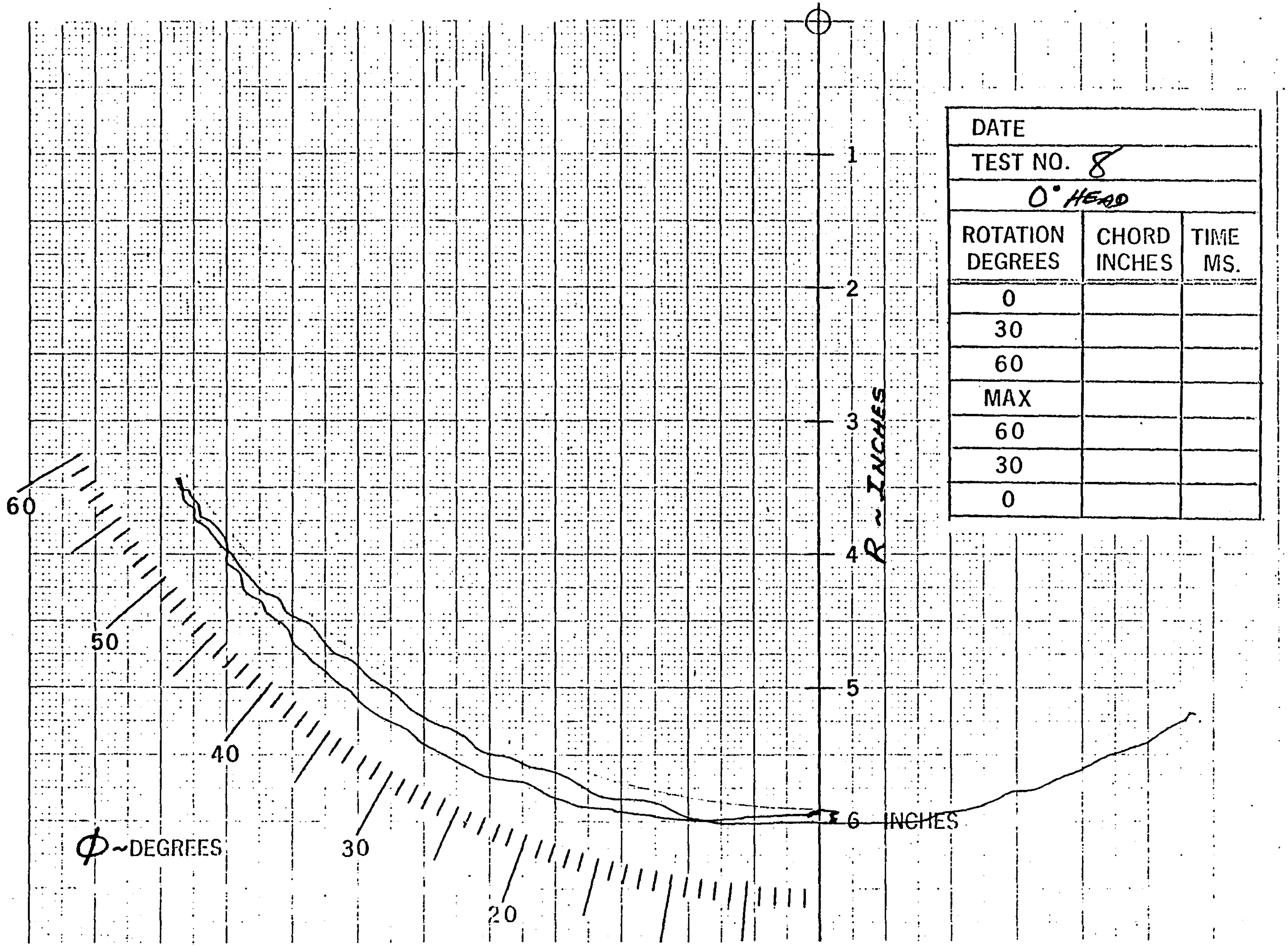

DATE		
TEST NO. 8		
0° HEAD		
ROTATION DEGREES	CHORD INCHES	TIME MS.
0		
30		
60		
MAX		
60		
30		
0		

Figure A-1 (Cont'd)

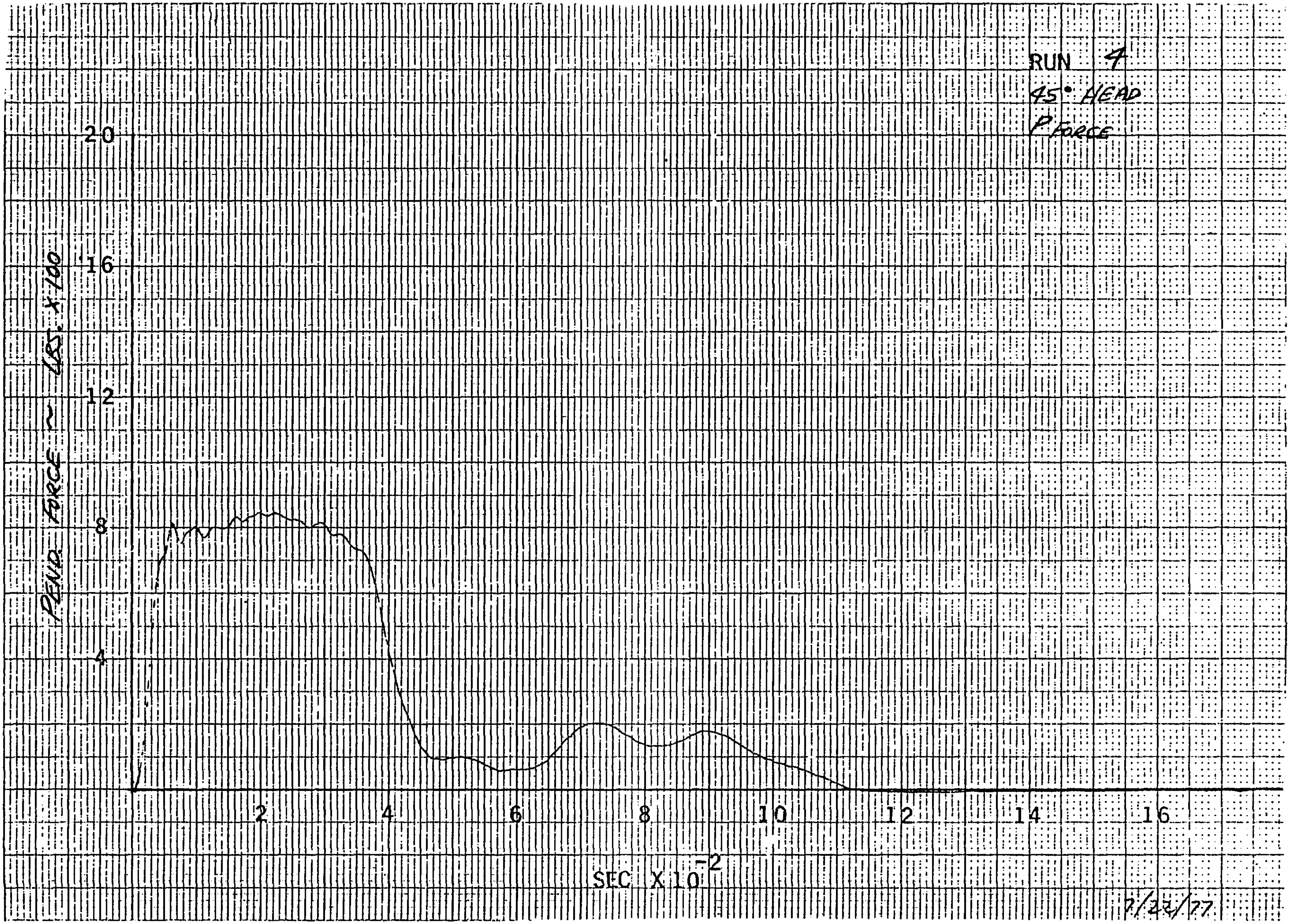

RUN 4
45° HEAD
P FORCE

7/22/77

Figure A-2 H/N TEST NO. 4 RESPONSES, 45° HEAD ORIENTATION

Figure A-2 (Cont'd)

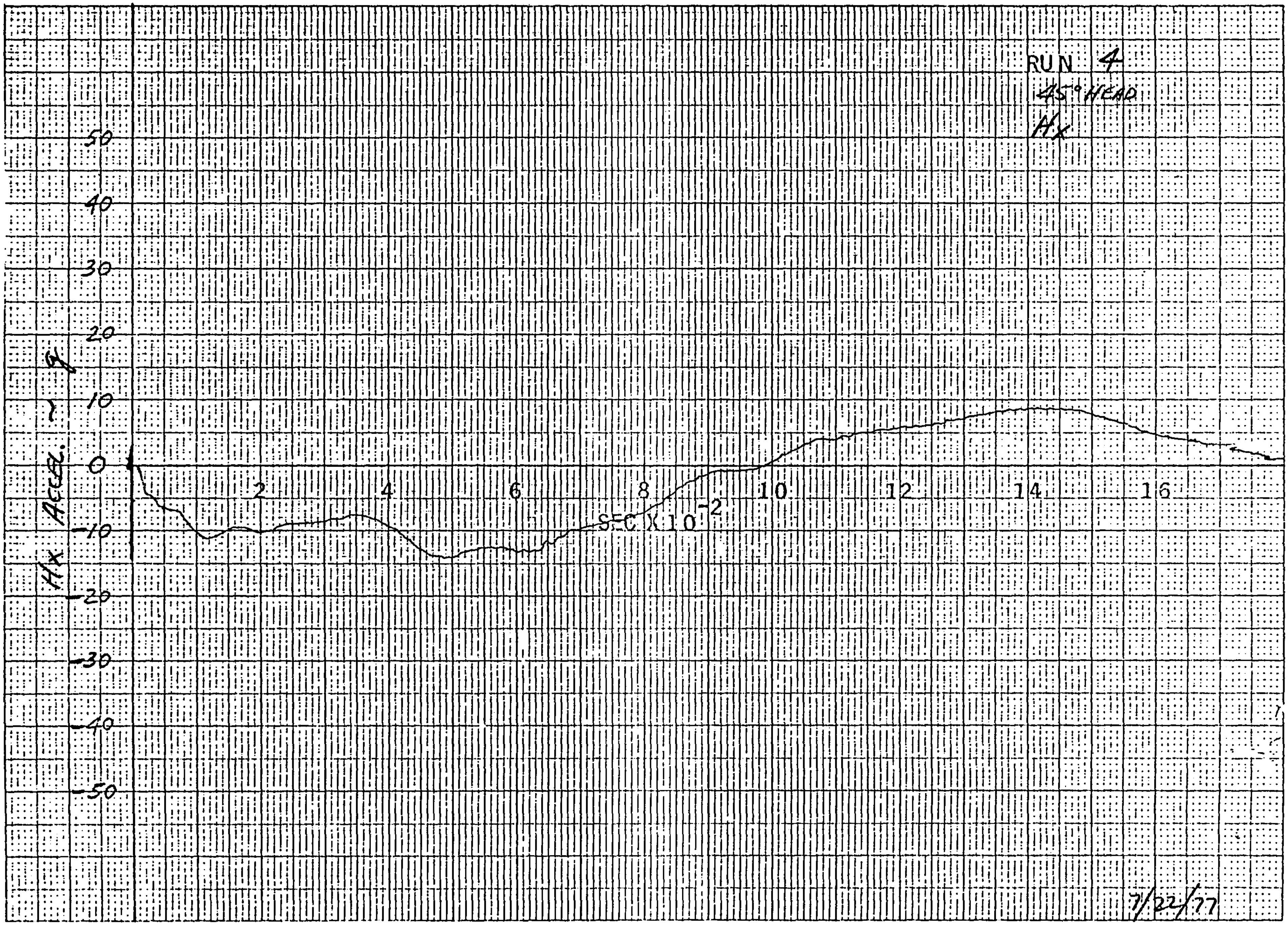

Figure A-2 (Cont'd)

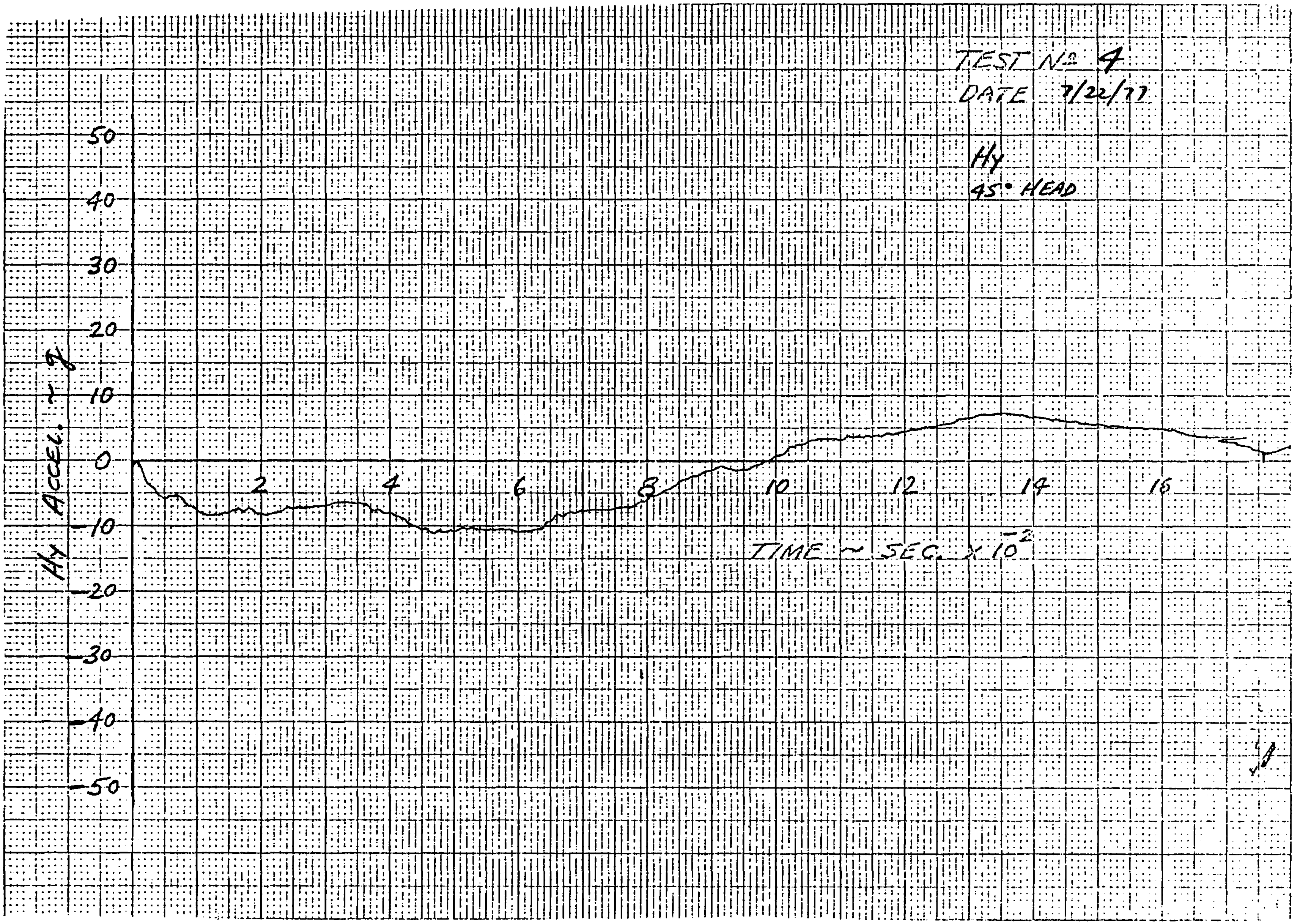

Figure A-2 (Cont'd)

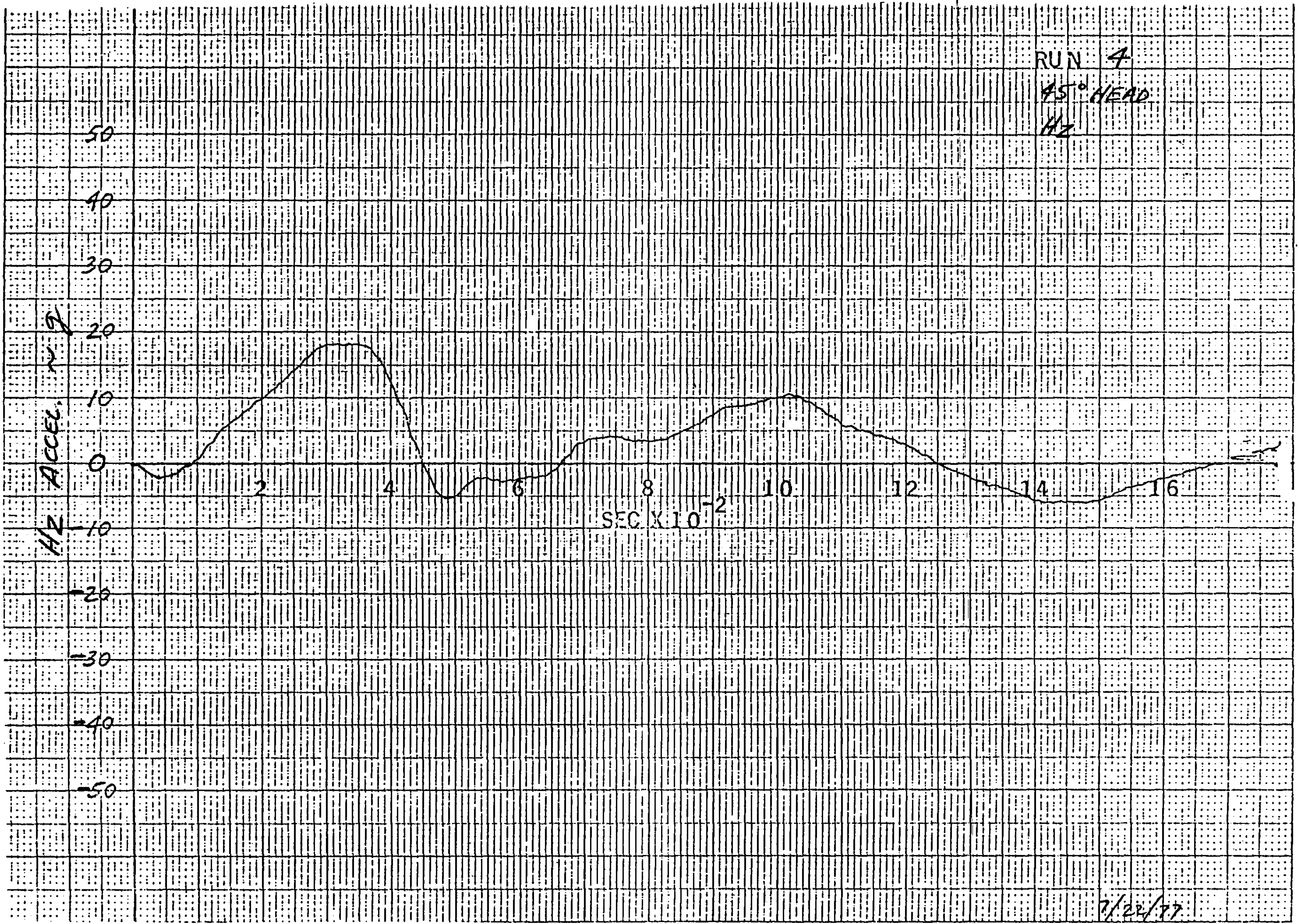

Figure A-2 (Cont'd)

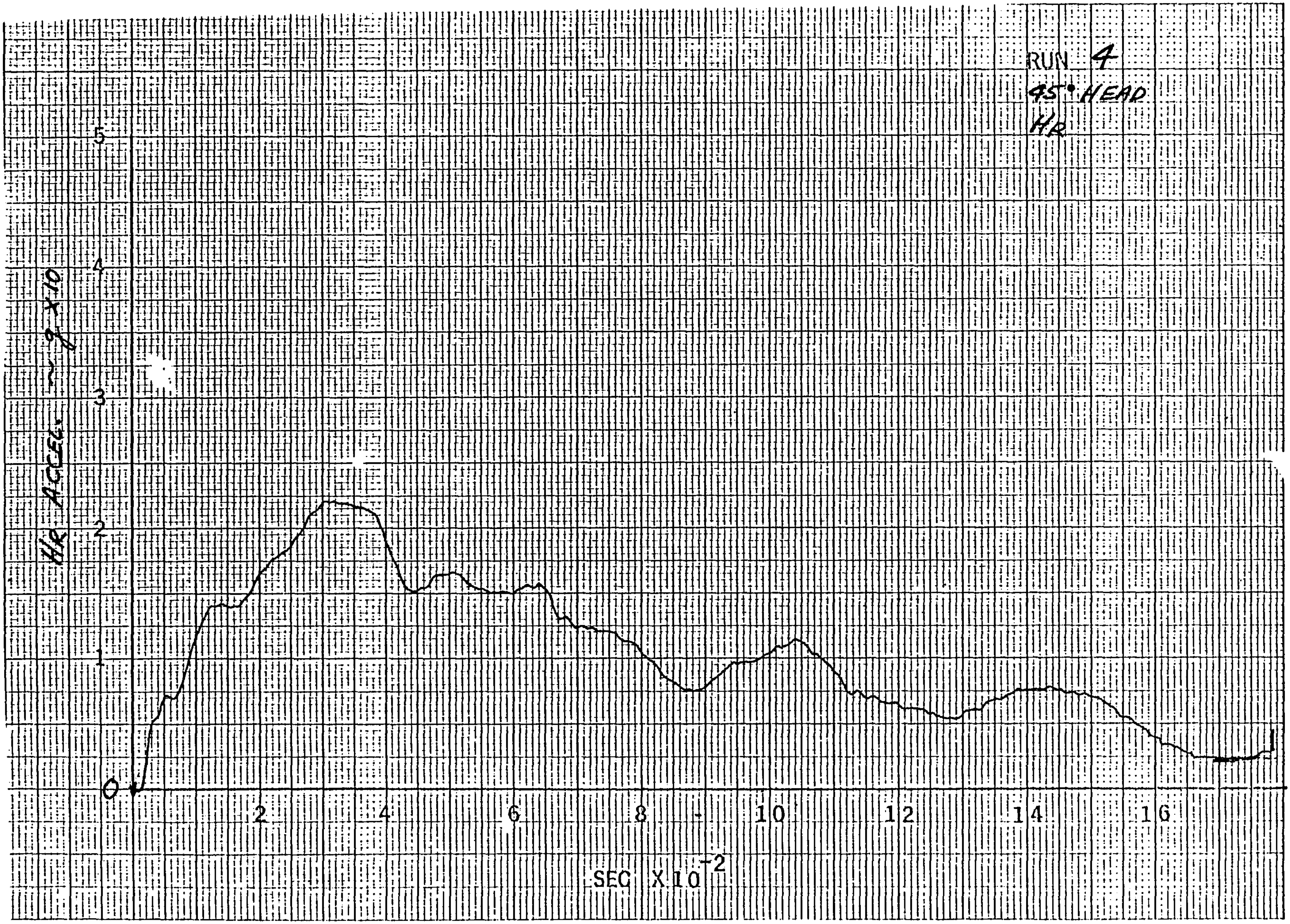

Figure A-2 (Cont'd)

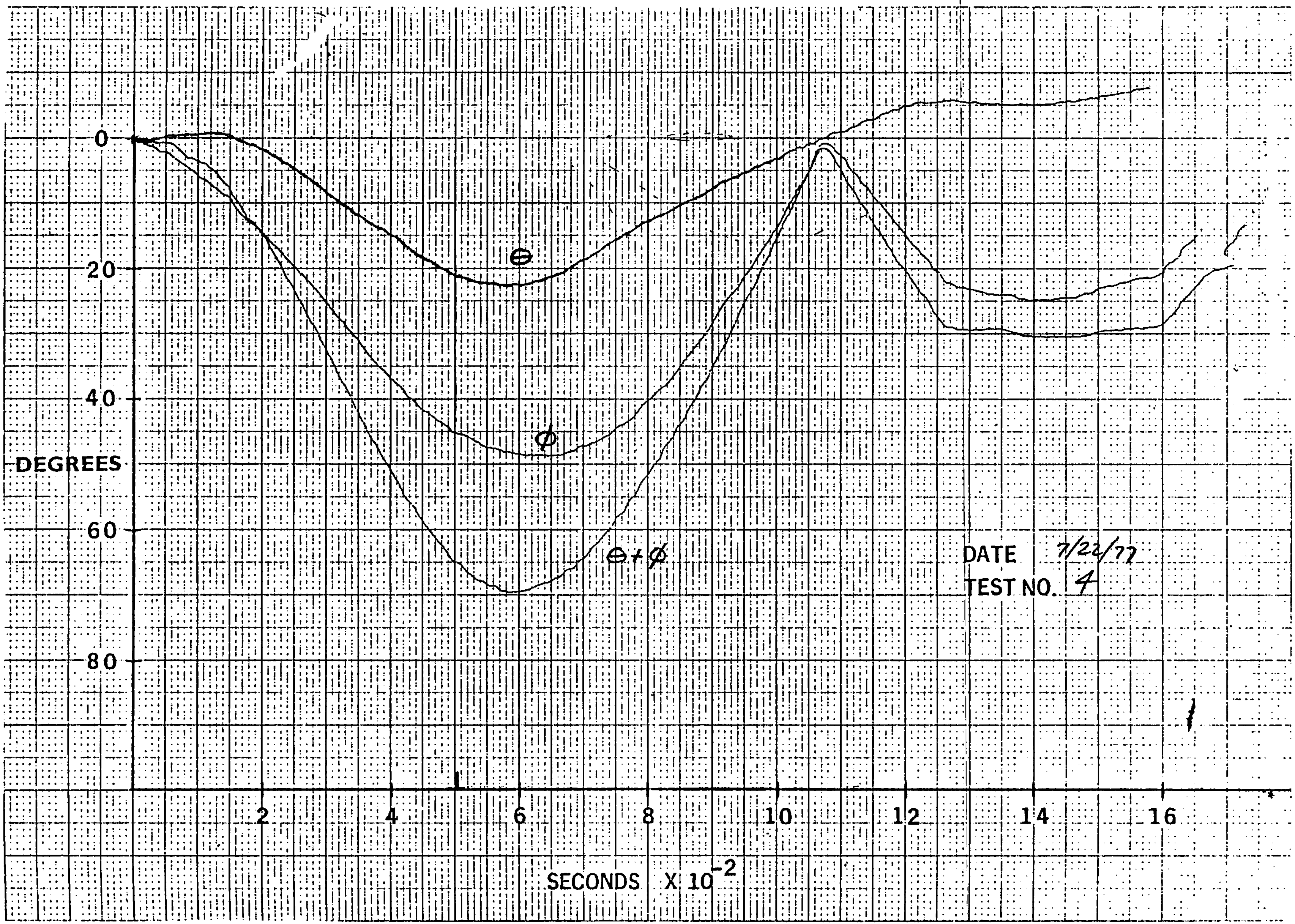

Figure A-2 (Cont'd)

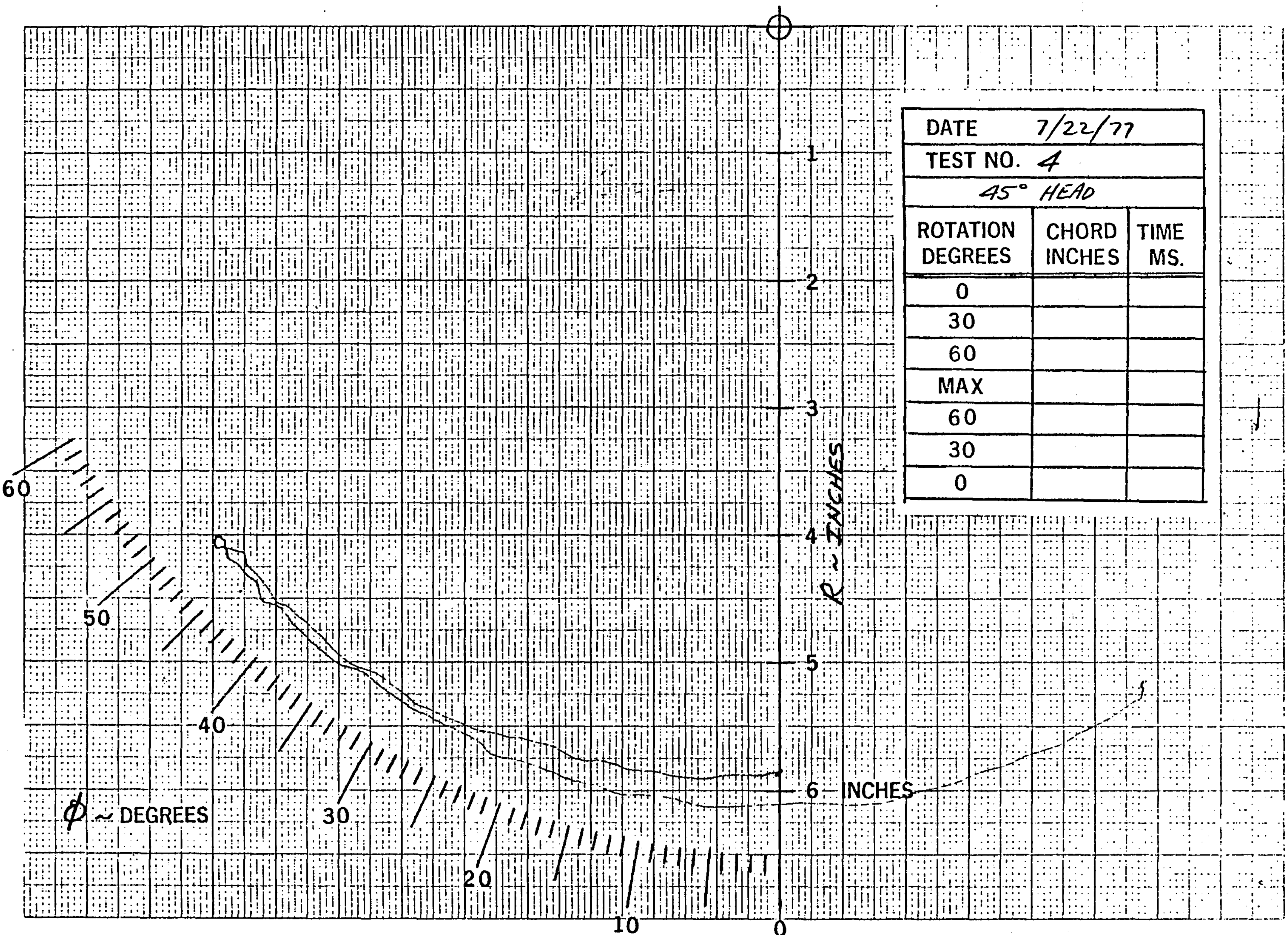

DATE	7/22/77
TEST NO.	4
45° HEAD	

ROTATION DEGREES	CHORD INCHES	TIME MS.
0		
30		
60		
MAX		
60		
30		
0		

Figure A-2 (Cont'd)

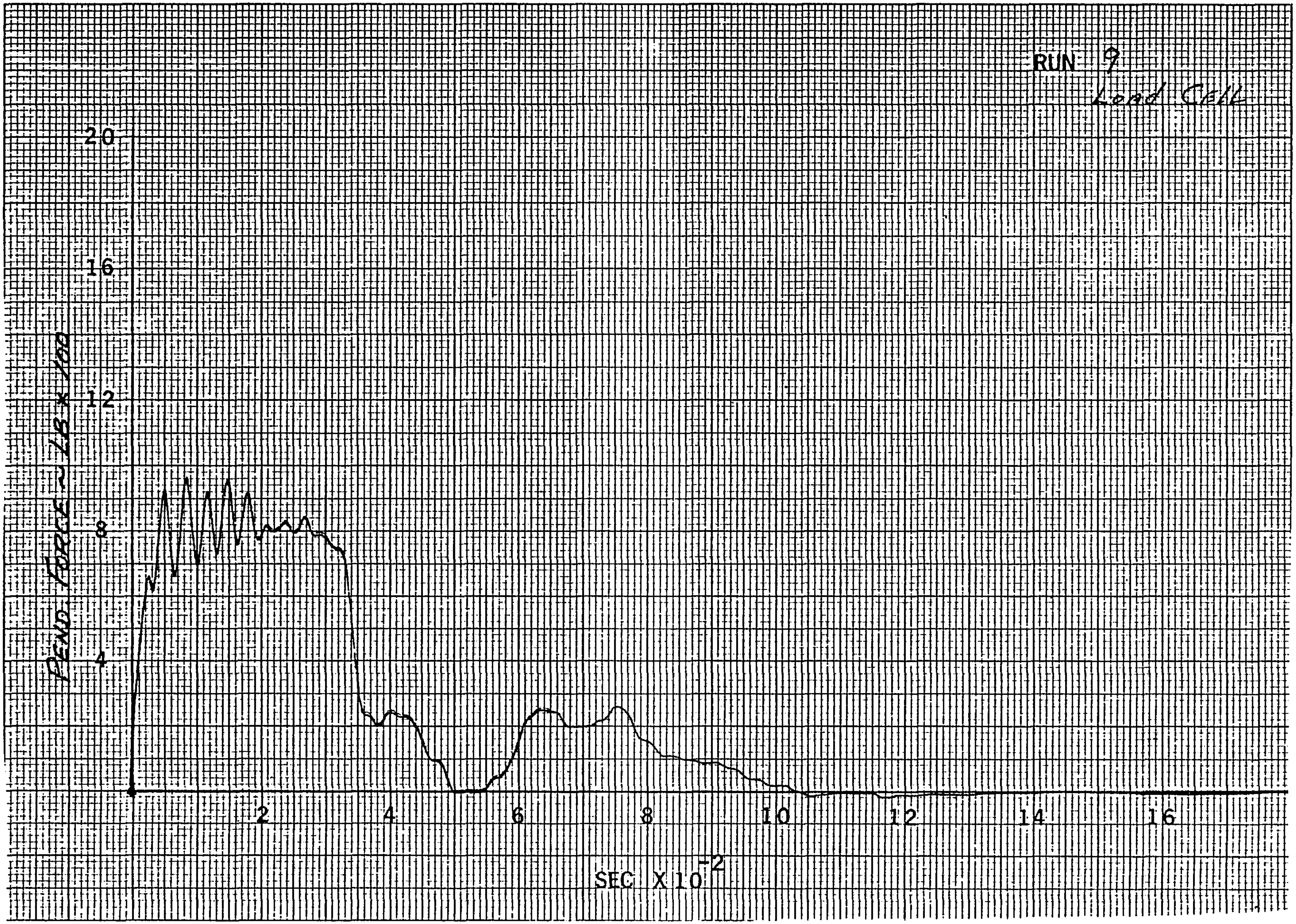

Figure A-3 H/N TEST NO. 9 RESPONSES, 90° HEAD ORIENTATION

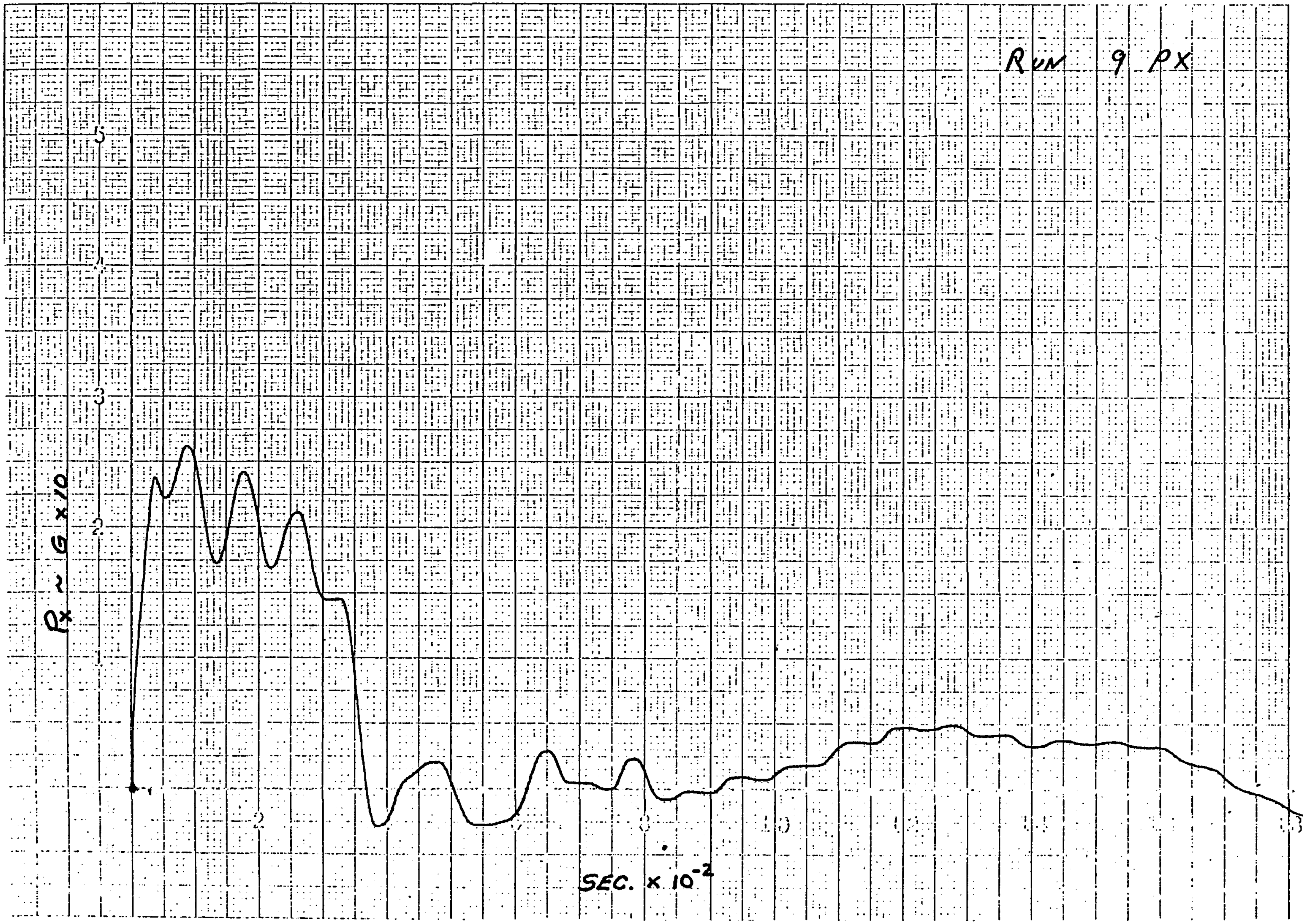

Figure A-3 (Cont'd)

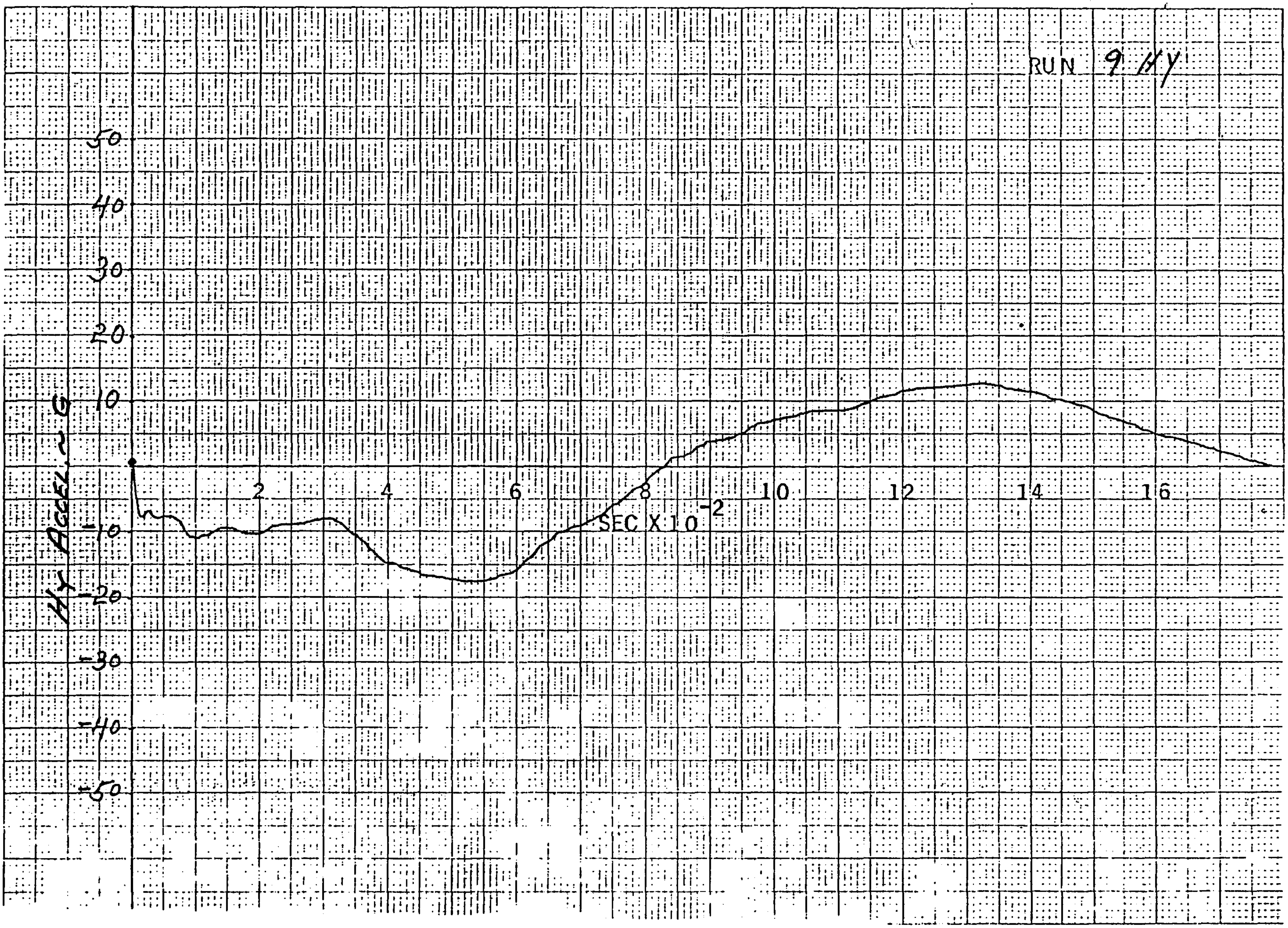

Figure A-3 (Cont'd)

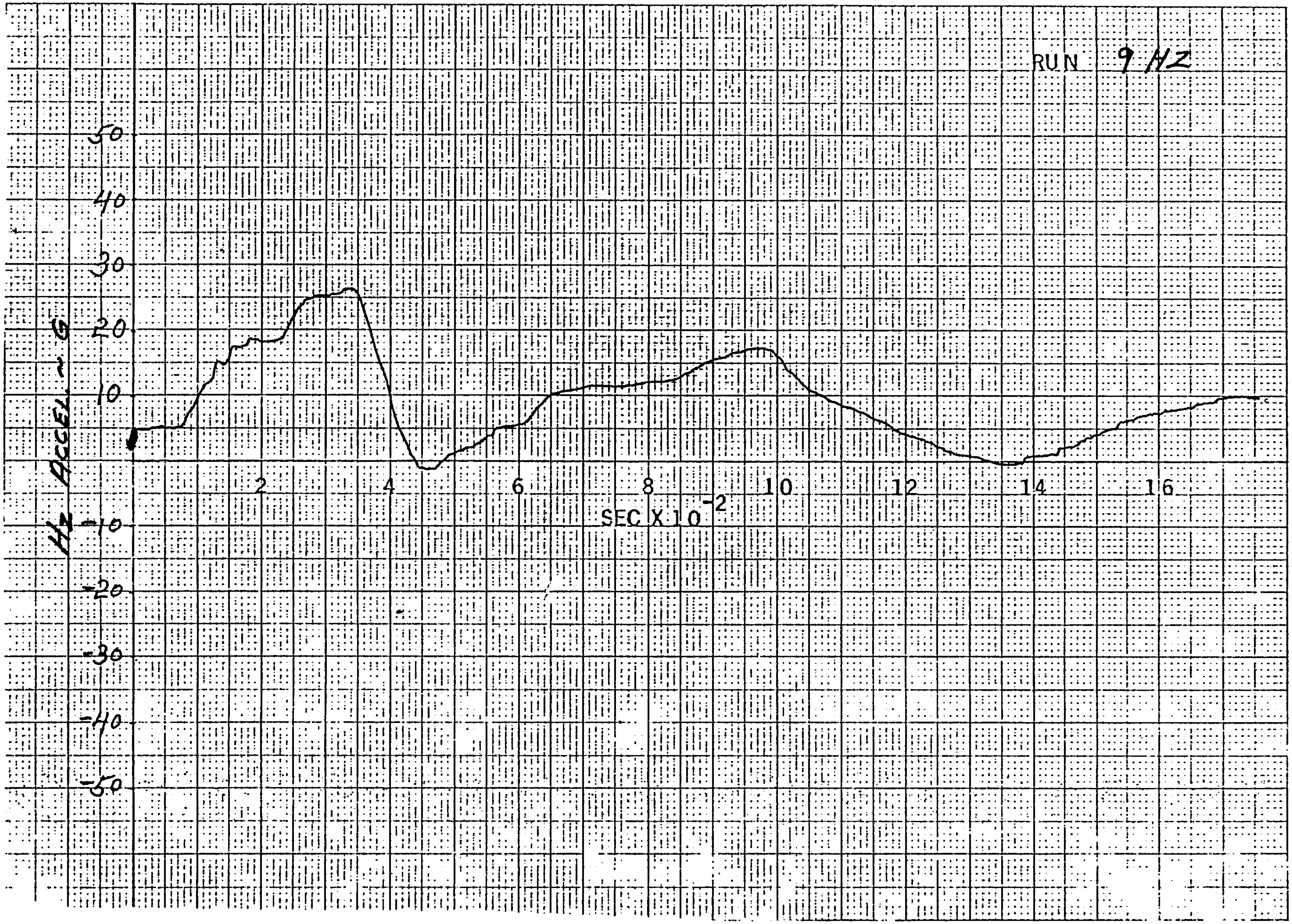

Figure A-3 (Cont'd)

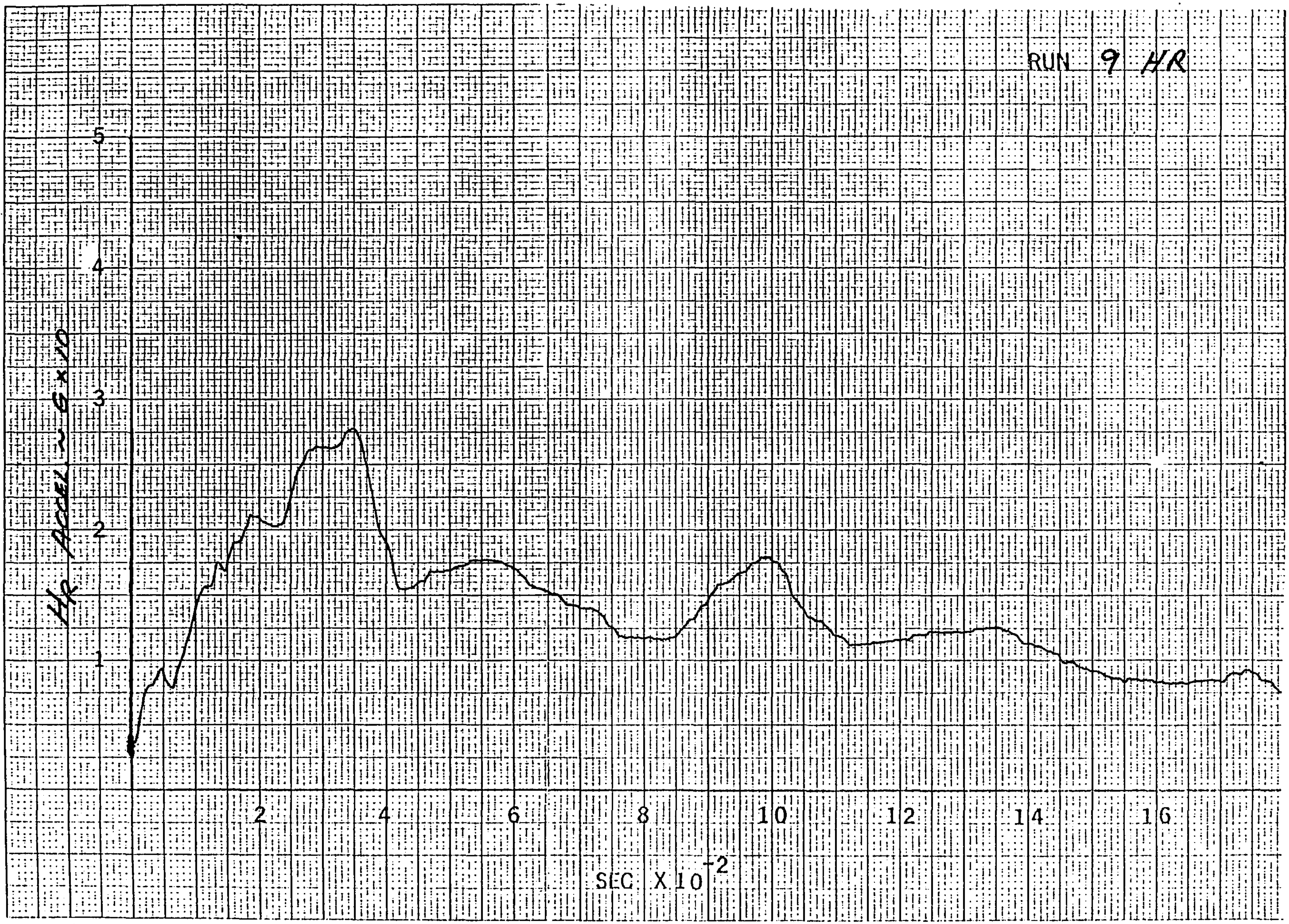

Figure A-3 (Cont'd)

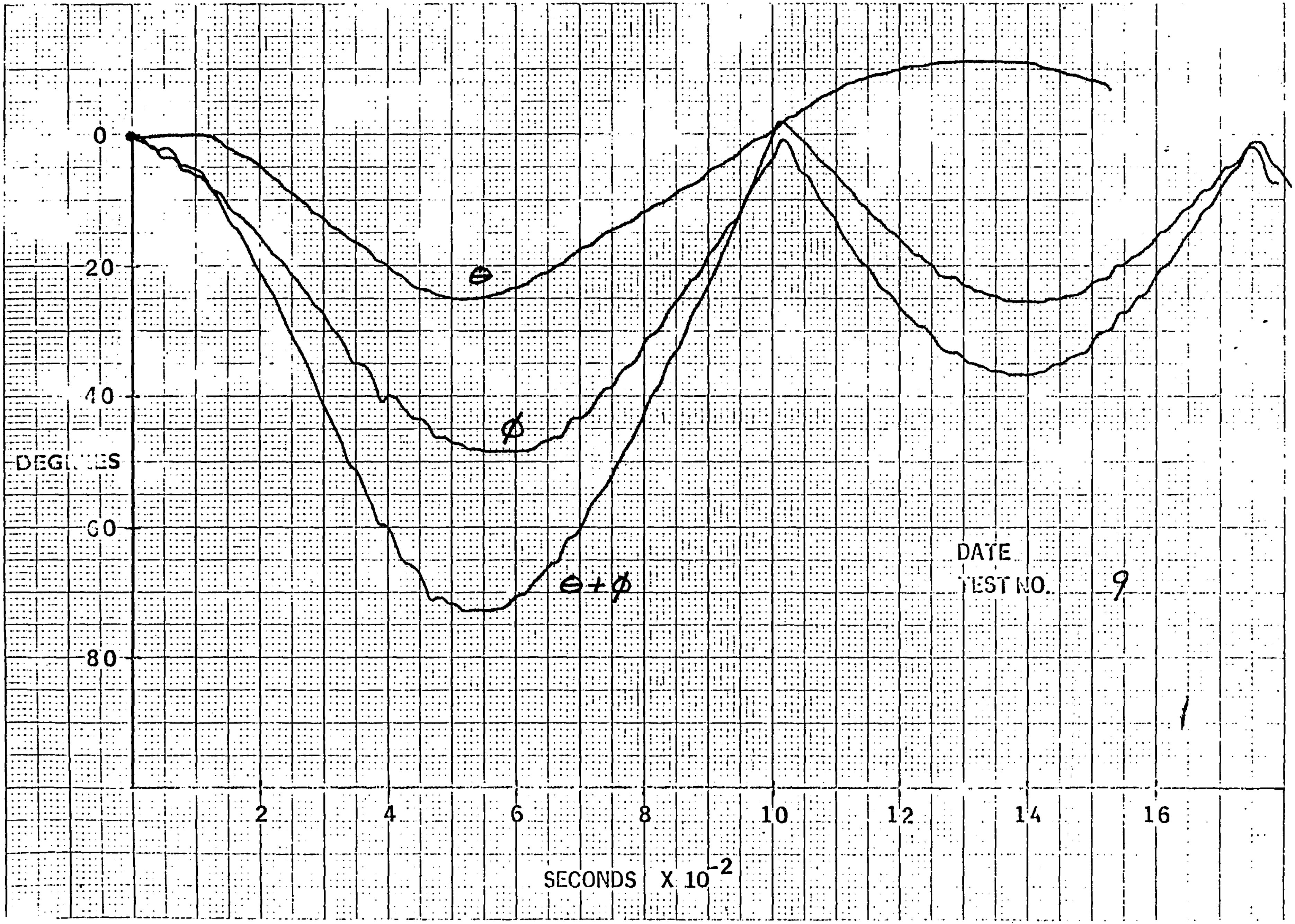

Figure A-3 (Cont'd)

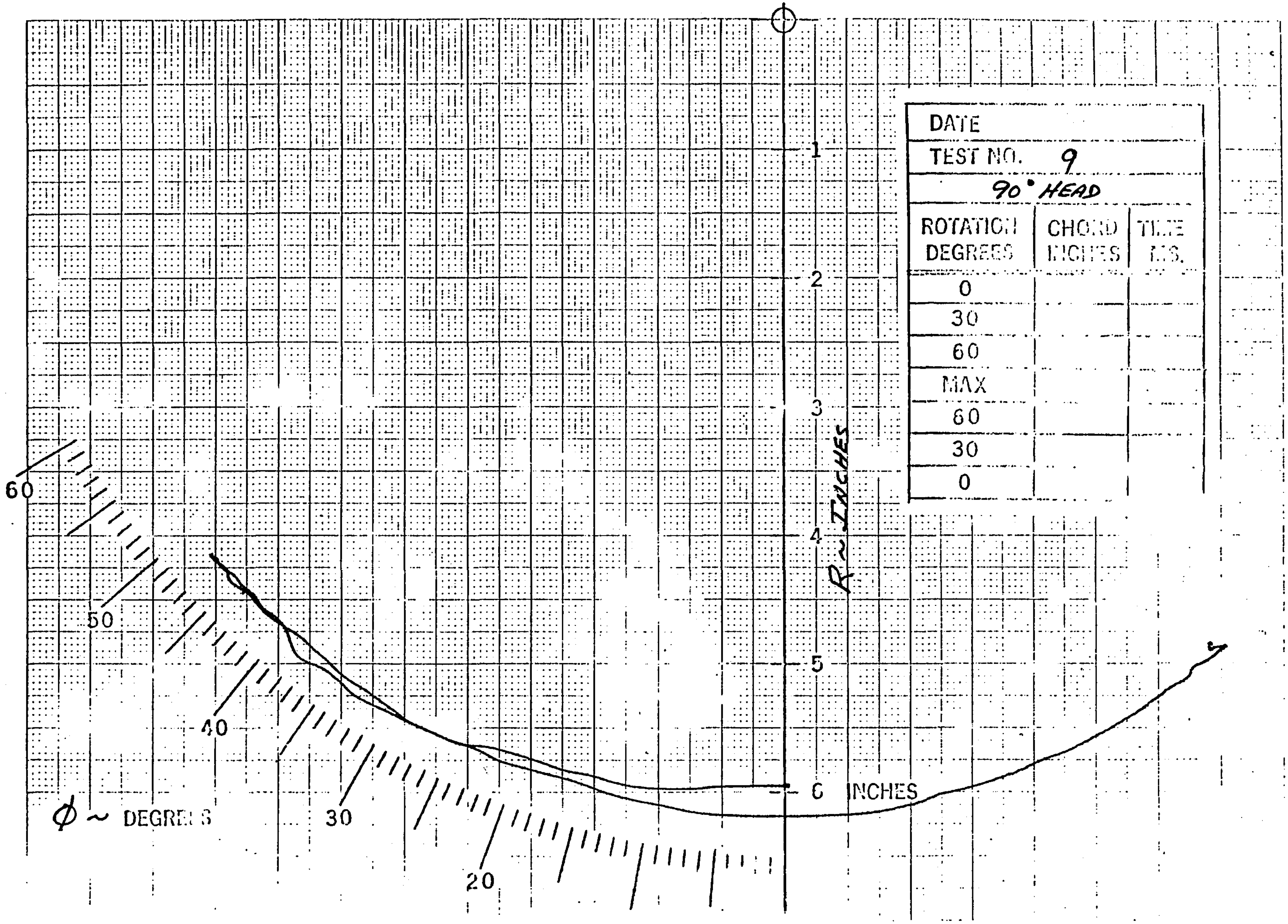

DATE		
TEST NO. 9		
90° HEAD		
ROTATION DEGREES	CHORD INCHES	TIME MS.
0		
30		
60		
MAX		
60		
30		
0		

Figure A-3 (Cont'd)

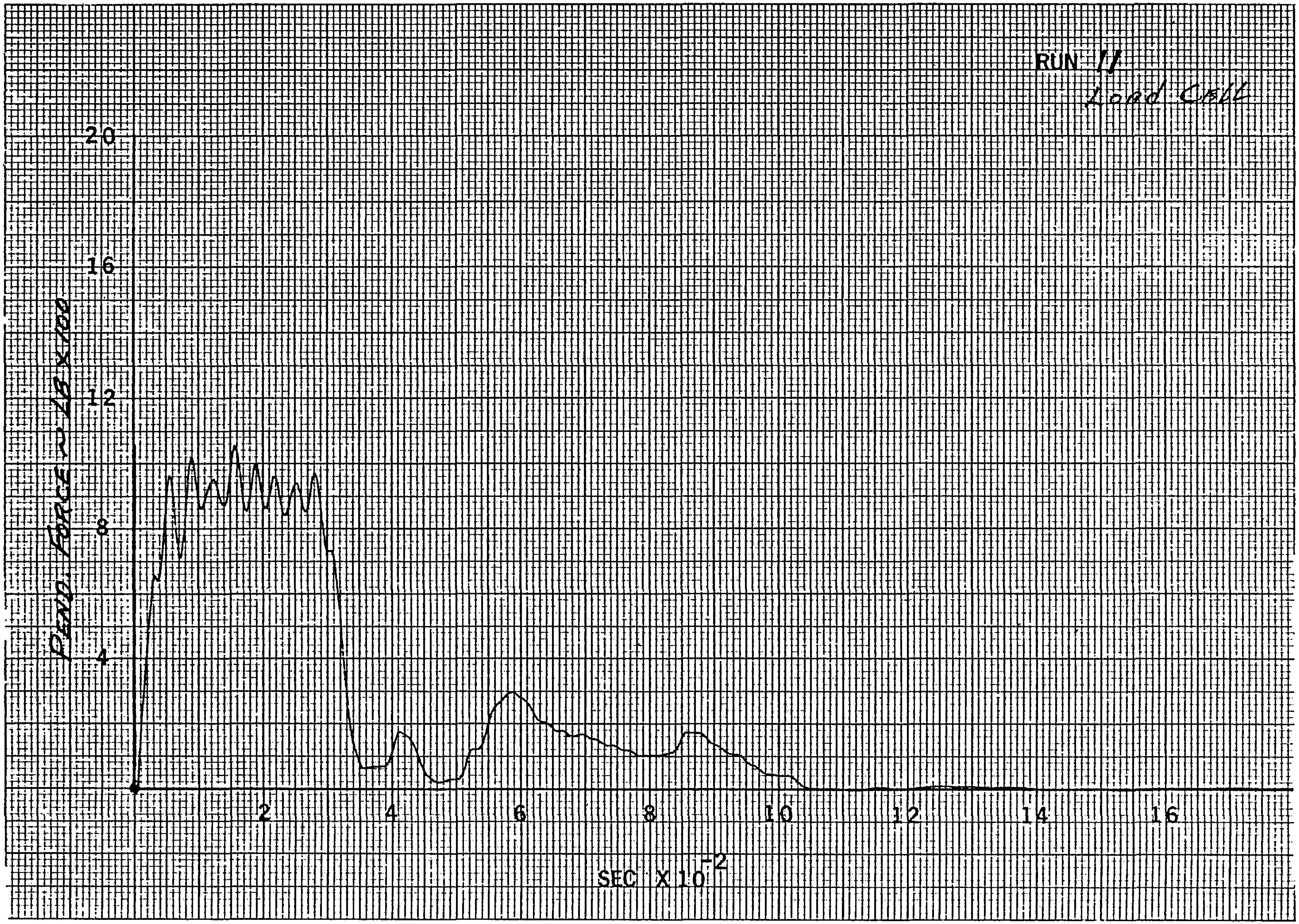

Figure A-4 H/N TEST NO. 11 RESPONSES, 180° HEAD ORIENTATION

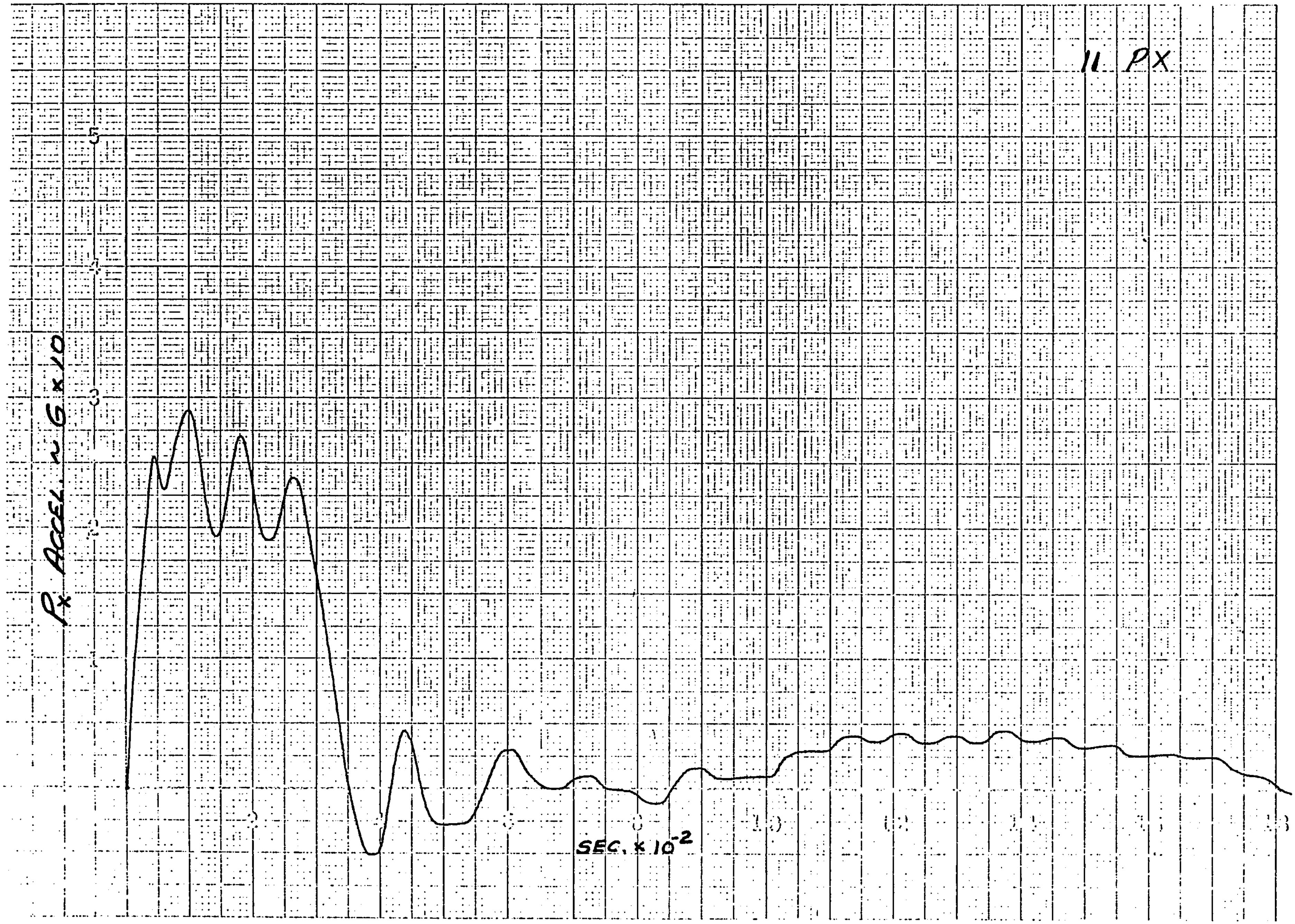

Figure A-4 (Cont'd)

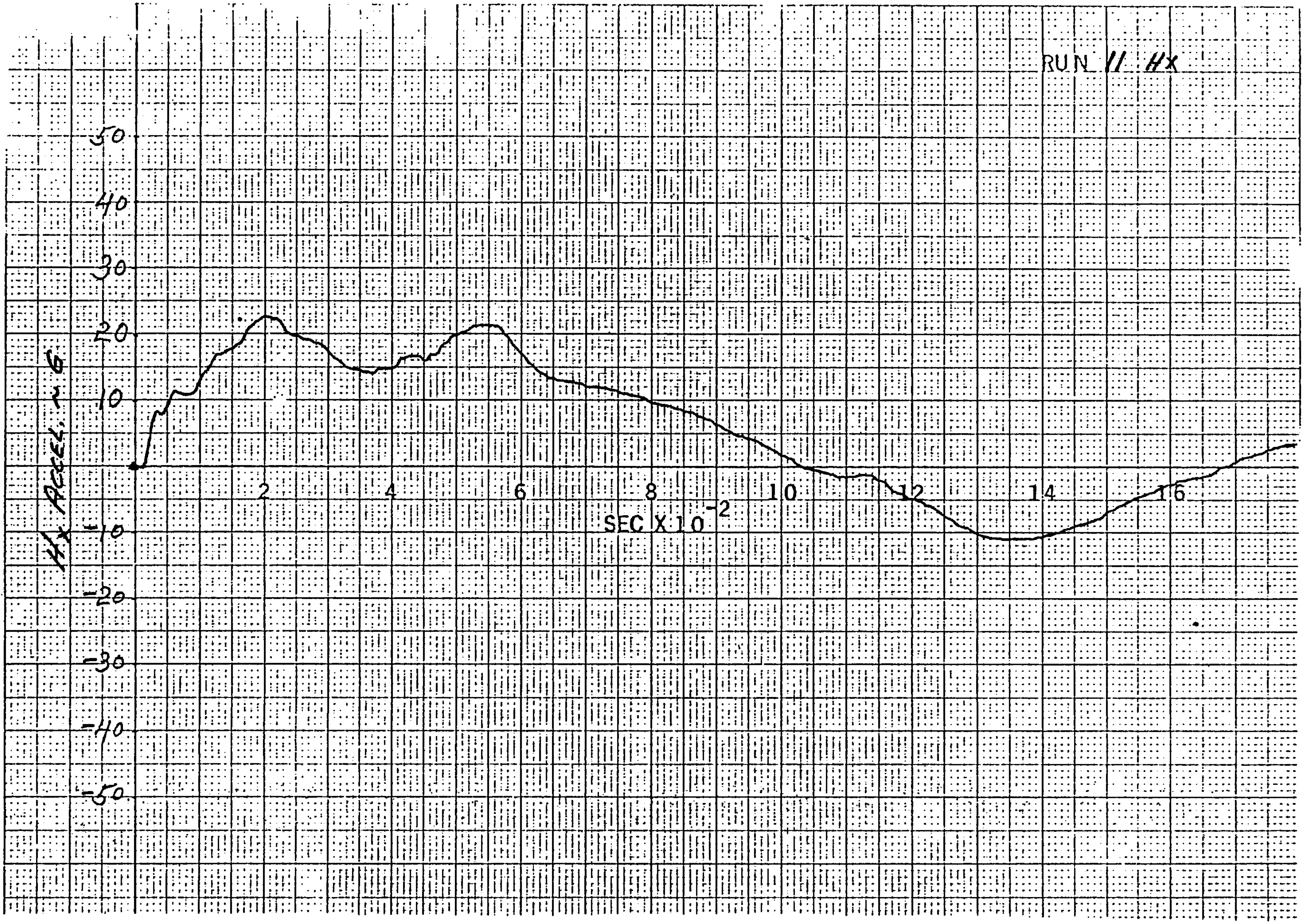

Figure A-4 (Cont'd)

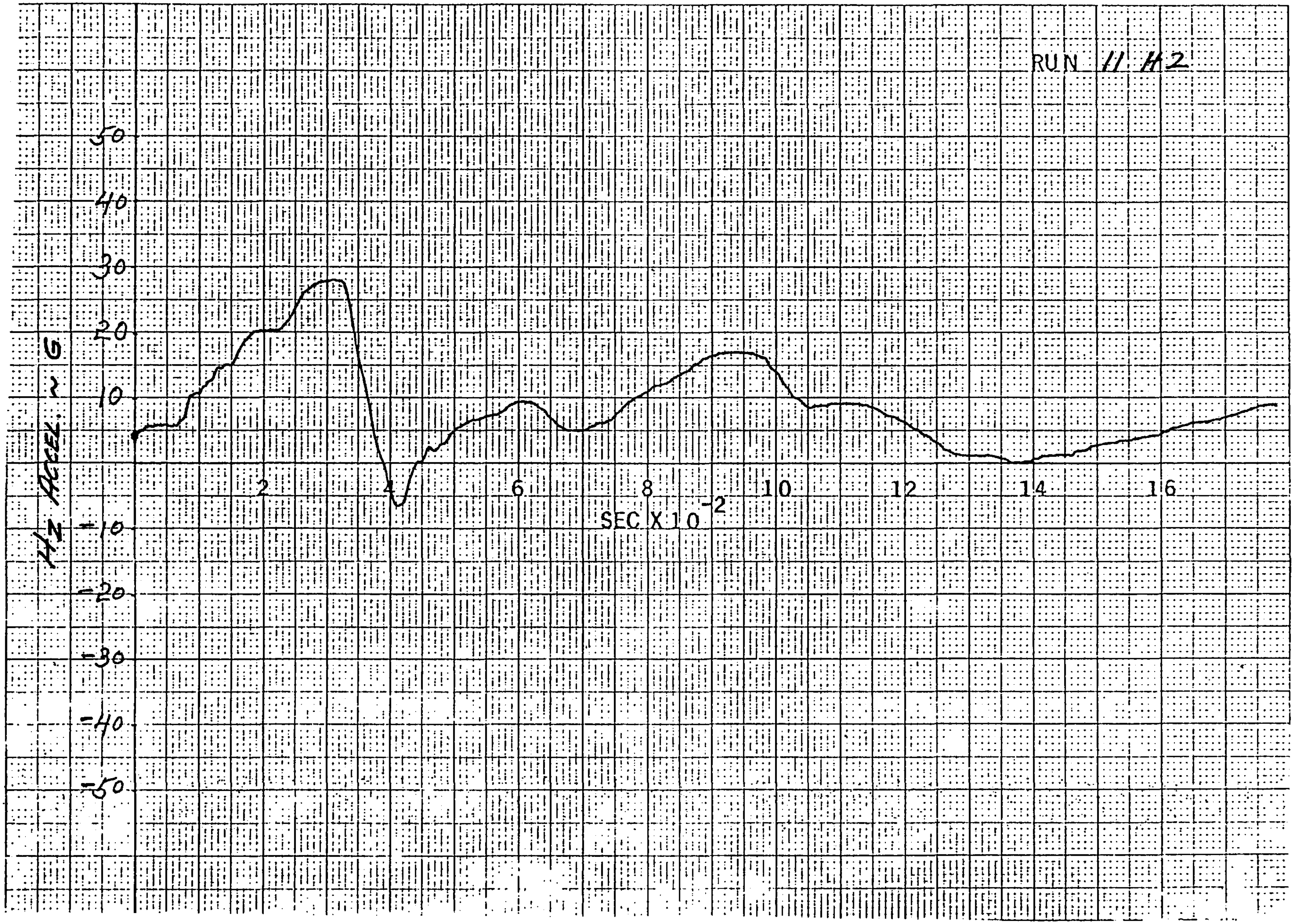

Figure A-4 (Cont'd)

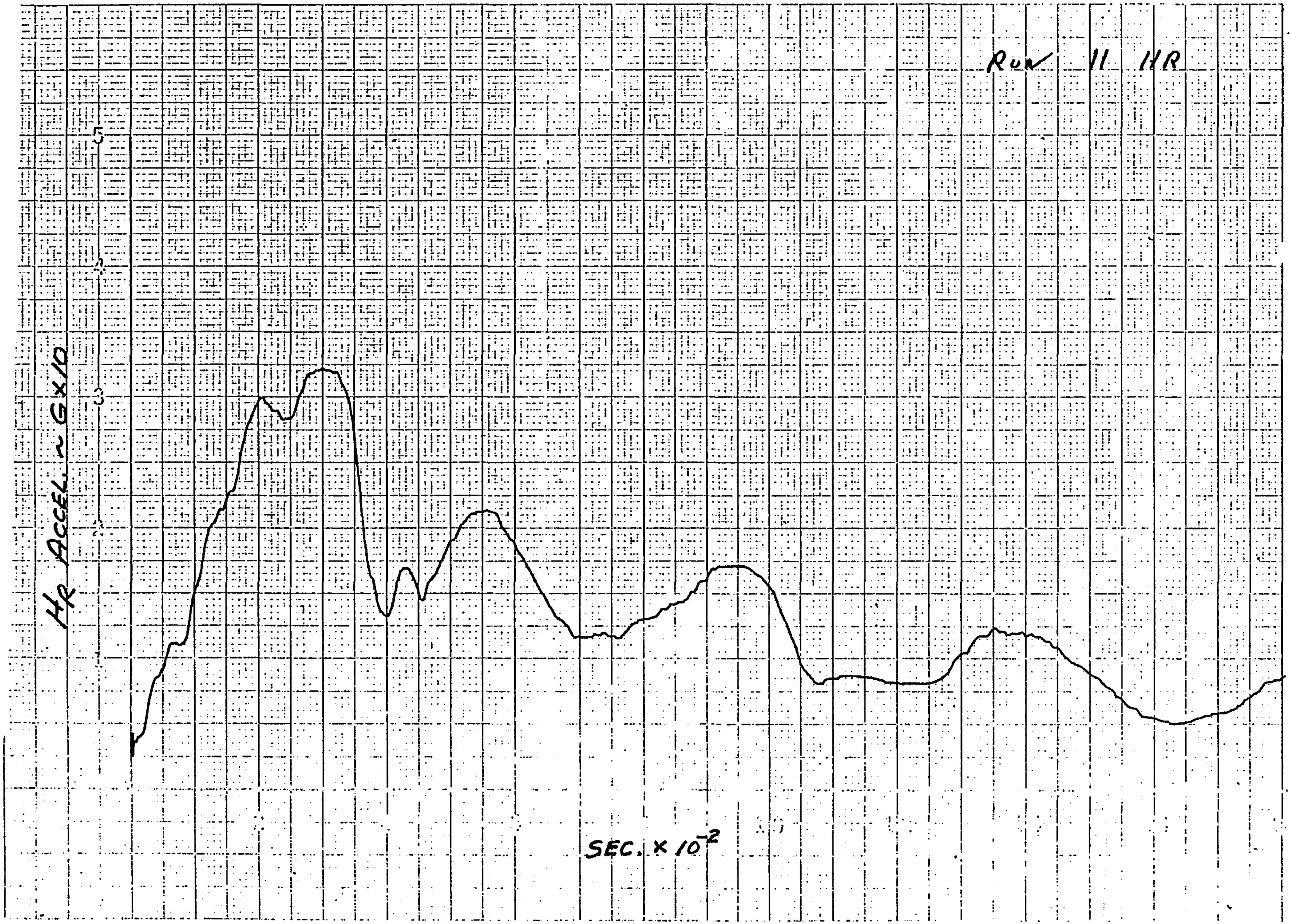

Figure A-4 (Cont'd)

APPENDIX B

Example Inputs for Simulation of Pendulum Test of Torso with Rubber Spine

```
                                       CALSPAN 3-D CRASH VICTIM SIMULATION PROGRAM

    7 APR 1977  IRSIN=   0  IRSOUT=   0  RSTIME =  0.0                                                              CARDS A

  SIMULATION OF TORSO PENDULUM RUN NO. 25
      PART 572 RESTART FROM 0  NEW DATA  720

   UNITL =  IN.      UNITM =  LB.      UNITT = SEC.      GRAVITY VECTOR = (    0.0     ,    0.0     , 386.0880)

   NDINT =    6      NSTEPS =    30      DT =0.010000      H0 =0.001000       HMAX =0.005000      HMIN =0.000125

 NPRT ARRAY
    1  2  3  4  5  6  7  8  9 10 11 12 13 14 15 16 17 18 19 20 21 22 23 24 25 26 27 28 29 30 31 32 33 34 35 36 37 38 39 40
    0  0  1  0  0  0  0  0  0  0  0  0  0  0  0  0  0  0  0  0  0  0  0  0  0  0  0  0  0  0  0  0  0  0  0  0  0  0  0  0
```

```
CRASH VICTIM       TORSO PENDULUM        4 SEGMENTS    4 JOINTS                                                         CARDS B.2

                                    SEGMENT MOMENT OF INERTIA                        SEGMENT CONTACT ELLIPSOID
 SEGMENT          WEIGHT             ( LB.-SEC.**2- IN.)                   SEMIAXES ( IN.)            CENTER ( IN.)
I  SYM PLOT       ( LB.)              X          Y          Z                X      Y      Z            X      Y      Z

1 PEND  P         72.350     137.95000  143.30000   17.67800             2.50   2.50   2.50         2.42    0.0   28.37
2  LT   5         65.800       1.78000    5.28700    1.71000             4.94   6.94   7.60          0.0    0.0     0.0
3  CT   4          1.380       0.32500    0.04000    0.14900             4.91   6.35   7.03          0.0    0.0   -2.00
4  UT   3         37.840       2.32000    1.63400    1.33000             4.41   6.78   4.94          0.0    0.0     0.0


                                                                                                                          CARDS B.3
 JOINT                   LOCATION( IN.) - SEG(JNT)   LOCATION( IN.) - SEG(J+1)  PRIN. AXIS(DEG) - SEG(JNT)  PRIN. AXIS(DEG) - SEG(J+1)
J SYM PLOT JNT PIN          X        Y        Z         X        Y        Z         YAW      PITCH      ROLL      YAW      PITCH      ROLL

1  PP   K    1 -2        -0.59      0.0    36.17     -3.75      0.0     2.10        0.0      0.0       0.0        0.0      0.0     180.00
2   P   P    2  0        -5.00      0.0    -5.15       0.0      0.0     2.70        0.0      0.0       0.0        0.0      0.0       0.0
3   W   O    3  0          0.0      0.0    -2.70     -1.12      0.0     6.72        0.0      0.0       0.0        0.0      0.0       0.0
4  PT   T    1  1        -0.59      0.0   -36.63       0.0      0.0      0.0        0.0      0.0       0.0        0.0      0.0       0.0
```

CARDS B.4

JOINT TORQUE CHARACTERISTICS

	FLEXURAL SPRING CHARACTERISTICS					TORSIONAL SPRING CHARACTERISTICS				
	SPRING COEF. (IN. LB./DEG**J)					SPRING COEF. (IN. LB./DEG**J)				
JOINT	LINEAR (J=1)	QUADRATIC (J=2)	CUBIC (J=3)	ENERGY DISSIPATION COEF.	JOINT STOP (DEG)	LINEAR (J=1)	QUADRATIC (J=2)	CUBIC (J=3)	ENERGY DISSIPATION COEF.	JOINT STOP (DEG)
1 PP	0.0	0.0	0.0	0.0	1.000	0.0	0.0	0.0	0.0	0.0
2 P	50.000	60.923	0.0	1.000	35.000	34.383	60.923	0.0	1.000	35.000
3 W	50.000	60.923	0.0	1.000	35.000	34.383	60.923	0.0	1.000	35.000
4 PT	0.0	0.0	0.0	0.0	1.000	0.0	0.0	0.0	0.0	0.0

CARDS B.5

JOINT VISCOUS CHARACTERISTICS AND LOCK-UNLOCK CONDITIONS

JOINT	VISCOUS COEFFICIENT (IN. LB.SEC./DEG)	COULOMB FRICTION COEF. (IN. LB.)	FULL FRICTION ANGULAR VELOCITY (DEG/SEC.)	MAX TORQUE FOR A LOCKED JOINT (IN. LB.)	MIN TORQUE FOR UNLOCKED JOINT (IN. LB.)	MIN. ANG. VELOCITY FOR UNLOCKED JOINT (RAD/SEC.)	IMPULSE RESTITUTION COEFFICIENT
1 PP	0.0	0.0	1.00	0.0	0.0	0.0	0.0
2 P	1.000	10.00	30.00	0.0	0.0	0.0	0.0
3 W	1.000	10.00	30.00	0.0	0.0	0.0	0.0
4 PT	0.0	0.0	1.00	0.0	0.0	0.0	0.0

```
                         SEGMENT INTEGRATION CONVERGENCE TEST INPUT                                                                          CARDS B.6

                       ANGULAR VELOCITIES               LINEAR VELOCITIES            ANGULAR ACCELERATIONS           LINEAR ACCELERATIONS
                          (RAD/SEC.)                       ( IN./SEC.)                  (RAD/SEC.**2)                   ( IN./SEC.**2)
SEGMENT          MAG.        ABS.       REL.      MAG.        ABS.       REL.      MAG.        ABS.       REL.      MAG.        ABS.       REL.
NO. SYM          TEST        ERROR      ERROR     TEST        ERROR      ERROR     TEST        ERROR      ERROR     TEST        ERROR      ERROR

 1 PEND           0.0         0.0       0.0        0.0         0.0       0.0        0.10        0.10      0.0010     1.00        1.00      0.0010
 2  LT            0.0         0.0       0.0        0.0         0.0       0.0        0.10        0.10      0.0010     0.0         0.0       0.0
 3  CT            0.0         0.0       0.0        0.0         0.0       0.0        0.10        0.10      0.0010     0.0         0.0       0.0
 4  UT            0.0         0.0       0.0        0.0         0.0       0.0        0.10        0.10      0.0010     0.0         0.0       0.0
```

```
VEHICLE DECELERATION INPUTS                                                                                          CARDS C

   NO VEHICLE

     YAW          PITCH        ROLL         VIPS         VTIME        X0(X)        X0(Y)        X0(Z)        NATAB    AT0         ADT
     0.0          0.0          0.0          0.0          1.000        0.0          0.0          0.0          0        0.0         0.0

PASSENGER COMPARTMENT DISPLACEMENT HISTORY
ANALYTICAL HALF-SINE WAVE DECELERATION
V0=   0.0    IN./SEC., OBLIQUE ANGLES =   0.0    0.0    0.0  DEGREES, TIME DURATION =  1.000 SEC.
```

```
PLANE INPUTS                                                              CARDS D.2

PLANE NO.   1        HONEYCOMB

                 X           Y           Z
POINT 1       2.5000     -5.0000     70.2500
POINT 2       2.5000      5.0000     70.2500
POINT 3       2.5000     -5.0000     60.2500

PLANE NO.   2       FRICTION PANEL

                 X           Y           Z
POINT 1       0.0         5.0000     67.0000
POINT 2       5.0000      5.0000     67.0000
POINT 3       0.0        -5.0000     67.0000
                                                                          CARD D.7
BODY SEGMENT SYMMETRY INPUT

SEG NO.    1    2    3    4

NSYM(J)    0    0    0    0
```

```
FUNCTION NO.   1      HONEYCOMB FORCE T8                  NTI( 1) =    1                                  CARDS E

         D0               D1              D2              D3              D4
        0.0            -5.0000           0.0             0.0             0.0

      FIRST PART OF FUNCTION -   13 TABULAR POINTS

       D                  F(D)
      0.0                 0.0
      0.100000           50.0000
      0.200000          190.0000
      0.300000          340.0000
      0.400000          530.0000
      0.500000          750.0000
      0.600000          930.0000
      0.700000         1000.0000
      0.800000         1000.0000
      0.900000          990.0000
      1.000000          950.0000
      1.100000          960.0000
      5.000000          960.0000




FUNCTION NO.   2      CONSTANT = 0.25                     NTI( 2) =   33                                  CARDS E

         D0               D1              D2              D3              D4
        0.0              0.0             0.2500          0.0             0.0

      FUNCTION IS CONSTANT    0.250000
```

```
FUNCTION NO.   3      CONSTANT = 0.010                    NTI( 3) =   38                        CARDS E
          D0                 D1                D2                D3                D4
          0.0                0.0               0.0100            0.0               0.0

     FUNCTION IS CONSTANT    0.010000


FUNCTION NO.   4      CONSTANT = 0.954                    NTI( 4) =   43                        CARDS E
          D0                 D1                D2                D3                D4
          0.0                0.0               0.9540            0.0               0.0

     FUNCTION IS CONSTANT    0.954000
```

```
                                                                                              CARDS E
FUNCTION NO.   5     VARIABLE FRICTION                        NTI( 5) =   48

        D0                 D1              D2             D3             D4
        0.0              -3.1000          0.0            0.0            0.0

      FIRST PART OF FUNCTION -    3 TABULAR POINTS

       D                   F(D)
      0.0                 0.2500
      2.900000            0.2500
      3.100000            3.0000



                                                                                              CARDS E
FUNCTION NO.   6      PANEL FRICTION 100                      NTI( 6) =   60

        D0                 D1              D2             D3             D4
        0.0                0.0         10000.0000        0.0            0.0

      FUNCTION IS CONSTANT10000.000000
```

```
ALLOWED CONTACTS AND ASSOCIATED FUNCTIONS
                                                                                                        CARDS F.1

    PLANE          SEGMENT  FORCE DEFLECTION     INERTIAL SPIKE       R FACTOR            G FACTOR         FRICTION COEF.
     1-  5          1-  1         1                   0                   3                   4                  2
  HONEYCOMB         PEND    HONEYCOMB FORCE T8                     CONSTANT = 0.010    CONSTANT = 0.954   CONSTANT = 0.25

     2-  5          1-  1         3                   0                   0                   0                  6
 FRICTION PANEL     PEND    CONSTANT = 0.010                                                              PANEL FRICTION 100
```

```
SUBROUTINE INITAL INPUT                                                                                  CARD G.1

  ZPLT(X)   ZPLT(Y)   ZPLT(Z)   I1    J1    I2    J2    I3
   30.00     30.00    145.00    0     0     0     0     1

INITIAL POSITIONS (INERTIAL REFERENCE)                                                                   CARDS G.2

SEGMENT          LINEAR POSITION ( IN.)              LINEAR VELOCITY ( IN./SEC.)
NO. SEG         X          Y           Z             X           Y           Z
 1 PEND     -1.58290      0.0       36.12820      72.45581      0.0        3.13078
 2  LT      -0.68333      0.0       74.52031     148.48601      0.0        1.34930
 3  CT      -6.22968      0.0       82.05439     163.67404      0.0       12.35807
 4  UT      -6.22611      0.0       91.55064     183.78219      0.0       12.33734

INITIAL ANGULAR ROTATION AND VELOCITY                                                                    CARDS G.3

SEGMENT          ANGULAR ROTATION (DEG)              ANGULAR VELOCITY (DEG/SEC.)
NO. SEG        YAW         PITCH      ROLL            X           Y           Z
 1 PEND        0.0       -3.38520      0.0           0.0      113.46627      0.0
 2  LT         0.0        3.38520   180.000000       0.0     -113.46627      0.0
 3  CT         0.0        5.33350   180.000000       0.0     -119.17465      0.0
 4  UT         0.0        7.32110   180.000000       0.0     -122.17122      0.0
```

```
      MAIN3D FUNCTIONS FOR TIME =  0.0      SEC.

                  ANGULAR ROTATION (DEG)              ANGULAR VELOCITY (RAD/SEC.)                 ANGULAR ACCELERATION (RAD/SEC.**2)
SEGMENT            YAW     PITCH     ROLL           X                Y                Z            X                Y               Z

 1 PEND           0.0     -3.3852   0.0            0.0          1.98036D+00      0.0          0.0          3.64890D-02     0.0
 2  LT            0.0     -3.3852 180.0000         0.0         -1.98036D+00      0.0          0.0         -3.64890D-02     0.0
 3  CT            0.0     -5.3335 180.0000         0.0         -2.07999D+00      0.0          0.0          1.91665D+01     0.0
 4  UT            0.0     -7.3211 180.0000         0.0         -2.13229D+00      0.0          0.0         -2.03723D+01     0.0
 5 VEH            0.0      0.0      0.0            0.0          0.0              0.0          0.0          0.0             0.0


                     LINEAR POSITION ( IN.)            LINEAR VELOCITY ( IN./SEC.)                 LINEAR ACCELERATIONS (G'S)
SEGMENT            X            Y         Z           X            Y            Z             X               Y               Z

 1 PEND         -1.5829       0.0       36.1282     72.45581      0.0          3.13078       0.019498        0.0            -0.371635
 2  LT          -0.6833       0.0       74.5203    148.48601      0.0          1.34930       0.013989        0.0            -0.761701
 3  CT          -6.2297       0.0       82.0544    163.67404      0.0         12.35807      -0.062406        0.0            -0.853006
 4  UT          -6.2261       0.0       91.5506    183.78219      0.0         12.33734       0.163181        0.0            -0.989193
 5 VEH            0.0         0.0        0.0         0.0          0.0          0.0           0.0            0.0             0.0


                    U1 ARRAY ( IN./SEC.**2)          U2 ARRAY (RAD/SEC.**2)
                 EXTERNAL LINEAR ACCELERATIONS    EXTERNAL ANGULAR ACCELERATIONS
SEGMENT            X            Y         Z           X         Y          Z

 1 PEND           0.0         0.0     386.0880       0.0       0.0        0.0
 2  LT            0.0         0.0     386.0880       0.0     16.69436     0.0
     CT           0.0         0.0     386.0880       0.0    155.55981     0.0
     UT           0.0         0.0     386.0880       0.0    -57.82466     0.0


                         JOINT FORCES ( LB.)              JOINT TORQUES ( IN. LB.)        RELATIVE ANGULAR
 JOINT  IPIN          X          Y          Z            X            Y            Z      VELOCITY (RAD/SEC.)

 1   PP   -2       7.0091       0.0     -193.7481       0.0      -423.33888      0.0          0.0
 2    P    0       6.0887       0.0      -77.8282       0.0       -88.26310      0.0          0.099630
 3    W    0       6.1748       0.0      -75.2710       0.0       -94.48549      0.0          0.052300
 4   PT    1      -8.4198       0.0      292.9859       0.0         0.0          0.0          1.980360
```

APPENDIX C

Example Inputs for Simulation of Pendulum Impact Test of Torso with Single Pin Spine Joint

```
CRASH VICTIM     TORSO WITH PIN JOINT    4 SEGMENTS    4 JOINTS                                                  CARD  B.1

                                PRINCIPAL MOMENTS OF INERTIA              SEGMENT CONTACT ELLIPSOID                       CARDS B.2
 SEGMENT            WEIGHT         ( LB.-SEC.**2- IN.)              SEMIAXES ( IN.)              CENTER ( IN.)         PRINCIPAL AXES (DEG)
I  SYM PLOT         ( LB.)          X          Y          Z         X         Y         Z         X         Y         Z         YAW        PITCH       ROLL

1 PEND   P          74.300     100.0000  148.4000  100.0000    10.000    10.000    10.000    -8.330     0.0      27.500       0.0        0.0         0.0
2 LT     L          65.280     100.0000    4.4400  100.0000     1.000     1.000     1.000     0.0       0.0       0.0         0.0        0.0         0.0
3 UT     U          39.620     100.0000    1.8300  100.0000     1.000     1.000     1.000     0.0       0.0       0.0         0.0        0.0         0.0
4 GSEG   G           0.001     100.0000    0.0010  100.0000     1.000     1.000     1.000     0.0       0.0       0.0         0.0        0.0         0.0

                                                                                                                           CARDS B.3
 JOINT                    LOCATION( IN.) - SEG(JNT)    LOCATION( IN.) - SEG(J+1)  PRIN. AXIS(DEG) - SEG(JNT)  PRIN. AXIS(DEG) - SEG(J+1)
J SYM PLOT JNT PIN           X         Y         Z          X         Y         Z        YAW       PITCH       ROLL       YAW       PITCH      ROLL

1 PDLT   L     1 -1       -0.700    0.0       35.250     -3.680    0.0       4.970     0.0       0.0         0.0        0.0       0.0       180.0
2 LTUT   S     2  1       -4.930    0.0       -5.160     -1.080    0.0       8.540     0.0       0.0         0.0        0.0       0.0         0.0
3 UTGS   U     3 -1        0.0      0.0       -3.560      0.0      0.0       0.0       0.0       0.0         0.0        0.0       0.0         0.0
4 PPIN   P     1  1       -0.700    0.0      -37.500      0.0      0.0       0.0       0.0       0.0         0.0        0.0       0.0         0.0
```

```
JOINT TORQUE CHARACTERISTICS                                                                                              CARDS B.4

                    FLEXURAL SPRING CHARACTERISTICS                                       TORSIONAL SPRING CHARACTERISTICS

                SPRING COEF. ( IN. LB./DEG**J)      ENERGY     JOINT      SPRING COEF. ( IN. LB./DEG**J)       ENERGY     JOINT
JOINT            LINEAR    QUADRATIC     CUBIC   DISSIPATION  STOP         LINEAR    QUADRATIC     CUBIC   DISSIPATION  STOP
                 (J=1)       (J=2)       (J=3)      COEF.     (DEG)        (J=1)       (J=2)       (J=3)      COEF.     (DEG)

1 PDLT            0.0         0.0         0.0        0.0      1.000         0.0         0.0         0.0        0.0       0.0
2 LTUT            8.250       1.250       0.0        0.450   40.000         0.0         0.0         0.0        0.0       0.0
3 UTGS            0.0         0.0         0.0        0.0      1.000         0.0         0.0         0.0        0.0       0.0
4 PPIN            0.0         0.0         0.0        0.0      0.0           0.0         0.0         0.0        0.0       0.0


                                                                                                                         CARDS B.5
                                   JOINT VISCOUS CHARACTERISTICS AND LOCK-UNLOCK CONDITIONS

             VISCOUS           COULOMB        FULL FRICTION    MAX TORQUE FOR   MIN TORQUE FOR   MIN. ANG. VELOCITY      IMPULSE
JOINT      COEFFICIENT     FRICTION COEF.  ANGULAR VELOCITY   A LOCKED JOINT   UNLOCKED JOINT   FOR UNLOCKED JOINT    RESTITUTION
     ( IN. LB.SEC./DEG).  ( IN. LB.)        (DEG/SEC.)         ( IN. LB.)       ( IN. LB.)          (RAD/SEC.)        COEFFICIENT

1 PDLT         0.0              0.0            1.00               0.0              0.0                 0.0               0.0
2 LTUT         0.0             10.00          10.00               0.0              0.0                 0.0               0.0
3 UTGS         0.0              0.0            1.00               0.0              0.0                 0.0               0.0
4 PPIN         0.0              0.0            1.00               0.0              0.0                 0.0               0.0
```

```
                                                                                                              CARDS B.6
                      SEGMENT INTEGRATION CONVERGENCE TEST INPUT

                    ANGULAR VELOCITIES             LINEAR VELOCITIES              ANGULAR ACCELERATIONS           LINEAR ACCELERATIONS
                        (RAD/SEC.)                     ( IN./SEC.)                    (RAD/SEC.**2)                   ( IN./SEC.**2)
SEGMENT          MAG.      ABS.      REL.      MAG.      ABS.      REL.      MAG.      ABS.      REL.      MAG.      ABS.      REL.
NO. SYM          TEST      ERROR     ERROR     TEST      ERROR     ERROR     TEST      ERROR     ERROR     TEST      ERROR     ERROR

 1 PEND         0.0       0.0       0.0       0.0       0.0       0.0       0.100     0.100     0.0010    1.000     1.000     0.0010
 2 LT           0.0       0.0       0.0       0.0       0.0       0.0       0.100     0.100     0.0010    0.0       0.0       0.0
 3 UT           0.0       0.0       0.0       0.0       0.0       0.0       0.100     0.100     0.0010    0.0       0.0       0.0
 4 GSEG         0.0       0.0       0.0       0.0       0.0       0.0       0.0       0.0       0.0       0.0       0.0       0.0
```

```
                                                                                                   CARDS C
VEHICLE DECELERATION INPUTS

 VEHICLE TREATED AS GROUND
                                                                                          ATO        ADT     MSEG
     YAW        PITCH       ROLL       VIPS       VTIME      XO(X)      XO(Y)      XO(Z)  NATAB
     0.0        0.0         0.0        0.0        1.000      0.0        0.0        0.0      0      0.0        0.0        0

PASSENGER COMPARTMENT DISPLACEMENT HISTORY
ANALYTICAL HALF-SINE WAVE DECELERATION
VO=   0.0    IN./SEC., OBLIQUE ANGLES =   0.0    0.0    0.0  DEGREES, TIME DURATION =  1.000 SEC.
```

```
                                                                                                  CARD D.1
  NPL    NBLT    NBAG    NELP     NQ     NSD  NHRNSS  NWINDF   NJNTF  NFORCE
    1       0       0       0      0       0       0       0       0       0                      CARDS D.2

PLANE INPUTS

PLANE NO.   1    HONEYCOMB

                  X          Y          Z
POINT 1       -0.6300   -10.0000    75.0000
POINT 2       -0.6300    10.0000    75.0000
POINT 3       -0.6300   -10.0000    55.0000                                                       CARD D.7

BODY SEGMENT SYMMETRY INPUT

SEG NO.    1   2   3   4

NSYM(J)    0   0   0   0
```

```
FUNCTION NO.   1    HONEYCOMB FORCE-DEFL                      NTI( 1) =    1                                    CARDS E
          D0               D1              D2              D3              D4
         0.0            -5.0000           0.0             0.0             0.0

     FIRST PART OF FUNCTION -    9 TABULAR POINTS

      D                  F(D)
     0.0                 0.0
     0.050000          880.0000
     0.150000         1235.0000
     0.230000         1040.0000
     0.320000         1200.0000
     0.380000         1090.0000
     0.480000         1360.0000
     0.580000         1230.0000
     5.000000         1230.0000



FUNCTION NO.   2    CONSTANT =0.01                            NTI( 2) =   25                                    CARDS E
          D0               D1              D2              D3              D4
         0.0              0.0            0.0100           0.0             0.0

     FUNCTION IS CONSTANT    0.010000
```

```
FUNCTION NO.   3    CONSTANT =0.920                          NTI( 3) =   30                                        CARDS E
         D0                 D1                D2                D3                D4
        0.0                0.0              0.9200             0.0               0.0

      FUNCTION IS CONSTANT    0.920000



FUNCTION NO.   4    CONSTANT =0.25                           NTI( 4) =   35                                        CARDS E
         D0                 D1                D2                D3                D4
        0.0                0.0              0.2500             0.0               0.0

      FUNCTION IS CONSTANT    0.250000
```

```
 ALLOWED CONTACTS AND ASSOCIATED FUNCTIONS
                                                                                                        CARDS F.1

     PLANE          SEGMENT  FORCE DEFLECTION    INERTIAL SPIKE      R FACTOR          G FACTOR        FRICTION COEF.

       1-  5          1-  1        1                  0                  2                 3                 4
 HONEYCOMB            PEND HONEYCOMB FORCE-DEFL                   CONSTANT =0.01    CONSTANT =0.920   CONSTANT =0.25
```

```
SUBROUTINE INITAL INPUT                                                                                          CARD G.1

 ZPLT(X)   ZPLT(Y)   ZPLT(Z)   I1    J1    I2    J2    I3    SPLT(1)   SPLT(2)   SPLT(3)
   30.       30.       60.      0     0     0     0     1     10.00      6.00      1.00

INITIAL POSITIONS (INERTIAL REFERENCE)                                                                           CARDS G.2

SEGMENT          LINEAR POSITION ( IN.)                  LINEAR VELOCITY ( IN./SEC.)
NO. SEG           X           Y          Z               X           Y           Z
 1 PEND        -1.03455      0.0      37.49226        44.85229      0.0       1.23764
 2 LT           0.08270      0.0      77.80703        93.08116      0.0      -0.09894
 3 UT          -4.39660      0.0      91.31438       132.70300      0.0       3.38939
 4 GSEG        -4.56119      0.0      94.87057       146.68117      0.0       4.03636

INITIAL ANGULAR ROTATION AND VELOCITY                                                                            CARDS G.3

SEGMENT          ANGULAR ROTATION (DEG)                  ANGULAR VELOCITY (DEG/SEC.)
NO. SEG        YAW        PITCH        ROLL              X           Y           Z                IYPR
 1 PEND        0.0      -2.65000       0.0              0.0       68.54338      0.0          1    2    3    0
 2 LT          0.0       2.65000    180.00000           0.0      -68.54338      0.0          1    2    3    0
 3 UT          0.0       2.65000    180.00000           0.0     -225.21000      0.0          1    2    3    0
 4 GSEG        0.0      -3.35000    180.00000           0.0     -225.21000      0.0          1    2    3    0
```